Low ppm Atom Transfer Radical Polymerization in Dispersed Media and Electrochemically Mediated Reversible Addition-Fragmentation Chain-Transfer Polymerization

Submitted in partial fulfillment of the requirements for the degree of

Doctor of Philosophy in

Department of Chemistry

Yi Wang

Carnegie Mellon University

Pittsburgh, PA

June, 2020

Abstract

This thesis summarizes my PhD research study in the mechanistic study of atom transfer radical polymerization (ATRP) in aqueous dispersed media and electrochemically mediated reversible addition-fragmentation chain-transfer (*e*RAFT) polymerization.

The introductory chapter (Chapter I) reviews the history and development of RDRP, focusing on ATRP and RAFT polymerization. Their principle, mechanism, media, kinetics, and resulting polymer materials are presented.

Chapters II – VI cover the mechanism study of ATRP in miniemulsion and emulsion under different low ppm ATRP techniques using an ion-pair catalyst. Chapter II presents the activator regenerated by electron transfer (ARGET) ATRP in miniemulsion. The selection of structure and concentration of the surfactant, copper concentration, target degree of polymerization, are discussed. The synthesis of block, star and brush copolymers are conducted. Chapter III discusses the key factor for application of the ion-pair catalyst to an *ab initio* emulsion. Chapters IV – V explores the application of photomediated ATRP in miniemulsion and *ab initio* emulsion. The impact of surfactant amount and solids content which influence the optical properties of the miniemulsion are investigated, as well as temporal control, chain extension and gradient copolymer preparation. Chapter VI presents an enzyme-deoxygenation system in miniemulsion and emulsion ATRP, which allows synthesis of hydrophobic polymers without physical displacement methods.

Chapters VII – VIII investigate the synthesis of block copolymers and hairy nanoparticles in miniemulsion ATRP. Chapter VII discusses the optimal conditions to

chain extend a less active macroinitiator with a more active monomer under low copper concentration. Chapter VIII explores approaches for chain extending a hydrophobic crosslinked nanoparticle with hydrophilic or zwitterionic polymer chains.

Chapters IX – XI discuss pathways to employ electrochemistry in the initiation and control over RAFT polymerization. Chapter IX presents initiation of RAFT polymerization by electrochemical reaction of an external diazonium salt initiator. Chapter X combines the benefit of *e*ATRP and RAFT in a synergistic mechanism. The radicals are generated in *e*ATRP, and controlled simultaneously by ATRP and RAFT. In sight of the RAFT chain-transfer agents (CTAs) as alkyl pseudohalides, Chapter XI employs copper catalysts in *e*ATRP to activate the CTAs. The contribution of ATRP and RAFT to the control is discussed.

Published works with minor relevance to this thesis are included as appendices.

Acknowledgements

I appreciate the support and care from my parents, Yinqiong Wu, Tongjun Wang, my parents-in-law, Qingli Shang and Ye Qian, and my husband, Shangyu Qian. They shared my happiness and sorrow during the five years of my graduate study. Whenever I need help, they were behind me. I acknowledge my uncle, Shunxing Wu, my aunt, Chunxian Wu, cousins, Qing Wang, Kangda Zhang, Yile Qian, Yixiao Qian, who gave me a lot of support and comfort. My grandmother, Junhua Sun, devoted her selfless love to everyone in the big family. Her kindness, optimism, and forgiveness influenced the way I understand life. I dedicate this thesis to my grandmother, and I wish her healthy and long-life.

I deeply acknowledge my advisor, Prof. Krzysztof Matyjaszewski, for providing me such a great opportunity to conduct research in the top Polymer group, and for his guidance and patience to me throughout the five years. His enthusiasm, inspiration diligence, have been of great value for me, which I am sure will influence my work even after I leave CMU.

I would like to acknowledge my committee members, Prof. Kevin Noonan and Prof. Robert Tilton for their insightful discussions, for reviewing my work and providing feedback. My gratitude goes to Dr. Rea Freeland, Prof. Linda Peteanu, Lorna Williams for their help and accommodations throughout the program.

I benefited a lot from Dr. Sangwoo Park, Dr. Marco Fantin, for their kind guidance in my first years of PhD study. Also many thanks to my collaborators, Dr. Pawel Chmielarz, Dr. Francesca Lorandi, Sajjad Dadashi-Silab, and Liye Fu for their significant

contributions and fruitful discussion. I would like to especially thank Dr. James Spanswick and Emilee Tkacik for their kind suggestions in scientific writing. I thank the friendship with Dr. Jiajun Yan, Dr. Zongyu Wang, Rui Yuan, Liye Fu, Dr. Taeheon Lee, Dr. Xuan Qin, Dr. Zhenhua Wang, and Dr. Patricia Borim.

Table of Contents

List of Tables

List of Figures

List of Schemes

Chapter 1 Reversible Deactivation Radical Polymerization in Dispersed Media and in Solution

1.1. Introduction to Reversible Deactivation Radical Polymerization

Radical polymerization has been advantageous over other polymerization mechanisms due to the broad range of compatible (co)monomers, reaction media, and tolerance to impurities. It is also widely used in industry, as it constitutes ~ 50% of commercial production worldwide.[1] However, the intrinsic high activity of radicals leads to inevitable termination reactions, thus the lifetime of radicals is only ~1 s, making it impossible to further tune the process, regarding polymer structure and chain length.

Regulation of polymer chain length and dispersity is important in polymer chemistry. Synthesis of polymers with pre-determined molecular weight (MW), low dispersity ($Đ$) and preserved chain end functionalities allows to fine tune the physical properties of materials and to manufacture macromolecules with complex architectures. With these requirements, various techniques have been employed to extend the lifetime of the radicals, termed reversible deactivation radical polymerizations (RDRPs).[1-2] Their essence is to "cut" the lifetime (~1 s) of a radical into thousands of ~ 1 ms active periods, and insert a long dormant states (> 1 min) between each short active state, taking advantage of reversible deactivation or chain-transfer. The multiple deactivation procedures decrease the possibility of radical termination, average the number of monomer addition per active periods, and result in polymers with predetermined molecular weight and low dispersity. Main techniques of RDRP include atom transfer radical polymerization (ATRP),[3-4]

reversible addition-fragmentation chain-transfer (RAFT) polymerization,[5-8] nitroxide-mediated polymerization (NMP),[9] iodine transfer polymerization (ITP),[10] organotellurium-mediated polymerization (TERP),[11] etc.

RDRPs have been employed to prepare polymers with various chain length and architectures, block copolymers, and bio-polymer hybrids, which could be used in many applications. Taking ATRP as an example, the incorporation of different compositions, topologies, functionalities, and architectures greatly enriched the world of polymers. These macromolecular engineering techniques made preparation of an array of functional materials accessible (**Scheme 1-1**).[12]

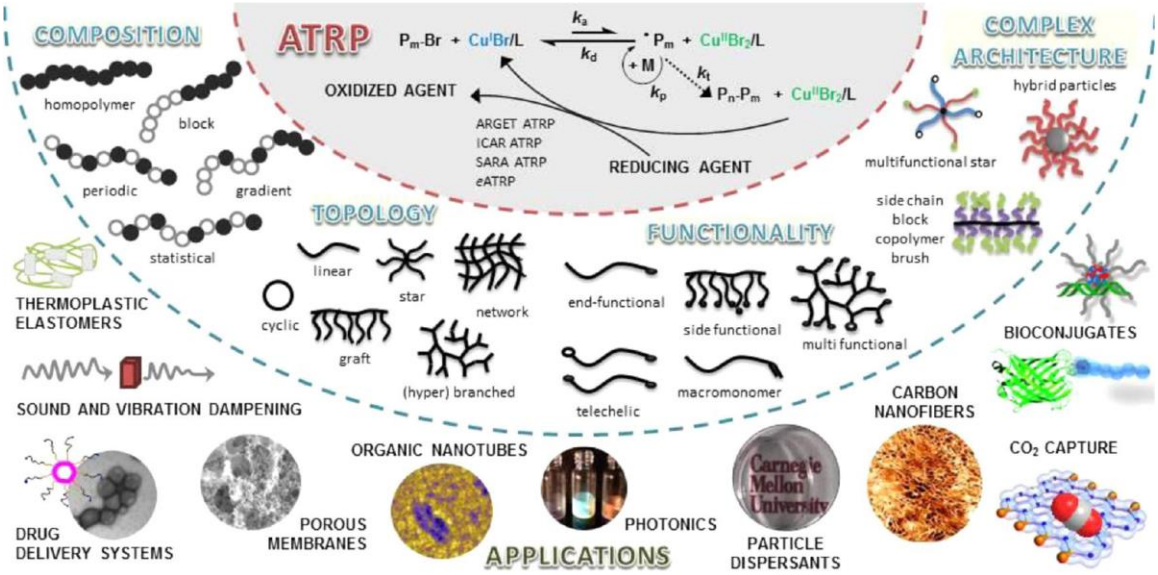

Scheme 1-1. Overview of ATRP and the resulting materials by macromolecular engineering. Reproduced with permission from ref[12].

1.2. Atom Transfer Radical Polymerization

1.2.1. Mechanistic Insights into Atom Transfer Radical Polymerization

ATRP is based on an inner sphere electron transfer process, which involves a reversible (pseudo)halogen transfer from a dormant species (R–X or P_n–X) to a transition metal complex (Cu^IL^+), generating propagating radicals (P_n·) and the metal complex in the higher oxidation state, X–$Cu^{II}L^+$ (**Scheme 1-2**). Radicals react reversibly with X–$Cu^{II}L^+$ to reform the dormant species, lowering the possibility of conventional radical termination (k_t). A small fraction of chains is active at one time and activation-deactivation equilibrium can be fast, therefore all chains grow simultaneously and termination reactions are minimized.[13]

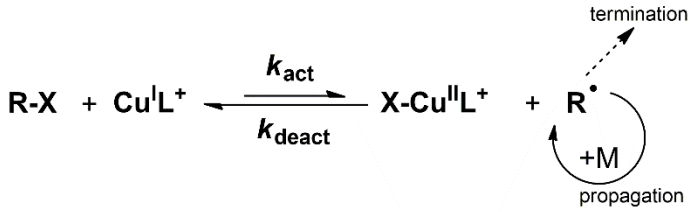

Scheme 1-2. Mechanism of ATRP. (k_{act} = activation rate constant, k_{deact} = deactivation rate constant, k_p = propagation rate constant, k_t = termination rate constant, M = monomer, L = ligand, X = halogen, and R−X = alkyl halide).

The equilibrium constant, K_{ATRP}, is expressed as:

$$K_{ATRP} = \frac{[P_n \cdot][X - Cu^{II}/L]}{[P_n - X][Cu^I/L]} \quad (1\text{-}1)$$

The rate of polymerization R_p at equilibrium state is expressed by Equation (1-2):

$$R_p = k_p[M][P_n \cdot] = k_p K_{ATRP}[M][P_n - X]\frac{[Cu^I/L]}{[X - Cu^{II}/L]} \quad (1\text{-}2)$$

where K_{ATRP} is the equilibrium constant. The rate of polymerization depends on the ratio of Cu^I/Cu^{II}. The dispersity $Đ = M_w/M_n$ of the resulting polymer decreases at higher Cu^{II}:

$$\frac{M_w}{M_n} = 1 + \frac{1}{DP_n} + \left(\frac{k_p[RX]_0}{k_d[X - Cu^{II}/L]}\right)\left(\frac{2}{p} - 1\right) \quad (1\text{-}3)$$

Where DP_n is the degree of polymerization, p is the conversion.

ATRP was first explored in high copper concentration conditions, i.e., Cu catalyst complex was in the equimolar to R–X. In normal ATRP, Cu^IBr was added directly, thus an oxygen free atmosphere was necessary.[14-15] Alternative methods were explored to avoid the use of Cu^IBr. In reverse ATRP, $Cu^{II}Br_2$ and a thermal initiator (for example, AIBN), were employed to build the ATRP equilibrium from the $Cu^{II}Br_2$ side.[16] The disadvantage of reverse ATRP is the limitation to polymer architectures and functionalities. To incorporate functional groups in the initiator and facilitate synthesis of polymer architectures, a mixture of thermal initiator and alkyl halide initiator could be used in simultaneous reverse and normal initiation (SR&NI).[17] The use of the thermal initiator was avoided by chemically generation of Cu^I using chemical reducing agents in activator generated by electron transfer (AGET) ATRP. [18-19]

1.2.2. Activator Regeneration Atom Transfer Radical Polymerization

The high concentration of Cu catalyst in the above mentioned ATRP techniques placed problems of limited solubility, toxicity and catalyst removal. Methods have been developed to conduct ATRP under decreased Cu concentration, yet not to sacrifice the kinetics and degree of control. Since the rate of polymerization depends on the ratio of

Cu^{I}/Cu^{II} (Equation (1-2)), an decreased Cu concentration does not necessarily result in slow polymerization. However, the inevitable termination reaction leads to accumulation of Cu^{II}, which causes slows down or even stops the polymerization. Thus, to maintain a proper Cu^{I}/Cu^{II}, regeneration of Cu^{I} is required (**Scheme 1-3**). These activator regeneration methods allowed for lower Cu amount (ppm level) and lower cost for ligands. In addition, the use of oxidatively stable $Cu^{II}Br_2$ and oxygen tolerance greatly simplified the reaction setup procedure. The main concept of activator regeneration methods is summarized below.

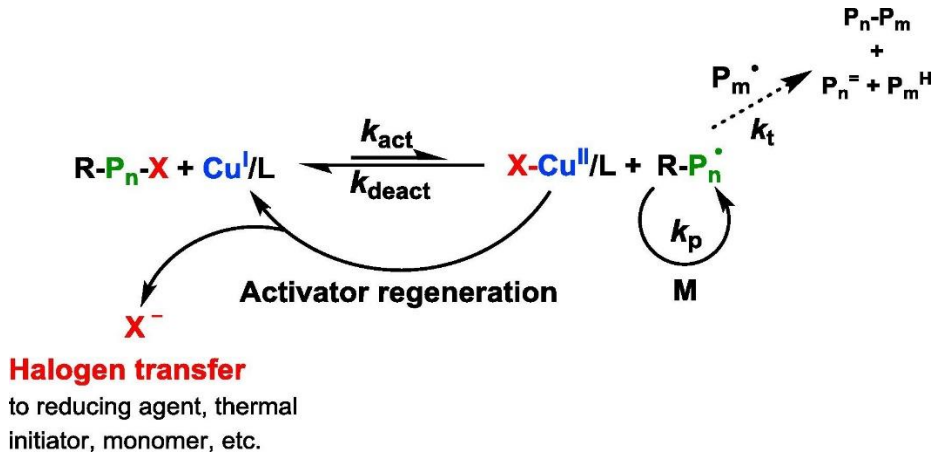

Scheme 1-3. General mechanism of activator regeneration ATRP. Reprinted with permission from ref[20].

Activators regenerated by electron transfer (ARGET) ATRP utilizes chemical reducing agents such as ascorbic acid (AsAc) or $Sn^{II}R_2$ compounds.[21-23] The rate of polymerization depends on the amount or feeding rate of the reducing agent. ARGET ATRP was widely used in polymer-inorganic hybrid material synthesis due to its robustness and high oxygen tolerance.[24-25]

Initiators for continuous activator regeneration (ICAR) ATRP employs a thermal radical initiator such as AIBN, whose slow decomposition continuously reduce the

deactivator back to the activator.[26] The kinetics of an ICAR ATRP is similar to that in RAFT, and a small fraction of the chains originate from the thermal initiator. Thus, it is not ideal for the synthesis of well-defined block copolymers.

Supplemental activator and reducing agent (SARA) ATRP uses zero-valent copper which acts as both a supplemental activator and a reducing agent.[27-30] The rate of polymerization depends on the surface area of Cu^0. Cu metal could be reused for multiple reactions.

Electrochemically mediated ATRP (*e*ATRP) takes advantage of electrochemical current.[31-33] No external chemicals are needed in *e*ATRP, thus *e*ATRP is a "cleaner" method than ARGET or ICAR. The rate of polymerization, affected by Cu^I/Cu^{II} ratio, could be directly correlated to the applied potential by Nernst equation. Temporal control was achieved by adjusting the potential.[32] The disadvantages of *e*ATRP include the complex reaction setup, expensive supporting electrolytes, and difficulty of scaling up.

In photoATRP, UV light or visible light reduces excited Cu^{II} complexes by a free aliphatic amine, usually an excess of ligand.[34-35] The rate of polymerization is influenced by the ratio of ligand to copper. Similar to *e*ATRP, the use of light as an external stimulus, thus temporal control was achieved in photo ATRP.[36] In recent years, some organocatalysts, such as 10-phenylphenothiazine (PTZ) acted as a good photocatalyst for photo ATRP.[37]

SonoATRP has been developed in recent years. There are two ways of radical generation. First, ultrasound induced electron transfer from piezoelectric materials such as $BaTiO_3$ or ZnO allowed activator regeneration in low ppm ATRP.[38-40] Second, in an aqueous media, ultrasonication produced hydroxyl radicals from water molecule. The

hydroxyl radicals reacted with methanol or alcohol, forming carbon based radicals which activate propagation.[41]

1.3. Atom Transfer Radical Polymerization in Dispersed Media

Polymerizations in heterogeneous media are characterized by good heat transfer, low environmental impact, low viscosity and low toxicity,[42] which are important advantages for commercial applications.[43] Moreover, they can be employed to prepare nanoparticles with various morphologies (*e.g.* core-shell, microcapsules and multilayered particles) for specific applications in biomedical, pharmaceutical, drug delivery or diagnostic areas.[42, 44-47]

Conducting RDRP in dispersed media brings additional benefits. The segregation of polymerization loci in dispersed media brings RDRP additional benefit of reduced termination reaction. This effect leads to increased degree of livingness in dispersed media polymerization compared to homogeneous polymerizations.[48]

In this section, various types of dispersed media polymerization are discussed. Since miniemulsion and emulsion polymerization are mainly explored in this thesis work, a brief overview of ATRP in miniemulsion and emulsion is presented. Finally, preparation of polymer architectures and functional materials is discussed.

1.3.1. Types of Dispersed Media Polymerization

Heterogeneous polymerization processes are generally two-phase systems, where the starting monomer(s) and/or the resulting polymer are well dispersed in an immiscible liquid. However, the definitions are somewhat unclear. In this section, a general

introduction about different types of dispersed media polymerization is given. Depending on four criteria: 1) initial state of the polymerization mixture; 2) kinetics of polymerization; 3) mechanism of particle formation; and 4) size of the final polymer particles, heterogeneous polymerizations are categorized into the following types: suspension, emulsion, miniemulsion, microemulsion, dispersion and precipitation.[49] The features of these types of dispersed media are discussed below.

Miniemulsion polymerization (**Scheme 1-4**). The oil-soluble monomer, initiator, and a hydrocarbon costabilizer are used in the organic phase, and the surfactant is dissolved in the aqueous phase. A miniemulsion is hydrodynamically unstable, so a strong homogenization process, like probe ultrasonication is needed. The surfactant is absorbed on the surface of the monomer droplets, and there is no mass transfer of monomer during the polymerization, thus the polymerization proceeds in each droplet like a "mini-bulk" polymerization. As a result, the size of the final polymer is similar to that of the initial monomer droplet size (50-500 nm).[50]

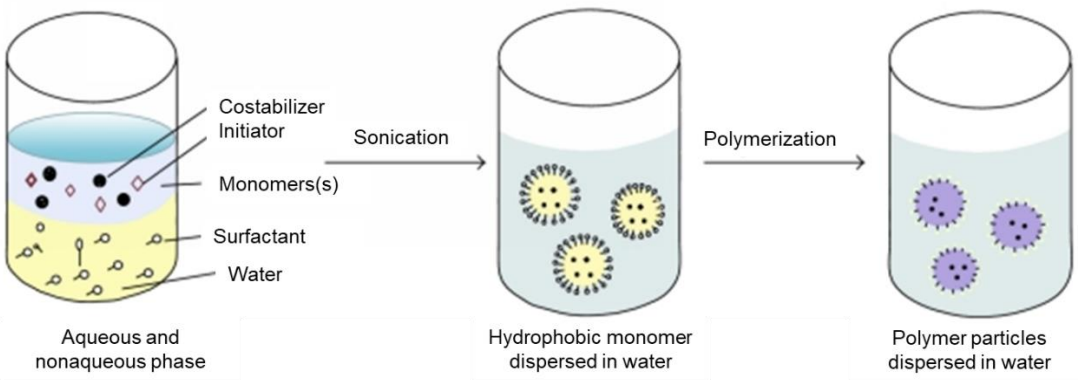

Scheme 1-4. Schematic illustration of a miniemulsion polymerization process within an oil-in-water (O/W) miniemulsion. Reproduced with permission from ref[51].

Suspension polymerization. In suspension polymerization, the initiator is dissolved in the monomer phase, which disperses in the aqueous phase to form droplets. Instead of strong homogenization in the presence of surfactant in miniemulsion, suspension is prepared by stirring in the presence of a droplet stabilizer (suspension agent). The monomer droplets are converted directly to the polymer microbeads with no significant size change. Suspension polymerization is usually used to produce polymer beads with a size of 20 μm -2 mm.[49]

Emulsion polymerization. A traditional emulsion polymerization system consists of a hydrophobic monomer, a water-soluble initiator, surfactant and water. At the very beginning of the polymerization, a large portion of monomer resides in monomer droplets (1-10 μm) under the aid of surfactants, and a small fraction is in surfactant-formed micelles. The initiators are decomposed in water, and initiate chain growth into oligoradicals. At a critical chain length, the hydrophobic oligoradicals enter the micelles rather than the monomer droplets, because the micelles have much higher surface area. The monomer in the droplets diffuses into aqueous phase, and enters the micelles to continuously propagate, resulting in polymer particles (**Scheme 1-5**). The final polymer particle size is 100-500 nm.[52]

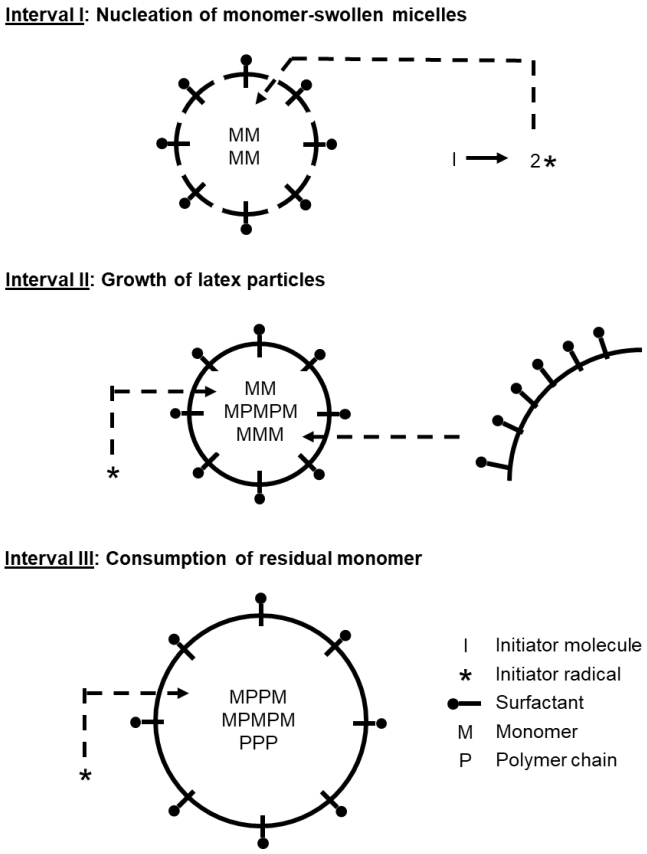

Scheme 1-5. Mechanism of emulsion polymerization. Reproduced with permission from ref[52].

Typical internal phase (dispersed phase) volume percentage is <74% (the maximum packing fraction of monodiperse, undeformable spheres). In special cases when the internal content exceeds 74%, the system turns into a high internal phase emulsion (HIPE). Instead of spheres, the dispersed phase possesses irregular polyhedral or polydisperse distribution of droplet sizes. The continuous phase could be loaded with monomers and crosslinkers. After polymerization and purification, a highly porous material with interconnecting voids is prepared, which is called polyHIPE (**Scheme 1-6**A). This emulsion template method is an important pathway for the synthesis of porous polymers, leading to a wide variety of highly interconnected, highly porous monolithic systems (**Scheme 1-6**B).[53-55]

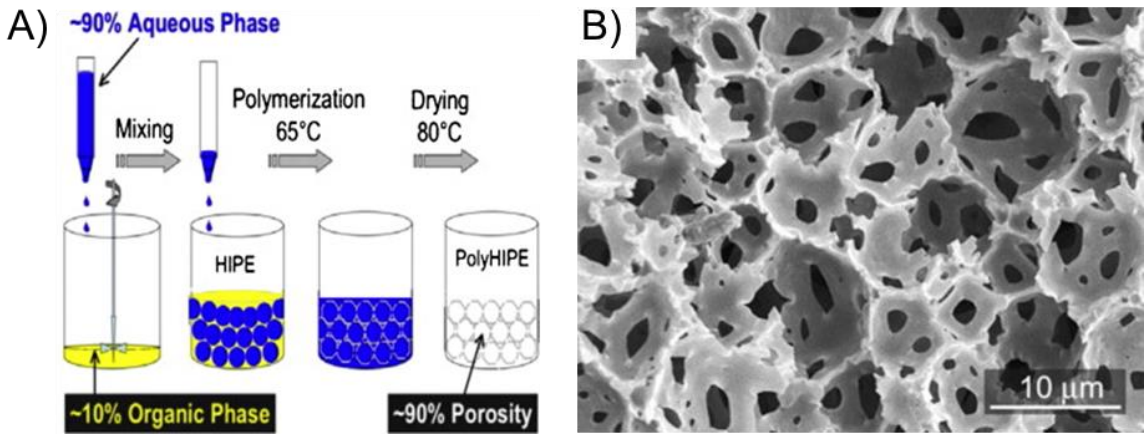

Scheme 1-6. A) Schematic illustration of HIPE formation and polyHIPE synthesis within a water-in-oil (W/O) HIPE; B) typical SEM of porous polyHIPE structure. Reproduced with permission from ref[54].

Dispersion and precipitation polymerization both start from a homogeneous solution, and quickly turn to a heterogeneous one since the polymer is not soluble in the reaction medium. In precipitation polymerization, the polymer is not soluble in its own monomer (for example, polyacrylonitrile is insoluble in acrylonitrile). Thus, the polymer precipitates at a critical chain length. Since the polymer precipitates are not swelled by the monomer, polymerization stops. In dispersion polymerization, however, the polymer is soluble in the monomer, and polymerization continues after nucleation. These two mechanisms are often seen in nonaqueous heterogeneous systems, providing polymer particles of 1-15 µm.[56]

1.3.2. Atom Transfer Radical Polymerization in Miniemulsion

As discussed in Section 1.3.1. , in miniemulsion polymerization, there is no migration of monomers during the polymerization. Miniemulsion polymerization behaves

like many “mini-bulk” systems, and a proper selection of ligands and surfactants results in a successful polymerization.

The most important component for a successful miniemulsion ATRP is the catalyst, which should be very hydrophobic and highly active. The commonly used catalysts in miniemulsion ATRP are summarized in **Scheme 1-7**.

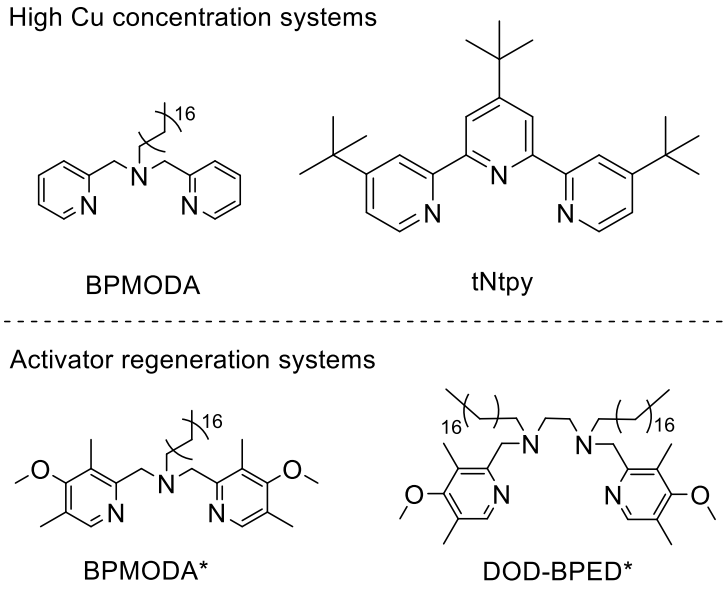

Scheme 1-7. Typical ligands used in miniemulsion ATRP systems.

Since its first report in 2000, application of high Cu content ATRP techniques were explored in miniemulsion. Normal ATRP, using equimolar concentration of $Cu^{I}Br$ and an initiator, was not suitable for miniemulsion ATRP due to the inevitable Cu^{I} oxidation in the probe ultrasonication process. [57] Then reverse and SR&NI ATRP were conducted to trigger the ATRP equilibrium from the $Cu^{II}Br_2$ side, leading to well-controlled polymerization.[58-59] In 2005, AGET ATRP employing AsAc as reducing agent to $Cu^{II}Br$ was developed.[19] AGET was advantageous over reverse and SR&NI ATRP, since the

polymer chains were exclusively formed from ATRP initiators, and excess AsAc provided oxygen tolerance.[60] Bis(2-pyridylmethyl)-octadecylamine (BPMODA) and 4,4',4''-tris(5-nonyl)-2,2':6',2''-terpyridine (tNtpy) were efficient ligands, since they formed hydrophobic and active ATRP catalysts with $CuBr_2$ (**Scheme 1-7**).[61-62]

Various activator regeneration ATRP methods were developed since 2006, and then rapidly employed in miniemulsion polymerization. ARGET ATRP was the most frequently used technique in miniemulsion polymerization due to its simplicity, high chain-end fidelity and oxygen tolerance. The low catalyst loading required ligands of high activity and high hydrophobicity. BPMODA and tNtpy were not suitable for ARGET ATRP, since the activity was not high enough. Typically used highly active ligands, Me_6TREN and TPMA, were hydrophilic. Thus, two highly active and highly hydrophobic ligands, bis[2-(4-methoxy-3,5-dimethyl)pyridylmethyl]octadecylamine (BPMODA*) and N',N''-dioctadecyl-N',N''-bis[2-(4-methoxy-3,5-dimethyl)pyridylmethyl]ethane-1,2-diamine (DOD-BPED*) were designed and synthesized (**Scheme 1-7**). The electron-donating groups increased the activity, and aliphatic chains improved the hydrophobicity,[63-64] allowing successful miniemulsion ATRP of *n*-butyl acrylate (BA) under as low as 50 ppm Cu catalyst.

1.3.3. Atom Transfer Radical Polymerization in Emulsion

The nucleation mechanism in emulsion ATRP is more complicated than miniemulsion ATRP. Initiation and oligomerization proceeds in the aqueous phase, and the hydrophobic oligoradicals enter micelles for further propagation (**Scheme 1-5**). Initiation loci and catalyst transport to micelles are big challenges for emulsion ATRP. [56]

Before 2006, various initiation methods in high Cu content ATRP were carried out. In normal ATRP, hydrophobic initiators resided predominantly in monomer droplets, leading to poor latex stability and thus coagulation.[65] The coagulation was eliminated in reverse ATRP using water-soluble initiators, V-50 and VA-044, leading to monomodal size distribution.[66] However, the transport of copper catalysts remained a problem.

The hydrophobic catalysts inefficient transport from droplets to aqueous media. An efficient catalyst should control ATRP in both aqueous oligomerization and the micelle propagation. However, the transport of Cu catalyst from the monomer droplets through the aqueous phase to the micelles was difficult.

A two-step approach was developed to locate the Cu catalyst in micelles. The first step was microemulsion ATRP, where initiators, Cu catalysts and a small proportion of monomers were encapsulated in microemulsion droplets. Then, the remaining monomer was fed to the microemulsion, diffused to the micelles like a normal emulsion polymerization process (**Scheme 1-8**).[67] This process avoided the catalyst transportation problem, leading to well-controlled polymerization and narrow particle size distribution. In addition, the feeding of a different monomer in the second step allowed *in situ* preparation of block copolymers.[67]

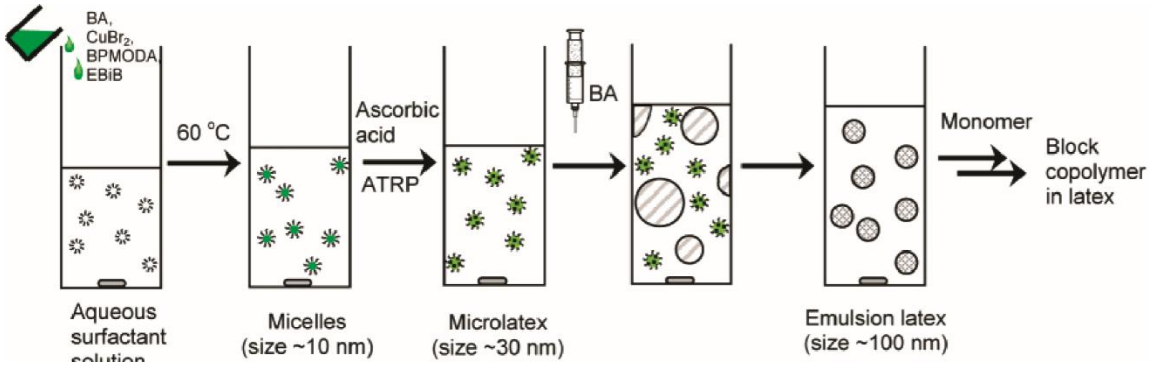

Scheme 1-8. *Ab initio* emulsion using a "two-step" microemulsion to emulsion procedure.

Tethering the Cu catalyst to the surfactant could also efficiently catalyze a true emulsion ATRP. A multidentate ligand was covalently attached to the hydrophobic part of the surfactant, forming a surfactant-ligand (SL) (**Scheme 1-9**). The micelles had much higher total surface area than monomer droplets, thus the Cu-surfactant mostly resided predominantly in the micelles. The complexation of Cu^{II} with SL diminished the leaking of traditional Cu complex to the aqueous media. The combination of free catalyst and surfactant-catalyst resulted in well-controlled polymerization, and the polymer dispersity reached 1.2.[68-69]

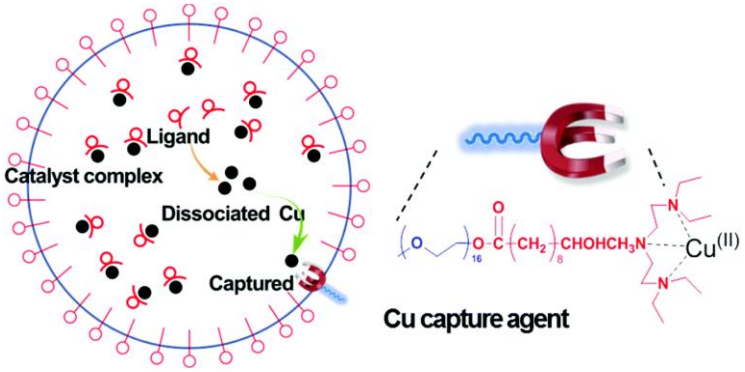

Scheme 1-9. Structure of the surfactant-ligand used as a Cu capture agent in emulsion ATRP.

Similarly, a surface-active initiator could regulate the polymerization initiation in the surface of micelles. This could diminish the monomer reservoir nucleation and improve the control. Both nonionic PEO and anionic moieties could be used for the hydrophilic end of the surface-active initiator (**Scheme 1-10**A).[70-71] Alternatively, the surfactant could also be modified with double bonds and covalently bond to the polymer particles, resulting in increased stability (**Scheme 1-10**B).[72]

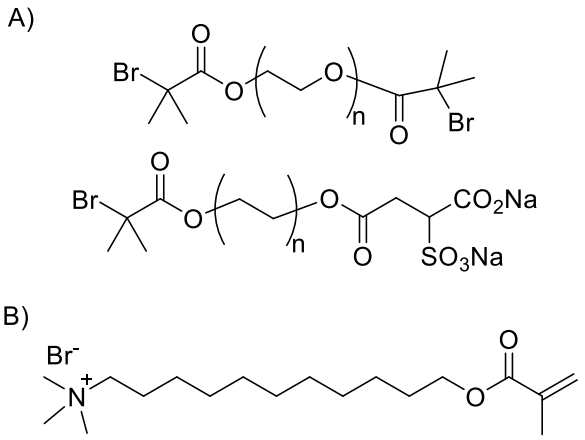

Scheme 1-10. Structure of representative bifunctional surfactants. A) surface-active initiators; B) surface-active monomer.

Besides, some organic moieties were incorporated to accelerate the transportation of catalysts. Emulsion ATRP of BMA was improved by addition of acetone and an organic salt, tetrabutylammonium bromide (TBABr). Acetone aided the reactant transport, and TBABr acted as phase transfer agents for halogen ion (**Scheme 1-11**).[73]

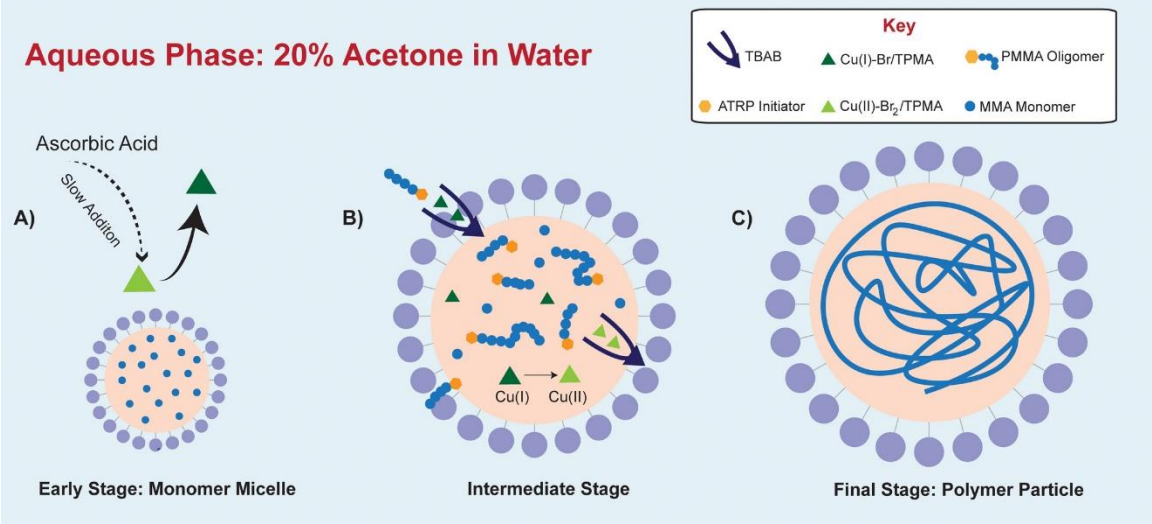

Scheme 1-11. Proposed mechanism for organic solvent and phase-transfer catalyst aided emulsion ATRP. Reproduced with permission from ref[73].

1.3.4. Architectures and Possible Applications by ATRP in Dispersed Media

The exploration of catalysts, surfactants and procedures allows well-controlled ATRP of polymers in various types of dispersed media. The inevitable biradical termination is greatly suppressed in miniemulsion compared to in solution or in bulk due to the physical segregation of radicals. This reduced termination makes miniemulsion polymerization extremely suitable for RDRP, especially for some special compositions and architectures.

ATRP in dispersed media for synthesis of homopolymers have been discussed in the previous sections. Diverse polymer compositions could also be prepared. Block copolymers could be prepared by chain extension from polymer macroinitiators.[61] Using multifunctional initiators, polymer stars and brushes were synthesized with high conversion and minimal termination reactions.[74] Gradient copolymers were prepared thanks to the difference of monomers in activity[62] or feeding rate.[75]

The reduced termination rate benefits significantly for synthesis of polymers with complex architectures. For example, a small proportion of intermolecular termination results in macroscopic gelation in a polymer bottlebrush synthesis in homogeneous conditions. However, the segregation of polymerization loci into isolated miniemulsion droplets allowed synthesis of polymer bottlebrushes in high conversion without macroscopic gelation.[74, 76] More interestingly, the "mini-bulk" character in microemulsion turns each oil droplet into a "nanoreactor". Miniemulsion ATRP in the presence of inimers produced hyperbranched polymers with uniform sizes, since theoretically each droplet contains only one hyperbranched polymer (**Scheme 1-12**). The hyperbranched polymer latex could be either be further swollen in hydrophobic monomers, and subsequent polymerization led to hyper-star polymers.[77]

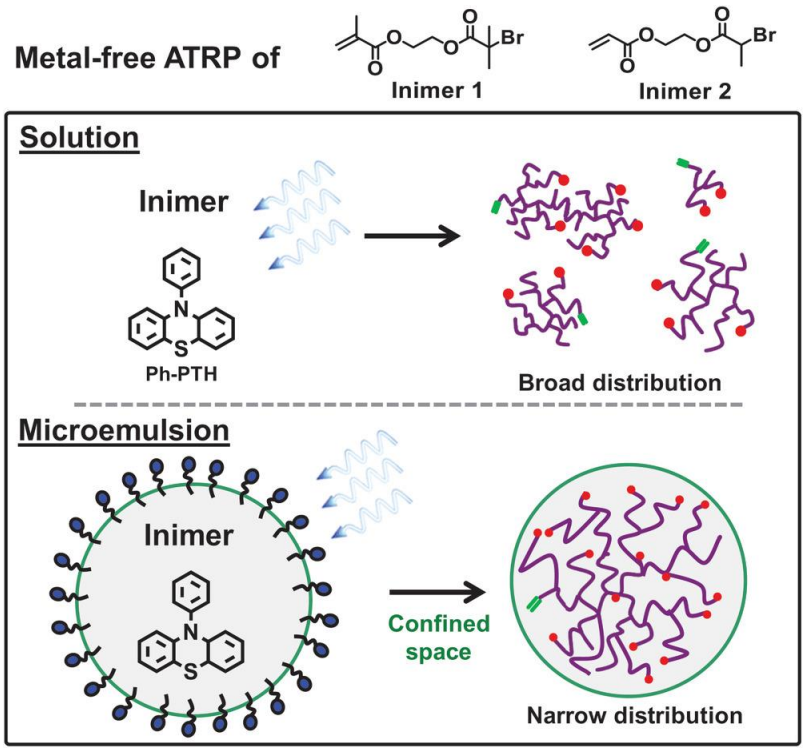

Scheme 1-12. Synthesis of hyperbranched polymers by solution and microemulsion ATRP. Reproduced with permission from ref[77].

Polymerization-induced self-assembly (PISA) is an important pathway for the synthesis of phase-separated nanoobjects since it is achieved simultaneously during polymerization at high solids content.[78] It originates from a homogeneous polymerization from a macroinitiator and forms a water-insoluble polymer. During propagation of the insoluble block increases, a transition from solution to micelles, worms, rods and vesicles could be observed.[78] ICAR ATRP was successful in PISA systems,[79] and could be used to synthesize core-crosslinked materials due to the ring opening of the pendant epoxy groups in the core (**Scheme 1-13**).[80]

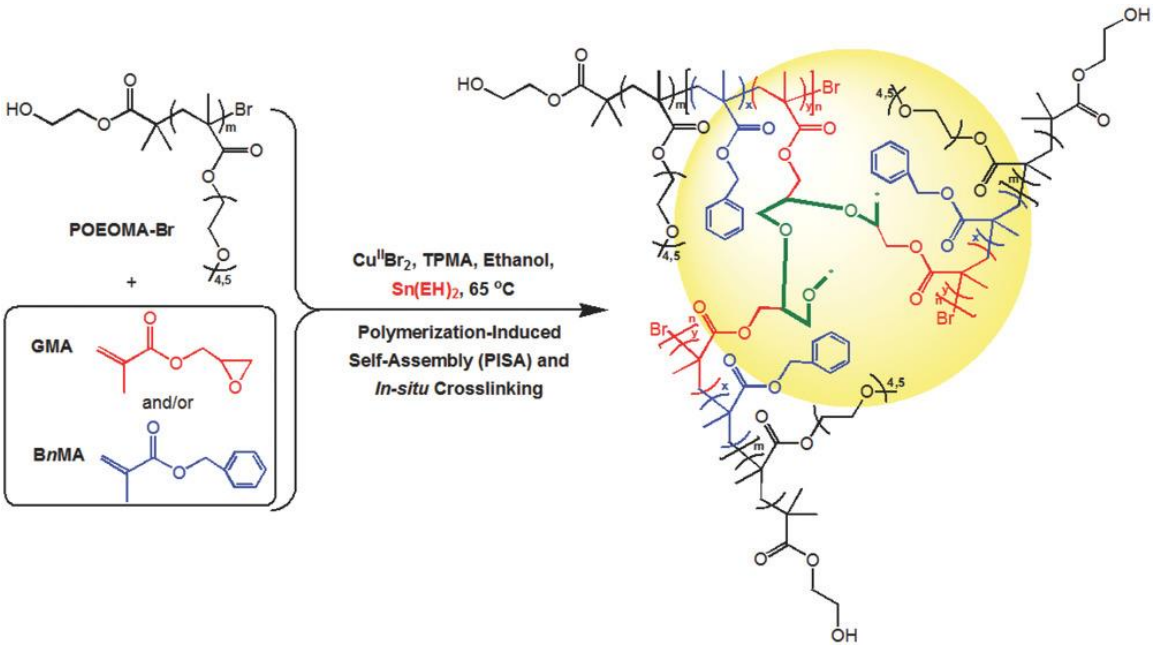

Scheme 1-13. One-pot synthesis of nanoparticles via *in situ* crosslinking during PISA. Reproduced with permission from ref[80].

Incorporation of multi-vinyl monomers as crosslinkers in miniemulsion ATRP is a robust way to synthesize crosslinked nanoobjects. A disulfide-based crosslinker could be utilized to prepare degradable networks.[81] Microemulsion ATRP of MMA in the presence

of a crosslinker led to polymer network "seeds", which could swell in BA and transform into an emulsion polymerization system, forming hairy nanoparticles with PMMA core and PBA "hair" (**Scheme 1-14**).[81-82] Crosslinking was also conducted by coupling ATRP with ring opening metathesis polymerization (ROMP),[83] click reactions,[84-85] or UV curing[86].

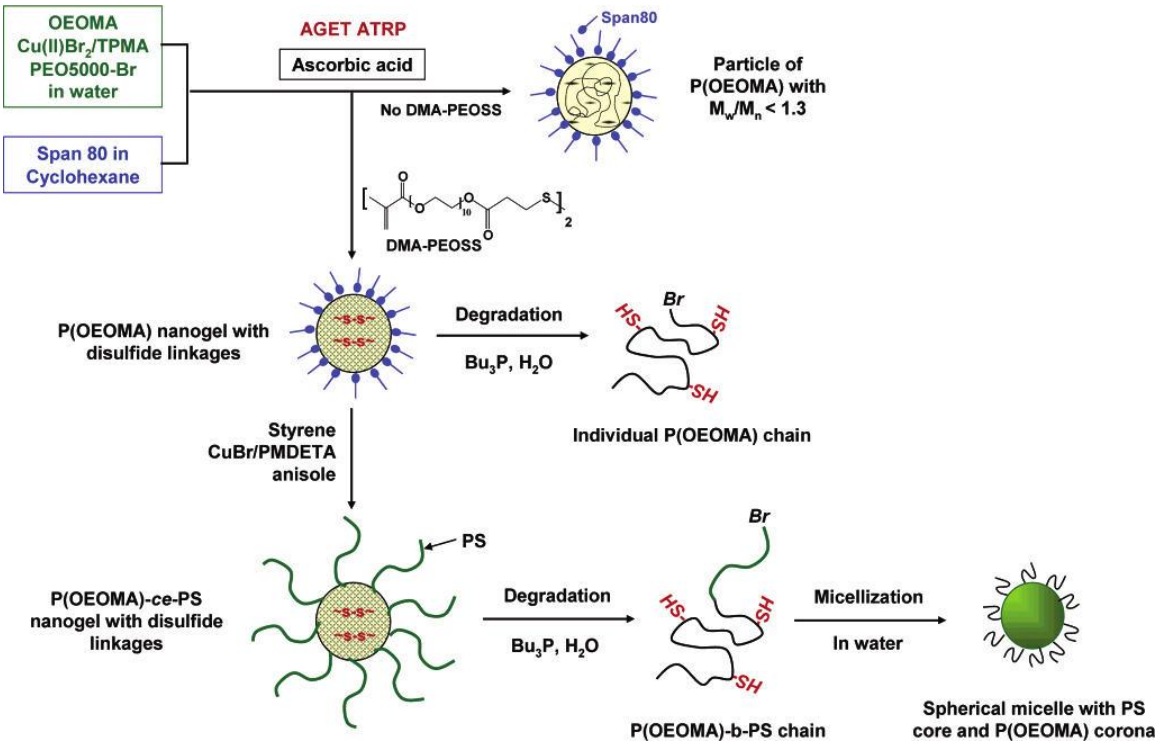

Scheme 1-14. Synthesis of degradable hairy nanoparticles in miniemulsion ATRP. Reproduced with permission from ref[81].

Hollow structures could be prepared by initiation of ATRP at the surface of the droplets. Such initiation could be achieved by surface-active initiators, usually an amphiphilic block copolymer with ATRP initiation site on the hydrophobic end. The surface-active initiators could initiate miniemulsion polymerization from the surface of the

droplets, forming nanocapsules which could load hydrophobic molecules or be further modified with functionalities on the surface (**Scheme 1-15**).[87-88]

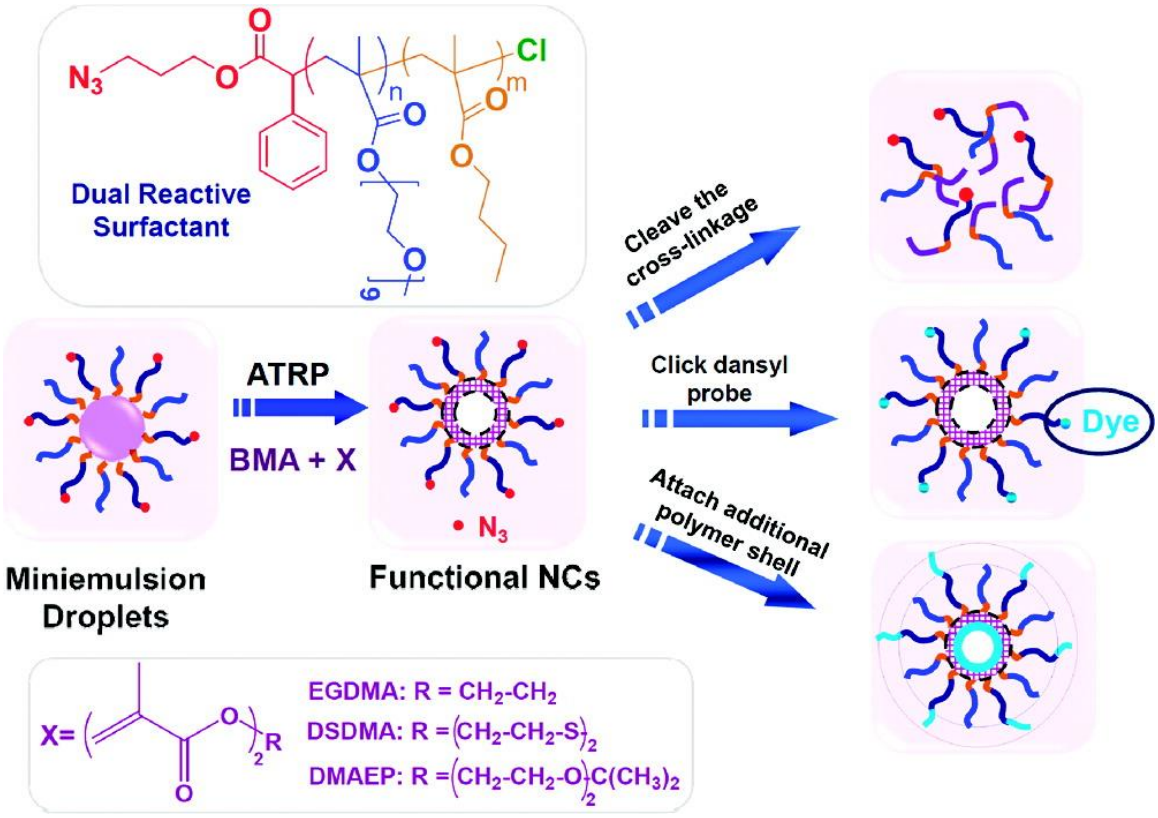

Scheme 1-15. Synthesis of polymer nanocapsules by miniemulsion ATRP using a mixture of dual and monofunctional reactive surfactants. Reproduced with permission from ref[88].

1.4. Reversible Addition-Fragmentation Chain-Transfer Polymerization

1.4.1. Mechanism of Reversible Addition-Fragmentation Chain-Transfer Polymerization

Besides ATRP, another important RDRP procedure is RAFT polymerization (**Scheme 1-16**),[5-8, 89-90] is based on degenerative transfer mediated by chain transfer agents (CTAs) such as dithioesters, dithiocarbamates, trithiocarbonates, or xanthates.[5] RAFT

polymerization is compatible with many vinyl monomers and solvents, including both homogeneous and heterogeneous conditions.[91]

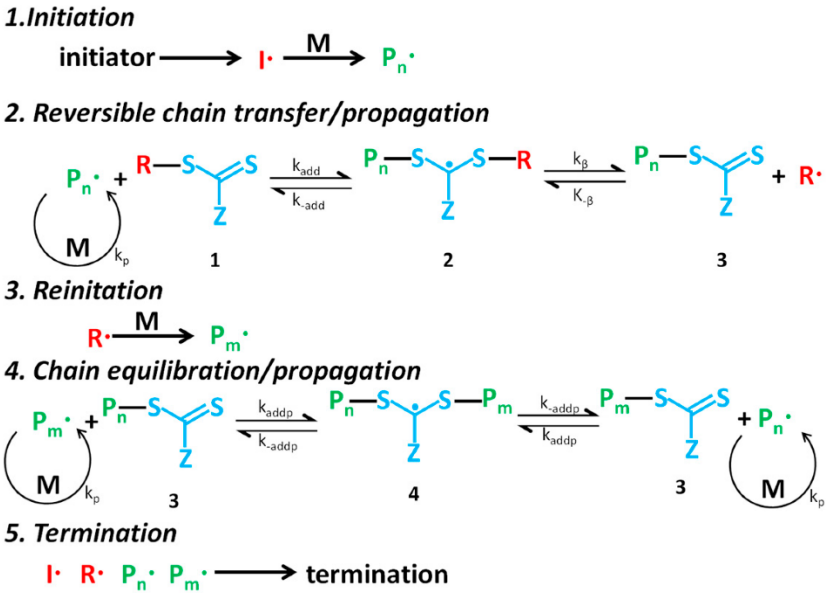

Scheme 1-16. Mechanism of RAFT polymerization initiated by thermal initiators. Reproduced with permission from ref[90].

Scheme 1-16 shows the mechanism of RAFT polymerization. The initiation, propagation and termination are similar to that in conventional radial polymerization. The key processes are step *2* and *4* (degenerative transfer), composed of the addition of polymer radicals (P_n·) to the carbon-sulfur double bonds in the CTA (**1**) or macroCTA (**3**) to form an intermediate radical (**2** or **4**), which could fragment in the carbon-sulfur double bond to release a new radical, which could further propagate, add to the CTA or terminate. This degenerative transfer process allows a quick equilibrium between active and dormant polymer chains, thus ensures the simultaneous growth of all polymer chains. Ideally the number of chains in RAFT polymerization is equal to the number of CTAs, thus the theoretical degree of polymerization (DP_T) determined by

$$DP_T = [M]_0/[CTA]_0 \quad (1\text{-}4)$$

Due to inevitable termination during RAFT polymerization, a continuous supply of radicals is required. The initiation step is commonly the thermal decomposition of traditionally used free radical polymerization initiators (for example, AIBN).

However, there are some intrinsic problems in the thermal initiation process. First, the addition of thermal initiators results in higher number of polymer chains than the number of CTAs. The external generated radicals generated slowly during the polymerization (often conducted a temperature which $t_{1/2}$ = 10 h) lead to a lower *DP* (Equation (1-5)) than the theoretical value (Equation (1-4)), and high dispersity.

$$DP = [M]_0/[[CTA]_0 + 2f[I]_0(1 - e^{-k_d t})] \quad (1\text{-}5)$$

Second, at elevated temperatures, side reactions, including irreversible chain transfer, self-initiation of monomer, may occur.[90] In addition, high temperatures may be not suitable for some functional monomers,[92] or for biological or thermo-responsive systems.[93] With these considerations, many new approaches for radical generation methods have been developed.

1.4.2. Initiation in Reversible Addition-Fragmentation Chain-Transfer Polymerization

Besides thermal initiation, there are a few initiation systems that generate radicals from external sources. Redox initiation systems, such as benzoyl peroxide/dimethyl aniline,

sodium thiosulfate/potassium persulfate, *tert*-butyl hydroperoxide/ascorbic acid, and Cu complex/dithioester generate radicals in room temperature.[94-96]

Enzymes could also catalyze redox reactions and generate radicals efficiently. For example, glucose oxidase (GOx) or pyranose oxidase (P2Ox) catalyzed the oxidation of glucose in the presence of oxygen in air and form H_2O_2, which homolyze into HO· and initiate RAFT polymerization (**Scheme 1-17**A).[97] GOx and P2Ox could both form an enzyme cascade with horse radish peroxide (HRP) in the presence of acetylacetone (AcAc), generating AcAc· which initiated polymerization more efficiently than HO· (**Scheme 1-17B**).[98] These enzyme-catalyzed redox reactions consumed oxygen, thus allowed RAFT polymerization in open-to-air conditions.

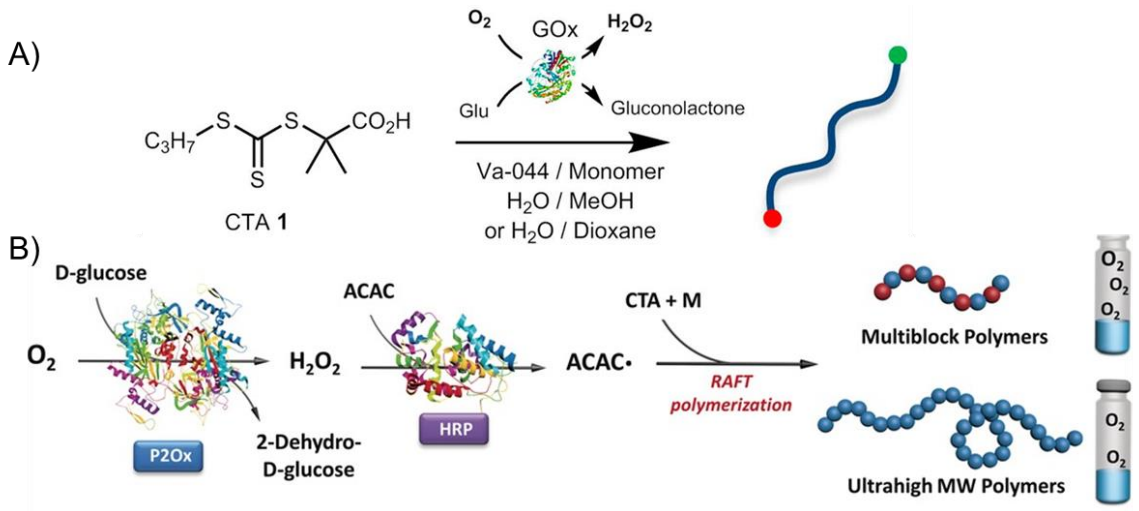

Scheme 1-17. Mechanism of enzyme-initiation in RAFT polymerization. A) GOx deoxygenation redox initiation; B) P2Ox-HRP cascade catalysis initiation in RAFT polymerization. Reprinted with permission from ref[97-98].

Radicals could also be generated by other chemical reactions. For example, acid catalyzed reaction of ketone with peroxide generated radicals and trigger RAFT

polymerization.[96] An air-stable alkylborane-amine complex liberated a reactive trialkylborane that reacts with oxygen and generated a series of oxygen and carbon centered radicals which could initiate polymerization.[99]

The more desired approaches, however, form radicals directly from CTAs. These methods avoid the generation of radicals from external sources, thus their molecular weight could be predetermined by Equation (1-4), and the chain end functionality is greatly improved.[60] Co γ-irradiation cleaves the bonds between benzyl group and sulfur in dibenzyl trithiocarbonate. [100]

Photoiniferter polymerization takes advantage of the photolysis of the C-S bond in CTAs. The high-energy UV light was efficient in the photolysis of a wide range of CTAs, but suffered from the slow degradation of RAFT agents, which caused poor control in high conversion. Thus, visible light was employed to initiate RAFT polymerizations (**Scheme 1-18**). [101] Taking advantage of the variation in the visible-light absorption wavelengths of different types of CTAs, selective activation of CTAs allowed the synthesis of polymer bottlebrushes and polymer gels.[102-103]

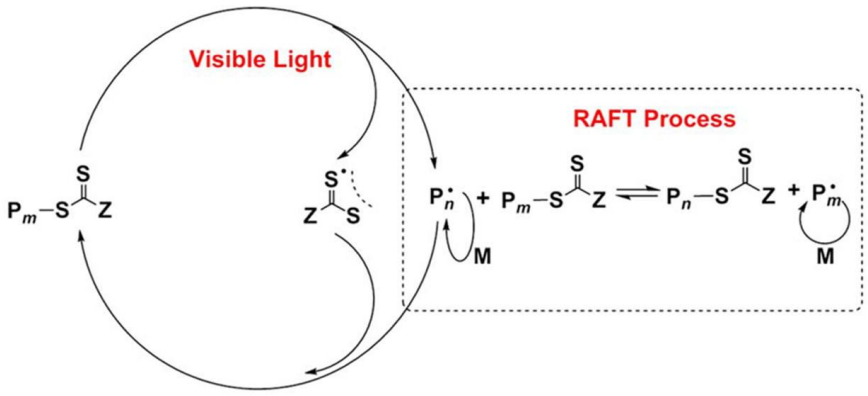

Scheme 1-18. Mechanism of photoiniferter RAFT polymerization under visible light. Reprinted with permission from ref [101].

Since, a more robust process, photoinduced electron/energy transfer RAFT (PET-RAFT) was invented (**Scheme 1-19**).[104] This process involves a photosensitizer catalyze the fragmentation of the CTA. During the past years, the development of different catalysts have been rapid, and the polymerization duration was shortened from a week to a few hours. It was compatible with both metal-based catalysts (Ir or Zn complexes), and some low toxicity organocatalysts (Eosin Y, chlorophyll).[105] The transformation of O_2 into inactive species by PET process provided oxygen tolerance, making it suitable for high-throughput synthesis and screening.[104 106]

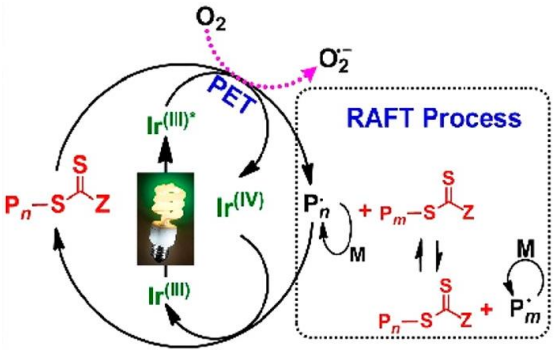

Scheme 1-19. Mechanism of PET-RAFT polymerization using Ir-based catalyst. Reproduced from ref[104].

Another interesting approach is coupling ATRP with RAFT. The radicals were directly generated from ATRP, either by copper-catalyzed activation of RAFT CTAs,[107] or by incorporating an ATRP initiator.[108] Activator regeneration methods could be incorporated in the concurrent ATRP/RAFT approach, and the control over molecular weight is enhanced.

1.5. Electrochemistry in Radical Polymerization

Electrochemical methods have been found to drive unspontaneous chemical reactions in the 1750s. Taking advantage of the electrons released/absorbed by the electrode, many reactions could be conducted, including cathodic reductions, anodic Electrosynthesis and electrocatalysis are important synthetic methods that have experienced a renaissance in the past two decades.[109] They are fundamental tools for chemical transformations, switchable catalysis, [110-111] and external regulation of controlled polymerizations.[112]

Among numerous electrochemichal reactions, many could produce radicals, cations or anions, which could initiate chain-growth and step-growth polymerizations. In addition, electrochemistry could tune the redox states of the catalysts for polymerizations, which in turn controls the on/off and the rate of polymerization.

Approaches for electrochemical initiation free radical polymerization are diverse. Nitrate ion,[113] perchlorate ion[114] and carboxylate[115] have been reported as radical sources in electropolymerizations by anodic current. However, these systems cannot be used in aqueous polymerization due to competitive oxidation of water.[116] Electropolymerizations based reduction of sulfuric acid, potassium persulfate (KPS) and arenediazonium salts were successful.[116-117] In addition to solution polymerization, polymerization reaction could also be conducted to graft polymer brushes from surfaces or to synthesize polymer microgels. [114, 118-119]

Besides generating radicals, electrochemistry could tune the oxidation state of the catalyst, and thus control the polymerization kinetics. A successful example is *e*ATRP, which is presented in 1.2.2. The facile temporal control and control over rate of

polymerization brings *e*ATRP extraordinary advantage among low ppm ATRP techniques.[32] In addition, electrochemistry is an important tool for characterization of catalysts. The redox properties, stability, and activity of ATRP catalysts were studied taking advantage of a series of techniques, including cyclic voltammetry (CV), chronoamperometry (CA), rotating disk electrode (RDE) technique, and in simulation tools, electrochemistry acted as important tools to investigate the thermodynamic and dynamic parameters related to ATRP.[120-121]

The mostly developed *e*ATRP system is a three-electrode cell, consisting of working electrode (WE), counter electrode (CE) and reference electrode (RE) (**Scheme 1-20**). By sweeping the potential in two directions, cyclic voltammetry (CV) profile can be obtained and provides important information about the redox properties. The cathodic and anodic peak potentials, E_{pc} and E_{pa}, respectively, Electrolysis can be carried under both potentiostatic conditions and galvanostatic conditions.

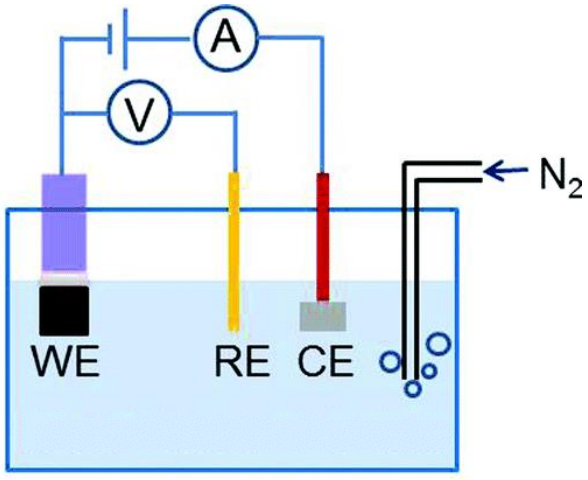

Scheme 1-20. Illustration of experimental setup in electrochemistry.[122]

1.6. Thesis Goal

As discussed above, conducting ATRP in dispersed media provides less termination and better control than its homogeneous polymerization counterpart. Specific hydrophobic catalysts were successful for miniemulsion polymerization, but resulted in high copper residual in the final polymer which was hard remove. The first goal of this thesis work was to study the kinetics and molecular weight control in miniemulsion and emulsion ATRP. Starting from using hydrophilic-hydrophobic dual catalyst combination in *e*ATRP, a hydrophilic ion-pair catalyst was developed and used in *e*ATRP, ARGET, photoATRP in miniemulsion for the synthesis of hydrophobic polymers. The polymerization kinetics, copper removal, and capability of different activator regeneration ATRP techniques were studied. Ab initio emulsion ATRP was developed by my collaborator, Dr. Francesca Lorandi and I expanded it in photomediated polymerization conditions. Enzyme-deoxygenated aqueous ATRP was explored by our group members, Dr. Alan Enciso and Liye Fu. I collaborated with Liye Fu to employ this system into miniemulsion and emulsion ATRP.

The low Cu residual and good control of MW makes it very beneficial to synthesize functional materials. The second goal was the preparation of block copolymers and hairy nanoparticles in dispersed media. Catalytic halogen exchange was studied in miniemulsion, aiming to extend a macroinitiator with a more active monomer. The conditions were employed and tested in the synthesis of block copolymers. Hairy nanoparticles were also synthesized in one-pot miniemulsion polymerization by addition of crosslinkers and hydrophilic comonomers.

RAFT is of similar importance in the world of RDRP. The drawbacks in traditional thermal initiation triggered researchers to investigate new ways to initiate RAFT polymerization, especially to generate radicals from CTAs. The success of *e*ATRP triggered my interest to employ electrochemistry in the initiation and control of the RAFT process.

The third goal of this thesis work was to employ electrochemistry to control a RAFT polymerization. The direct electrochemical activation of CTAs was not successful due to the low reduction potential and irreversible reduction feature. Thus, indirect activation pathways were studied, including incorporating external redox initiators, coupling with ATRP, and catalytic activation of CTAs.

1.7. References

(1) Braunecker, W. A.; Matyjaszewski, K., Controlled/Living Radical Polymerization: Features, Developments, and Perspectives. *Prog Polym Sci* **2007,** *32* (1), 93-146.
(2) Matyjaszewski, K.; Spanswick, J., Controlled/Living Radical Polymerization. *Mater Today* **2005,** *8* (3), 26-33.
(3) Matyjaszewski, K.; Xia, J. H., Atom Transfer Radical Polymerization. *Chem Rev* **2001,** *101* (9), 2921-2990.
(4) Matyjaszewski, K., Advanced Materials by Atom Transfer Radical Polymerization. *Advanced Materials* **2018,** *30*, 1706441.
(5) Moad, G.; Rizzardo, E.; Thang, S. H., Living Radical Polymerization by the RAFT Process. *Aust J Chem* **2005,** *58* (6), 379-410.
(6) Moad, G.; Rizzardo, E.; Thang, S. H., Living Radical Polymerization by the RAFT Process - A first update. *Aust J Chem* **2006,** *59* (10), 669-692.
(7) Moad, G.; Rizzardo, E.; Thang, S. H., Living Radical Polymerization by the RAFT Process - A second update. *Aust J Chem* **2009,** *62* (11), 1402-1472.
(8) Moad, G.; Rizzardo, E.; Thang, S. H., Living Radical Polymerization by the RAFT Process - A third update. *Aust J Chem* **2012,** *65* (8), 985-1076.
(9) Nicolas, J.; Guillaneuf, Y.; Lefay, C.; Bertin, D.; Gigmes, D.; Charleux, B., Nitroxide-Mediated Polymerization. *Prog Polym Sci* **2013,** *38* (1), 63-235.
(10) Ni, Y. Y.; Zhang, L. F.; Cheng, Z. P.; Zhu, X. L., 1 Iodine-mediated reversible-deactivation radical polymerization: a powerful strategy for polymer synthesis. *Polym. Chem.* **2019,** *10* (20), 2504-2515.

(11) Goto, A.; Kwak, Y.; Fukuda, T.; Yamago, S.; Iida, K.; Nakajima, M.; Yoshida, J., Mechanism-based Invention of High-Speed Living Radical Polymerization Using Organotellurium Compounds and Azo-Initiators. *J Am Chem Soc* **2003,** *125* (29), 8720-8721.
(12) Matyjaszewski, K.; Tsarevsky, N. V., Macromolecular Engineering by Atom Transfer Radical Polymerization. *J Am Chem Soc* **2014,** *136* (18), 6513-6533.
(13) De Paoli, P.; Isse, A. A.; Bortolamei, N.; Gennaro, A., New Insights into the Mechanism of Activation of Atom Transfer Radical Polymerization by Cu(I) Complexes. *Chem Commun* **2011,** *47* (12), 3580-3582.
(14) Wang, J. S.; Matyjaszewski, K., Controlled Living Radical Polymerization - Halogen Atom-Transfer Radical Polymerization Promoted by a Cu(I)/Cu(II) Redox Process. *Macromolecules* **1995,** *28* (23), 7901-7910.
(15) Wang, J. S.; Matyjaszewski, K., Controlled Living Radical Polymerization - Atom-Transfer Radical Polymerization In the Presence Of Transition-Metal Complexes. *J Am Chem Soc* **1995,** *117* (20), 5614-5615.
(16) Wang, J. S.; Matyjaszewski, K., Living Controlled Radical Polymerization - Transition-Metal-Catalyzed Atom-Transfer Radical Polymerization In the Presence Of a Conventional Radical Initiator. *Macromolecules* **1995,** *28* (22), 7572-7573.
(17) Gromada, J.; Matyjaszewski, K., Simultaneous Reverse and Normal Initiation in Atom Transfer Radical Polymerization. *Macromolecules* **2001,** *34* (22), 7664-7671.
(18) Jakubowski, W.; Matyjaszewski, K., Activator Generated by Electron Transfer for Atom Transfer Radical Polymerization. *Macromolecules* **2005,** *38* (10), 4139-4146.
(19) Bai, L. J.; Zhang, L. F.; Cheng, Z. P.; Zhu, X. L., Activators Generated by Electron Transfer for Atom Transfer Radical Polymerization: Recent Advances in Catalyst and Polymer Chemistry. *Polym Chem-Uk* **2012,** *3* (10), 2685-2697.
(20) Krys, P.; Matyjaszewski, K., Kinetics of Atom Transfer Radical Polymerization. *Eur Polym J* **2017,** *89*, 482-523.
(21) Jakubowski, W.; Min, K.; Matyjaszewski, K., Activators Regenerated by Electron Transfer for Atom Transfer Radical Polymerization of Styrene. *Macromolecules* **2006,** *39* (1), 39-45.
(22) Simakova, A.; Averick, S. E.; Konkolewicz, D.; Matyjaszewski, K., Aqueous ARGET ATRP. *Macromolecules* **2012,** *45* (16), 6371-6379.
(23) Payne, K. A.; D'hooge, D. R.; van Steenberge, P. H. M.; Reyniers, M. F.; Cunningham, M. F.; Hutchinson, R. A.; Marin, G. B., ARGET ATRP of Butyl Methacrylate: Utilizing Kinetic Modeling To Understand Experimental Trends. *Macromolecules* **2013,** *46* (10), 3828-3840.
(24) Wang, Z. Y.; Liu, T.; Zhao, Y. Q.; Lee, J. J.; Wei, Q. B.; Yan, J. J.; Li, S. P.; Olszewski, M.; Yin, R. G.; Zhai, Y.; Bockstaller, M. R.; Matyjaszewski, K., Synthesis of Gradient Copolymer Grafted Particle Brushes by ATRP. *Macromolecules* **2019,** *52* (24), 9466-9475.
(25) Wang, Z. Y.; Yan, J. J.; Liu, T.; Wei, Q. B.; Li, S. P.; Olszewski, M.; Wu, J. N.; Sobieski, J. L.; Fantin, M.; Bockstaller, M. R.; Matyjaszewski, K., Control of Dispersity and Grafting Density of Particle Brushes by Variation of ATRP Catalyst Concentration. *Acs Macro Lett* **2019,** *8* (7), 859-864.
(26) Matyjaszewski, K.; Jakubowski, W.; Min, K.; Tang, W.; Huang, J. Y.; Braunecker, W. A.; Tsarevsky, N. V., Diminishing Catalyst Concentration in Atom Transfer Radical Polymerization with Reducing Agents. *P Natl Acad Sci USA* **2006,** *103* (42), 15309-15314.

(27) Matyjaszewski, K.; Tsarevsky, N. V.; Braunecker, W. A.; Dong, H.; Huang, J.; Jakubowski, W.; Kwak, Y.; Nicolay, R.; Tang, W.; Yoon, J. A., Role of Cu0 in Controlled/"Living" Radical Polymerization. *Macromolecules* **2007,** *40* (22), 7795-7806.
(28) Zhang, Y.; Wang, Y.; Matyjaszewski, K., ATRP of Methyl Acrylate with Metallic Zinc, Magnesium, and Iron as Reducing Agents and Supplemental Activators. *Macromolecules* **2011,** *44* (4), 683-685.
(29) Konkolewicz, D.; Wang, Y.; Zhong, M. J.; Krys, P.; Isse, A. A.; Gennaro, A.; Matyjaszewski, K., Reversible-Deactivation Radical Polymerization in the Presence of Metallic Copper. A Critical Assessment of the SARA ATRP and SET-LRP Mechanisms. *Macromolecules* **2013,** *46* (22), 8749-8772.
(30) Konkolewicz, D.; Wang, Y.; Krys, P.; Zhong, M. J.; Isse, A. A.; Gennaro, A.; Matyjaszewski, K., SARA ATRP or SET-LRP. End of Controversy? *Polym Chem-Uk* **2014,** *5* (15), 4396-4417.
(31) Bortolamei, N.; Isse, A. A.; Magenau, A. J. D.; Gennaro, A.; Matyjaszewski, K., Controlled Aqueous Atom Transfer Radical Polymerization with Electrochemical Generation of the Active Catalyst. *Angew Chem Int Ed* **2011,** *50* (48), 11391-11394.
(32) Magenau, A. J. D.; Strandwitz, N. C.; Gennaro, A.; Matyjaszewski, K., Electrochemically Mediated Atom Transfer Radical Polymerization. *Science* **2011,** *332* (6025), 81-84.
(33) Chmielarz, P.; Fantin, M.; Park, S.; Isse, A. A.; Gennaro, A.; Magenau, A. J. D.; Sobkowiak, A.; Matyjaszewski, K., Electrochemically Mediated Atom Transfer Radical Polymerization (eATRP). *Prog Polym Sci* **2017,** *69*, 47-78.
(34) Konkolewicz, D.; Schroder, K.; Buback, J.; Bernhard, S.; Matyjaszewski, K., Visible Light and Sunlight Photoinduced ATRP with ppm of Cu Catalyst. *Acs Macro Lett* **2012,** *1* (10), 1219-1223.
(35) Pan, X. C.; Tasdelen, M. A.; Laun, J.; Junkers, T.; Yagci, Y.; Matyjaszewski, K., Photomediated Controlled Radical Polymerization. *Prog Polym Sci* **2016,** *62*, 73-125.
(36) Chantasirichot, S.; Inoue, Y.; Ishihara, K., Photoinduced atom transfer radical polymerization in a polar solvent to synthesize a water-soluble poly(2-methacryloyloxyethyl phosphorylcholine) and its block-type copolymers. *Polymer* **2015,** *61*, 55-60.
(37) Treat, N. J.; Sprafke, H.; Kramer, J. W.; Clark, P. G.; Barton, B. E.; de Alaniz, J. R.; Fors, B. P.; Hawker, C. J., Metal-Free Atom Transfer Radical Polymerization. *J Am Chem Soc* **2014,** *136* (45), 16096-16101.
(38) Mohapatra, H.; Kleiman, M.; Esser-Kahn, A. P., Mechanically Controlled Radical Polymerization Initiated by Ultrasound. *Nat Chem* **2017,** *9* (2), 135-139.
(39) Wang, Z. H.; Pan, X. C.; Yan, J. J.; Dadashi-Silab, S.; Xie, G. J.; Zhang, J. N.; Wang, Z. H.; Xia, H. S.; Matyjaszewski, K., Temporal Control in Mechanically Controlled Atom Transfer Radical Polymerization Using Low ppm of Cu Catalyst. *Acs Macro Lett* **2017,** *6* (5), 546-549.
(40) Wang, Z. H.; Pan, X. C.; Li, L. C.; Fantin, M.; Yan, J. J.; Wang, Z. Y.; Wang, Z. H.; Xia, H. S.; Matyjaszewski, K., Enhancing Mechanically Induced ATRP by Promoting Interfacial Electron Transfer from Piezoelectric Nanoparticles to Cu Catalysts. *Macromolecules* **2017,** *50* (20), 7940-7948.

(41) Wang, Z. H.; Wang, Z. H.; Pan, X. C.; Fu, L. Y.; Lathwal, S.; Olszewski, M.; Yan, J. J.; Enciso, A. E.; Wang, Z. Y.; Xia, H. S.; Matyjaszewski, K., Ultrasonication-Induced Aqueous Atom Transfer Radical Polymerization. *Acs Macro Lett* **2018,** *7* (3), 275-280.
(42) Zetterlund, P. B.; Kagawa, Y.; Okubo, M., Controlled/Living Radical Polymerization in Dispersed Systems. *Chem Rev* **2008,** *108* (9), 3747-3794.
(43) Jennings, J.; He, G.; Howdle, S. M.; Zetterlund, P. B., Block Copolymer Synthesis by Controlled/Living Radical Polymerisation in Heterogeneous Systems. *Chem Soc Rev* **2016,** *45* (18), 5055-5084.
(44) Cunningham, M. F., Controlled/Living Radical Polymerization in Aqueous Dispersed Systems. *Prog Polym Sci* **2008,** *33* (4), 365-398.
(45) Wu, M.; Ramirez, L. M. F.; Lozano, A. R.; Quemener, D.; Babin, J.; Durand, A.; Marie, E.; Six, J. L.; Nouvel, C., First Multi-reactive Dextran-Based Inisurf for Atom Transfer Radical Polymerization in Miniemulsion. *Carbohyd Polym* **2015,** *130*, 141-148.
(46) Saade, J.; Bordes, C.; Raffin, G.; Hangouet, M.; Marote, P.; Faure, K., Response Surface Optimization of Miniemulsion: Application to UV Synthesis of Hexyl Acrylate Nanoparticles. *Colloid Polym Sci* **2016,** *294* (1), 27-36.
(47) Wu, L.; Glebe, U.; Boker, A., Synthesis of Hybrid Silica Nanoparticles Densely Grafted with Thermo and pH Dual-Responsive Brushes via Surface-Initiated ATRP. *Macromolecules* **2016,** *49* (24), 9586-9596.
(48) Khan, M.; Guimaraes, T. R.; Zhou, D. W.; Moad, G.; Perrier, S.; Zetterlund, P. B., Exploitation of Compartmentalization in RAFT Miniemulsion Polymerization to Increase the Degree of Livingness. *J Polym Sci Pol Chem* **2019,** *57* (18), 1938-1946.
(49) Arshady, R., Suspension, Emulsion, And Dispersion Polymerization - a Methodological Survey. *Colloid Polym Sci* **1992,** *270* (8), 717-732.
(50) Asua, J. M., Miniemulsion Polymerization. *Prog Polym Sci* **2002,** *27* (7), 1283-1346.
(51) Lohani, A.; Singh, G.; Bhattacharya, S.; Verma, A., Interpenetrating Polymer Networks as Innovative Drug Delivery Systems. *Journal of Drug Delivery* **2014,** *2014*, 583612.
(52) Chern, C. S., Emulsion Polymerization Mechanisms and Kinetics. *Prog Polym Sci* **2006,** *31* (5), 443-486.
(53) Cameron, N. R., High Internal Phase Emulsion Templating as a Route to Well-Defined Porous Polymers. *Polymer* **2005,** *46* (5), 1439-1449.
(54) Silverstein, M. S., PolyHIPEs: Recent Advances in Emulsion-Templated Porous Polymers. *Prog Polym Sci* **2014,** *39* (1), 199-234.
(55) Zhang, T.; Sanguramath, R. A.; Israel, S.; Silverstein, M. S., Emulsion Templating: Porous Polymers and Beyond. *Macromolecules* **2019,** *52* (15), 5445-5479.
(56) Min, K.; Matyjaszewski, K., Atom Transfer Radical Polymerization in Aqueous Dispersed Media. *Cent Eur J Chem* **2009,** *7* (4), 657-674.
(57) Matyjaszewski, K.; Qiu, J.; Tsarevsky, N. V.; Charleux, B., Atom Transfer Radical Polymerization of n-Butyl Methacrylate in an Aqueous Dispersed system: A Miniemulsion Approach. *J Polym Sci Pol Chem* **2000,** *38*, 4724-4734.
(58) Simms, R. W.; Cunningham, M. F., Reverse Atom Transfer Radical Polymerization of butyl Methacrylate in a Miniemulsion Stabilized with a Cationic Surfactant. *J Polym Sci Pol Chem* **2006,** *44* (5), 1628-1634.

(59) Simms, R. W.; Cunningham, M. F., High Molecular Weight Poly(butyl Methacrylate) by Reverse Atom Transfer Radical Polymerization in Miniemulsion Initiated by a Redox System. *Macromolecules* **2007,** *40* (4), 860-866.
(60) Min, K.; Jakubowski, W.; Matyjaszewski, K., AGET ATRP in the presence of air in miniemulsion and in bulk. *Macromol. Rapid Commun.* **2006,** *27* (8), 594-598.
(61) Li, M.; Jahed, N. M.; Min, K.; Matyjaszewski, K., Preparation of Linear and Star-Shaped block Copolymers by ATRP Using Simultaneous Reverse and Normal Initiation Process in Bulk and Miniemulsion. *Macromolecules* **2004,** *37* (7), 2434-2441.
(62) Min, K.; Li, M.; Matyjaszewski, K., Preparation of Gradient Copolymers via ATRP using a Simultaneous Reverse and Normal Initiation Process. I. Spontaneous Gradient. *J Polym Sci Pol Chem* **2005,** *43* (16), 3616-3622.
(63) Elsen, A. M.; Burdynska, J.; Park, S.; Matyjaszewski, K., Active Ligand for Low PPM Miniemulsion Atom Transfer Radical Polymerization. *Macromolecules* **2012,** *45* (18), 7356-7363.
(64) Elsen, A. M.; Burdynska, J.; Park, S.; Matyjaszewski, K., Activators Regenerated by Electron Transfer Atom Transfer Radical Polymerization in Miniemulsion with 50 ppm of Copper Catalyst. *Acs Macro Lett* **2013,** *2* (9), 822-825.
(65) Gaynor, S. G.; Qiu, J.; Matyjaszewski, K., Controlled/"Living" Radical Polymerization Applied to Water-Borne Systems. *Macromolecules* **1998,** *31* (17), 5951-5954.
(66) Qiu, J.; Gaynor, S. G.; Matyjaszewski, K., Emulsion Polymerization of n-Butyl Methacrylate by Reverse Atom Transfer Radical Polymerization. *Macromolecules* **1999,** *32* (9), 2872-2875.
(67) Min, K.; Gao, H. F.; Matyjaszewski, K., Development of an Ab Initio Emulsion Atom Transfer Radical Polymerization: From Microemulsion to Emulsion. *J Am Chem Soc* **2006,** *128* (32), 10521-10526.
(68) Wei, Y. P.; Jia, Y. Y.; Wang, W. J.; Li, B. G.; Zhu, S. P., Surfactant-Ligand Design for ab Initio Emulsion Atom Transfer Radical Polymerization. *Macromolecules* **2014,** *47* (22), 7701-7706.
(69) Wei, Y. P.; Liu, P. W.; Wang, W. J.; Li, B. G.; Zhu, S. P., Well-Controlled and Stable Emulsion ATRP of MMA with Low Surfactant Concentration using Surfactant-Ligand Design as the Copper Capture Agent. *Polym Chem-Uk* **2015,** *6* (15), 2837-2843.
(70) Cheng, C. J.; Shu, J. B.; Shen, L.; Peng, H. F.; Qiao, Y. L.; Fu, C. Q., Synthesis of ATRP Initiators with Surface Activities and Their Application in Emulsifier-free Emulsion Polymerization. *Chinese Journal of Synthetic Chemistry* **2010,** *18* (3), 285-289.
(71) Shu, J. B.; Cheng, C. J.; Zheng, Y.; Shen, L.; Qiao, Y. L.; Fu, C. Q., "One Pot" Synthesis of Fluorinated Block Copolymers using a Surface-Active ATRP Initiator under Emulsion Polymerization Conditions. *Polym Bull* **2011,** *67* (7), 1185-1200.
(72) Li, W. W.; Matyjaszewski, K., Cationic Surface-Active Monomers as Reactive Surfactants for AGET Emulsion ATRP of n-Butyl Methacrylate. *Macromolecules* **2011,** *44* (14), 5578-5585.
(73) Cordero, R.; Jawaid, A.; Hsiao, M. S.; Lequeux, Z.; Vaia, R. A.; Ober, C. K., Mini Monomer Encapsulated Emulsion Polymerization of PMMA Using Aqueous ARGET ATRP. *Acs Macro Lett* **2018,** *7* (4), 459-463.

(74) Min, K.; Yu, S.; Lee, H. I.; Mueller, L.; Sheiko, S. S.; Matyjaszewski, K., High Yield Synthesis of Molecular Brushes via ATRP in Miniemulsion. *Macromolecules* **2007,** *40* (18), 6557-6563.
(75) Min, K.; Oh, J. K.; Matyjaszewski, K., Preparation of Gradient Copolymers via ATRP in Miniemulsion. II. Forced Gradient. *J Polym Sci Pol Chem* **2007,** *45* (8), 1413-1423.
(76) Wang, Y.; Lorandi, F.; Fantin, M.; Chmielarz, P.; Isse, A. A.; Gennaro, A.; Matyjaszewski, K., Miniemulsion ARGET ATRP via Interfacial and Ion-Pair Catalysis: From ppm to ppb of Residual Copper. *Macromolecules* **2017,** *50* (21), 8417-8425.
(77) Wang, X. F.; Graff, R. W.; Shi, Y.; Gao, H. F., One-Pot Synthesis of Hyperstar Polymers via Sequential ATRP of Inimers and Functional Monomers in Aqueous Dispersed Media. *Polym Chem-Uk* **2015,** *6* (37), 6739-6745.
(78) Derry, M. J.; Fielding, L. A.; Armes, S. P., Polymerization-Induced Self-Assembly of Block Copolymer Nanoparticles via RAFT Non-Aqueous Dispersion Polymerization. *Prog Polym Sci* **2016,** *52*, 1-18.
(79) Wang, G.; Schmitt, M.; Wang, Z. Y.; Lee, B.; Pan, X. C.; Fu, L. Y.; Yan, J. J.; Li, S. P.; Xie, G. J.; Bockstaller, M. R.; Matyjaszewski, K., Polymerization-Induced Self-Assembly (PISA) Using ICAR ATRP at Low Catalyst Concentration. *Macromolecules* **2016,** *49* (22), 8605-8615.
(80) Wang, J.; Wu, Z. G.; Wang, G. W.; Matyjaszewski, K., In Situ Crosslinking of Nanoparticles in Polymerization-Induced Self-Assembly via ARGET ATRP of Glycidyl Methacrylate. *Macromol Rapid Comm* **2019,** *40* (2).
(81) Oh, J. K.; Tang, C. B.; Gao, H. F.; Tsarevsky, N. V.; Matyjaszewski, K., Inverse Miniemulsion ATRP: A New Method for Synthesis and Functionalization of Well-Defined Water-Soluble/Cross-Linked Polymeric Particles. *J Am Chem Soc* **2006,** *128* (16), 5578-5584.
(82) Min, K.; Gao, H.; Yoon, J. A.; Wu, W.; Kowalewski, T.; Matyjaszewski, K., One-Pot Synthesis of Hairy Nanoparticles by Emulsion ATRP. *Macromolecules* **2009,** *42* (5), 1597-1603.
(83) Airaud, C.; Ibarboure, E.; Gaillard, C.; Heroguez, V., Nanostructured Polymer Composite Nanoparticles Synthesized in a Single Step via Simultaneous ROMP and ATRP under Microemulsion Conditions. *J Polym Sci Pol Chem* **2009,** *47* (16), 4014-4027.
(84) Xu, L. Q.; Yao, F.; Fu, G. D.; Shen, L., Simultaneous "Click Chemistry" and Atom Transfer Radical Emulsion Polymerization and Prepared Well-Defined Cross-Linked Nanoparticles. *Macromolecules* **2009,** *42* (17), 6385-6392.
(85) Yao, F.; Yan, G. C.; Xu, L. Q.; Fu, G. D.; Yin, L. H.; Pu, Y. P.; Kang, E. T., Hairy Fluorescent Nanoparticles from One-Pot Click Chemistry and Atom Transfer Radical Emulsion Polymerization. *Polym Int* **2014,** *63* (2), 237-243.
(86) Cheng, C. J.; Fu, Q. L.; Liu, Z. B.; Shen, L.; Qiao, Y. L.; Fu, C. Q., Emulsifier-Free Synthesis of Crosslinkable ABA Triblock Copolymer Nanoparticles via AGET ATRP. *Macromol Res* **2011,** *19* (10), 1048-1055.
(87) Li, W. W.; Matyjaszewski, K.; Albrecht, K.; Moller, M., Reactive Surfactants for Polymeric Nanocapsules via Interfacially Confined Miniemulsion ATRP. *Macromolecules* **2009,** *42* (21), 8228-8233.
(88) Li, W. W.; Yoon, J. A.; Matyjaszewski, K., Dual-Reactive Surfactant Used for Synthesis of Functional Nanocapsules in Miniemulsion. *J Am Chem Soc* **2010,** *132* (23), 7823-+.

(89) Moad, G.; Chiefari, J.; Chong, Y. K.; Krstina, J.; Mayadunne, R. T. A.; Postma, A.; Rizzardo, E.; Thang, S. H., Living Free Radical Polymerization with Reversible Addition-Fragmentation Chain Transfer (the life of RAFT). *Polym Int* **2000,** *49* (9), 993-1001.
(90) Tian, X. Y.; Ding, J. J.; Zhang, B.; Qiu, F.; Zhuang, X. D.; Chen, Y., Recent Advances in RAFT Polymerization: Novel Initiation Mechanisms and Optoelectronic Applications. *Polymers-Basel* **2018,** *10* (3).
(91) Hill, M. R.; Carmean, R. N.; Sumerlin, B. S., Expanding the Scope of RAFT Polymerization: Recent Advances and New Horizons. *Macromolecules* **2015,** *48* (16), 5459-5469.
(92) Li, Y.; Yang, J.; Benicewicz, B. C., Well-controlled polymerization of 2-azidoethyl methacrylate at near room temperature and click functionalization Journal of Polymer Science Part A: Polymer Chemistry Volume 45, Issue 18. *J. Polym. Sci., Part A: Polym. Chem.* **2007,** *45* (18), 4300-4308.
(93) Convertine, A. J.; Lokitz, B. S.; Vasileva, Y.; Myrick, L. J.; Scales, C. W.; Lowe, A. B.; McCormick, C. L., Direct synthesis of Thermally Responsive DMA/NIPAM Diblock and DMA/NIPAM/DMA Triblock Copolymers via Aqueous, Room Temperature RAFT Polymerization. *Macromolecules* **2006,** *39* (5), 1724-1730.
(94) Martin, L.; Gody, G.; Perrier, S., Preparation of Complex Multiblock Copolymers via Aqueous RAFT Polymerization at Room Temperature. *Polym Chem-Uk* **2015,** *6* (27), 4875-4886.
(95) Nicolay, R.; Kwak, Y.; Matyjaszewski, K., A Green Route to Well-Defined High-Molecular-Weight (Co)polymers Using ARGET ATRP with Alkyl Pseudohalides and Copper Catalysis. *Angew Chem Int Ed* **2010,** *49* (3), 541-544.
(96) Vandenbergh, J.; Schweitzer-Chaput, B.; Klussmann, M.; Junkers, T., Acid-Induced Room Temperature RAFT Polymerization: Synthesis and Mechanistic Insights. *Macromolecules* **2016,** *49* (11), 4124-4135.
(97) Chapman, R.; Gormley, A. J.; Herpoldt, K. L.; Stevens, M. M., Highly Controlled Open Vessel RAFT Polymerizations by Enzyme Degassing. *Macromolecules* **2014,** *47* (24), 8541-8547.
(98) Liu, Z. F.; Lv, Y.; An, Z. S., Enzymatic Cascade Catalysis for the Synthesis of Multiblock and Ultrahigh-Molecular-Weight Polymers with Oxygen Tolerance. *Angew Chem Int Ed* **2017,** *56* (44), 13852-13856.
(99) Lv, C. N.; He, C. Z.; Pan, X. C., Oxygen-Initiated and Regulated Controlled Radical Polymerization under Ambient Conditions. *Angew Chem Int Ed* **2018,** *57* (30), 9430-9433.
(100) Bai, R. K.; You, Y. Z.; Pan, C. Y., Co-60 Gamma-Irradiation-Initiated "Living" Free-Radical Polymerization in the Presence of Dibenzyl Trithiocarbonate. *Macromol Rapid Comm* **2001,** *22* (5), 315-319.
(101) Xu, J. T.; Shanmugam, S.; Corrigan, N. A.; Boyer, C., Catalyst-Free Visible Light-Induced RAFT Photopolymerization. *Acs Sym Ser* **2015,** *1187*, 247-+.
(102) Shanmugam, S.; Cuthbert, J.; Kowalewski, T.; Boyer, C.; Matyjaszewski, K., Catalyst-Free Selective Photoactivation of RAFT Polymerization: A Facile Route for Preparation of Comblike and Bottlebrush Polymers. *Macromolecules* **2018,** *51* (19), 7776-7784.
(103) Shanmugam, S.; Cuthbert, J.; Flum, J.; Fantin, M.; Boyer, C.; Kowalewski, T.; Matyjaszewski, K., Transformation of Gels via Catalyst-Free Selective RAFT Photoactivation. *Polym Chem-Uk* **2019,** *10* (19), 2477-2483.

(104) Xu, J. T.; Jung, K.; Atme, A.; Shanmugam, S.; Boyer, C., A Robust and Versatile Photoinduced Living Polymerization of Conjugated and Unconjugated Monomers and Its Oxygen Tolerance. *J Am Chem Soc* **2014,** *136* (14), 5508-5519.
(105) Wu, C. Y.; Shanmugam, S.; Xu, J. T.; Zhu, J.; Boyer, C., Chlorophyll a Crude Extract: Efficient Photo-Degradable Photocatalyst for PET-RAFT Polymerization. *Chem Commun* **2017,** *53* (93), 12560-12563.
(106) Ng, G.; Yeow, J.; Chapman, R.; Isahak, N.; Wolyetang, E.; Cooper-White, J. J.; Boyer, C., Pushing the Limits of High Throughput PET-RAFT Polymerization. *Macromolecules* **2018,** *51* (19), 7600-7607.
(107) Kwak, Y.; Nicolay, R.; Matyjaszewski, K., Concurrent ATRP/RAFT of Styrene and Methyl Methacrylate with Dithioesters Catalyzed by Copper(I) Complexes. *Macromolecules* **2008,** *41* (18), 6602-6604.
(108) Elsen, A. M.; Nicolay, R.; Matyjaszewski, K., Dual Concurrent ATRP/RAFT of Methyl Acrylate Co-initiated by Alkyl Halides. *Macromolecules* **2011,** *44* (7), 1752-1754.
(109) Yan, M.; Kawamata, Y.; Baran, P. S., Synthetic Organic Electrochemical Methods Since 2000: On the Verge of a Renaissance. *Chem Rev* **2017,** *117* (21), 13230-13319.
(110) Teator, A. J.; Lastovickova, D. N.; Bielawski, C. W., Switchable Polymerization Catalysts. *Chem Rev* **2016,** *116* (4), 1969-1992.
(111) Blanco, V.; Leigh, D. A.; Marcos, V., Artificial Switchable Catalysts. *Chem Soc Rev* **2015,** *44* (15), 5341-5370.
(112) Leibfarth, F. A.; Mattson, K. M.; Fors, B. P.; Collins, H. A.; Hawker, C. J., External Regulation of Controlled Polymerizations. *Angew Chem Int Ed* **2013,** *52* (1), 199-210.
(113) Bhadani, S. N.; Prasad, Y. K., Anodic Gel Polymerization Of Acrylamide. *J Polym Sci Pol Lett* **1977,** *15* (12), 721-728.
(114) Yan, S. T.; Wu, Q. S.; Chang, A. P.; Lu, F.; Xu, H. C.; Wu, W. T., Electrochemical Synthesis of Polymer Microgels. *Polym Chem-Uk* **2015,** *6* (21), 3979-3987.
(115) Smith, W. B.; Gilde, H. G., The Kolbe Electrolysis as a Source Of Free Radicals In Solution. *J Am Chem Soc* **1959,** *81* (20), 5325-5329.
(116) Zhang, X.; Bell, J. P., Studies of Arenediazonium Salts as a New Class of Electropolymerization Initiator. *J Appl Polym Sci* **1999,** *73* (11), 2265-2272.
(117) Lee, C. S.; Bell, J. P., Polymer-Coatings by Electropolymerization Of Some Vinyl Monomers. *J Appl Polym Sci* **1995,** *57* (8), 931-938.
(118) Tessier, L.; Deniau, G.; Charleux, B.; Palacin, S., Surface Electroinitiated Emulsion Polymerization (SEEP): A Mechanistic Approach. *Chem Mater* **2009,** *21* (18), 4261-4274.
(119) Deniau, G.; Azoulay, L.; Bougerolles, L.; Palacin, S., Surface Electroinitiated Emulsion Polymerization: Grafted Organic Coatings From aqueous solutions. *Chem Mater* **2006,** *18* (23), 5421-5428.
(120) Fantin, M.; Lorandi, F.; Gennaro, A.; Isse, A. A.; Matyjaszewski, K., Electron Transfer Reactions in Atom Transfer Radical Polymerization. *Synthesis-Stuttgart* **2017,** *49* (15), 3311-3322.
(121) Lorandi, F.; Fantin, M.; Isse, A. A.; Gennaro, A., Electrochemical Triggering and Control of Atom Transfer Radical Polymerization. *Curr Opin Electroche* **2018,** *8*, 1-7.
(122) Wang, Z. J.; Cao, X. H.; Ping, J. F.; Wang, Y. X.; Lin, T. T.; Huang, X.; Ma, Q. L.; Wang, F. K.; He, C. B.; Zhang, H., Electrochemical Doping of Three-Dimensional Graphene Networks used as Efficient Electrocatalysts for Oxygen Reduction Reaction. *Nanoscale* **2015,** *7* (21), 9394-9398.

Chapter 2 Miniemulsion Activators Regenerated by Electron Transfer Atom Transfer Radical Polymerization via Interfacial and Ion-pair Catalysis: From ppm to ppb of Residual Copper

2.1. Preface

The content of this chapter was published in *Macromolecules.* (Yi Wang, Francesca Lorandi, Marco Fantin, Paweł Chmielarz, Abdirisak A. Isse, Armando Gennaro, Krzysztof Matyjaszewski, "Miniemulsion ARGET ATRP via Interfacial and Ion-Pair Catalysis: From ppm to ppb of Residual Copper", *Macromolecules* **2017**, *50*, 8417-8425.)

The combination of hydrophilic catalyst Cu/TPMA and the anionic surfactant SDS was first demonstrated in *e*ATRP miniemulsion polymerization of acrylates and published in *Macromolecules* (Marco Fantin, Paweł Chmielarz, Yi Wang, Francesca Lorandi, Abdirisak A. Isse, Armando Gennaro, Krzysztof Matyjaszewski, " Harnessing the Interaction between Surfactant and Hydrophilic Catalyst To Control *e*ATRP in Miniemulsion", *Macromolecules* **2017**, *50*, 3726-3732.) I was a new graduate student at that time and my contributions were relatively minor, therefore it is attached at the end of this Thesis as Appendix 1.

The work presented in Chapters II – VI is the continuation of the miniemulsion electrochemically mediated ATRP (*e*ATRP) project. The ion-pair catalyst was employed for various activator regeneration ATRP methods in different dispersed media. Oxygen tolerance in the presence of enzyme was also explored.

In this chapter, ARGET ATRP was conducted due to the significantly easier reaction setup. A systematic kinetic study was conducted in ARGET ATRP in miniemulsion using the ion-pair catalyst, and the synthesis of block, star and brush copolymers was successfully carried out.

I conducted most of the experiments and summarized the results. I want to thank Dr. Francesca Lorandi, Dr. Marco Fantin and Dr. Paweł Chmielarz for their contribution and helpful discussions and revisions of the paper. I acknowledge Dr. Xiaoyu Gao for his kind help in ICP-MS tests and Dr. Guojun Xie for the preparation of $PBiBM_{100}$ macroinitiator and useful discussions.

This project was completed with a financial support from the NSF (CHE-1707490) and the National Institutes of Health (R01DE020843).

2.2. Introduction

Reversible-deactivation radical polymerizations (RDRPs) in heterogeneous media are characterized by good heat transfer, low environmental impact, low viscosity and low toxicity,[1] which are important advantages for commercial applications.[2] Moreover, polymerization in dispersed media, including microemulsion, miniemulsion, emulsion and dispersion, can be used to prepare nanoparticles with various morphologies (*e.g.* core-shell, microcapsules and multilayered particles) for specific applications in biomedical, pharmaceutical, drug delivery or diagnostic areas.[1, 3-6]

RDRPs provide well-defined polymers with low dispersity (*Đ*), limited amount of radical termination, and pre-determined architecture and molecular weight (MW).[7-9] The

most often used RDRP methods are atom transfer radical polymerization (ATRP), reversible addition-fragmentation chain-transfer (RAFT) polymerization, and nitroxide mediated polymerization (NMP), which have been successfully developed in both homogeneous and heterogeneous media.[9-15] Moreover, heterogeneous systems additionally limit radical termination through radical segregation and compartmentalization.[16-18] Despite the benefits offered by dispersed media, the vast majority of RDRPs are still performed in homogeneous systems.

A promising technique for heterogeneous polymerization is ATRP, which is based on radical generation by an active catalyst, generally a copper-amine complex in its lower oxidation state, *i.e.* $Cu^{I}L^{+}$ (**Scheme 2-1**).[19] The $Cu^{I}L^{+}$ complex activates an alkyl halide initiator (R–X) or dormant chain end (P_n–X), forming a propagating radical and a higher oxidation state deactivator complex X–$Cu^{II}L^{+}$. A small fraction of chains is active at one time and initiation can be fast, therefore all chains grow homogeneously and termination reactions are minimized.[20]

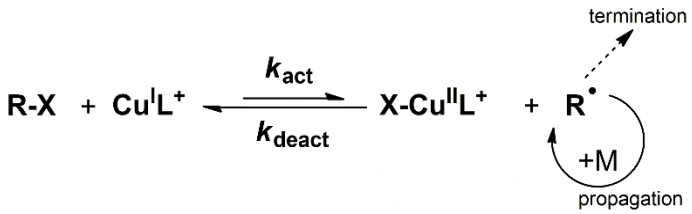

Scheme 2-1. Mechanism of ATRP.

During the last decade, catalyst loading was reduced by the development of "low-ppm" ATRP techniques. These methods comprise activators re-generated by electron transfer (ARGET) ATRP,[21-22] initiators for continuous activator regeneration (ICAR)

ATRP,[23] supplemental activator and reducing agent (SARA) ATRP,[24-28] electrochemically mediated ATRP (*e*ATRP)[29-33]photoATRP,[34-35] and mechanoATRP.[36-37] Nevertheless, for some applications, residual catalyst should be removed, using column filtration, electrodeposition, or more complex methods, depending on the desired degree of purity.[38-43]

The biphasic nature of heterogeneous polymerizations can simplify catalyst removal. Indeed, in miniemulsion systems, the large surface area of the organic/water interface helps mass transport of the catalyst from the polymer particles to the aqueous phase, if a sufficiently hydrophilic catalyst is used. The catalyst, however, should be also sufficiently hydrophobic to enter the hydrophobic monomer droplets, where it starts and controls the miniemulsion polymerization.[1, 44]

In this context, we recently developed a novel catalytic system for *e*ATRP, based on a strongly hydrophilic complex, Br–Cu^{II}TPMA^{+}. Despite its insoluble nature in *n*-butyl acrylate (BA), the catalyst enters hydrophobic BA droplets when combined with an anionic surfactant, sodium dodecyl sulfate (SDS).[45] The interaction between catalyst and SDS formed neutral ion pairs, Br–Cu^{II}TPMA^{+}/DS^{-}, that resided either at the surface or inside the BA droplets. This concept could be considered as a paradigm shift for miniemulsion ATRP, which previously required very hydrophobic catalysts that were predominately confined to the organic phase.[46-50] With the Br–Cu^{II}TPMA^{+}/SDS system, only ~1% of the catalyst was inside the hydrophobic droplets as ion pairs, 95% was bound at the monomer/water interface, and ~4% was in the aqueous phase. Therefore, such a combination of ion-pair and interfacial catalysis (cf. **Scheme 2-2**) allowed for the

successful *e*ATRP of BA. Relevant for industrial application, ≤ 1% of total Cu was detected inside the final latex after centrifugation.

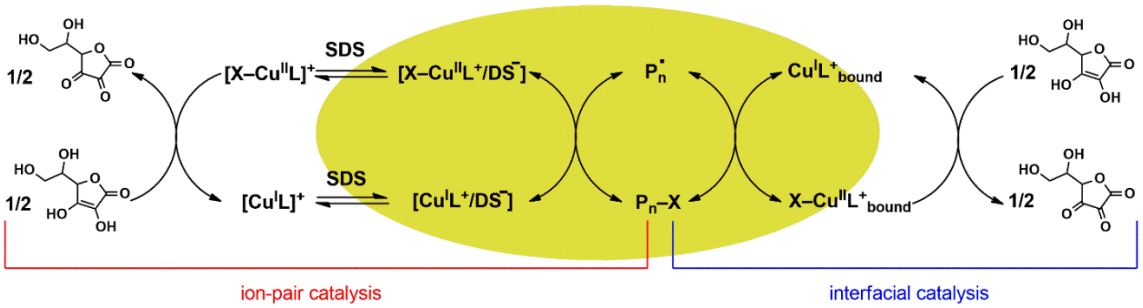

Scheme 2-2. Mechanism of ion-pair and interfacial catalysis in ARGET ATRP in miniemulsion with ascorbic acid as reducing agent.

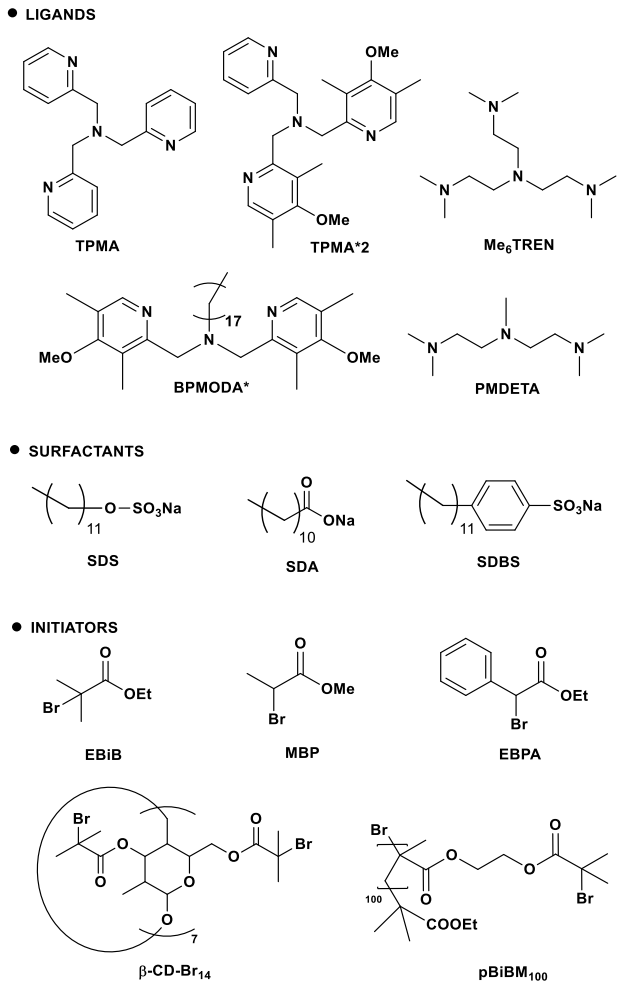

Scheme 2-3. Chemical structures of copper ligands, surfactants, and initiators used in this work.

In the present work, the concept of ion-pair and interfacial catalysis was exploited in miniemulsion ARGET ATRP of BA and *n*-butyl methacrylate (BMA), with ascorbic acid (AsAc) as reducing agent (**Scheme 2-2**). Several hydrophilic ligands and anionic surfactants were evaluated (**Scheme 2-3**). The effect of SDS concentration on particles size, polymerization kinetics, and degree of control was studied, providing some mechanistic insights. Cu concentration was reduced to minimize contamination in the final product. Both low and high degrees of polymerization (200-1200) were targeted. The livingness of

the process was confirmed by chain-extending a poly(*n*-butyl methacrylate)–Br macroinitiator (PBMA-MI) with both acrylic and methacrylic monomers, confirming the high retention of chain-end functionality. Synthesis of polymers with complex architecture, such as stars and brushes, was successful.[51]

2.3. Results and Discussion

Effect of Ligand Structure on Miniemulsion ATRP of BA. Different copper complexes were tested in ARGET ATRP with 20 vol% BA in water, using ultrasonication to form a miniemulsion with the composition reported in **Table 2-1**. NaBr (0.1 M) was added to increase the stability of the $Br–Cu^{II}L^{+}$ deactivator, which could otherwise dissociate to $Cu^{II}L^{2+} + Br^{-}$ in aqueous media.[52-53] The appropriate amount of AsAc was injected dropwise during the first 3 minutes of the reaction, considering that reduction of all Cu^{II} requires $[AsAc]/[Cu^{II}] = 0.5$.[46]

The Cu complexes with pyridinic ligands, $Br–Cu^{II}TPMA^{+}$ and $Br–Cu^{II}(TPMA*2)^{+}$, provided well-controlled PBA with $Đ \approx 1.2$ and experimental MW ($M_{n,app}$) close to theoretical values (**Table 2-2, entries 1-3**). The obtained latex was stable for several months, and particle size varied less than 15% before and after polymerizations, as measured by dynamic light scattering (DLS). Comparable results were obtained using either NaBr or Et_4NBr as a source of Br^{-} to stabilize $Br–Cu^{II}TPMA^{+}$ (**Table 2-2, entry 1 vs. 2**). Et_4NBr, however, formed larger monomer droplets, indicating that Et_4N^{+} can slightly destabilize latex formation.

Table 2-1. Composition of Organic and Aqueous Phases in a Typical Miniemulsion ARGET ATRP.[a]

Component	Weight (g)	Comments
Organic phase		
Monomer	1.79	20 vol% (18 wt%)
R–X [b,c]	0.0098 (EBiB)	[Monomer]/[R–X] = 280/1
	0.012 (EBPA)	
Hexadecane	0.19	10.8 wt% to monomer
Aqueous phase		
Water	8	Deionized water
SDS[c]	0.082	4.6 wt% to monomer
NaBr	0.103	[NaBr] = 0.1 M[d]
$Cu^{II}Br_2$	2.2×10^{-3}	1 mM[d]
TPMA[c]	3.2×10^{-3}	1.1 mM[d]
AsAc	varied	cf. Tables 2-2 through 2-5

[a]Conditions: T = 65 °C, V_{tot} = 10 mL. The miniemulsion was prepared by ultrasonication as described in the Supporting Information. [b][R–X] was varied to target different degrees of polymerization (DPs). [c]Chemical structure of surfactants, initiators, and ligands are presented in **Scheme 2-3**. [d]With respect to the total volume.

The polymerization rates were almost the same with $Br–Cu^{II}TPMA^{+}$ and $Br–Cu^{II}(TPMA*2)^{+}$, despite the much higher redox activity of the latter catalyst. On the other hand, the interactions between SDS and either $Br–Cu^{II}(TPMA*2)^{+}$ or $Br–Cu^{II}TPMA^{+}$ were similar.[45] This indicates that the intrinsic catalyst activity, catalyst interaction with the surfactant, and the partitioning of the catalyst between the organic and aqueous phases are all important parameters.

Table 2-2. Effect of Various Ligand-Surfactant Combinations in ARGET ATRP Miniemulsion Polymerization of BA.[a]

Entry	Ligand	Surfactant	t (h)	Conv. (%)	k_p^{app} [b] (h^{-1})	$M_{n,app}$ ($\times10^{-3}$)	$M_{n,th}$ ($\times10^{-3}$)	$Đ$	d_Z[c] (nm)
1	TPMA	SDS	6	66	0.25	30.9	24.4	1.17	117±2
2	TPMA[d]	SDS	5	70	0.31	24.1	25.5	1.14	152±1
3	TPMA*2	SDS	3	40	0.21	10.0	14.5	1.24	114±1
4	PMDETA	SDS	2	79	1.42	38.5	28.8	5.02	161±1
5	Me_6TREN	SDS	1.1	89	2.21	32.4	32.2	2.65	152±2
6	TPMA	SDBS	3	84	0.63	29.8	30.4	1.32	153±1
7	TPMA	SDS+SDA[e]	5	74	0.31	27.4	27.0	1.25	273±3

[a]General conditions as in **Table 2-1**. [AsAc]/[Cu^{II}] = 0.5, AsAc injected dropwise at t = 0 h. [b]The slope of the $\ln([M]_0/[M])$ vs. time plot. [c]Z-Average particles diameter, measured by DLS. [d] Et_4NBr replaced NaBr. [e] [SDS] = 4.6 wt% and [SDA] = 0.5 wt% relative to BA.

Me_6TREN and PMDETA were also tested as ligands under otherwise identical conditions. These aliphatic-amine ligands led to 6–9 times faster polymerizations than with TPMA, but poorly controlled (**Table 2-2, entries 3-4**). Similar poor control was previously observed in *e*ATRP with Me_6TREN and attributed to a much weaker interaction between SDS and Br–$Cu^{II}Me_6TREN^+$ than with Br–$Cu^{II}TPMA^+$. Moreover, previous electrochemical studies showed that the interaction between Cu/Me_6TREN and SDS was stronger for Cu^I than Cu^{II} species. Abundant $Cu^IMe_6TREN^+/DS^-$ explains the faster polymerization, while scarce Br-$Cu^{II}Me_6TREN^+/DS^-$ suggests that insufficient deactivator was present at the polymerization loci.[45] In fact, GPC traces revealed a sharp peak followed by a broad signal at high MWs, indicating the presence of droplets with very low deactivator concentration .

Under homogenous conditions, Cu^{I}/Me_6TREN^{+} is one order of magnitude more reactive than $Cu^{I}/TPMA^{+}$. Therefore, in miniemulsion the following strategies were attempted to slow down the reaction and improve control with $Cu^{I}Me_6TREN^{+}$: *i*) reduce catalyst and/or ascorbic acid loadings, *ii*) use of NaCl instead of NaBr, *iii*) replace the EBiB initiator by MBP, with a secondary less reactive alkyl structure.[54] Nevertheless, all polymerization were fast and polymers with high *Đ* were obtained (**Table 2-3**).

Table 2-3. ARGET ATRP of BA in miniemulsion catalyzed by Cu^{II}/Me_6TREN.[a]

Entry	Surfactant	Cu^{II} (ppm)	[AsAc]/[Cu^{II}]	NaX	R–X	*t* (h)	Conv. (%)	k_p^{app} [b] (h^{-1})	$M_{n,th}$ ($\times10^{-3}$)	$M_{n,app}$ ($\times10^{-3}$)	*Đ*	d_Z (nm)[c]
1	SDS	720	0.5	NaBr	EBiB	1.1	89	2.21	32.2	32.4	2.65	152±2
2	SDS+SDA[d]	720	0.5	NaBr	EBiB	1	85	2.22	30.9	33.4	2.61	149±2
3	SDS+SDA[d]	360	0.5	NaBr	EBiB	1	90	2.63	32.9	31.9	3.56	138±1
4	SDS+SDA[d]	72	0.5	NaBr	EBiB	4	0	-	-	-	-	-
5	SDS	720	0.25	NaBr	EBiB	1	93	3.29	33.8	38.6	1.82	144±2
6	SDS	720	0.125	NaBr	EBiB	2	87	1.30	31.7	32.1	2.36	133±1
7	SDS	720	0.5	NaCl	EBiB	1	85	2.20	30.9	27.4	3.24	128±1
8	SDS	720	0.5	NaBr	MBP	1	88	2.62	31.9	32.7	2.43	129±1

[a]General conditions: ARGET ATRP of BA 20 % vol in H_2O + 0.1 M NaX, *T* = 65 °C; V_{tot} = 10 mL, [BA]/[EBiB]/ $[Cu^{II}Me_6TREN]^{2+}$ = 280/1/0.2, [surfactant] = 4.6 % wt and [HD] = 10.8 % wt rel. to BA. AsAc added dropwise at the beginning. [b]The slope of the $\ln([M]_0/[M])$ vs. time plot. [c]Z-Average particle diameter measured by DLS. [d][SDS] = 4.6 % wt, [SDA] = 0.5 % wt rel. to BA.

The $Cu^{I}PMDETA^{+}$ catalyst is much less active than either $Cu^{I}Me_6TREN^{+}$ or $Cu^{I}TPMA^{+}$.[55-56] Therefore, the poor control observed with $Br–Cu^{II}PMDETA^{+}$ suggests that

the interaction of this complex with SDS is very weak. In conclusion, pyridinic ligands, such as TPMA, are better suited for miniemulsion ARGET ATRP due to the specific interactions between catalyst and surfactant, which enables both Cu^{I} and Cu^{II} species to enter the hydrophobic droplets and tune the polymerization process.

Effect of Structure and Amount of Surfactant on Miniemulsion ATRP of BA. Several anionic surfactants were evaluated to form ion-pair complexes (**Scheme 2-3**): SDS, sodium dodecylbenzenesulfonate (SDBS), and sodium dodecanoate (SDA).

SDBS provided a fast polymerization (**Table 2-2, entry 6, Figure 2-1**), reaching 84% conversion in 3 h, but polymers with $Đ$ = 1.32, higher than with SDS under identical conditions, were obtained. The higher polymerization rate and the decreased control may be caused by a weaker interaction between $Br–Cu^{II}TPMA^{+}$ and SDBS, leading to a lower amount of the Cu^{II} species inside the droplets.

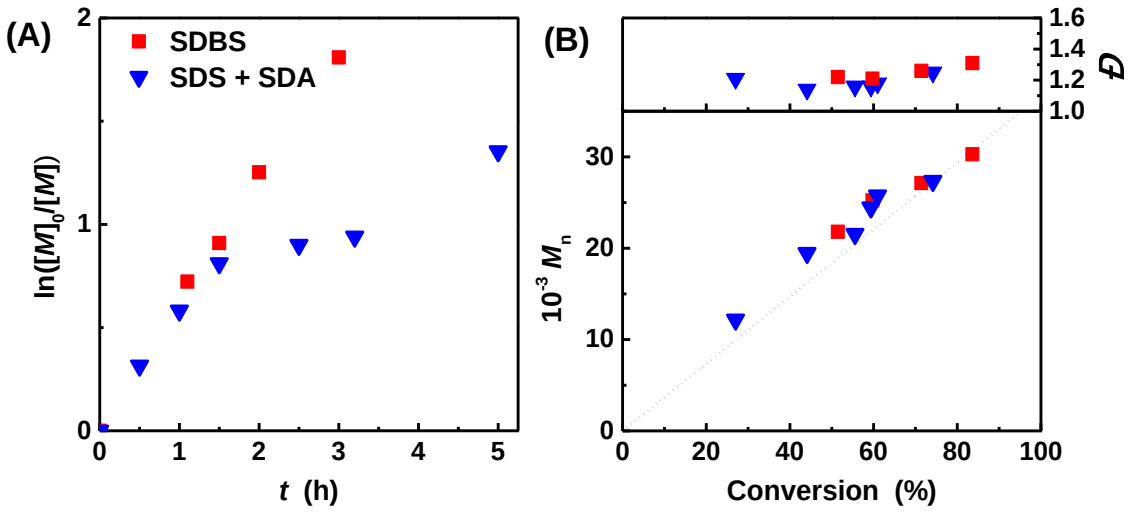

Figure 2-1. ARGET ATRP miniemulsion polymerization of BA with Cu^{II}/TPMA as catalyst and different anionic surfactants (Table 2 main text, entries 6-7). (A) Semi-logarithmic kinetic plots and (B) MW and $Đ$ evolution vs. monomer conversion. Reaction

conditions: [BA]/[EBiB] = 280/1, [BA] = 1.39 M, [NaBr] = 0.1 M, [HD] = 85 mM, T = 65 °C. SDBS 4.6 % wt relative to BA, or SDS 4.6 % wt + SDA 0.5 % wt relative to BA.

SDA alone could not stabilize the BA miniemulsion, therefore a combination of SDS and SDA was tested (4.6 wt % SDS + 0.5 wt % SDA relative to BA, **Table 2-2, entry 7, Figure 2-1**). The obtained miniemulsion was stable, but particle size increased to *ca.* 270 nm (almost twice larger than with other surfactants). Polymerization was slightly faster than with SDS alone, with $Đ$ = 1.25, suggesting the presence of a different Cu^{I}/Cu^{II} ratio. SDA seemed to slightly destabilize the system, while SDS ensured the effective interaction with the Cu complex. Therefore, SDA can be used in combination with SDS, to tune the particle size but preserving most of the polymerization control and the latex stability.

Finally, the amount of SDS was varied to change latex properties and polymerization kinetics (**Table 2-4** and **Figure 2-2**). By lowering [SDS], k_p^{app} decreased and first-order kinetics deviated from linearity. A controlled polymerization was even obtained with [SDS] as low as 1.15 wt% relative to monomer, which is below the critical micellar concentration (cmc) of the surfactant in the polymerization media (cmc = 8.9 mM for SDS in water + 0.1 M NaBr, T = 65 °C, which corresponds to 1.46 wt% relative to BA)[45]. Reducing [SDS] resulted in decreased control because less ion pairs were formed and less catalyst was bound to the surface of the droplets. Polymerization rate decreased because the droplets size increased, lowering the overall interfacial area, which slowed down the kinetics of mass transport. Nevertheless, the process remained controlled ($Đ$ = 1.1–1.3) and the final latexes were stable, meaning that the amount of SDS can be varied to tune particles dimensions.

Table 2-4. ARGET ATRP Miniemulsion Polymerization of BA with Different Amounts of SDS.[a]

Entry	[SDS] (wt% rel. to BA)	t (h)	Conv. (%)	k_p^{app} [b] (h^{-1})	$M_{n,app}$ ($\times10^{-3}$)	$M_{n,th}$ ($\times10^{-3}$)	$Đ$	d_Z [c] (nm)
1	9.2	4	81	0.50	30.2	29.4	1.12	106±2
2	4.6	6	66	0.25	30.9	24.4	1.17	117±2
3	2.3	13	74	0.12	30.2	26.7	1.30	161±1
4	1.15	20	74	0.16	35.2	27.2	1.32	207±2

[a]General conditions as in Table 2-1. [AsAc]/[Cu^{II}] = 0.5, AsAc injected dropwise at t = 0 h. [b]The linear slope of the ln([M]$_0$/[M]) vs. time in the first 10 h of polymerization. [c]Z-Average particle diameter measured by DLS.

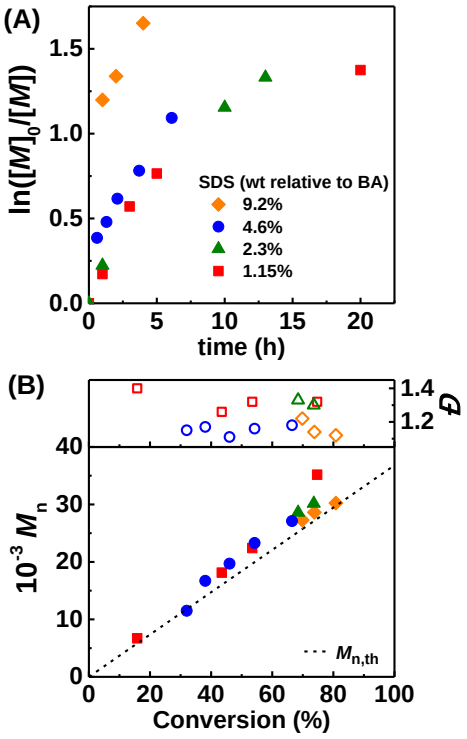

Figure 2-2. ARGET miniemulsion ATRP of BA with different amounts of SDS (**Table 2-4**). (A) Semilogarithmic kinetic plot and (B) MW and $Đ$ evolution vs. conversion. [AsAc]/[Cu^{II}] = 0.5 added dropwise at t = 0 h. Other conditions as in **Table 2-1**.

Effect of Catalyst Loading on Miniemulsion ARGET ATRP of BA and BMA. The Br–$Cu^{II}TPMA^{+}$ loading was reduced from 719, to 360, and to 144 ppm in a miniemulsion ARGET ATRP of BA, and resulted in maintaining comparable polymerization rates (

Table 2-5, Figure 2-3). However, the dispersity increased with decreasing catalyst loading, in agreement with Eq. 1: _ENREF_8[7, 57]

$$Đ = 1 + \left(\frac{k_p[\text{R–X}]}{k_{deact}[\text{X–Cu}^{II}\text{L}^{+}]}\right)\left(\frac{2}{p} - 1\right) \quad (1)$$

where k_p is the propagation rate constant, k_{deact} is the deactivation rate constant and p is conversion.

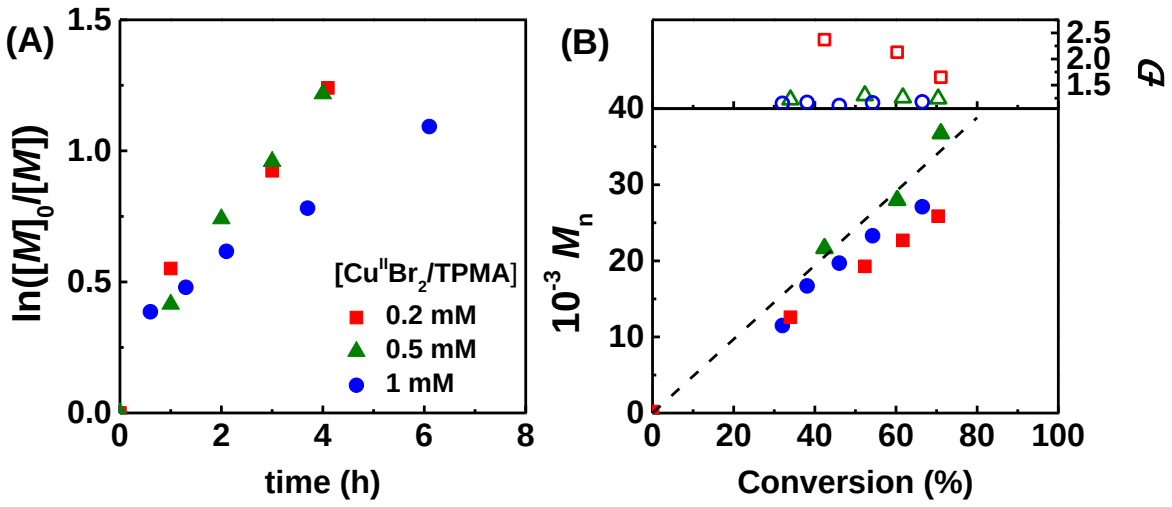

Figure 2-3. ARGET ATRP miniemulsion polymerization of BA with different concentrations of catalyst. (A) Semi-logarithmic kinetic plots and (B) MW and $Đ$ evolution

vs. monomer conversion. Reaction conditions: [BA]/[EBiB] = 280/1, [BA] = 1.39 M, [NaBr] = 0.1 M, [SDS] = 28 mM, [HD] = 85 mM, T = 65 °C.

Table 2-5. ARGET ATRP Miniemulsion Polymerization of BA and BMA with Different Catalyst Loadings and Targeted DP.[a]

Entry	[Br–Cu^{II}TPMA^{+}] (ppm)	target DP	t (h)	Conv. (%)	k_p^{app} [b] (h^{-1})	$M_{n,app}$ ($\times10^{-3}$)	$M_{n,th}$ ($\times10^{-3}$)	$Đ$	d_Z [c] (nm)
monomer = BA, R–X = EBiB[d]									
1	719	280	6	66	0.25	24.4	30.9	1.17	117±2
2	360	280	4	70	0.34	25.6	34.1	1.24	126±2
3	144	280	4	71	0.31	26.1	36.7	1.65	121±1
4	719	1000	20	71	0.07	91.6	101.8	1.25	126±1
monomer = BMA, R–X = EBPA[e]									
5	800	280	1	82	1.60	36.3	32.9	1.26	135±2
6	200	280	2	90	1.05	36.3	36.1	1.33	132±3
7	50	280	2	77	0.72	31.6	30.9	1.31	139±3
8	800	600	2.5	82	0.52	70.0	70.2	1.20	138±2
9	800	1200	4	76	0.38	118.6	129.3	1.42	131±2
10[f]	800	280	6	92	0.35	34.5	36.9	1.18	193±1

[a]General conditions as in **Table 2-1**. [b]The slope of the $\ln([M]_0/[M])$ vs. time plot. [c]Z-Average particles diameter by DLS before polymerization. [d][AsAc]/[Cu^{II}] = 0.5, AsAc injected dropwise at t = 0 h. [e][AsAc]/[Cu^{II}] = 0.4 injected dropwise every 30 minutes, unless otherwise noted. [f]Br–Cu^{II}BPMODA*$^{+}$ was used as catalyst; [AsAc]/[Cu^{II}] = 0.5 injected at t = 0 h.

Control over BA polymerization was lost when 144 ppm of catalyst was used, which resulted in polymers with $Đ$ = 1.65. Conversely, 360 ppm of catalyst ensured a well-controlled polymerization, even if, based on previous analysis, less than 10 ppm of copper species were present inside the monomer droplets under these conditions.[45]

ARGET ATRP of BMA was similar to BA polymerization. In fact, Br–Cu^{II}TPMA$^+$ is poorly soluble in either BA or BMA (**Figure 2-4**), and therefore it entered monomer droplets only when paired with SDS.

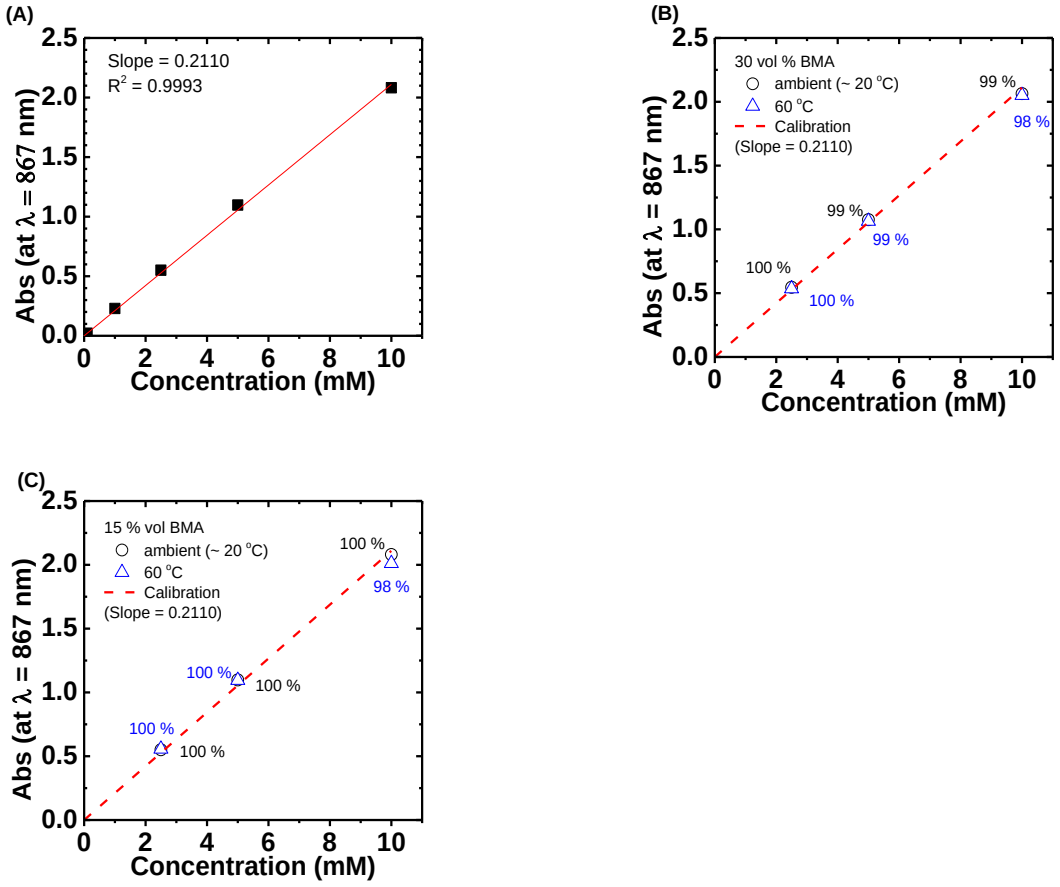

Figure 2-4 Partition experiments of $Cu^{II}Br_2$/TPMA. (A) Calibration curve (absorbance vs. $Cu^{II}Br_2$/TPMA concentration) obtained from the UV-Vis spectra (R^2 = 0.9993). (B) Partition experiments in 70/30 water/BMA mixtures (by v/v), *T* = ambient (~ 20 °C) or 60 °C; (C) Partition experiments in 85/15 water/BMA mixtures (by v/v), *T* = ambient (~ 20 °C) or 60 °C.

ARGET ATRP of BMA required careful selection of the initiator: tertiary alkyl halides, such as EBiB, are less efficient initiators for methacrylates, due to the penultimate

unit effect.[58] Indeed, with EBiB polymerization was slow resulting in polymers with $Đ$ = 1.35 (**Figure 2-5**). Instead, ethyl 2-bromophenylacetate (EBPA), which is much more reactive than EBiB,[59-60] provided a well-controlled process, reaching 34% conversion in 2 h and polymers with $Đ$ = 1.13 (**Table 2-6**).

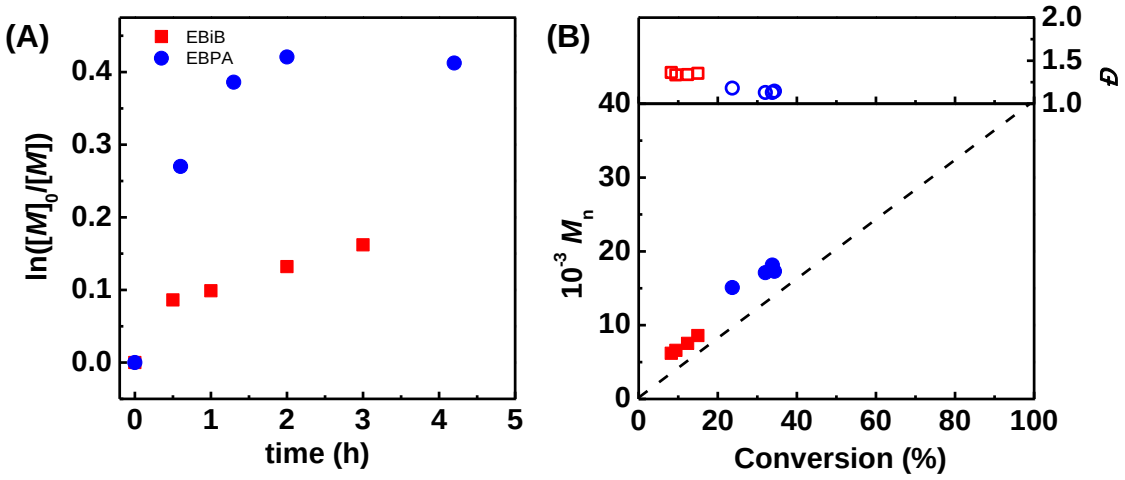

Figure 2-5. Miniemulsion ARGET ATRP of BMA with R–X = EBiB or EBPA. (A) Kinetic plot and (B) MW and $Đ$ evolution vs. monomer conversion. Reaction conditions: [BMA]/ [R–X]/[Br–Cu^{II}TPMA$^+$] = 280/1/0.2, [BMA] = 1.25 M, [Br–Cu^{II}TPMA$^+$] = 1.00 mM, [NaBr] = 0.1 M, [SDS] = 28 mM, [HD] = 85 mM, T = 65 °C.

Table 2-6. ARGET miniemulsion ATRP of BMA with different AsAc feeding procedures.[a]

Entry	AsAc feeding procedure	[AsAc]/[Cu^{II}]	t (h)	Conv. (%)	k_p^{app} [b] (h^{-1})	$M_{n,app}$ ($\times10^{-3}$)	$M_{n,th}$ ($\times10^{-3}$)	$Đ$	d_z (nm)[c]
1	Dropwise at t = 0 h	0.5	2	34	0.25	14.6	13.8	1.13	144±3
2	Syringe pump (rate = 0.125 eq/h) [d]	0.375	3	64	0.35	23.4	25.8	1.22	146±4
3	Dropwise at t = 0 and 1 h	0.5 + 0.5	3	70	0.41	33.7	28.1	1.25	153±2

4	Dropwise at t = 0 h and syringe pump (rate = 0.3 eq/h)	0.2 + 0.6	2	79	0.98	32.0	31.7	1.25	137±2
5	Dropwise at t = 0 and 0.5 h	0.4 + 0.4	1	82	1.60	36.3	32.9	1.26	135±2

[a]General conditions: ARGET ATRP of BMA 20% vol in H_2O + 0.1 M NaBr, T = 65 °C; V_{tot} = 10 mL, [BMA]/[EBPA]/[$Cu^{II}Br_2$/TPMA] = 280/1/0.2, [BMA] = 1.25 M, [SDS] = 4.6 % wt relative to BMA, [HD] = 10.8 % wt rel. to BMA. [b]The slope of the $\ln([M]_0/[M])$ vs. time plot. [c]Z-Average particle diameter measured by DLS before polymerization. [d]eq = $[AsAc]/[Cu^{II}]_0$ = 1.

Polymerization stopped after 2 h, suggesting that the initial addition of AsAc ([AsAc]/[Br–$Cu^{II}TPMA^+$] = 0.5) did not provide continuous regeneration of the active catalyst. Hence, the feeding of AsAc was optimized (**Table 2-6** and **Figure 2-6**); a fast and well-controlled polymerization was obtained by simply injecting initially 0.4 equivalents of AsAc, with respect to initial Br–$Cu^{II}TPMA^+$, at t = 0 h and then subsequently every 30 minutes. 82% conversion in 1 h and polymers with $Đ$ = 1.26 were obtained, with good agreement between experimental and theoretical MWs (

Table 2-5, entry 5 and **Figure 2-7**).

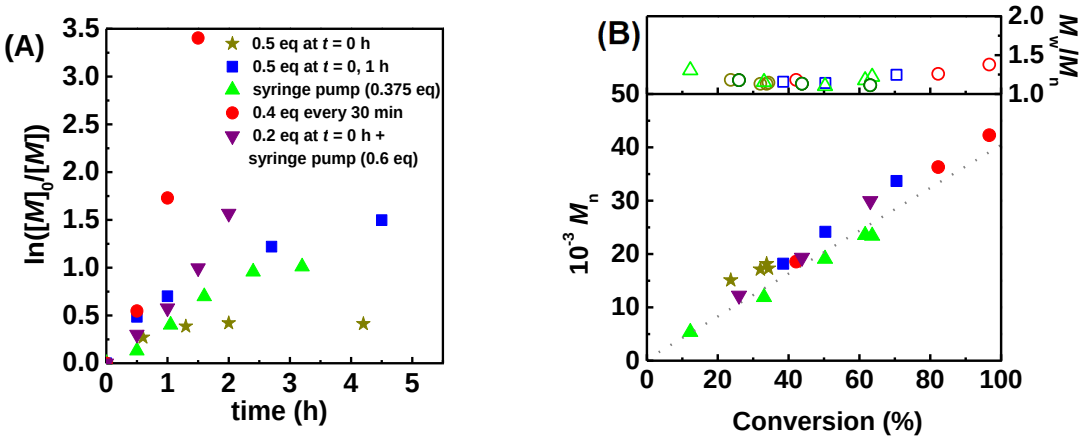

Figure 2-6. ARGET miniemulsion ATRP of BMA with different AsAc feeding procedure. (A) Kinetic plot and (B) MW and $Đ$ evolution vs. monomer conversion. Reaction conditions: [BMA]/[EBPA]/[Br–Cu^{II}/TPMA^{+}] = 280/1/0.2, [BMA] = 1.3 M, [Br–Cu^{II}/TPMA^{+}] = 1.00 mM, [NaBr] = 0.1 M, [SDS] = 28 mM, [HD] = 85 mM, T = 65 °C (**Table 2-6**, entries 1-5).

Catalyst loading was successfully reduced from 800 ppm to 50 ppm in ARGET ATRP of BMA (**Table 2-5,** entries 5-7). Polymerization rate (R_p) decreased with decreasing amount of Cu, exhibiting a good proportionality between R_p and the square root of [Br–Cu^{II}TPMA^{+}], as predicted from Eq. 2:[61]

$$R_p = k_p^{app}[M] = k_p[M][P^\bullet] = k_p[M]\sqrt{\frac{k_{red}[AsAc][Br-Cu^{II}L^+]}{2k_t}} \quad (2)$$

where k_{red} is the reduction rate constant of Br–Cu^{II}TPMA^{+} and k_t is the termination rate constant. 50 ppm of Br–Cu^{II}TPMA^{+}, corresponding to 6.25 × 10^{-5} M, provided 77% conversion in 2 h with a final polymer with $Đ$ = 1.31. However, MWD was broader during the first hour, due to the slow ATRP deactivation with very low catalyst loadings (**Figure**

2-7). The much lower propagation rate constant, k_p, of BMA than of BA permitted good control and low dispersity with few ppm of catalyst (cf. Eq. 1).[62]

Interestingly, polymerization rate of BMA varied with initial [Cu^{II}], while polymerization rate of BA did not. This is likely due to the different extent of radical termination in the two systems. The BMA system, with high ATRP activity and lower k_p, was characterized by higher radical concentration, which increased the extent of radical termination. Therefore, a large portion of Cu^{I} catalyst was regenerated and the kinetics agreed with eq. 2. In the BA system, on the contrary, radical concentration was lower and termination was almost negligible. In this case, addition of AsAc established a fixed [Cu^{I}]/[Cu^{II}] ratio, so that the kinetics did not depend on [Cu^{II}]. (Note that a constant [AsAc]/[Cu^{II}] was used in each case).

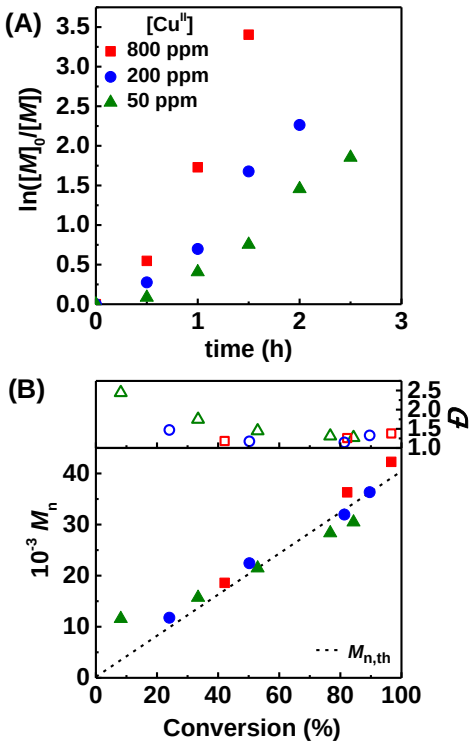

Figure 2-7. Miniemulsion ARGET ATRP of BMA with various catalyst loadings. (A) Semilogarithmic kinetic plot and (B) MW and *Đ* evolution vs. monomer conversion. [AsAc]/[Cu^{II}] = 0.4, injected dropwise every 30 min. Other reaction conditions are listed in **Table 2-1**.

ICP-MS measurements of the precipitated PBMA revealed residual copper contents as low as 4.5, 1.6 and 0.3 ppm, with initial catalyst loadings of respectively 800, 200 and 50 ppm (over the total amount of monomer). Less than 1% of the initial copper content remained in the final polymer after precipitation. Metal contamination in the ppb range makes the polymer suitable for some applications without any purification procedure.[63]

For comparison, ARGET ATRP of BMA in miniemulsion was carried out with a traditionally used hydrophobic complex (**Table 2-5,** entry 10 and **Figure 2-8**), namely

BPMODA*, which was specifically designed to form a highly active and hydrophobic copper catalyst.[49] BPMODA* was prepared as described in the Supporting Information. Under the same conditions used for Cu/TPMA, Cu/BPMODA* gave well-controlled polymers, but particles size was 80% larger, suggesting potential destabilization of the droplets' surface.[43] Starting from 800 ppm of Br–Cu^{II}BPMODA*$^{+}$, ICP-MS measurements determined 45 ppm of residual copper in the precipitated polymer, 10 times higher than with Br–Cu^{II}TPMA^{+}/SDS.

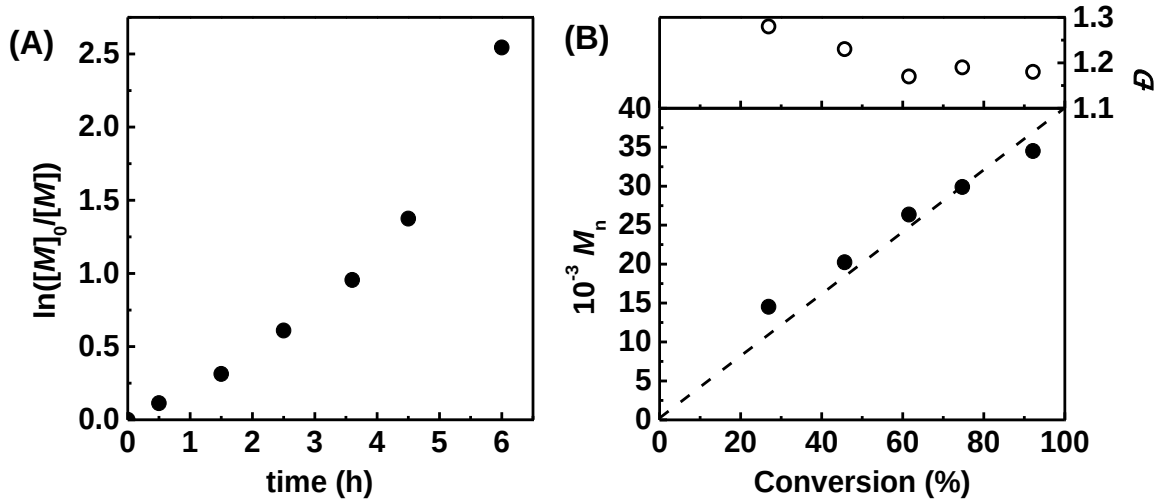

Figure 2-8. ARGET ATRP miniemulsion polymerization of BMA with BPMODA* as ligand. (A) Kinetic plot and (B) MW and *Đ* vs. monomer conversion. Reaction conditions: [BMA] = 1.25 M, [Br–Cu^{II}/BPMODA*$^{+}$] = 1.00 mM, [NaBr] = 0.1 M, [SDS] = 28 mM, [HD] = 85 mM, *T* = 65 °C. Details in **Table 2-5**, entry 10 in the main text.

Effect of Targeted DP on Miniemulsion ATRP of BA and BMA. Higher degrees of polymerization were targeted by lowering initiator concentration. PBA with DP > 700, *Đ* = 1.25, and good agreement between theoretical and experimental MWs was obtained.

Polymerization rate decreased for lower [R–X], as expected from Eq. 2, due to lower amount of generated radicals (**Table 2-5,** entry 4).[61]

High MW PBMA was obtained when targeting DP = 600 and 1200 (**Table 2-5**, entries 8, 9). Once again, polymerization rates were proportional to [R–X]. By switching from targeted DP = 280 to 600, *Đ* diminished from 1.25 to 1.20, in agreement with Eq. 1. However, *Đ* increased to 1.42 for DP = 1200 (Figure 2-9A), possibly due to the high viscosity in the polymerizing droplets. An increase of viscosity, besides slowing down termination events, can hamper radical deactivation by the small amount of Cu^{II} present inside the droplets. High viscosity can be related to the "auto-acceleration" of the polymerization after 2 h (**Figure 2-9**A), which was concomitant with the increase in dispersity (**Figure 2-9**B).

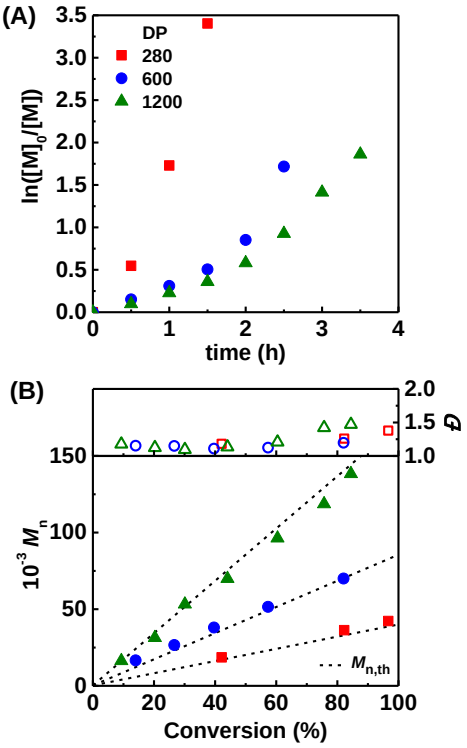

Figure 2-9. Miniemulsion ARGET ATRP of BMA with different target DPs (280, 600 and 1200). (A) Kinetic plot and (B) MW and $Đ$ vs. monomer conversion. [AsAc]/[Cu^{II}] = 0.5. Other reaction conditions listed in **Table 2-1**.

Chain Extension Experiments. To test chain-end fidelity of the obtained polymers, a PBMA macroinitiator (PBMA-MI) was prepared by miniemulsion ARGET ATRP with Br–Cu^{II}TPMA$^+$/SDS, see details in Supporting Information. After purification, the macroinitiator had $M_{n,app}$ = 4000 and $Đ$ = 1.31. Chain extension polymerizations were performed with both BA (

Table 2-7, entry 1) and *tert*-butyl methacrylate (*t*BMA,

Table 2-7, entry 2). **Figure 2-10A** and **B** show a clean shift of MWs in both cases, with monomodal MW distributions, confirming the high retention of chain-end functionality in the first block. The second block was also well-controlled, with $Đ_2$ = 1.34 for *t*BMA and

$Đ_2$ = 1.15 for BA, calculated as $Đ - 1 = w_1^2(Đ_1 - 1) + w_2^2(Đ_2 - 1)$, where w_1 and w_2 are the weight fractions of the first and second block, respectively.[64] Thus, PBMA-MI was successfully chain-extended with both methacrylates and acrylates. High chain-end fidelity, indicating well-controlled polymerizations, motivated the synthesis of more complex structures by miniemulsion ARGET ATRP, such as star and brush-like polymers.

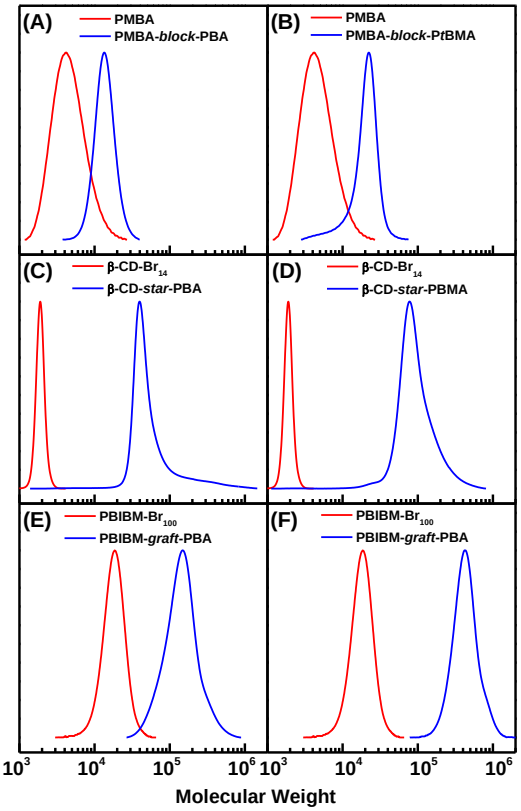

Figure 2-10. GPC traces of polymers with different architectures, prepared by ARGET miniemulsion ATRP. Chain extensions of PBMA-MI with (A) *t*BMA and (B) BA; multi-arm star polymers from β-CD-Br_{14} macroinitiator and (C) BA or (D) BMA; PBA molecular brushes with DP target (E) 25 and (F) 100. Detailed conditions are listed in

Table 2-7.

Synthesis of Polymer Stars. PBA and PBMA stars were prepared by grafting from a β-cyclodextrin core that was functionalized with 14 ATRP initiators (β-CD-Br_{14}).[65] The structure of β-CD-Br_{14} is illustrated in **Scheme 2-3**, while its synthesis is described in the Supporting Information. A clean shift of MW was observed in the GPC traces during the "grafting from" polymerizations with both BA and BMA (**Figure 2-10C** and **D**). PBA star polymers were well-defined (

Table 2-7, entry 3), with $M_{n,app} < M_{n,th}$ since the hydrodynamic volume of a star polymer is lower than its linear analogue with the same MW.[65] The formation of the PBMA star polymer was less controlled (

Table 2-7, entry 4).

Table 2-7. Preparation of Polymers with Complex Structures by ARGET ATRP in Miniemulsion.[a]

Entry	Initiator	Polymer	t (h)	Conv. (%)	k_p^{app} [b] (h^{-1})	$M_{n,app}$ ($\times10^{-3}$)	$M_{n,th}$ ($\times10^{-3}$)	$Đ$	d_Z [c] (nm)
1[d]	PBMA-Br	PBMA-*block*-PBA	2	30	0.20	13.0	11.7	1.10	118±1
2[e]	PBMA-Br	PBMA-*block*-P*t*BMA	1	30	0.35	16.1	12.6	1.19	119±1
3[e]	β-CD-Br_{14}	β-CD-*star*-PBA	2	73	0.70	47.7	65.7	1.39	118±2
4[e]	β-CD-Br_{14}	β-CD-*star*-PBMA	2	76	0.95	82.2	78.1	1.54	138±2
5[f]	$PBiBM_{100}$	$PBiBM_{100}$-*graft*-PBA	4	94	0.44	357	125	1.29	194±2
6[f]	$PBiBM_{100}$	$PBiBM_{100}$-*graft*-PBA	7	57	0.15	775	347	1.28	155±1

[a]General conditions: monomer 20 vol% in H_2O + 0.1 M NaBr, T = 65 °C; V_{tot} = 10 mL, [$Cu^{II}Br_2$/TPMA] = 1 mM, [SDS] = 4.6 wt%, [hexadecane] = 10.8 wt% relative to monomer. [b]The slope of the $\ln([M]_0/[M])$ vs. time plot. [c]Z-Average particle diameter by DLS before

polymerization. [d]AsAc feeding rate = 3 μmol/h. [e]AsAc feeding rate = 2 μmol/h. [f]AsAc feeding rate = 50 nmol/h and [SDS] = 2.3 wt% relative to monomer.

Synthesis of Polymer Brushes. Molecular brushes were successfully prepared in a miniemulsion by grafting BA from a poly(2-(2-bromoisobutyryloxy)ethyl methacrylate) ($PBiBM_{100}$) macroinitiator, comprising a methacrylate backbone functionalized with ca. 100 α-bromoisobutyrate initiating sites. The structure of $PBiBM_{100}$ is illustrated in **Scheme 2-3.** Successful synthesis of molecular brushes requires minimal termination to avoid coupling between the multifunctional macromolecules. Indeed, direct injection of AsAc at the beginning of the reaction produced too many radicals and resulted in coupled chains, *i.e.* gelation. Therefore, the concentration of radicals was lowered by *i*) decreasing SDS concentration (cf. **Table 2-4**) and *ii*) gradually feeding AsAc to the reaction in order to slowly reduce Cu^{II} to the activator Cu^{I} state (

Table 2-7, entries 5 and 6). Slightly larger particles were obtained according to DLS, as expected from the lower C_{SDS}, but the final miniemulsion was stable and no gelation was observed. Molecular brushes with side-chain length of DP = 24 and 57 were prepared. In both cases, radical termination by coupling was minimal, according to the low intensity of high MW shoulders in the GPC traces (**Figure 2-10E** and **F**). Again, $M_{n,app}$ was lower than $M_{n,th}$, due to the very compact nature of molecular brushes.

2.4. Conclusion

The interaction between hydrophilic catalysts and SDS provided ion-pair and interfacial catalysts suitable for controlled ARGET ATRP of BA, BMA, and *t*BMA in a

miniemulsion polymerization. The setup was simple, with the use of commercially available reagents to prepare *in situ* a Br–Cu^{II}TPMA^{+}/DS^{-} ion-pair complex, followed by reduction with ascorbic acid to activate the polymerization.

The final latexes contained very low amount of residual copper, possibly avoiding the need for any further purification. Indeed, the hydrophilic Br–Cu^{II}TPMA^{+} complex migrated to the aqueous phase when crashing the miniemulsion by dilution. Low dispersity PBMA was obtained by lowering Cu loading to 50 ppm, which resulted in 300 ppb Cu in the final latex. Residual copper content was 10 times lower than when using traditional hydrophobic complexes.

High degrees of polymerization were successfully targeted with both BA and BMA. Moreover, chain extension of a PBMA macroinitiator showed excellent retention of chain-end functionality. Monomodal block copolymers PBMA-*b*-PBA and PBMA-*b*-P*t*BMA with $Đ < 1.2$ were formed in few hours. Well-defined star and brush polymers were also prepared, showing minimal radical termination by coupling.

Compared to traditional super-hydrophobic catalysts, miniemulsion ATRP by interfacial and ion-pair catalysis employs commercially available reagents, readily affording polymers with high purity. The hydrophilic ion-pair catalysts can also potentially be used with water-soluble or amphiphilic initiating systems, opening new avenues for controlled polymerizations in dispersed media that are currently being investigated.

2.5. Experimental Section

Materials. Copper(II) bromide ($Cu^{II}Br_2$, 99%), sodium dodecyl sulfate (SDS, 99%), sodium dodecylbenzenesulfonate (SDBS, technical grade), hexadecane (HD, 99%),

tetrahydrofuran (THF, > 99%), ethyl α-bromoisobutyrate (EBiB, 98%), ethyl α-bromophenylacetate (EBPA, 97%), methyl 2-bromopropionate (MBP, 98%), 2-bromopropionitrile (BPN, 97%), tris[2-(dimethylamino)ethyl]amine (Me_6TREN, 97%) and ascorbic acid (AsAc) were purchased from Sigma-Aldrich. Sodium bromide (NaBr, 99%) was purchased from Acros. Tris(2-pyridylmethyl)amine (TPMA), 1-(4-methoxy-3,5-dimethylpyridin-2-yl)-*N*-((4-methoxy-3,5-dimethylpyridin-2-yl)methyl)-*N*-(pyridin-2-ylmethyl)methanamine (TPMA*2), bis[2-(4-methoxy-3,5-dimethyl)pyridylmethyl]octadecylamine (BPMODA*), EBiB-modified β-cyclodextrin (β-CD-Br_{14}), and poly(2-(2-bromoisobutyryloxy)ethyl methacrylate) ($PBiBM_{100}$) were prepared according to published procedures.[50, 65-68] _ENREF_1*n*-Butyl methacrylate (BMA, 99%, Aldrich), *t*-butyl methacrylate (*t*BMA, 99%, Aldrich) and *n*-butyl acrylate (BA, 99%, Aldrich) were passed through a column filled with basic alumina prior to use to remove polymerization inhibitors. Dodecanoic acid (DA, 98%, Aldrich) was neutralized with NaOH to prepare sodium dodecanoate (SDA).

Typical procedure for a partition experiment. Aqueous solutions of $Cu^{II}Br_2$/TPMA were prepared at various concentrations, *i.e.*, 0.1, 1, 2.5, 5 and 10 mM. Catalyst concentration was followed by UV-Vis spectroscopy at maximum-absorption wavelength, λ_{max} = 867 nm. A linear calibration was obtained from the correlation between absorbance and catalyst concentration (R^2 = 0.9993, see **Figure 2-4A**). Solutions of the copper complex in water were prepared at various concentrations and then mixed with BMA to obtain 70/30 and 85/15 water/BMA ratios (by v/v). The mixtures were vigorously stirred using a Vortex Mixer and stored at either room temperature (r.t.) or 60 °C for 1 day. The aqueous phase was collected and absorbance at λ_{max} was recorded by UV-Vis

spectrometer. Percentages of copper complex remaining in the aqueous phase were then calculated.

Instrumentation. Ultrasound treatment to prepare miniemulsion samples was carried out using Ultrasonics W-385 sonicator.

UV-Vis spectra were recorded by Agilent 8453 with a glass cuvette (length = 1 cm).

$M_{n,app}$ and $Đ$ were determined by GPC equipped with Polymer Standards Services (PSS) columns (guard, 10^5, 10^3, and 10^2 Å) and a differential refractive index detector (Waters, 2410), with THF as eluent at a flow rate of 1.00 mL/min (T = 35 °C). GPC traces were processed by WinGPC 8.0 software (PSS) using a calibration based on linear polystyrene (PS) standards.

Monomer conversion was determined by gravimetric analysis, evaporating the samples at 110 °C for at least 30 min.

Particle size and size distribution were determined by using a Zetasizer Nano from Malvern Instruments, Ltd.

Samples for inductively coupled plasma−mass spectrometry (ICP-MS) were prepared by digesting the samples in 10 mL of HNO_3:HCl 1:3 mixture at 90 °C for 30 min, and then diluted in 2% HNO_3 matrix. Acids with "Traceselect" purity were used. The concentrations of copper (Cu) in precipitated polymers were determined using Thermo-Finnigan Element XR ICP-MS. The instrument was calibrated with standard solutions. The samples were analyzed immediately after the initial calibration, and the elemental results were within the calibration range. Cu residual (ppm) = (mass of Cu)/(total mass) × 10^6.

Note that this is different from the definition of ppm for initial catalyst loading, which is usually expressed as Cu loading (ppm) = C_{Cu} / C_M × 10^6.

General procedure for a miniemulsion ARGET ATRP of BA. BA (2 mL, 13.95 mmol), EBiB (7.2 μL, 0.05 mmol) to target degree of polymerization (DP) = 280 (the amount of EBiB was adjusted for different targeted DPs), and HD (0.25 mL, 0.85 mmol) were mixed to form the organic phase. $Cu^{II}Br_2$/TPMA stock solution (0.20 mL, 0.01 mmol), NaBr (0.103 g, 1 mmol), and SDS (0.082 g, 0.28 mmol) were dissolved in 8 mL of distilled water. The organic and aqueous solutions were mixed (total volume ≈ 10 mL), placed in an ice bath, and dispersed by probe sonicator, amplitude = 70% for 15 min (application and rest time of 1 s each). Nitrogen was bubbled through the miniemulsion solution for 0.5 h. The flask was immersed in a 65 °C oil bath and then AsAc solution (0.02 M in water) was slowly injected over 3 minutes to start the reaction. Samples were withdrawn periodically to follow the monomer conversion by gravimetric analysis, while $M_{n,app}$ and $Đ$ were determined by GPC.

General procedure for miniemulsion ARGET ATRP of BMA. A solution of BMA (2 mL, 12.57 mmol), EBPA (7.86 μL, 0.045 mmol) to target DP = 280 (the amount of EBPA was adjusted for different targeted DPs), and HD (0.25 mL, 0.85 mmol) was prepared. $Cu^{II}Br_2$/TPMA stock solution (0.20 mL, 0.01 mmol), NaBr (0.103 g, 1 mmol), and SDS (0.082 g, 0.28 mmol) were dissolved in 8 mL of distilled water. The organic and aqueous solutions were mixed (total volume ≈ 10 mL), placed in an ice bath, and dispersed by a probe sonicator, amplitude = 70% for 15 min (application and rest time of 1 s each). Nitrogen was bubbled through the miniemulsion solution for 0.5 h. The flask was immersed in a 65 °C oil bath and then AsAc solution was slowly injected over 3 min to start the

reaction. Samples were withdrawn periodically to follow the monomer conversion by gravimetric analysis, while $M_{n,app}$ and $Đ$ were determined by GPC.

Preparation of PBMA-MI. A solution of BMA (4 mL, 25.15 mmol), EBPA (88.0 μL, 0.50 mmol, to target DP = 50), and HD (0.50 mL, 1.71 mmol) was prepared. $Cu^{II}Br_2$/TPMA stock solution (0.40 mL, 0.02 mmol), NaBr (0.206 g, 2 mmol), and SDS (0.164 g, 0.57 mmol) were dissolved in 16 mL of distilled water. 2 mL of the organic solution were mixed with 8 mL of the aqueous solution, then the mixture was placed in an ice bath, and dispersed by a probe sonicator, amplitude = 70% for 15 min (application and rest time of 1 s each). Nitrogen was bubbled through the miniemulsion solution for 0.5 h. The flask was immersed in a 65 °C oil bath and a degassed AsAc solution fed by a syringe pump at 0.2 mmol/h. Samples were withdrawn periodically to follow the monomer conversion by gravimetric analysis, while $M_{n,app}$ and $Đ$ were determined by GPC. The product was precipitated into MeOH/H_2O (1/1 by v/v), redissolved in THF, passed through neutral alumina column and dried in vacuum.

General procedure for chain extension from PBMA-MI. A solution of *t*BMA (2 mL, 12.31 mmol), PBMA-MI (0.25 g, 0.062 mmol) to target DP = 200, and HD (0.25 mL, 0.85 mmol) was prepared. $Cu^{II}Br_2$/TPMA stock solution (0.20 mL, 0.01 mmol), NaBr (0.103 g, 1 mmol), and SDS (0.082 g, 0.28 mmol) were dissolved in 8 mL of distilled water. The organic and aqueous solutions were mixed (total volume ≈ 10 mL), placed in an ice bath, and dispersed by a probe sonicator, amplitude = 70% for 15 min (application and rest time of 1 s each). Nitrogen was bubbled through the miniemulsion solution for 0.5 h. The flask was immersed in a 65 °C oil bath and then a degassed AsAc solution was added by a

syringe pump at 0.2 mmol/h. Samples were withdrawn periodically to follow the monomer conversion by gravimetric analysis, while $M_{n,app}$ and $Đ$ were determined by GPC.

General procedure for synthesis of star polymers *via* ARGET ATRP in miniemulsion. A solution of BA (2 mL, 13.95 mmol), β-CD-Br_{14} (0.064 g, 0.020 mmol, to target DP = 50, calculated per -Br), and HD (0.25 mL, 0.85 mmol) was prepared. $Cu^{II}Br_2$/TPMA stock solution (0.20 mL, 0.01 mmol), NaBr (0.103 g, 1 mmol), and SDS (0.082 g, 0.28 mmol) were dissolved in 8 mL of distilled water. The organic and aqueous solutions were mixed (total volume ≈ 10 mL), placed in an ice bath, and dispersed by a probe sonicator, amplitude = 70% for 15 min (application and rest time of 1 s each). Nitrogen was bubbled through the miniemulsion solution for 0.5 h. The flask was immersed in a 65 °C oil bath and then a degassed AsAc solution was added by a syringe pump at 0.3 mmol/h. Samples were withdrawn periodically to follow the monomer conversion by gravimetric analysis, while $M_{n,app}$ and $Đ$ were determined by GPC.

General procedure for synthesis of PBiBM-*graft*-PBA molecular brushes *via* ARGET ATRP in miniemulsion. BA (1 mL, 6.9 mmol), $PBiBM_{100}$ (78 mg, 0.0028 mmol, to target DP = 25; 19 mg, 0.0007 mmol, to target DP = 100), and HD (0.125 mL, 0.43 mmol) were mixed to form the organic phase. $Cu^{II}Br_2$/TPMA stock solution (0.10 mL, 0.005 mmol), NaBr (0.052 g, 0.5 mmol), and SDS (41 mg, 0.14 mmol or 21 mg, 0.07 mmol) were dissolved in 4 mL of distilled water. The organic and aqueous solutions were mixed (total volume ≈ 5 mL), placed in an ice bath, and dispersed by a probe sonicator, amplitude = 70% for 15 min (application and rest time of 1 s each). Nitrogen was bubbled through the miniemulsion solution for 0.5 h. The flask was immersed in a 65 °C oil bath and then a degassed AsAc solution was slowly injected through a syringe pump at 50 nmol/h.

Samples were withdrawn periodically to follow the monomer conversion by gravimetric analysis, while $M_{n,app}$ and $Đ$ were determined by GPC.

General procedure for polymer precipitation. 5 mL of polymerization solution were transferred to a 50 mL centrifuge tube. 20 mL of water and 20 mL of MeOH were added and then the tubes were placed in the centrifuge for 20 min at 5000 rpm. The precipitated polymer was recovered and prepared for the ICP-MS analysis as previously described. About 90% of the polymer was recovered after precipitation.

2.6. References

(1) Zetterlund, P. B.; Kagawa, Y.; Okubo, M., Controlled/Living Radical Polymerization in Dispersed Systems. *Chem Rev* **2008,** *108* (9), 3747-3794.
(2) Jennings, J.; He, G.; Howdle, S. M.; Zetterlund, P. B., Block Copolymer Synthesis by Controlled/Living Radical Polymerisation in Heterogeneous Systems. *Chem Soc Rev* **2016,** *45* (18), 5055-5084.
(3) Cunningham, M. F., Controlled/Living Radical Polymerization in Aqueous Dispersed Systems. *Prog Polym Sci* **2008,** *33* (4), 365-398.
(4) Wu, M.; Ramirez, L. M. F.; Lozano, A. R.; Quemener, D.; Babin, J.; Durand, A.; Marie, E.; Six, J. L.; Nouvel, C., First Multi-reactive Dextran-Based Inisurf for Atom Transfer Radical Polymerization in Miniemulsion. *Carbohyd Polym* **2015,** *130*, 141-148.
(5) Saade, J.; Bordes, C.; Raffin, G.; Hangouet, M.; Marote, P.; Faure, K., Response Surface Optimization of Miniemulsion: Application to UV Synthesis of Hexyl Acrylate Nanoparticles. *Colloid Polym Sci* **2016,** *294* (1), 27-36.
(6) Wu, L.; Glebe, U.; Boker, A., Synthesis of Hybrid Silica Nanoparticles Densely Grafted with Thermo and pH Dual-Responsive Brushes via Surface-Initiated ATRP. *Macromolecules* **2016,** *49* (24), 9586-9596.
(7) Matyjaszewski, K., Atom Transfer Radical Polymerization (ATRP): Current Status and Future Perspectives. *Macromolecules* **2012,** *45* (10), 4015-4039.
(8) Moad, G.; Rizzardo, E.; Thang, S. H., Living Radical Polymerization by the RAFT Process - A third update. *Aust J Chem* **2012,** *65* (8), 985-1076.
(9) Nicolas, J.; Guillaneuf, Y.; Lefay, C.; Bertin, D.; Gigmes, D.; Charleux, B., Nitroxide-Mediated Polymerization. *Prog Polym Sci* **2013,** *38* (1), 63-235.
(10) Airaud, C.; Heroguez, V.; Gnanou, Y., Bicompartmentalized Polymer Particles by Tandem ROMP and ATRP in miniemulsion. *Macromolecules* **2008,** *41* (9), 3015-3022.
(11) Airaud, C.; Ibarboure, E.; Gaillard, C.; Heroguez, V., Nanostructured Polymer Composite Nanoparticles Synthesized in a Single Step via Simultaneous ROMP and ATRP under Microemulsion Conditions. *J Polym Sci Pol Chem* **2009,** *47* (16), 4014-4027.

(12) Min, K.; Matyjaszewski, K., Atom Transfer Radical Polymerization in Aqueous Dispersed Media. *Cent Eur J Chem* **2009,** *7* (4), 657-674.
(13) Sun, J. T.; Hong, C. Y.; Pan, C. Y., Recent Advances in RAFT Dispersion Polymerization for Preparation of Block Copolymer Aggregates. *Polym Chem-Uk* **2013,** *4* (4), 873-881.
(14) Cao, J.; Zhang, L. F.; Jiang, X. W.; Tian, C.; Zhao, X. N.; Ke, Q.; Pan, X. Q.; Cheng, Z. P.; Zhu, X. L., Facile Iron-Mediated Dispersant-Free Suspension Polymerization of Methyl Methacrylate via Reverse ATRP in Water. *Macromol Rapid Comm* **2013,** *34* (22), 1747-1754.
(15) Li, Z.; Chen, W. J.; Zhang, Z. B.; Zhang, L. F.; Cheng, Z. P.; Zhu, X. L., A Surfactant-Free Emulsion RAFT Polymerization of Methyl Methacrylate in a Continuous Tubular Reactor. *Polym Chem-Uk* **2015,** *6* (11), 1937-1943.
(16) Kagawa, Y.; Zetterlund, P. B.; Minami, H.; Okubo, M., Compartmentalization in Atom Transfer Radical Polymerization (ATRP) in Dispersed Systems. *Macromol Theor Simul* **2006,** *15* (8), 608-613.
(17) Zetterlund, P. B.; Okubo, M., Compartmentalization in Nitroxide-Mediated Radical Polymerization in Dispersed Systems. *Macromolecules* **2006,** *39* (26), 8959-8967.
(18) Thomson, M. E.; Cunningham, M. F., Compartmentalization Effects on the Rate of Polymerization and the Degree of Control in ATRP Aqueous Dispersed Phase Polymerization. *Macromolecules* **2010,** *43* (6), 2772-2779.
(19) Wang, J. S.; Matyjaszewski, K., Controlled Living Radical Polymerization - Atom-Transfer Radical Polymerization In the Presence Of Transition-Metal Complexes. *J Am Chem Soc* **1995,** *117* (20), 5614-5615.
(20) De Paoli, P.; Isse, A. A.; Bortolamei, N.; Gennaro, A., New Insights into the Mechanism of Activation of Atom Transfer Radical Polymerization by Cu(I) Complexes. *Chem Commun* **2011,** *47* (12), 3580-3582.
(21) Simakova, A.; Averick, S. E.; Konkolewicz, D.; Matyjaszewski, K., Aqueous ARGET ATRP. *Macromolecules* **2012,** *45* (16), 6371-6379.
(22) Payne, K. A.; D'hooge, D. R.; van Steenberge, P. H. M.; Reyniers, M. F.; Cunningham, M. F.; Hutchinson, R. A.; Marin, G. B., ARGET ATRP of Butyl Methacrylate: Utilizing Kinetic Modeling To Understand Experimental Trends. *Macromolecules* **2013,** *46* (10), 3828-3840.
(23) Matyjaszewski, K.; Jakubowski, W.; Min, K.; Tang, W.; Huang, J. Y.; Braunecker, W. A.; Tsarevsky, N. V., Diminishing Catalyst Concentration in Atom Transfer Radical Polymerization with Reducing Agents. *P Natl Acad Sci USA* **2006,** *103* (42), 15309-15314.
(24) Matyjaszewski, K.; Tsarevsky, N. V.; Braunecker, W. A.; Dong, H.; Huang, J.; Jakubowski, W.; Kwak, Y.; Nicolay, R.; Tang, W.; Yoon, J. A., Role of Cu0 in Controlled/"Living" Radical Polymerization. *Macromolecules* **2007,** *40* (22), 7795-7806.
(25) Zhang, Y.; Wang, Y.; Matyjaszewski, K., ATRP of Methyl Acrylate with Metallic Zinc, Magnesium, and Iron as Reducing Agents and Supplemental Activators. *Macromolecules* **2011,** *44* (4), 683-685.
(26) Konkolewicz, D.; Wang, Y.; Krys, P.; Zhong, M. J.; Isse, A. A.; Gennaro, A.; Matyjaszewski, K., SARA ATRP or SET-LRP. End of Controversy? *Polym Chem-Uk* **2014,** *5* (15), 4396-4417.

(27) Williams, V. A.; Matyjaszewski, K., Expanding the ATRP Toolbox: Methacrylate Polymerization with an Elemental Silver Reducing Agent. *Macromolecules* **2015,** *48* (18), 6457-6464.
(28) Williams, V. A.; Ribelli, T. G.; Chmielarz, P.; Park, S.; Matyjaszewski, K., A silver bullet: elemental silver as an efficient reducing agent for atom transfer tadical polymerization of acrylates. *J. Am. Chem. Soc.* **2015,** *137* (4), 1428-1431.
(29) Bortolamei, N.; Isse, A. A.; Magenau, A. J. D.; Gennaro, A.; Matyjaszewski, K., Controlled Aqueous Atom Transfer Radical Polymerization with Electrochemical Generation of the Active Catalyst. *Angew Chem Int Ed* **2011,** *50* (48), 11391-11394.
(30) Magenau, A. J. D.; Strandwitz, N. C.; Gennaro, A.; Matyjaszewski, K., Electrochemically Mediated Atom Transfer Radical Polymerization. *Science* **2011,** *332* (6025), 81-84.
(31) Park, S.; Chmielarz, P.; Gennaro, A.; Matyjaszewski, K., Simplified Electrochemically Mediated Atom Transfer Radical Polymerization using a Sacrificial Anode. *Angew Chem Int Ed* **2015,** *54* (8), 2388-2392.
(32) Lorandi, F.; Fantin, M.; Isse, A. A.; Gennaro, A., Electrochemically Mediated Atom Transfer Radical Polymerization of n-Butyl Acrylate on Non-Platinum Cathodes. *Polym Chem-Uk* **2016,** *7* (34), 5357-5365.
(33) Chmielarz, P.; Fantin, M.; Park, S.; Isse, A. A.; Gennaro, A.; Magenau, A. J. D.; Sobkowiak, A.; Matyjaszewski, K., Electrochemically Mediated Atom Transfer Radical Polymerization (eATRP). *Prog Polym Sci* **2017,** *69*, 47-78.
(34) Konkolewicz, D.; Schroder, K.; Buback, J.; Bernhard, S.; Matyjaszewski, K., Visible Light and Sunlight Photoinduced ATRP with ppm of Cu Catalyst. *Acs Macro Lett* **2012,** *1* (10), 1219-1223.
(35) Pan, X. C.; Tasdelen, M. A.; Laun, J.; Junkers, T.; Yagci, Y.; Matyjaszewski, K., Photomediated Controlled Radical Polymerization. *Prog Polym Sci* **2016,** *62*, 73-125.
(36) Mohapatra, H.; Kleiman, M.; Esser-Kahn, A. P., Mechanically Controlled Radical Polymerization Initiated by Ultrasound. *Nat Chem* **2017,** *9* (2), 135-139.
(37) Wang, Z. H.; Pan, X. C.; Yan, J. J.; Dadashi-Silab, S.; Xie, G. J.; Zhang, J. N.; Wang, Z. H.; Xia, H. S.; Matyjaszewski, K., Temporal Control in Mechanically Controlled Atom Transfer Radical Polymerization Using Low ppm of Cu Catalyst. *Acs Macro Lett* **2017,** *6* (5), 546-549.
(38) Tayal, A.; Kelly, R. M.; Khan, S. A., Rheology and Molecular Weight Changes During Enzymatic Degradation of a Water-Soluble Polymer. *Macromolecules* **1999,** *32* (2), 294-300.
(39) Paik, H. J.; Kickelbick, G.; Matyjaszewski, K., Immobilization of the Copper Catalyst in Atom-Transfer Radical Polymerization. *Abstr Pap Am Chem S* **1999,** *218*, U542-U542.
(40) Matyjaszewski, K.; Pintauer, T.; Gaynor, S., Removal of Copper-Based Catalyst in Atom Transfer Radical Polymerization using Ion Exchange Resins. *Macromolecules* **2000,** *33* (4), 1476-1478.
(41) Gromada, J.; Spanswick, J.; Matyjaszewski, K., Synthesis and ATRP Activity of New TREN-Based Ligands. *Macromol Chem Phys* **2004,** *205* (5), 551-566.
(42) Jasinski, N.; Lauer, A.; Stals, P. J. M.; Behrens, S.; Essig, S.; Walther, A.; Godmann, A. S.; Barner-Kowollik, C., Cleaning the Click: A Simple Electrochemical Avenue for Copper Removal from Strongly Coordinating Macromolecules. *Acs Macro Lett* **2015,** *4* (3), 298-301.

(43) Wei, Y. P.; Zhang, Q.; Wang, W. J.; Li, B. G.; Zhu, S. P., Improvement on Stability of Polymeric Latexes Prepared by Emulsion ATRP through Copper Removal using Electrolysis. *Polymer* **2016,** *106*, 261-266.
(44) Tsarevsky, N. V.; Matyjaszewski, K., "Green" Atom Transfer Radical Polymerization: From Process Design to Preparation of Well-Defined Environmentally Friendly Polymeric Materials. *Chem Rev* **2007,** *107* (6), 2270-2299.
(45) Fantin, M.; Chmielarz, P.; Wang, Y.; Lorandi, F.; Isse, A. A.; Gennaro, A.; Matyjaszewski, K., Harnessing the Interaction between Surfactant and Hydrophilic Catalyst to Control eATRP in Miniemulsion. *Macromolecules* **2017,** *50* (9), 3726-3732.
(46) Min, K.; Gao, H. F.; Matyjaszewski, K., Preparation of Homopolymers and Block Copolymers in Miniemulsion by ATRP using Activators Generated by Electron Transfer (AGET). *J Am Chem Soc* **2005,** *127* (11), 3825-3830.
(47) Kagawa, Y.; Minami, H.; Okubo, M.; Zhou, H., Preparation of Block Copolymer Particles by Two-Step Atom Transfer Radical Polymerization in Aqueous Media and its Unique Morphology. *Polymer* **2005,** *46* (4), 1045-1049.
(48) Simms, R. W.; Cunningham, M. E., High Molecular Weight Poly(butyl Methacrylate) via ATRP Miniemulsions. *Macromol Symp* **2008,** *261*, 32-35.
(49) Elsen, A. M.; Burdynska, J.; Park, S.; Matyjaszewski, K., Active Ligand for Low PPM Miniemulsion Atom Transfer Radical Polymerization. *Macromolecules* **2012,** *45* (18), 7356-7363.
(50) Fantin, M.; Park, S.; Wang, Y.; Matyjaszewski, K., Electrochemical Atom Transfer Radical Polymerization in Miniemulsion with a Dual Catalytic System. *Macromolecules* **2016,** *49* (23), 8838-8847.
(51) Min, K.; Yu, S.; Lee, H. I.; Mueller, L.; Sheiko, S. S.; Matyjaszewski, K., High Yield Synthesis of Molecular Brushes via ATRP in Miniemulsion. *Macromolecules* **2007,** *40* (18), 6557-6563.
(52) Teo, V. L.; Davis, B. J.; Tsarevsky, N. V.; Zetterlund, P. B., Successful Miniemulsion ATRP using an Anionic Surfactant: Minimization of Deactivator Loss by Addition of a Halide Salt. *Macromolecules* **2014,** *47* (18), 6230-6237.
(53) Fantin, M.; Isse, A. A.; Gennaro, A.; Matyjaszewski, K., Understanding the Fundamentals of Aqueous ATRP and Defining Conditions for Better Control. *Macromolecules* **2015,** *48* (19), 6862-6875.
(54) Tang, W.; Kwak, Y.; Tsarevsky, N. V.; Matyjaszewski, K., Effect of Ligand and Initiator Structures on the Equilibrium Constants in ATRP. *Abstr Pap Am Chem S* **2007,** *233*.
(55) Tang, W.; Kwak, Y.; Braunecker, W.; Tsarevsky, N. V.; Coote, M. L.; Matyjaszewski, K., Understanding Atom Transfer Radical Polymerization: Effect of Ligand and Initiator Structures on the Equilibrium Constants. *J Am Chem Soc* **2008,** *130* (32), 10702-10713.
(56) Fantin, M.; Isse, A. A.; Bortolamei, N.; Matyjaszewski, K.; Gennaro, A., Electrochemical Approaches to the Determination of Rate Constants for the Activation Step in Atom Transfer Radical Polymerization. *Electrochim Acta* **2016,** *222*, 393-401.
(57) Mastan, E.; Zhu, S. P., A Molecular Weight Distribution Polydispersity Equation for the ATRP System: Quantifying the Effect of Radical Termination. *Macromolecules* **2015,** *48* (18), 6440-6449.
(58) Nanda, A. K.; Matyjaszewski, K., Effect of Penultimate Unit on the Activation Process in ATRP. *Macromolecules* **2003,** *36* (22), 8222-8224.

(59) Jakubowski, W.; Matyjaszewski, K., Activators Regenerated by Electron Transfer for Atom-Transfer Radical Polymerization of (Meth)acrylates and Related Block Copolymers. *Angew Chem Int Ed* **2006,** *45* (27), 4482-4486.
(60) Tang, W.; Matyjaszewski, K., Effects of Initiator Structure on Activation Rate Constants in ATRP. *Macromolecules* **2007,** *40* (6), 1858-1863.
(61) Krys, P.; Matyjaszewski, K., Kinetics of Atom Transfer Radical Polymerization. *Eur Polym J* **2017,** *89*, 482-523.
(62) Beuermann, S.; Buback, M.; Davis, T. P.; Gilbert, R. G.; Hutchinson, R. A.; Kajiwara, A.; Klumperman, B.; Russell, G. T., Critically evaluated rate coefficients for free-radical polymerization, 3 - Propagation rate coefficients for alkyl methacrylates. *Macromol. Chem. Phys.* **2000,** *201* (12), 1355-1364.
(63) Egorova, K. S.; Ananikov, V. P., Which Metals are Green for Catalysis? Comparison of the Toxicities of Ni, Cu, Fe, Pd, Pt, Rh, and Au Salts. *Angew Chem Int Ed* **2016,** *55* (40), 12150-12162.
(64) Fukuda, T.; Goto, A., Gel permeation chromatographic determination of activation rate constants in nitroxide-controlled free radical polymerization .2. Analysis of evolution of polydispersities. *Macromol. Rapid Commun.* **1997,** *18* (8), 683-688.
(65) Chmielarz, P.; Park, S.; Sobkowiak, A.; Matyjaszewski, K., Synthesis of Beta-Cyclodextrin-Based Star Polymers via a Simplified Electrochemically Mediated ATRP. *Polymer* **2016,** *88*, 36-42.
(66) Beers, K. L.; Gaynor, S. G.; Matyjaszewski, K.; Sheiko, S. S.; Moller, M., The synthesis of densely grafted copolymers by atom transfer radical polymerization. *Macromolecules* **1998,** *31* (26), 9413-9415.
(67) Xia, J. H.; Matyjaszewski, K., Controlled/"Living" Radical Polymerization. Atom Transfer Radical Polymerization Catalyzed by Copper(I) and Picolylamine Complexes. *Macromolecules* **1999,** *32* (8), 2434-2437.
(68) Kaur, A.; Ribelli, T. G.; Schroder, K.; Matyjaszewski, K.; Pintauer, T., Properties and ATRP Activity of Copper Complexes with Substituted Tris(2-pyridylmethyl)amine-Based Ligands. *Inorg Chem* **2015,** *54* (4), 1474-1486.

Chapter 3 *Ab Initio* Emulsion Atom Transfer Radical Polymerization

3.1. Preface

The content of this chapter was published in *Angewwandte Chemie International Edition* (“Ab Initio Emulsion Atom‐Transfer Radical Polymerization”, F. Lorandi, Y. Wang, M. Fantin, K. Matyjaszewski, *Angewwandte Chemie International Edition*, **2018**, 57(27), 8270-8274.)

This is a continuation of the work presented in Appendix 1, where the ion-pair catalyst efficiently controlled the miniemulsion polymerization of (meth)acrylates. In this chapter, the application of the ion-pair catalyst in emulsion polymerization is presented. The polymerization kinetics, evolution of molecular weight and particle size, emulsion stability were investigated. Block, gradient copolymers were prepared *in situ*. The variation of solids content and reaction scale-up were conducted to evaluate the industrial potential.

The main experimental work was conducted by Dr. Francesca Lorandi. I contributed methacrylate polymerization experiments and the *in situ* block copolymerization. Acknowledgements are made to Dr. Xiaoyu Gao for his kind help in ICP-MS tests, and Guojun Xie and Liye Fu for the preparation of the initiators PEO_{1K}BiB and PEO_{2K}BPA, respectively.

The support from the National Science Foundation (CHE 1707490) was acknowledged. F. Lorandi acknowledged Fondazione Aldo Gini, Università di Padova.

3.2. Introduction

Emulsion polymerizations are relevant in many large-volume industrial applications because of the low environmental impact, low operation cost, good thermal properties, and accessibility to high-molecular-weight polymers. Nevertheless, conventional emulsion polymerization procedures cannot finely tune polymer topology and composition. Instead, polymer architecture is typically controlled by reversible deactivation radical polymerization (RDRP) techniques, which exploit a catalyst, a reversible trapping agent, or a chain transfer agent (CTA) to continuously activate and deactivate radicals. However, the implementation of RDRP in a true *ab initio* emulsion polymerization procedure is challenging.[1]

The main concern in emulsion RDRP is controlling the localization of the reaction. In conventional *ab initio* emulsion polymerization, initiation and particle nucleation spontaneously occur in the aqueous phase; then, the hydrophobic monomer continuously diffuses from large monomer droplets to nanometric polymer particles, and the polymerization proceeds inside the monomer-swollen particles. In emulsion RDRPs, the species that regulate the polymerization need to "follow" the growing chains in such a dynamic system, from the aqueous phase to the interior of hydrophobic polymer particles.

One effective strategy to this end is the polymerization-induced self-assembly (PISA) technique, in which amphiphilic block copolymers self-assemble into particles with precise morphologies.[2] The PISA approach was developed in aqueous emulsion reversible addition-fragmentation chain-transfer (RAFT) polymerization,[3] nitroxide mediated polymerization (NMP),[4] and organotellurium-mediated radical polymerization (TERP),[5]

by chain extending hydrophilic macroinitiators or macro-CTAs with hydrophobic monomers. Instead, *ab initio* emulsion RDRP with small molecule hydrophilic initiators is less explored. In this regard, the photo-induced *ab initio* emulsion TERP of methyl methacrylate (MMA) was recently reported, initiated by a hydrophilic TERP agent.[6]

Another technique to control polymerizations in "green" aqueous media is atom transfer radical polymerization (ATRP),[7] in which the catalytic couple $Cu^{I}L^{+}/X–Cu^{II}L^{+}$ (X = Cl, Br) finely tunes the equilibrium between active radicals and halogen-capped dormant species. In emulsion ATRP, however, both catalysts and initiators partition between the aqueous phase and hydrophobic monomer droplets, causing limited polymerization control and latex instability.[8] Undesired nucleation of large monomer droplets was observed when employing poorly water-soluble catalysts or initiators.[9] To avoid these issues, microemulsion,[10] miniemulsion,[11] and *seeded* emulsion[12] ATRP were developed: hydrophobic catalysts and initiators were confined inside the polymerizing droplets that acted as mini-bulk reactors in which the whole polymerization process occurred, providing well-defined polymers. Nevertheless, the requirement of very high surfactant concentration and/or shearing forces makes these procedures less industrially viable than a true *ab initio* emulsion ATRP.

Two approaches to an *ab initio* emulsion ATRP were recently reported. One employed a hydrophilic catalyst and a tetraalkylammonium salt as phase transfer agent.[13] However, acetone was added to aid monomer solubility, while low solid content (5 wt%) and high surfactant loading (26 wt% to monomer) were employed. The other approach exploited an amphiphilic surfactant-catalyst, composed of a ligand with a long hydrophobic "tail" and a hydrophilic "head" that bound to Cu ions.[14] Particles were effectively

nucleated in the aqueous phase, but polymerization was poorly controlled due to the low mobility of this catalyst, which was bound to the particles' surface. Therefore, it appears that the ideal catalyst for an *ab initio* emulsion ATRP should be amphiphilic and have high mobility to control polymer growth both in the aqueous phase and within the nucleated hydrophobic particles.

Recently, we developed an effective amphiphilic catalytic system for miniemulsion ATRP, based on a hydrophilic complex, Cu/tris(2-pyridylmethyl)amine (Cu/TPMA), and an anionic surfactant, sodium dodecyl sulfate (SDS).[15] These two species strongly interacted, resulting in a large fraction of Cu/TPMA (~90%) bonded to SDS at the interface of monomer droplets, while a smaller fraction (~1%) entered the droplets as neutral ion pairs [$Cu^{I}TPMA^{+}$/dodecyl sulfate $(DS)^{-}$] or [Br-$Cu^{II}TPMA^{+}/DS^{-}$] (**Scheme 3-1**). A third small fraction of Cu/TPMA remained in the aqueous phase. This catalytic system effectively controlled a miniemulsion ATRP, demonstrating good mobility/transfer between phases,[15] and thus emerged as a promising candidate for *ab initio* emulsion ATRP.

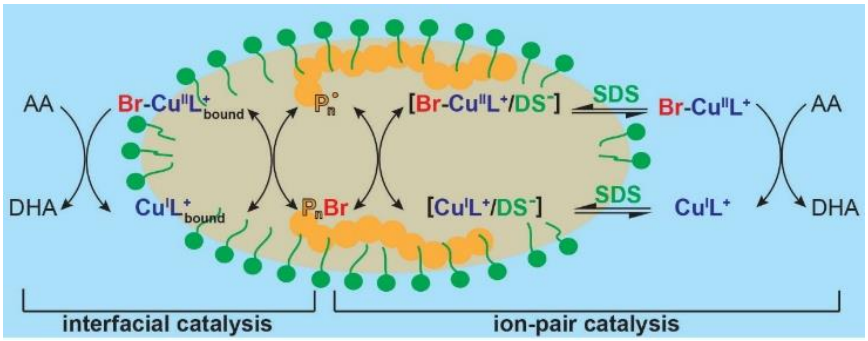

Scheme 3-1. Mechanism of activators regenerated by electron transfer (ARGET) ATRP in hydrophobic particles dispersed in water, with Br–$Cu^{II}L^{+}$ (L = TPMA) as catalyst, SDS as surfactant, and ascorbic acid (AA) as reducing agent that is oxidized to dehydroascorbic acid (DHA). Combination of ion-pair catalysts ([Br–$Cu^{II}L^{+}/DS^{-}$], [$Cu^{I}L^{+}/DS^{-}$]) and interfacial catalysts (Br–$Cu^{II}L^{+}_{bound}$, $Cu^{I}L^{+}_{bound}$).

Herein, a true *ab initio* emulsion ATRP is reported for polymerization of various (meth)acrylates, employing Cu/TPMA as catalyst and SDS as surfactant. Water-soluble initiators ensured that initiation occurred in the aqueous phase, thereby inducing aqueous particle nucleation. Small amounts of the active Cu^{I} species were (re)generated by ascorbic acid as water-soluble reducing agent (**Figure 1**). Final latexes were stable for more than one year, and polymers had low dispersity (*Đ*), and molecular weights (MWs) that matched theoretical values.

3.3. Results and Discussion

The polymerization of *n*-butyl acrylate (BA) was initially investigated at T = 65 °C and with 18.4 wt% of SDS relative to BA. NaBr was added to prevent dissociation of Br-$Cu^{II}L^{+}$ due to complexation of $Cu^{II}L^{+}$ with water or DS^{-}.[7, 16] 2-Hydroxyethyl-2-bromoisobutyrate (HEBiB) was selected as the water-soluble initiator. 77% Conversion was measured after 7 h, obtaining PBA with $Đ$ = 1.15 (**Table 3-1, entry 1** and **Figure 3-1**). Dynamic light scattering (DLS) revealed monodisperse nanoparticles with final volumetric average size d_v = 106.3 ± 0.6 nm. Indeed, d_v increased with conversion (**Figure 3-2a**), as typical for an emulsion polymerization.

Table 3-1. *Ab initio* emulsion ARGET ATRP of (meth)acrylic monomers.[a]

Entry	M	RBr	C_{SDS} (wt%)[b]	Stirring rate	t (h)	Conv. (%)	k_p^{app} (h^{-1})	$M_{n,th}$ × 10^{-3}	M_n × 10^{-3}	$Đ$	d_v (nm)
1	BA	HEBiB	18.4	500	7	77	0.23	49.9	55.8	1.15	106.3 ± 0.6
2	BA	HEBiB	9.2	500	8	75	0.17	48.1	62.0	1.13	119.9 ± 0.3

3	BA	HEBiB	4.6	250	18	77	0.08	49.7	64.2	1.16	186.2 ± 1.6
4	BA	HEBiB	2.3	150	24	83	0.07	53.9	80.3	1.36	473.2 ± 4.8
5[c]	BA	HEBiB	4.6	250	21	60	0.05	38.9	64.1	1.19	135.5 ± 0.4
6[d]	BA	HEBiB	4.6	250	21	61[e]	0.05	38.9	58.2	1.26	277.0 ± 7.3
7[f]	BA	PEO_{1K}BiB	18.4	500	7	74	0.20	28.7	30.1	1.15	100 ± 14
8	BA	PEO_{1K}BiB	4.6	500	18	78	0.08	52.0	69.9	1.27	427 ± 54
9[g]	MMA	PEO_{2K}BPA	18.4	250	7	>99	0.49	54.4	49.7	1.15	33.8 ± 0.9
10[g]	MMA	PEO_{2K}BPA	2.3	250	24	67	0.04	39.9	37.4	1.37	103.0 ± 1.3
11[g]	BMA	PEO_{2K}BPA	18.4	250	8	52	0.09	40.3	34.8	1.20	468 ± 32
12[g]	BMA	OH-BPA	18.4	250	6	82	0.29	62.3	54.5	1.13	n.d.

[a] 20 vol% monomer (M) in H_2O, V_{tot} = 10 mL, C_M/C_{RBr} = 500/1, $C_{NaBr}/C_{Cu^{II}TPMA^{2+}}$ = 100, $C_{Cu^{II}TPMA^{2+}} = C_{Cu^{II}L^{2+}} 10^{-3}$ M (L = TPMA), T = 65 °C. AA: 0.16 molar equivalents to Cu (eq.) injected at t = 0 + 0.16 eq./h feeding. [b] relative to monomer. [c] V_{tot} = 100 mL. [d] 40 vol% BA. [e] coagulum < 2 % (wt/wt polymer). [f] C_M/C_{RBr} = 280/1. [g] $C_{Cu^{II}TPMA^{2+}} = 5.6 \times 10^{-4}$ M, T = 45 °C. AA: 0.29 eq. injected at t = 0 + 0.29 eq./h feeding.

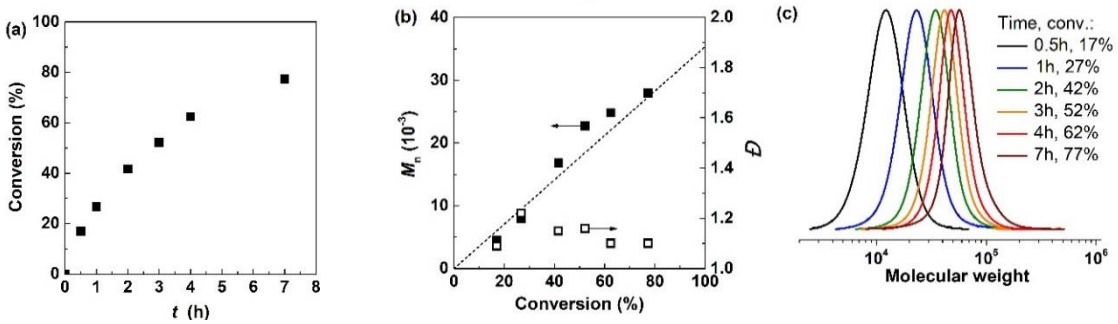

Figure 3-1. Kinetic plot (a), evolution of MW and *Đ* with conversion (b), and GPC traces (c) for *ab initio* emulsion ARGET ATRP of BA 20 vol% (conditions in **Table 3-1, entry 1**).

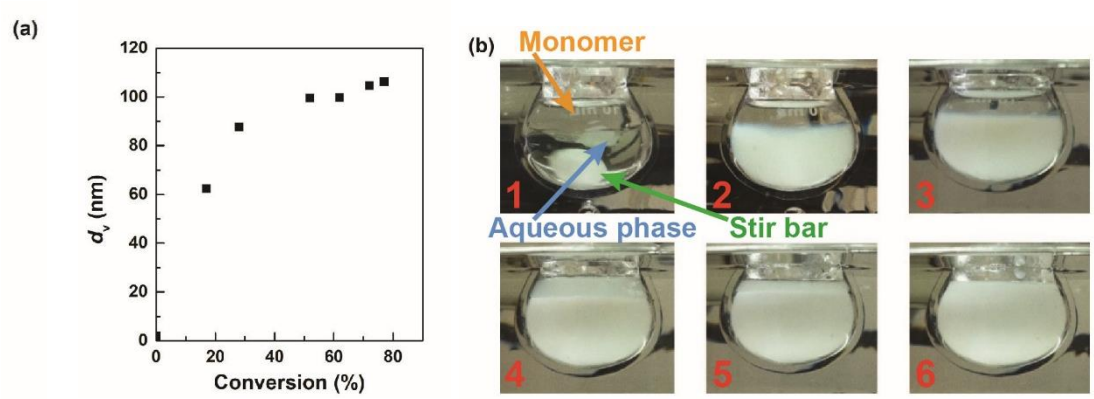

Figure 3-2. Evolution of particle size measured by DLS (a). Photographs of the polymerization mixture during *ab initio* emulsion ARGET ATRP of BA 20 vol% (b). Photographs taken at interval of ca. 30 minutes (**Table 3-1**, **entry 1**).

A well-controlled *ab initio* emulsion ATRP requires initiation and nucleation to occur in the aqueous phase, without migration of catalyst and initiator to the large monomer droplets. This was achieved by a simple experimental procedure: first, the aqueous phase containing SDS, $Cu^{II}Br_2$/TPMA, NaBr, and initiator (RBr) was degassed in a Schlenk flask; then, the degassed monomer was slowly fed into the flask without stirring. Two separated layers were obtained, with the low-density monomer on top of the aqueous phase (**Figure 3-2b, picture 1**). Then, AA was injected and stirring was activated to start the polymerization. As the polymerization progressed, the dispersed monomer slowly diffused to the growing polymer particles (**Figure 3-2b**, **pictures 2-5**). In summary, avoiding pre-mixing of the two phases prevented undesired partitioning of catalyst and initiator. Conversely, when the two phases were extensively mixed before starting the polymerization, both micelles and larger monomer droplets were nucleated, thus leading to a bimodal distribution of MW and high $Đ$ (**Table 3-2** and **Figure 3-3**). Additionally, the stirring rate should be low (≤ 500 rpm) to promote an effective aqueous nucleation and

preserve the colloidal stability. A higher stirring rate (1000 rpm) caused the polymerization to stop at low conversion (**Table 3-3** and **Figure 3-4**) after coagulation of polymer particles.

Table 3-2. *Ab initio* emulsion ARGET ATRP of BA with different pre-mixing procedures.[a]

Entry	Pre-mixing time (min) [b]	t (h)	Conv. (%)	k_p^{app} (h^{-1})	$M_{n,th}$ ($\times 10^{-3}$)	M_n ($\times 10^{-3}$)	$Đ$	d_v (nm)
1 [c]	60	5	89	0.45	32.9	34.4	2.11	1265±130
2	10	5	74	0.25	27.3	34.0	1.67	166.6±1.3
3	No mixing	5	82	0.33	30.0	30.4	1.59	213.4±4.0

[a] BA 20 vol% in H_2O, V_{tot} = 10 mL, C_{BA}/C_{HEBiB} = 280/1, C_{NaBr} = 0.1 M, $C_{Cu^{II}TPMA^{2+}} = 10^{-3}$ M. C_{SDS} = 18.4% wt. rel to BA. AA: 0.16 eq. injected at t = 0 + feeding at 0.16 eq./h. Stirring rate = 500 rpm, T = 65 °C. [b] duration of monomer and water phase mixing, before injecting AA to start the polymerization. [c] Stirring rate = 1500 rpm.

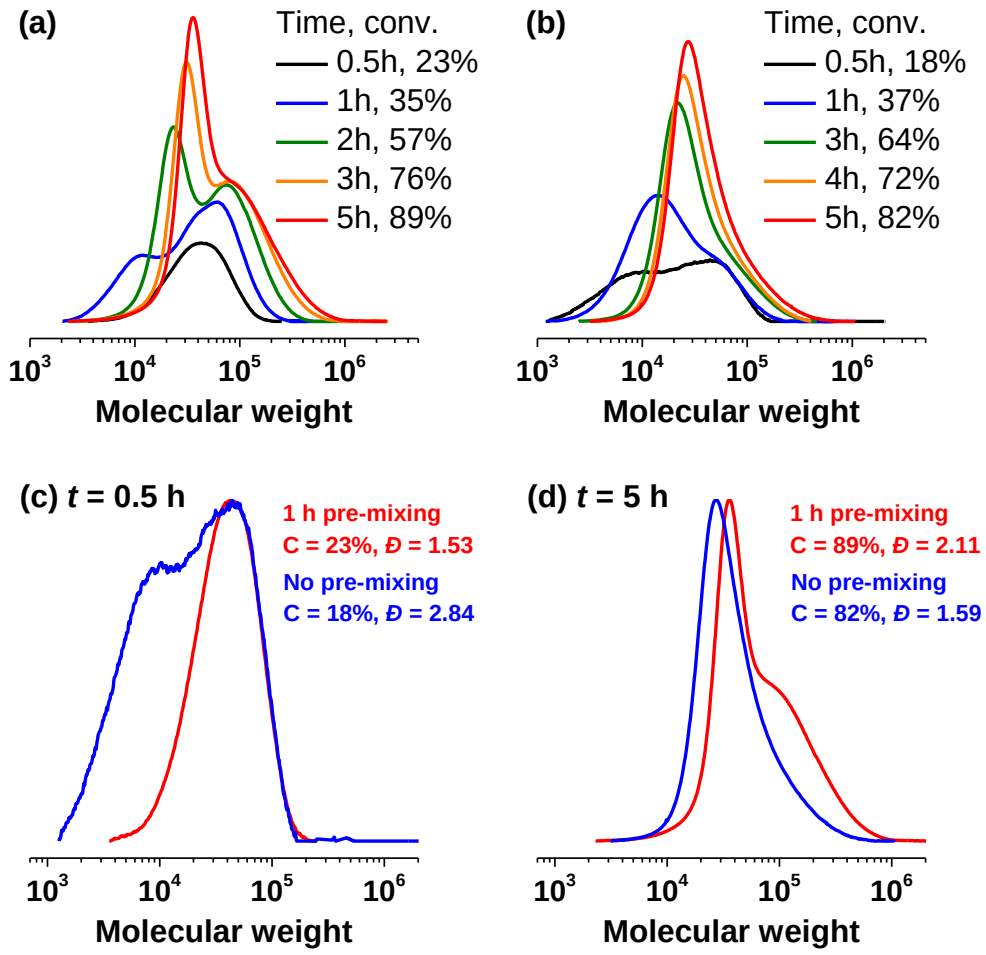

Figure 3-3. GPC traces of PBA from *ab initio* emulsion ARGET ATRP with different preparative procedures: a) 1 h pre-mixing of water phase and monomer, b) no pre-mixing, c) and d) comparison of the GPC traces for polymers prepared at the same reaction time, for the two different pre-activation conditions in **Table 3-2** entry 1 and 3).

Table 3-3. Effect of stirring rate on an *ab initio* emulsion ARGET ATRP of BA, RBr = HEBiB, C_{SDS} = 4.6% wt. relative to BA, T = 65 °C.[a]

Entry	Stirring rate	t (h)	Conv. (%)	k_p^{app} (h^{-1})	$M_{n,th}$ (× 10^{-3})	M_n (× 10^{-3})	$Đ$	d_v (nm)	*Remark (see table S4)*
1[b]	250	18	77	0.08	49.7	64.2	1.16	176.6±0.2	
2	500	6	61	0.16	39.2	55.8	1.21	1069±122	low coagulation

3	1000	5	26	0.07	17.0	14.9	1.43	-	unstable

[a] $C_{BA}/C_{HEBiB}/C_{NaBr}/C_{Cu^{II}TPMA^{2+}}$ = 500/1/36/0.36, BA 20 vol% in H_2O, V_{tot} = 10 mL. AA: 0.16 eq. injected at t = 0 + feeding at 0.16 eq./h. [b] also in **Table 3-1, entry 3**.

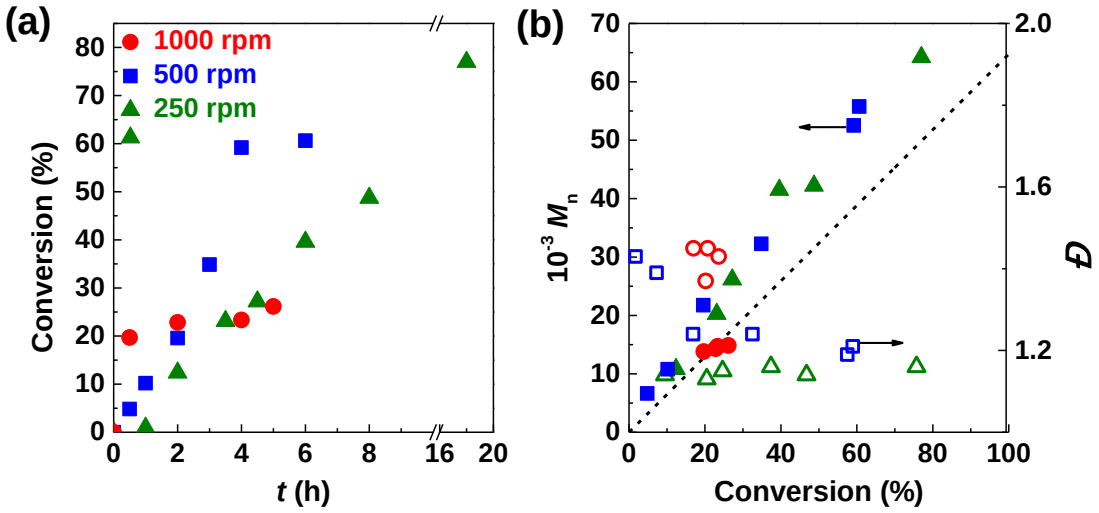

Figure 3-4. *Ab initio* emulsion ARGET ATRP of BA with C_{SDS} = 4.6% wt. rel. to BA and different stirring rates. Conversion vs. time (a) and MWs and dispersity evolution vs. conversion (b). Conditions in **Table 3-3**.

Aqueous initiation in emulsion ATRP was ensured by the combination of the hydrophilic Cu/TPMA catalyst with a water-soluble RBr. In fact, replacing the hydrophilic HEBiB initiator with the hydrophobic ethyl α-bromoisobutyrate (EBiB) resulted in a 7-times slower and much less controlled polymerization (**Table 3-4**). EBiB partitioned itself between the aqueous phase and the monomer phase, causing very poor initiation efficiency and a tailing toward low MWs in the gel permeation chromatography (GPC) traces (**Figure 3-5**). In another control experiment, the catalyst Cu/TPMA was replaced by the similarly active, but much more hydrophobic Cu/bis[2-(4-methoxy-3,5-dimethyl)-

pyridylmethyl]octadecylamine) (Cu/BPMODA*) catalyst complex. Again, the polymerization was much slower, with a bimodal MW distribution and $M_n >> M_{n,th}$ (**Table 3-4, Figure 3-6**). These results confirmed that both water-soluble RBr and hydrophilic catalyst were necessary for efficient aqueous initiation and nucleation. The preparative procedure helped the aqueous nucleation by minimizing the undesired monomer nucleation, but was not sufficient to guarantee well-controlled polymerization with more hydrophobic catalyst or initiator.

Table 3-4. Emulsion ARGET ATRP of BA with different ligands and initiators.[a]

Entry	L	RBr	t (h)	Conv. (%)	k_p^{app} (h^{-1})	$M_{n,th}$ ($\times 10^{-3}$)	M_n ($\times 10^{-3}$)	$Đ$	d_v (nm)
1	TPMA	EBiB	5.5	13	0.03	8.8	46.6	1.11	65.9 ± 0.9
2	BPMODA*	HEBiB	9	26	0.04	16.9	41.8	1.32	unstable

[a] $C_{BA}/C_{RX}/C_{NaBr}/C_{Cu^{II}L^{2+}}$ = 500/1/36/0.36, BA 20 vol% in H_2O, V_{tot} = 10 mL, T = 65 °C, C_{SDS} = 18.4% wt. rel. to BA. AA: 0.16 eq. injected at t = 0 + feeding at 0.16 eq./h. Stirring rate = 500 rpm.

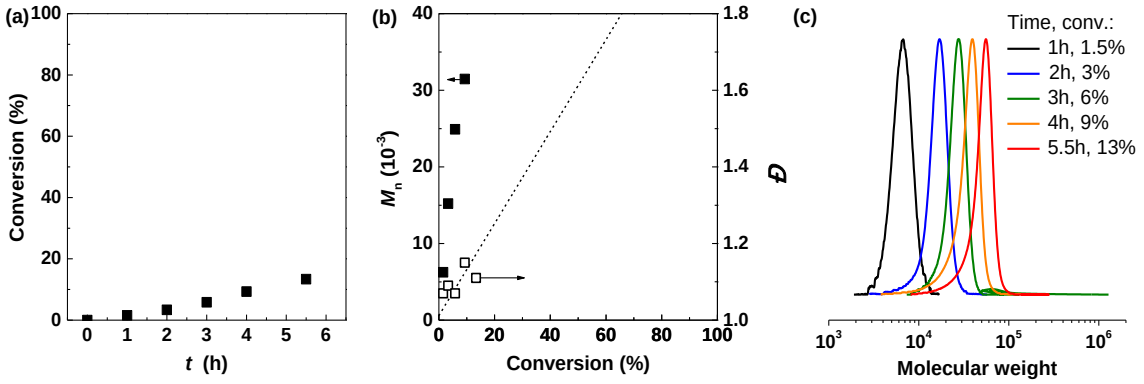

Figure 3-5. Emulsion ARGET ATRP of BA with RBr = EBiB. Conversion vs. time (a) and MWs and dispersity evolution vs. conversion (b), and GPC traces (c). Conditions in **Table 3-4**, **entry 1**.

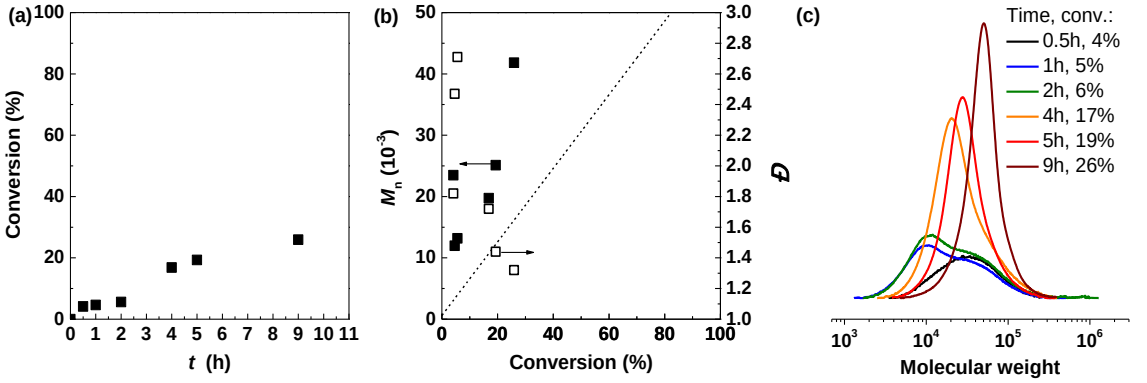

Figure 3-6. Emulsion ARGET ATRP of BA catalyzed by Cu/BPMODA*. Conversion vs. time (a) and MWs and dispersity evolution vs. conversion (b), and GPC traces (c). Conditions in **Table 3-4**, **entry 2**.

The amount of SDS was progressively reduced from 18.4 wt% to 2.3 wt% relative to BA (**Table 3-1, entries 2-4**). The stirring rate was also reduced to ensure effective nucleation and stability of the formed latex. The polymerization rate decreased with decreasing C_{SDS} and stirring rate, whereas the particle size increased with decreasing C_{SDS} while maintaining a monomodal distribution. In particular, much larger particles (ca. 473 nm) were obtained with 2.3 wt% SDS, which is a low amount of surfactant for an emulsion

polymerization (0.4 wt% of total), and is only slightly above the critical micelle concentration.[1]

The procedure was scaled to a larger size by increasing the reaction volume from 10 to 100 mL, with 4.6 wt% of SDS relative to BA (**Table 3-1, entry 5**). The same magnetic-stirring setup was used for both experiments. A stable latex was obtained with $Đ$ = 1.19 and d_v = 135.5 ± 0.4 nm. The slightly lower polymerization rate, if compared to the smaller 10 mL dispersion ($k_p^{app} = 0.05$ vs. $k_p^{app} = 0.08$), could be due to a slightly less efficient stirring in the higher-volume reaction.

The solid content was successfully increased from 20 to 40 vol%, with constant 4.6 wt% of SDS (**Table 3-1, entry 6**). At 40 vol% monomer, the process was well-controlled, and minimal coagulum was observed, < 2% of total polymer mass. Particle size gradually increased with conversion, reaching d_v = 277.0 ± 7.3 nm (**Figure 3-7**). Similar polymerization rates were obtained with either 20 vol% or 40 vol% monomer.

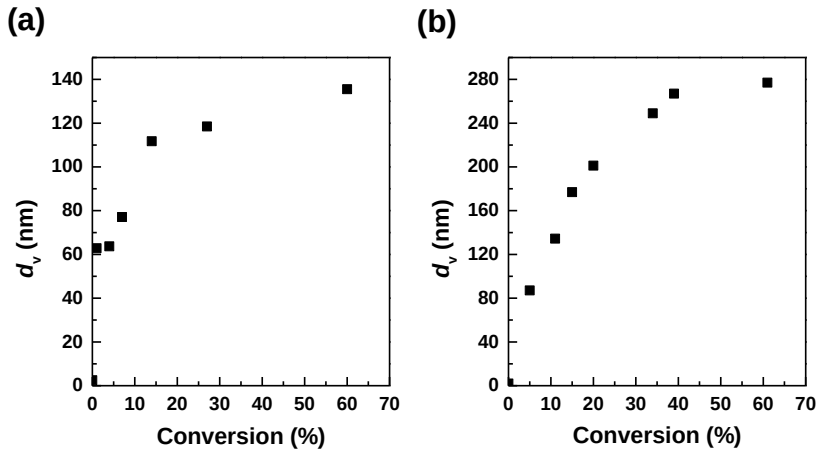

Figure 3-7. Evolution of particles size measured by DLS, during *ab initio* emulsion ARGET ATRP of (a) BA 20 vol% in H_2O, V_{tot} = 100 mL, (b) BA 40 vol% in H_2O, V_{tot} = 10 mL. Other conditions: C_{BA}/C_{HEBiB} = 500/1, C_{NaBr} = 0.1 M, $C_{Cu^{II}TPMA^{2+}} = 10^{-3}$ M, C_{SDS}

= 4.6% wt. rel. to BA, stirring rate = 250 rpm, T = 65 °C. AA: 0.16 eq. injected at t = 0 + feeding at 0.16 eq./h.

The versatility of the technique was tested by varying the nature of the hydrophilic initiator. When RBr = poly(ethylene oxide) α-bromoisobutyrate ($PEO_{1K}BiB$, MW_{PEO} = 1,000), BA polymerizations were well-controlled, even when targeting a lower degree of polymerization (DP) and decreasing the SDS loading (**Table 3-1, entries 6-7**). The obtained latex was less stable, showing complete sedimentation ~10 minutes after the stirring was stopped (**Figure 3-8**). There was no coagulum and the particles could be re-dispersed by stirring, allowing to measure a monomodal distribution of nanometric particles. This phenomenon was observed only for RX = $PEO_{1K}BiB$, and it was exploited to purify the polymer: after sedimentation, the supernatant was collected, and the polymer particles were washed with water 4 times. Following this procedure, (96.6 ± 0.6)% of the Cu loading remained in the aqueous fractions, as measured by inductively coupled plasma mass spectrometry analysis of the obtained polymer. Similarly, part-per-billion amounts of residual Cu was detected in polymers prepared *via* miniemulsion ATRPs conducted with Cu/TPMA and SDS.[1-2] Essentially, after crashing the (mini)emulsion, the hydrophilic Br-$Cu^{II}TPMA^{+}$ catalyst migrated into the aqueous phase leaving a "pure" product. The spontaneous separation of the polymer matrix with low level of Cu contamination observed herein can simplify separation and purification procedures and could provide a procedure for catalyst recycling.

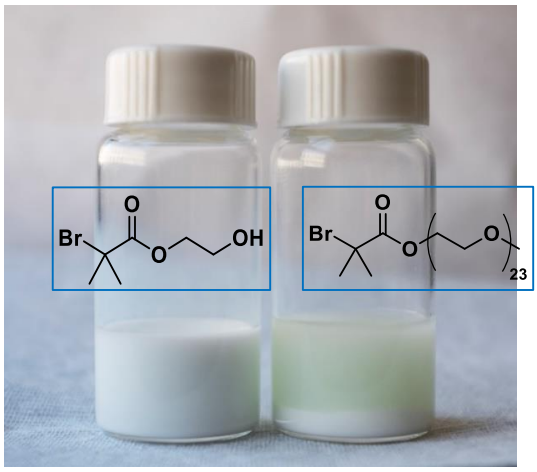

Figure 3-8. Latexes stability soon after polymerizations were stopped, for *ab initio* emulsion ARGET ATRP of BA 20 vol%, with RBr = HEBiB (left), RBr = $PEO_{1K}BiB$ (right). Experimental details in **Figure 3-1, main text** (left) and **错误!未找到引用源。** (right).

Methacrylate monomers were also polymerized (**Table 3-1, entries 9-12**); temperature was reduced to 45 °C due to their higher ATRP reactivity.[3] Poly(ethylene oxide) 2-bromo-2-phenylacetate ($PEO_{2K}BPA$, MW_{PEO} = 2,000) was used as the water-soluble initiator. An *ab initio* emulsion ATRP of MMA with 18.4 wt% SDS reached full conversion in 7 h, with $Đ$ = 1.15 and d_v = 33.8 ± 0.9 nm (**Table 3-1, entry 8**). Lower SDS loading, 2.3 wt% relative to MMA, slowed down the polymerization ($k_p^{app} = 0.04$ vs. $k_p^{app} = 0.49$, **Table 3-1**, **entry 9**), as observed for BA. Moreover, particles size increased, d_v = 103.0 ± 1.3 nm, and dispersity was slightly higher, $Đ$ = 1.37, because of the diminished concentration of [Br-Cu^{II}TPMA$^+$/DS^-] ion pairs. PMMA particles were much smaller than PBA particles formed with the same C_{SDS}; this is consistent with MMA having a higher nucleation efficiency because of its higher solubility in water.[4]

Ab initio emulsion ARGET ATRP of *n*-butyl methacrylate (BMA) was conducted with 18.4 wt% SDS relative to BMA, resulting in 52% conversion and polymer with $Đ$ = 1.20 in 8h (**Table 3-1, entry 10**), forming a latex that was stable for at least 6 months. Interestingly, the polymerization of BMA with a different water-soluble initiator, 2-hydroxyethyl 2-bromo-2-phenylacetate (OH-BPA), gave a 3-fold faster polymerization, with lower $Đ$ = 1.13 (**Table 3-1, entry 11**).

Cu/TPMA loading was diminished in both BA and BMA polymerizations (**Table 3-5**). In the case of BA, C_{Cu} was successfully reduced to 100 ppm, reaching 88% conversion in 5 h. At constant feeding rate of AA, the polymerization rate increased with decreasing Cu content because a relatively higher amount of active Cu^{I} species was generated.[2] In the case of BMA polymerization, as low as 55 ppm of Cu gave polymer with $Đ$ < 1.45, small coagulation (< 10% wt/wt polymer) and a larger particle size.

Table 3-5. Effect of catalyst loading in *ab initio* emulsion ARGET ATRPs.[a]

Entry	M	C_{Cu} (ppm)	AA feeding (eq./h)	t (h)	Conv. (%)	k_p^{app} (h^{-1})	$M_{n,th}$ × 10^{-3}	M_n × 10^{-3}	$Đ$	d_v (nm)	*Remark*
1	BA	200	0.57	8	88	0.25	56.9	46.5	1.23	141.3±8.6	
2	BA	100	1.14	5	88	0.46	57.0	60.3	1.34	296.7±1.5	
3	BA	50	2.29	4	82	0.42	52.7	56.8	2.72	> 5000	
4	BMA	221	0.57	14	80	0.098	60.6	67.7	1.43	629±30	< 10% coagulation
5	BMA	111	1.14	9	74	0.15	57.1	58.4	1.29	1639±251	< 10% coagulation
6	BMA	55	2.29	5	72	0.24	54.8	29.5	1.50	> 5000	
7	BMA	55	0.28	9	69	0.12	52.6	43.3	1.42	> 5000	

[a] C_M/C_{RX} = 500/1, $C_{NaBr}/C_{Cu^{II}TPMA^{2+}}$ = 100/1, M 20 vol% in H_2O, V_{tot} = 10 mL, C_{SDS} = 18.4% wt. rel. to monomer. BA: RX = HEBiB, T = 65 °C, stirring rate = 500 rpm. BMA: RX =PEO_{2K}BPA, T = 45 °C, stirring rate = 250 rpm.

The retention of chain-end functionality was tested by chain extension of a PBA-Br macroinitiator prepared by emulsion ARGET ATRP (**Figure 3-9a**). The polymerization of the first BA block was driven to 92% conversion (DP = 135); then, *t*-butyl acrylate (*t*BA) was injected, and good chain extension-initiation efficiency was observed with low dispersity, $Đ$ < 1.2 (**Table 3-6**).

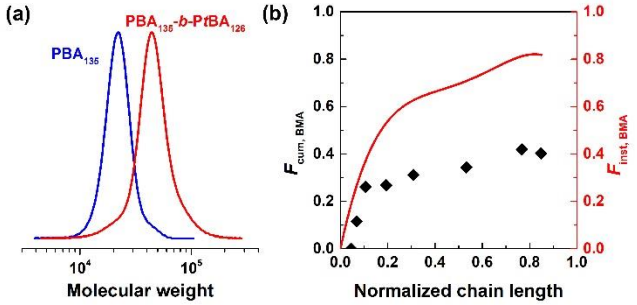

Figure 3-9. (a) GPC traces of PBA-Br and PBA-*b*-P*t*BA prepared by *ab initio* emulsion ARGET ATRP: $C_{BA}/C_{RBr}/C_{NaBr}/C_{Cu^{II}TPMA^{2+}}$= 150/1/20/0.2, BA 6 vol% in H_2O, V_{tot} = 10 mL, SDS 8 wt% relative to final solids. AA: 0.16 eq. injected at t = 0 + feeding at 0.16 eq./h. Stirring rate = 250 rpm. 0.8 mL of *t*BA injected after BA reached 92% conversion. (b) PMMA-*grad*-PBMA by *ab initio* emulsion ARGET ATRP: instantaneous and cumulative fraction of BMA. $C_{MMA}/C_{BMA}/C_{PEO2KBPA}/C_{NaBr}/C_{Cu^{II}TPMA^{2+}}$= 299/201/1/20/0.2, MMA 10 vol% + BMA 10 vol% in H_2O, V_{tot} = 20 mL. AA: 0.28 eq. injected at t = 0 + feeding at 0.28 eq./h. Stirring rate = 250 rpm, T = 45 °C.

Table 3-6. *Ab initio* emulsion ARGET ATRP with *in situ* generation of random, block and gradient copolymers.

Entry	RX	M	DP	C_{SDS}	t	Conv.	k_p^{app}	$M_{n,th}$	M_n	$Đ$	d_v
					(h)	(%)	(h^{-1})	× 10^{-3}	× 10^{-3}		(nm)

1 [a]	HEBiB	BA	150	18.4	6	92	0.38	18.1	19.4	1.12	
	PBA-Br	*t*BA	182		16.5	69	0.07	35.5	36.0	1.14	n.d.
2 [a]	HEBiB	BA	150	8	6	53	0.13	10.6	13.2	1.12	
	PBA-Br	*t*BA	182		18	59	0.05	32.4	39.1	1.13	55.8±0.6
3 [a]	HEBiB	BA	150	8	13	90	0.18	17.7	21.0	1.09	
	PBA-Br	*t*BA	182		22	69	0.05	37.1	41.4	1.18	51.5±0.3
4 [b]	$PEO_{2K}BPA$	MMA+BMA	500 [c]	9.2	13	85	0.12	53.8	45.5	1.23	540±61

[a] $C_{BA}/C_{HEBiB}/C_{NaBr}/C_{Cu^{II}TPMA^{2+}}$ = 150/1/20/0.2, BA 6 vol% in H_2O, V_{tot} = 10 mL. AA: 0.16 eq. injected at t = 0 + feeding at 0.16 eq./h. Stirring rate = 250 rpm, T = 65 °C. 0.8 mL of *t*BA injected dropwise *in situ*. [b] $C_{MMA}/C_{BMA}/C_{PEO2KBPA}/C_{NaBr}/ C_{Cu^{II}TPMA^{2+}}$ = 299/201/1/20/0.2, MMA 10 vol% + BMA 10 vol% in H_2O, V_{tot} = 20 mL. AA: 0.28 eq. injected at t = 0 + feeding at 0.28 eq./h. Stirring rate = 250 rpm, T = 45 °C. [c] $DP_{MMA}+DP_{BMA}$.

Emulsion RDRP procedures are straightforward techniques to prepare gradient copolymers by taking advantage of the different water solubility of monomers that would otherwise have similar reactivity ratios. When mixing equal volumes of MMA and BMA, MMA was preferentially polymerized in the initial stage of the reaction due to its higher water-solubility. Then, the polymer gradually incorporated BMA, with its cumulative and instantaneous fractions, $F_{cum,BMA}$ and $F_{inst,BMA}$,[5] constantly increasing during polymerization (**Figure 3-9b**). A total conversion of 85% was obtained in 13h, and the final copolymer showed $Đ$ = 1.23 (Figure 3-10).

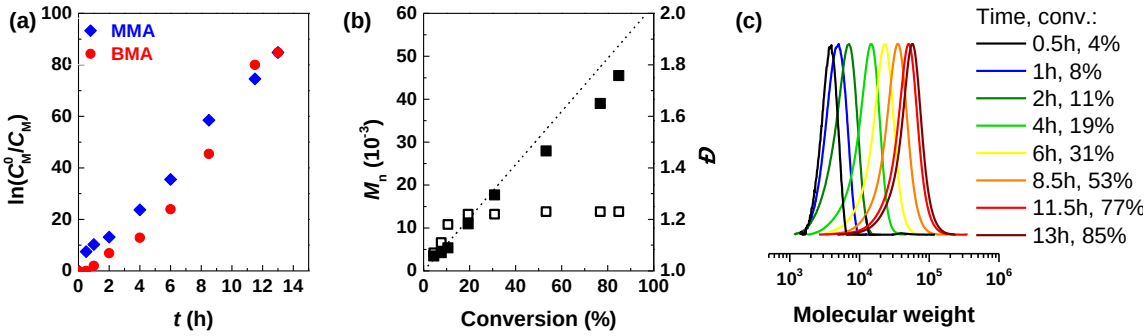

Figure 3-10. PMMA-*grad*-PBMA copolymer by *ab initio* emulsion ARGET ATRP (**Table 3-6**, **entry 4**). a), b) conversion vs. time for the two monomers, and evolution of MW and dispersity with conversion, and c) GPC traces.

3.4. Conclusion

In conclusion, a true *ab initio* emulsion ARGET ATRP of (meth)acrylic monomers was developed. Polymer particles were efficiently nucleated in the aqueous phase by using water-soluble initiators in combination with a hydrophilic catalyst, Cu/TPMA, which tuned the polymerization in the aqueous phase and in the polymer particles thanks to the strong interaction with the SDS surfactant. Polymers showed pre-determined MWs and low dispersity. Long-term stable latexes were obtained, even for SDS loading < 3 wt% relative to monomer. Gradient and block copolymers were simply generated *in situ*. Reaction volume and solid content were successfully increased to 100 mL and 40 vol%, respectively, suggesting a facile scale-up of this technique. The proposed setup could be directly integrated in existing industrial plants used for emulsion free radical polymerization.

3.5. Experimental Section

Materials. Copper(II) bromide ($Cu^{II}Br_2$, 99%), sodium dodecyl sulfate (SDS, 99%), tetrahydrofuran (THF, > 99%), ethyl α-bromoisobutyrate (EBiB, 98%), 2-hydroxyethyl 2-bromoisobutyrate (HEBiB, 95%) and ascorbic acid (AA) were purchased from Sigma-Aldrich. Sodium bromide (NaBr, 99%) was purchased from Acros. Tris(2-pyridylmethyl)amine (TPMA), bis[2-(4-methoxy-3,5-dimethyl)pyridylmethyl]octadecyl-amine (BPMODA*), poly(ethylene oxide) bromophenyl acetate ($PEO_{2K}BPA$), poly(ethylene oxide) isobutyryl bromide ($PEO_{1K}BiB$) were prepared according to published procedures.[6-8] *n*-Butyl acrylate (BA, 99%, Aldrich), *n*-butyl methacrylate (BMA, 99%, Aldrich), *t*-butyl acrylate (*t*BA, 98%, Aldrich), methyl methacrylate (MMA, 99%, Aldrich) were passed through a column filled with basic alumina prior to use, to remove polymerization inhibitors.

Instrumentation

M_n and $Đ$ were determined by gel permeation chromatography (GPC), with Polymer Standards Services (PSS) columns (guard, 10^5, 10^3, and 10^2 Å) and a differential refractive index detector (Waters, 2410), with THF as eluent at a flow rate of 1.00 mL/min (T = 35 °C). GPC traces were processed by WinGPC 8.0 software (PSS) using a calibration based on linear polystyrene (PS) or poly(methyl methacrylate) (PMMA) standards, for acrylates and methacrylates, respectively.

Monomer conversion was determined by gravimetric analysis, by evaporating samples at 110 °C for at least 30 min.

Particles size was determined by using a Zetasizer Nano from Malvern Instruments, Ltd. For all samples, the measurement was repeated after few weeks, and after few months. Samples mentioned in the main text as possessing long-term stability exhibited a particles size variation of less than 10%, even after > 10 months.

The sample for inductively coupled plasma−mass spectrometry (ICP-MS) was prepared by decanting the final solution. The decantation was repeated 4 times, by adding fresh distilled water each time. The recovered polymer was dissolved in 3 mL of HCl/HNO_3 3/1 (aqua regia) by mixing at 90 °C for 30 min. **Caution**! This is an extremely corrosive solution; the temperature should be carefully increased, and every possible measure should be taken to avoid exposure to vapors or spills. Then, the solution was diluted with water (Fischer Chemicals, HPLC grade) to obtain a 2% HNO_3 matrix. The concentrations of copper (Cu) in the solution and in a blank sample (pure water + 2% HNO_3 matrix) were determined using Thermo Scientific (Finnigan) Element XR ICP-MS. The instrument was calibrated with standard solutions.

General procedure for an ab initio emulsion ARGET ATRP

The aqueous phase was prepared in a Schlenk flask, by mixing SDS, $CuBr_2$, TPMA, the selected initiator (RBr) and NaBr, in deionized water. The solution was degassed at room temperature for about 30 minutes. In the meantime, the desired monomer and an aqueous solution of AA (0.02 or 0.04 M, V = 2 mL) were separately degassed at room temperature. The monomer was withdrawn with a syringe and slowly injected into the flask, without stirring the system. The aqueous phase and the monomer remained separated, with the monomer on top. The flask was then placed into a pre-heated oil-bath. A 1 mL syringe was filled with the solution of AA and placed on a syringe pump, with the needle inserted

into the flask, in a way to be as close as possible to the liquid level. The injection rate was set to the desired value: for instance, a rate of 40 μL/h introduced 800 nmol/h of AA, which corresponded to 0.16 eq./h with respect to copper, on the basis of a 10^{-3} M Cu solution in a 10 mL flask. A small volume of AA solution was withdrawn with another syringe and injected dropwise into the flask, to start the polymerization: in the case of the previous example, 40 μL of AA solution were injected to start the process. Simultaneously, the stirring plate and syringe pump were activated. Samples were periodically withdrawn with a syringe and placed on weighing aluminum plates, for further characterization.

3.6. References

(1) Fantin, M.; Chmielarz, P.; Wang, Y.; Lorandi, F.; Isse, A. A.; Gennaro, A.; Matyjaszewski, K., Harnessing the Interaction between Surfactant and Hydrophilic Catalyst To Control eATRP in Miniemulsion. *Macromolecules* **2017,** *50* (9), 3726-3732.
(2) Wang, Y.; Lorandi, F.; Fantin, M.; Chmielarz, P.; Isse, A. A.; Gennaro, A.; Matyjaszewski, K., Miniemulsion ARGET ATRP via Interfacial and Ion-Pair Catalysis: From ppm to ppb of Residual Copper. *Macromolecules* **2017,** *50* (21), 8417-8425.
(3) Fantin, M.; Isse, A. A.; Matyjaszewski, K.; Gennaro, A., ATRP in Water: Kinetic Analysis of Active and Super-Active Catalysts for Enhanced Polymerization Control. *Macromolecules* **2017,** *50* (7), 2696-2705.
(4) Lau, W., Emulsion Polymerization of Hydrophobia Monomers. *Macromol Symp* **2002,** *182* (1), 283-289.
(5) Matyjaszewski, K.; Ziegler, M. J.; Arehart, S. V.; Greszta, D.; Pakula, T., Gradient Copolymers by Atom Transfer Radical Copolymerization. *Journal of Physical Organic Chemistry* **2000,** *13* (12), 775-786.
(6) Xia, J.; Matyjaszewski, K., Controlled/"Living" Radical Polymerization. Atom Transfer Radical Polymerization Catalyzed by Copper(I) and Picolylamine Complexes. *Macromolecules* **1999,** *32* (8), 2434-2437.
(7) Elsen, A. M.; Burdyńska, J.; Park, S.; Matyjaszewski, K., Active Ligand for Low PPM Miniemulsion Atom Transfer Radical Polymerization. *Macromolecules* **2012,** *45* (18), 7356-7363.
(8) Fu, L.; Simakova, A.; Fantin, M.; Wang, Y.; Matyjaszewski, K., Direct ATRP of Methacrylic Acid with Iron-Porphyrin Based Catalysts. *Acs Macro Lett* **2018,** *7* (1), 26-30.

Chapter 4 Photoinduced Miniemulsion Atom Transfer Radical Polymerization

4.1. Preface

This content of this chapter was published in *ACS Macro Letters* (Yi Wang, Sajjad Dadashi-Silab, "Photoinduced Miniemulsion Atom Transfer Radical Polymerization", *ACS Macro Letters*, **2018**, 7, 275–280.).

This research was a continuation of my work presented in Chapter II. The ion-pair catalyst was demonstrated as an efficient catalysis system for miniemulsion ATRP using low ppm of catalyst. However, a miniemulsion ATRP was for the first time conducted using photoATRP, an environmentally friendly approach and was capable of spatial temporal control. In this project, a systematic investigation of photoATRP in miniemulsion was conducted.

I designed this project and carried out most of the experiments. Sajjad Dadashi-Silab conducted part of the synthetic work and contributed in photochemistry part. I want to thank Liye Fu for providing poly(ethylene oxide) bromophenyl acetate ($PEO_{5k}BPA$).

This project received financial support from the NSF (CHE-1707490).

4.2. Introduction

Aqueous dispersed systems, including microemulsion, miniemulsion, emulsion, and dispersion have been intensely studied.[1-2] Polymerizations in dispersed media result in formation of products with zero-volatile organic content (zero-VOC) while providing

facile heat transfer and low viscosity. Consequently, they are considered environmentally benign. As a result, these systems are extensively applied in various industrial applications. For example, polyacrylates, polyacrylamide, polyacrylonitrile, poly(vinyl acetate) and polymerized styrene butadiene rubber have been produced in dispersed media on an industrial scale. Emulsion polymerized polyacrylates can be directly used as waterborne coatings. In addition, dispersed media provide the possibility of loading organic/inorganic species, liquids and solids, to form polymeric nanoparticles or nanocapsules by encapsulation of magnetic nanoparticles,[3] enzymes,[4] pigments,[5] and so on.[6]

Several robust reversible-deactivation radical polymerization (RDRP) techniques, including atom transfer radical polymerization (ATRP),[7-11] _ENREF_6 reversible addition-fragmentation chain transfer (RAFT),[12] nitroxide-mediated polymerization (NMP),[13] organotellurium-mediated radical polymerization (TERP),[14] have been developed to synthesize polymers with predetermined molecular weight and low dispersity (*Đ*). RDRP procedures in dispersed media are especially beneficial for obtaining multifunctional polymers with low *Đ*, as the segregation and compartmentalization decrease the rate of termination processes.[15-18] _ENREF_18_ENREF_6 Various polymer structures, including gradient,[19-20] block,[21-23] star[21, 23] and brush[23-26] polymers have been synthesized in water dispersed RDRP. [27]

In addition to traditional methods, RDRP reactions have been successfully tuned by external stimuli, including photo, electrical current and mechanical. Regulation of polymerization by external stimuli eliminates the need for addition of chemicals to activate the reaction and provides efficient temporal control.[28-31] Among them, photo-mediated

ATRP is a viable candidate due to the high energy efficiency, and possibilities for spatiotemporal control.[32-35]

Currently, there have been a few reports where photo-mediated RDRP was conducted in microemulsion, miniemulsion or emulsion media. They include photoiniferter RAFT and photoinduced energy/electron transfer (PET)-RAFT polymerizations studied in miniemulsion.[36-37] Moreover, recently an *ab initio* emulsion polymerization was developed with TERP.[38] In microemulsion, particle sizes are typically in the range of 10–50 nm,[39-41] which are much smaller than the wavelength of visible light. Thus, the reaction mixture is optically transparent. From this point of view, microemulsion polymerization is particularly suitable for photomediated RDRPs. For polymerizations in miniemulsion and emulsion, the particle sizes are typically 50–500 nm, which is comparable to the light wavelength, and the systems are quite opaque. The turbidity hampers the light penetration, therefore, in these systems the impact of light scattering and absorption in the polymerization cannot be neglected.

In this contribution, we investigate photoATRP of (meth)acrylate monomers in miniemulsion, taking advantage of an SDS–Cu/TPMA ion-pair catalyst (SDS = sodium dodecyl sulfate; TPMA = tris(2-pyridylmethyl)amine).[22-23, 42] The key parameters in the reaction, including vial sizes, TPMA/$CuBr_2$ ratio, amount of SDS, solids content, and concentration of the Cu catalyst were examined. Moreover, temporal control was achieved by switching the UV light ON and OFF.

4.3. Results and Discussion

The efficacy of photochemical processes depends, among other factors, on the ability of light to penetrate through reaction medium. In regards to dispersed media,

turbidity of the solution may prevent deep penetration of the incident light. As a result, photochemical reactions may take place mainly at the surface of the reaction vial where absorption of the incident light is higher. To examine the efficiency of light in mediating miniemulsion ATRP, the polymerization of *n*-butyl methacrylate (BMA) was initially tested using vials with different sizes and under UV light irradiation. A small vial with an inner diameter of 12 mm was used to run a miniemulsion with 3 mL volume, whereas a larger vial with a diameter of 25 mm contained 10 mL of miniemulsion (**Figure 4-1**). The volume of the miniemulsion was adjusted to make sure that a similar height of the mixture is exposed to the UV light in both vials. Well-controlled polymerization was observed in both cases. Kinetic results presented in **Figure 4-2** show that polymerizations in the small vial were slightly faster than that in the larger vial. This could be attributed to the higher surface/volume ratio in the small vial enabling a better exposure to light, as was observed in continuous flow systems.[43-45] Although the polymerization in the smaller vial was faster, the majority of the experiments were performed in the larger vial due to the easy setup and facile preparation. For comparison, aqueous photoATRP of oligo(ethylene oxide) methyl ether methacrylate ($OEOMA_{500}$) was conducted in the above mentioned vials. Similar kinetics were observed in the photoATRP of $OEOMA_{500}$ regardless of the vial size (**Figure 4-3**). These results suggest that the miniemulsion system was more sensitive to vial size, due to the scattering effect of particles.

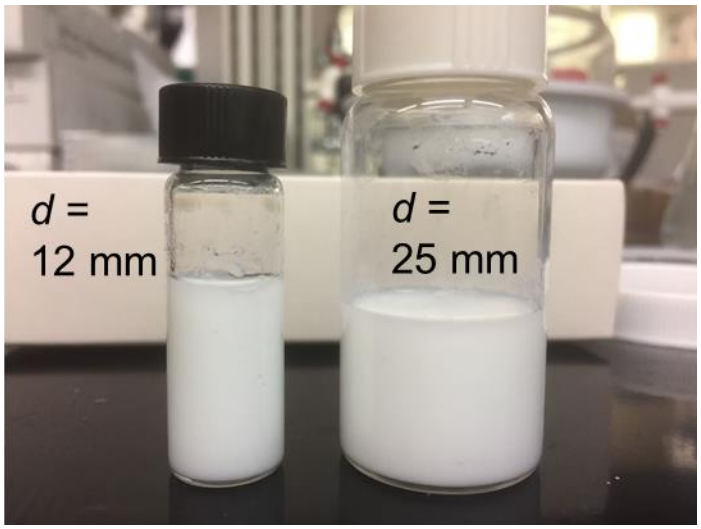

Figure 4-1. Photograph of the experiment setup for polymerizations in different vial sizes.

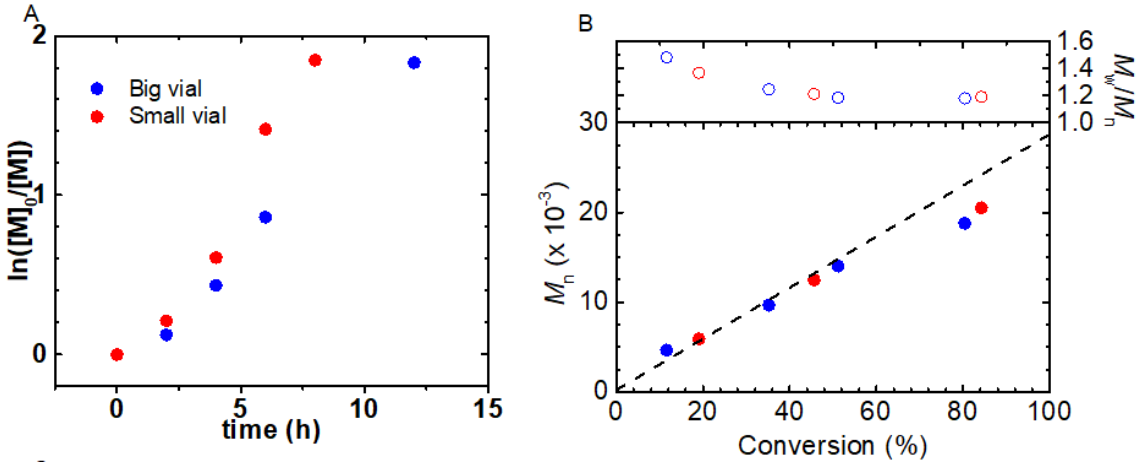

Figure 4-2. PhotoATRP of BMA in miniemulsion using vials of different diameters. (A) Kinetic plots; (B) evolution of M_n and $Đ$. Reaction conditions: BMA 2mL (20 vol%),[BMA]/[EBPA]/[$CuBr_2$]/[TPMA] = 200/1/0.16/0.64, [HD] = 10 wt% relative to BMA, [SDS] = 4.6 wt% relative to BMA, [NaBr] = 0.1 M, λ_{max} = 370 nm, intensity = 5 mW/cm^2.

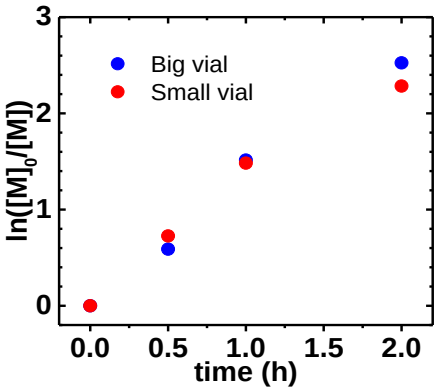

Figure 4-3. PhotoATRP of $OEOMA_{500}$ in water using vials of different diameters. Reaction conditions: $[OEOMA_{500}]/[PEO_{5k}BPA]/[CuBr_2/3TPMA] = 200/1/0.16$, [NaBr] = 5 mM, λ_{max} = 370 nm, intensity = 5 mW/cm^2.

Another factor that directly affects light absorption is particle size, which could be adjusted by varying the amount of SDS surfactant. The Zeta-average diameter of the organic droplets decreased from 167.4 ± 0.2, 138.5 ± 1.0, 122.4 ± 0.7, 120.4 ± 1.9 and 110.0 ± 3.0 nm when the SDS content was increased from 1.2 to 18.4 wt% relative to monomer, respectively, as measured by dynamic light scattering (DLS). When the amount of SDS was 1.2 wt% to BMA (0.4 wt% in total), < 10% coagulation was observed after polymerization, whereas at higher SDS amounts coagulation did not happen. **Figure 4-4A** shows a clear trend that the rate of the polymerization increased with increasing SDS content. This increase in the rate can be attributed to the formation of smaller particles, and hence higher number of particles, leading to segregation of propagating radicals.[46] All the polymerizations resulted in well-defined polymers with low *Đ* and predetermined molecular weight.

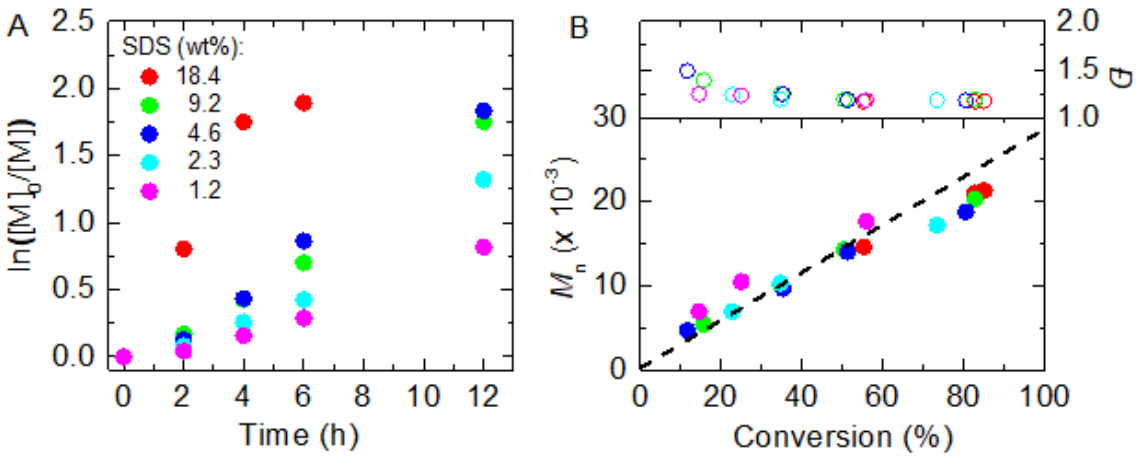

Figure 4-4. Miniemulsion photoATRP of BMA in the presence of various SDS concentrations. (A) Kinetic plots; (B) evolution of M_n and $Đ$. Reaction conditions: BMA 2mL (20 vol%), [BMA]/[EBPA]/[$CuBr_2$]/[TPMA] = 200/1/0.16/0.48, [HD] = 10 wt% relative to BMA, [SDS] = 2.3-18.4 wt% relative to BMA, [NaBr] = 0.1 M, λ_{max} = 370 nm, intensity = 5 mW/cm^2.

The effect of the ratio of TPMA/$CuBr_2$ on the kinetics of the polymerization was studied. In photoATRP, TPMA also serves as an electron donor to photochemically (re)generate Cu^I activator, so an excess of TPMA was required. **Figure 4-5** summarizes the results of the polymerization of BMA with various [TPMA]/[$CuBr_2$] ratios. The rate of the polymerization increased with increasing [TPMA]/[$CuBr_2$] ratio. Indeed, the presence of more TPMA facilitated faster photoreduction of Cu^{II} and (re)generation of Cu^I catalyst. These polymerizations were well-controlled with molecular weights in agreement with theoretical values and low $Đ$ (~1.2), indicating a high initiation efficiency. Notably, when TPMA was used at a ratio of 6/1 with respect to $CuBr_2$, an increase in $Đ$ was observed at higher conversions. This can possibly be attributed to the generation of higher concentration of radicals and consequently higher extent of radical termination.[23] Therefore the ratio of [TPMA]/[Cu] was fixed at 3/1 for other experiments.

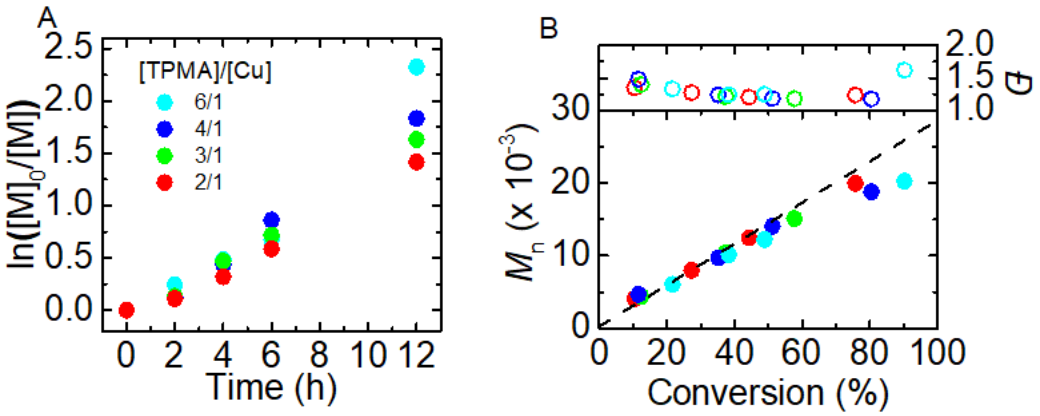

Figure 4-5. Miniemulsion photoATRP of BMA in the presence of different ratios of TPMA/Cu. (A) Kinetic plots; (B) evolution of M_n and $Đ$. Reaction conditions: BMA 2mL (20 vol%), [BMA]/[EBPA]/[$CuBr_2$]/[TPMA] = 200/1/0.16/0.32-0.96, [HD] = 10 wt% relative to BMA, [SDS] = 4.6 wt% relative to BMA, [NaBr] = 0.1 M, λ_{max} = 370 nm, intensity = 5 mW/cm^2.

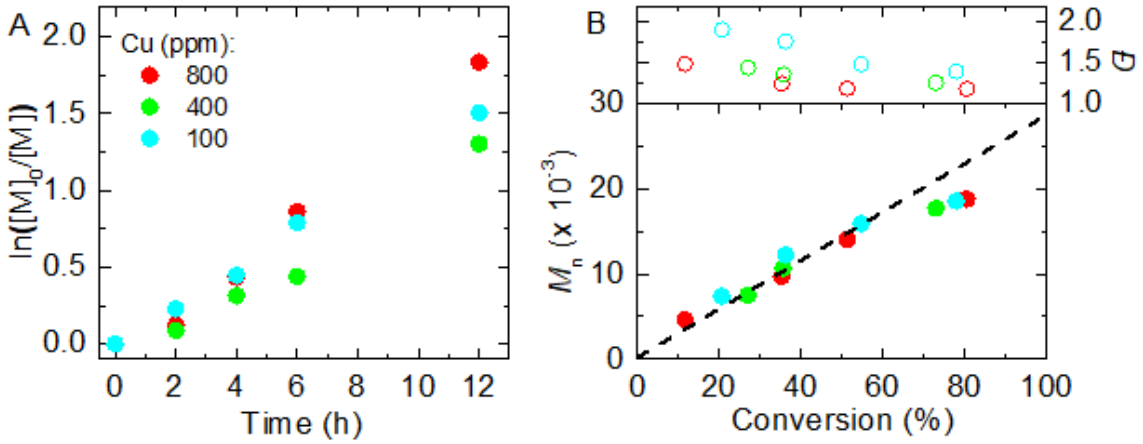

Figure 4-6. PhotoATRP of BMA in miniemulsion with different Cu catalyst loadings. (A) Kinetic plots; (B) evolution of M_n and $Đ$. Reaction conditions: BMA 2mL (20 vol%), [BMA]/[EBPA]/[$CuBr_2$/3TPMA] = 200/1/0.02-0.16, [HD] = 10 wt% relative to BMA, [SDS] = 4.6 wt% relative to BMA, [NaBr] = 0.1 M, λ_{max} = 370 nm, intensity = 5 mW/cm^2.

PhotoATRP of BMA in miniemulsion was also studied in the presence of different concentrations of the Cu catalyst. The catalyst loading was reduced from 800 to 100 ppm

relative to monomer (**Figure 4-6**). The polymerization kinetics were similar, and molecular weight showed good correlation with the theoretical value. However, a clear trend was observed, namely that *Đ* increased with decreasing amount of catalyst. This phenomenon was especially pronounced at the early stages of the polymerization. For example, at ~ 35% conversion, *Đ* was 1.24, 1.36 and 1.76 for 800, 400 and 100 ppm Cu, respectively. This observation can be explained by eq. 1 where the *Đ* is related to the concentration of dormant species (R–X) and of deactivator (X–$Cu^{II}L^{+}$), rate constants of propagation (k_p) and deactivation (k_{deact}), and monomer conversion (p):

$$Đ = 1 + \frac{1}{DP_n} + \left(\frac{k_p[R-X]}{k_{deact}[X-Cu^{II}L^{+}]}\right)\left(\frac{2}{p} - 1\right) \qquad \text{(eq. 1)}$$

The smaller amount of deactivator should lead to the higher *Đ* observed. Nevertheless, all polymerizations resulted in final *Đ* of ~1.3. The concentration of effective deactivator inside monomer droplets can indeed be estimated using eq. 1. For example, using values obtained for the polymerization of BMA in the presence of 800 ppm of $CuBr_2$ initially added, it was calculated that ~ 0.5 % of L/Cu^{II} was present inside the droplets that controlled the polymerization (see Supporting Information for more details).

Solids content of 30–70% is optimal for industrial applications, as increasing the solids content increases the energy efficiency of the polymerization. Furthermore, high solids content is desired in coating applications. However, higher solids content may lead to lower latex stability and more scattering. No significant coagulation was observed in the

photo ATRP of BMA in miniemulsion when the solids content was varied between 5 and 50 wt%, under a moderate surfactant loading, 4.6 wt % with respective to monomer. With increasing solids content, the rate of the polymerization was slower at the early stages, because the larger number of oil droplets resulted in more light scattering, thus the photoreduction of Cu^{II} was slower (**Figure 4-7**).[47] Nevertheless, the polymerization reached similar $[Cu^{II}]/[Cu^{I}]$ ratios exhibiting similar polymerization rates. All polymerizations reached more than 70% monomer conversion in 12 h exhibiting low *Đ*'s.

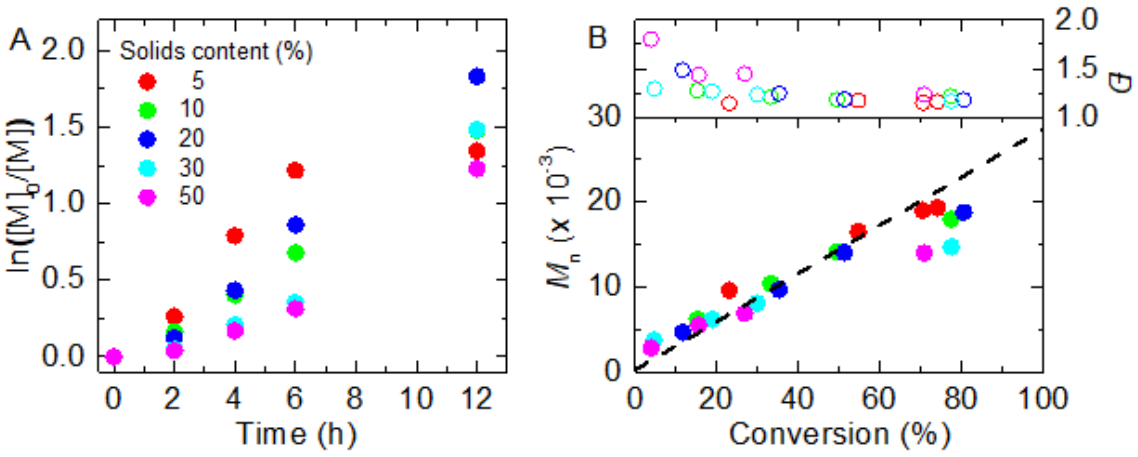

Figure 4-7. Miniemulsion photoATRP of BMA at various solids content, monomer vol%. (A) Kinetic plots; (B) evolution of M_n and *Đ*. Reaction conditions: BMA 0.5-5mL (5-50 vol%), [BMA]/[EBPA]/[$CuBr_2$]/[TPMA] = 200/1/0.16/0.48, [HD] = 10 wt% relative to BMA, [SDS] = 4.6 wt% relative to BMA, [NaBr] = 0.1 M, λ_{max} = 370 nm, intensity = 5 mW/cm^2.

Temporal control in photoATRP in miniemulsion was investigated by switching the UV light ON/OFF. Under intermittent switching of the UV light, the reaction was switched between ON/OFF states multiple times. The polymerization showed precise agreement of molecular weights with the theoretical value, and maintained low *Đ*, throughout multiple cycles (**Figure 4-8**).

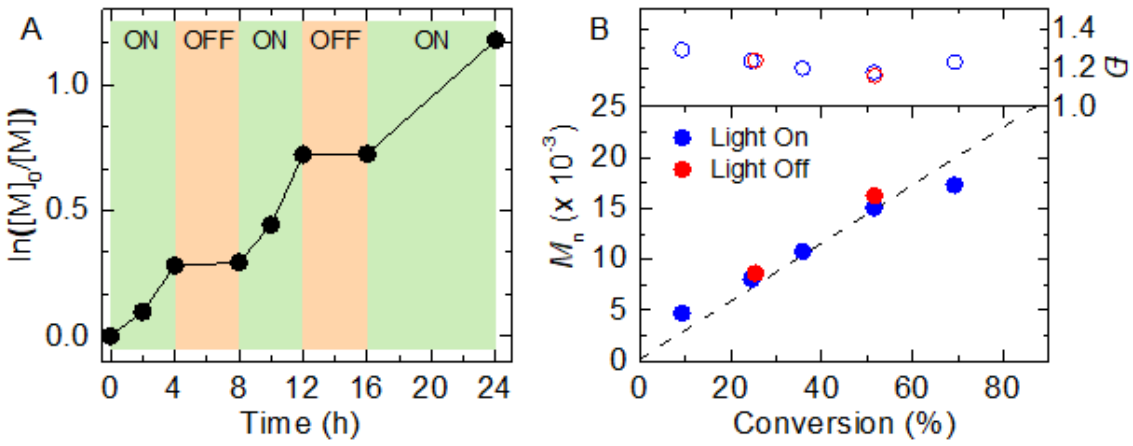

Figure 4-8. Temporal control in photoATRP miniemulsion. Reaction condition: BMA 2mL (20 vol%), [BMA]/[EBPA]/[$CuBr_2$]/[TPMA] = 200/1/0.16/0.48, [HD] = 10 wt% relative to BMA, [SDS] = 4.6 wt% relative to BMA, [NaBr] = 0.1 M, λ_{max} = 370 nm, intensity = 5 mW/cm^2.

In addition to methacrylate, the ion-pair photoATRP in miniemulsion was applied to the polymerization of *n*-butyl acrylate (BA) using ethyl α-bromoisobutyrate (EBiB) as initiator. As shown in **Figure 4-9** a well-controlled polymerization of BA was achieved with molecular weights in agreement with theoretical values and low *Đ*.

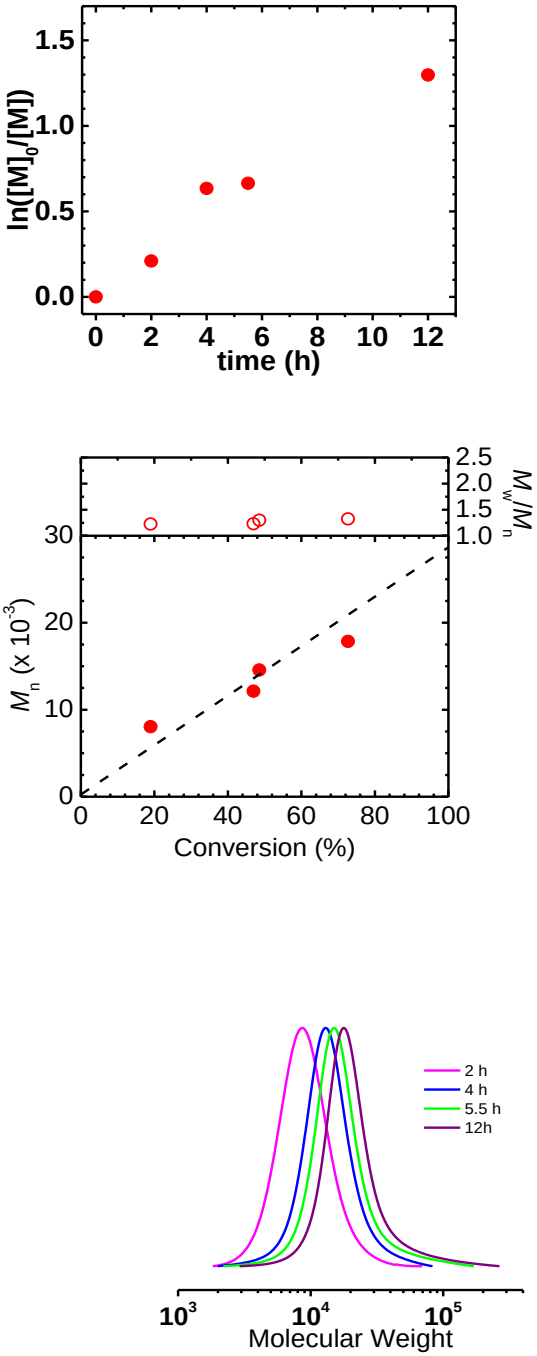

Figure 4-9. PhotoATRP of BA in miniemulsion. BA 2mL (20 vol%), [BA]/[**EBiB**]/[$CuBr_2$]/[TPMA] = 200/1/0.16/0.48, [HD] = 10 wt% relative to BA, [SDS] = 4.6 wt% relative to BMA, [NaBr] = 0.1 M, λ_{max} = 370 nm, intensity = 5 mW/cm^2.

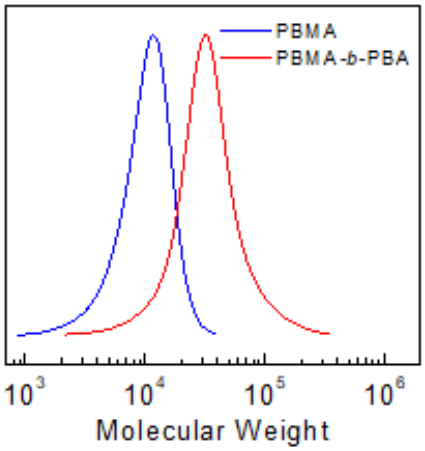

Figure 4-10. Chain extension of PBMA-MI with BA in miniemulsion. Reaction condition: BA 2mL (20 vol%), [BA]/[PBMA MI]/[$CuBr_2$]/[TPMA] = 200/1/0.16/0.48, [HD] = 10 wt% relative to BA, [SDS] = 4.6 wt% relative to BMA, [NaBr] = 0.1 M, λ_{max} = 370 nm, intensity = 5 mW/cm^2.

To confirm the chain-end functionality of the obtained polymers, a PBMA macroinitiator (PBMA-MI; M_n = 8700, $Đ$ = 1.28) was synthesized by miniemulsion photoATRP using the ion-pair catalyst (see synthesis and purification procedures in Supporting Information). The PBMA-MI was chain extended with BA after re-homogenization. Well-defined PBMA-*b*-PBA copolymer (M_n = 19900, $Đ$ = 1.36) was synthesized, as evidenced by a clear shift of the monomodal GPC traces toward higher molecular weights (**Figure 4-10**).

4.4. Conclusion

In conclusion, a miniemulsion photoATRP was conducted under UV light using an *in situ* formed ion-pair catalyst. The reaction conditions were optimized to provide polymers with well-defined properties. This system was conducted in the presence of a low concentration of surfactant, low Cu catalyst concentration, and solids content of up to 50

wt%. The progress of polymerization could be regulated by switching the UV light on and off resulting in temporal control over the polymerization. The versatility of this system was demonstrated by successful polymerization of butyl methacrylate and butyl acrylate from small-molecular initiators as well as a macroinitiator. The comparison between polymerizations in different vial sizes show that the polymerization could be accelerated upon increasing the surface to volume ratio of the reactor without sacrificing the degree of control over the polymerization. Conducting polymerization in a continuous flow reactor will be a good pathway for scaling up this procedure.[48]

4.5. Experimental Section

Materials. Copper(II) bromide ($Cu^{II}Br_2$, 99%), sodium dodecyl sulfate (SDS, 99%), hexadecane (HD, 99%), tetrahydrofuran (THF, > 99%), ethyl α-bromoisobutyrate (EBiB, 98%) and ethyl α-bromophenylacetate (EBPA, 97%), were purchased from Sigma-Aldrich. Sodium bromide (NaBr, 99%) was purchased from Acros. Tris(2-pyridylmethyl)amine (TPMA) was provided by KOEI Chemical. The reagents above were used as received. _ENREF_1*n*-Butyl methacrylate (BMA, 99%, Sigma-Aldrich), poly(ethylene glycol) methyl ether methacrylate (average M_n = 500, $OEOMA_{500}$, Sigma-Aldrich) and *n*-butyl acrylate (BA, 99%, Sigma-Aldrich) were passed through a column filled with basic alumina prior to use to remove polymerization inhibitors. poly(ethylene oxide) bromophenyl acetate ($PEO_{5k}BPA$) was prepared according to previously published procedures.[49]

Instrumentation. Ultrasound treatment to prepare miniemulsion samples was carried out using Autotune Series High Intensity Ultrasonic Processor, 1500 Watt Model.

All polymerizations were conducted in a 4.9 mW/cm^2 MelodySusie® UV lamp.

M_n and $Đ$ were determined by GPC equipped with Polymer Standards Services (PSS) columns (guard, 10^5, 10^3, and 10^2 Å) and a differential refractive index detector (Waters, 2410), with THF as eluent at a flow rate of 1.00 mL/min (T = 35 °C). GPC traces were processed by WinGPC 8.0 software (PSS) using a calibration based on linear polystyrene (PS) standards.

Monomer conversion was determined by gravimetric analysis, evaporating the samples at 110 °C for at least 30 min.

Particle size and size distribution were determined by using a Zetasizer Nano from Malvern Instruments, Ltd.

General procedure for miniemulsion photo ATRP of BMA. A solution of BMA (2.0 mL, 12.57 mmol), EBPA (11.0 μL, 0.063 mmol) to target DP = 200, and HD (0.25 mL, 0.85 mmol) was prepared. A stock solution of $Cu^{II}Br_2$/3TPMA (0.20 mL, 0.01 mmol), NaBr (0.103 g, 1 mmol), and SDS (0.082 g, 4.6 wt% to BMA) was prepared in 8 mL of distilled water. The organic and aqueous solutions were mixed (total volume ≈ 10 mL), placed in an ice-water bath, and dispersed by a probe sonicator, amplitude = 20% for 20 min (application and rest time of 1 s each). Nitrogen was bubbled through the miniemulsion solution for 30 min. The UV lamp was placed on a stir plate with a stir rate = 500 rpm. The flask was inserted into the cavity of the UV lamp. The lamp was turned on to start the reaction. Samples were withdrawn periodically to follow the monomer conversion by gravimetric analysis, while M_n and $Đ$ were determined by GPC.

Procedure for a miniemulsion photo ATRP of BA. BA (2 mL, 13.95 mmol), EBiB (10.0 μL, 0.070 mmol) to target a degree of polymerization (DP) = 200, and HD (0.25 mL,

0.85 mmol) were mixed to form the organic phase. $Cu^{II}Br_2$/3TPMA stock solution (0.20 mL, 0.01 mmol), NaBr (0.103 g, 1 mmol), and SDS (0.082 g, 4.6 wt% to BA) were dissolved in 8 mL of distilled water. The organic and aqueous solutions were mixed (total volume ≈ 10 mL), placed in an ice-water bath, and dispersed by a probe sonicator, amplitude = 20% for 20 min (application and rest time of 1 s each). Nitrogen was bubbled through the miniemulsion solution for 30 min. The UV lamp was placed on a stir plate with a stir rate = 500 rpm. The flask was inserted into the cavity of the UV lamp. The lamp was turned on to start the reaction. Samples were withdrawn periodically to follow the monomer conversion by gravimetric analysis, while M_n and M_w/M_n were determined by GPC.

Preparation of PBMA-MI. A photo ATRP polymerization was conducted following the same procedure for BMA polymerization as mentioned above. After 6 h, the polymerization was quenched by turning off the UV lamp and exposure to the air. 5 mL of polymerization solution were transferred to a 50 mL centrifuge tube. 20 mL of water and 20 mL of MeOH were added and then the tubes were placed in the centrifuge for 20 min at 5000 rpm. About 90% of the polymer was recovered after precipitation. The PBMA-MI was re-dissolved in THF, passed through neutral alumina column and dried in vacuum.

Procedure for chain extension from PBMA-MI. A solution of BA (2 mL, 12.31 mmol), PBMA-MI (0.25 g, 0.062 mmol) to target DP = 300, and HD (0.25 mL, 0.85 mmol) was prepared. $Cu^{II}Br_2$/TPMA stock solution (0.20 mL, 0.01 mmol), NaBr (0.103 g, 1 mmol), and SDS (0.082 g, 0.28 mmol) were dissolved in 8 mL of distilled water. The organic and aqueous solutions were mixed (total volume ≈ 10 mL), placed in an ice-water bath, and dispersed by a probe sonicator, amplitude = 20% for 20 min (application and rest

time of 1 s each). Nitrogen was bubbled through the miniemulsion solution for 30 min. The UV lamp was placed on a stir plate with a stir rate = 500 rpm. The flask was inserted into the cavity of the UV lamp. The lamp was turned on to start the reaction. Samples were withdrawn periodically to follow the monomer conversion by gravimetric analysis, while M_n and $Đ$ were determined by GPC.

General procedure for polymer precipitation. 5 mL of polymerization solution were transferred to a 50 mL centrifuge tube. 20 mL of water and 20 mL of MeOH were added and then the tubes were placed in the centrifuge for 20 min at 5000 rpm. About 90% of the polymer was recovered after precipitation.

4.6. References

(1) Zetterlund, P. B.; Kagawa, Y.; Okubo, M., Controlled/Living Radical Polymerization in Dispersed Systems. *Chem Rev* **2008,** *108* (9), 3747-3794.
(2) Zetterlund, P. B.; Thickett, S. C.; Perrier, S.; Bourgeat-Lami, E.; Lansalot, M., Controlled/Living Radical Polymerization in Dispersed Systems: An Update. *Chem Rev* **2015,** *115* (18), 9745-9800.
(3) Dou, J. B.; Zhang, Q. Y.; Jian, L. A.; Gu, J. W., Magnetic Nanoparticles Encapsulated Latexes Prepared with Photo-Initiated Miniemulsion Polymerization. *Colloid Polym Sci* **2010,** *288* (18), 1751-1756.
(4) Ishizuka, F.; Chapman, R.; Kuchel, R. P.; Coureault, M.; Zetterlund, P. B.; Stenzel, M. H., Polymeric Nanocapsules for Enzyme Stabilization in Organic Solvents. *Macromolecules* **2018,** *51* (2), 438-446.
(5) Hakeim, O. A.; Diab, H. A.; Adams, J., Preparation and characterization of UV curable-encapsulated phthalocyanine blue pigment. *Prog. Org. Coat.* **2015,** *84*, 70-78.
(6) Landfester, K.; Weiss, C. K., Encapsulation by Miniemulsion Polymerization. *Adv Polym Sci* **2010,** *229*, 1-49.
(7) Wang, J. S.; Matyjaszewski, K., Controlled Living Radical Polymerization - Atom-Transfer Radical Polymerization In the Presence Of Transition-Metal Complexes. *J Am Chem Soc* **1995,** *117* (20), 5614-5615.
(8) Matyjaszewski, K.; Xia, J. H., Atom Transfer Radical Polymerization. *Chem Rev* **2001,** *101* (9), 2921-2990.
(9) Matyjaszewski, K., Atom Transfer Radical Polymerization (ATRP): Current Status and Future Perspectives. *Macromolecules* **2012,** *45* (10), 4015-4039.

(10) Matyjaszewski, K.; Tsarevsky, N. V., Macromolecular Engineering by Atom Transfer Radical Polymerization. *J Am Chem Soc* **2014,** *136* (18), 6513-6533.
(11) Matyjaszewski, K., Advanced Materials by Atom Transfer Radical Polymerization. *Advanced Materials* **2018,** *30*, 1706441.
(12) Moad, G.; Rizzardo, E.; Thang, S. H., Living Radical Polymerization by the RAFT Process - A third update. *Aust J Chem* **2012,** *65* (8), 985-1076.
(13) Nicolas, J.; Guillaneuf, Y.; Lefay, C.; Bertin, D.; Gigmes, D.; Charleux, B., Nitroxide-Mediated Polymerization. *Prog Polym Sci* **2013,** *38* (1), 63-235.
(14) Yamago, S., Development of organotellurium-mediated and organostibine-mediated living radical polymerization reactions. *J. Polym. Sci., Part A: Polym. Chem.* **2006,** *44* (1), 1-12.
(15) Engelis, N. G.; Anastasaki, A.; Nurumbetov, G.; Truong, N. P.; Nikolaou, V.; Shegiwal, A.; Whittaker, M. R.; Davis, T. P.; Haddleton, D. M., Sequence-Controlled Methacrylic Multiblock Copolymers via Sulfur-Free RAFT Emulsion Polymerization. *Nat Chem* **2017,** *9* (2), 171-178.
(16) Asua, J. M., Miniemulsion Polymerization. *Prog Polym Sci* **2002,** *27* (7), 1283-1346.
(17) Kagawa, Y.; Zetterlund, P. B.; Minami, H.; Okubo, M., Compartmentalization in Atom Transfer Radical Polymerization (ATRP) in Dispersed Systems. *Macromol Theor Simul* **2006,** *15* (8), 608-613.
(18) Min, K.; Matyjaszewski, K., Atom Transfer Radical Polymerization in Aqueous Dispersed Media. *Cent Eur J Chem* **2009,** *7* (4), 657-674.
(19) Min, K.; Li, M.; Matyjaszewski, K., Preparation of Gradient Copolymers via ATRP using a Simultaneous Reverse and Normal Initiation Process. I. Spontaneous Gradient. *J Polym Sci Pol Chem* **2005,** *43* (16), 3616-3622.
(20) Min, K.; Oh, J. K.; Matyjaszewski, K., Preparation of Gradient Copolymers via ATRP in Miniemulsion. II. Forced Gradient. *J Polym Sci Pol Chem* **2007,** *45* (8), 1413-1423.
(21) Min, K.; Gao, H. F.; Matyjaszewski, K., Preparation of Homopolymers and Block Copolymers in Miniemulsion by ATRP using Activators Generated by Electron Transfer (AGET). *J Am Chem Soc* **2005,** *127* (11), 3825-3830.
(22) Fantin, M.; Chmielarz, P.; Wang, Y.; Lorandi, F.; Isse, A. A.; Gennaro, A.; Matyjaszewski, K., Harnessing the Interaction between Surfactant and Hydrophilic Catalyst to Control eATRP in Miniemulsion. *Macromolecules* **2017,** *50* (9), 3726-3732.
(23) Wang, Y.; Lorandi, F.; Fantin, M.; Chmielarz, P.; Isse, A. A.; Gennaro, A.; Matyjaszewski, K., Miniemulsion ARGET ATRP via Interfacial and Ion-Pair Catalysis: From ppm to ppb of Residual Copper. *Macromolecules* **2017,** *50* (21), 8417-8425.
(24) Min, K.; Yu, S.; Lee, H. I.; Mueller, L.; Sheiko, S. S.; Matyjaszewski, K., High Yield Synthesis of Molecular Brushes via ATRP in Miniemulsion. *Macromolecules* **2007,** *40* (18), 6557-6563.
(25) Oh, J. K.; Perineau, F.; Charleux, B.; Matyjaszewski, K., AGET ATRP in Water and Inverse Miniemulsion: A Facile Route for Preparation of High-Molecular-Weight Biocompatible Brush-Like Polymers. *J Polym Sci Pol Chem* **2009,** *47* (7), 1771-1781.
(26) Li, H.; Wang, W. W.; Li, C. M.; Tan, J. J.; Yin, D. Z.; Zhang, H. P.; Zhang, B. L.; Yin, C. J.; Zhang, Q. Y., Synthesis and Characterization of Brush-Like Multigraft Copolymers PnBA-g-PMMA by a Combination of Emulsion AGET ATRP and Emulsion Polymerization. *J Colloid Interf Sci* **2015,** *453*, 226-236.

(27) Fantin, M.; Park, S.; Wang, Y.; Matyjaszewski, K., Electrochemical Atom Transfer Radical Polymerization in Miniemulsion with a Dual Catalytic System. *Macromolecules* **2016,** *49* (23), 8838-8847.
(28) Leibfarth, F. A.; Mattson, K. M.; Fors, B. P.; Collins, H. A.; Hawker, C. J., External Regulation of Controlled Polymerizations. *Angew Chem Int Ed* **2013,** *52* (1), 199-210.
(29) Shanmugam, S.; Boyer, C., Stereo-, Temporal and Chemical Control through Photoactivation of Living Radical Polymerization: Synthesis of Block and Gradient Copolymers. *J Am Chem Soc* **2015,** *137* (31), 9988-9999.
(30) Chmielarz, P.; Yan, J. J.; Krys, P.; Wang, Y.; Wang, Z. Y.; Bockstaller, M. R.; Matyjaszewski, K., Synthesis of Nanoparticle Copolymer Brushes via Surface-Initiated seATRP. *Macromolecules* **2017,** *50* (11), 4151-4159.
(31) Wang, Z. H.; Pan, X. C.; Yan, J. J.; Dadashi-Silab, S.; Xie, G. J.; Zhang, J. N.; Wang, Z. H.; Xia, H. S.; Matyjaszewski, K., Temporal Control in Mechanically Controlled Atom Transfer Radical Polymerization Using Low ppm of Cu Catalyst. *Acs Macro Lett* **2017,** *6* (5), 546-549.
(32) Chen, M.; Zhong, M. J.; Johnson, J. A., Light-Controlled Radical Polymerization: Mechanisms, Methods, and Applications. *Chem Rev* **2016,** *116* (17), 10167-10211.
(33) Corrigan, N.; Shanmugam, S.; Xu, J. T.; Boyer, C., Photocatalysis in Organic and Polymer Synthesis. *Chem Soc Rev* **2016,** *45* (22), 6165-6212.
(34) Pan, X. C.; Tasdelen, M. A.; Laun, J.; Junkers, T.; Yagci, Y.; Matyjaszewski, K., Photomediated Controlled Radical Polymerization. *Prog Polym Sci* **2016,** *62*, 73-125.
(35) Dadashi-Silab, S.; Doran, S.; Yagci, Y., Photoinduced Electron Transfer Reactions for Macromolecular Syntheses. *Chem Rev* **2016,** *116* (17), 10212-10275.
(36) Jung, K.; Xu, J. T.; Zetterlund, P. B.; Boyer, C., Visible-Light-Regulated Controlled/Living Radical Polymerization in Miniemulsion. *Acs Macro Lett* **2015,** *4* (10), 1139-1143.
(37) Jung, K.; Boyer, C.; Zetterlund, P. B., RAFT Iniferter Polymerization in Miniemulsion Using Visible Light. *Polym Chem-Uk* **2017,** *8* (27), 3965-3970.
(38) Fan, W.; Tosaka, M.; Yamago, S.; Cunningham, M. F., Living Ab Initio Emulsion Polymerization of Methyl Methacrylate in Water Using a Water‐Soluble Organotellurium Chain Transfer Agent under Thermal and Photochemical Conditions. *Angewandte Chemie International Edition* **2018,** *57* (4), 962-966.
(39) Wang, L. J.; Liu, X. J.; Li, Y. Z., Synthesis and Evaluation of a Surface-Active Photoinitiator for Microemulsion Polymerization. *Macromolecules* **1998,** *31* (11), 3446-3453.
(40) Full, A. P.; Kaler, E. W.; Arellano, J.; Puig, J. E., Microemulsion Polymerization of Styrene: The Effect of Salt and Structure. *Macromolecules* **1996,** *29* (8), 2764-2775.
(41) Ciftci, M.; Tasdelen, M. A.; Li, W.; Matyjaszewski, K.; Yagci, Y., Photoinitiated ATRP in Inverse Microemulsion. *Macromolecules* **2013,** *46* (24), 9537-9543.
(42) Teo, V. L.; Davis, B. J.; Tsarevsky, N. V.; Zetterlund, P. B., Successful Miniemulsion ATRP using an Anionic Surfactant: Minimization of Deactivator Loss by Addition of a Halide Salt. *Macromolecules* **2014,** *47* (18), 6230-6237.
(43) Penconi, M.; Lobry, E.; Jasinski, F.; Chemtob, A.; Croutxe-Barghorn, C.; Criqui, A.; Braun, A. M.; Oliveros, E., The use of Chemical Actinometry for the Evaluation of the Light Absorption efficiency in Scattering Photopolymerizable Miniemulsions. *Photoch Photobio Sci* **2015,** *14* (2), 308-319.

(44) Wenn, B.; Conradi, M.; Carreiras, A. D.; Haddleton, D. M.; Junkers, T., Photo-Induced Copper-Mediated Polymerization of Methyl Acrylate in Continuous Flow Reactors. *Polym Chem-Uk* **2014,** *5* (8), 3053-3060.
(45) Kurek, P. N.; Kloster, A. J.; Weaver, K. A.; Manahan, R.; Allegrezza, M. L.; De Alwis Watuthanthrige, N.; Boyer, C.; Reeves, J. A.; Konkolewicz, D., How Do Reaction and Reactor Conditions Affect Photoinduced Electron/Energy Transfer Reversible Addition–Fragmentation Transfer Polymerization? *Industrial & Engineering Chemistry Research* **2018,** *57* (12), 4203-4213.
(46) Zetterlund, P. B., Controlled/Living Radical Polymerization in Nanoreactors: Compartmentalization Effects. *Polym Chem-Uk* **2011,** *2* (3), 534-549.
(47) Lobry, E.; Jasinski, F.; Penconi, M.; Chemtob, A.; Ley, C.; Croutxe-Barghorn, C.; Oliveros, E.; Braun, A. M.; Criqui, A., Absorption and Scattering in Concentrated Monomer Miniemulsions: Static and Dynamic Investigations. *Macromol Chem Phys* **2014,** *215* (12), 1201-1211.
(48) Chemtob, A.; Rannee, A.; Chalan, L.; Fischer, D.; Bistac, S., Continuous Flow Reactor for Miniemulsion Chain Photopolymerization: Understanding Plugging Issue. *Eur Polym J* **2016,** *80*, 247-255.
(49) Fu, L. Y.; Simakova, A.; Fantin, M.; Wang, Y.; Matyjaszewski, K., Direct ATRP of Methacrylic Acid with Iron-Porphyrin Based Catalysts. *Acs Macro Lett* **2018,** *7* (1), 26-30.

Chapter 5 Photomediated Atom Transfer Radical Polymerization in *Ab Initio* Emulsion

5.1. Preface

This content of this chapter was published in *Polymer* (Yi Wang, S. Dadashi-Silab, F. Lorandi, K. Matyjaszewski, "Photoinduced Atom Transfer Radical Polymerization in *Ab Initio* Emulsion" *Polymer*, **2019**, 165, 163-167.)

This project was a continuation of results presented in Chapters III – IV. The robustness of the ion-pair catalyst in both miniemulsion and emulsion triggered my interest to conduct further study. After the miniemulsion photoATRP project, I extended application of photoATRP to *ab initio* emulsion polymerization. The influence of light source and monomer hydrophobicity was studied, and very hydrophobic monomers were incorporated through copolymerization.

I designed the project and conducted most of the experiments. My collaborators Sajjad Dadashi-Silab and Dr. Francesca Lorandi contributed to some experiments and to a draft of the manuscript. I thank Liye Fu for the synthesis of water-soluble initiators.

The financial support from NSF (CHE-1707490) is acknowledged.

5.2. Introduction

Polymerizations in dispersed aqueous media, such as oil-in-water emulsion and miniemulsion are highly relevant for their environmentally friendly character. Facile heat transfer, absence of volatile organic compounds, and low viscosity make these processes attractive for large-scale polymer productions. Moreover, polymeric nano-objects are easily prepared in (mini)emulsion systems.

Control over molecular weight (MW), MW distribution, and composition of polymers can be achieved using reversible deactivation radical polymerization (RDRP) techniques. RDRPs have been implemented in dispersed media, to combine the control over polymer properties with tuning of polymer particles' size and morphology.[1-5] However, these systems are typically more challenging than conventional homogenous polymerizations.[5]

In ab initio emulsion polymerizations, radicals are generated in the aqueous phase, then particles are nucleated and stabilized by surfactant molecules. The growing particles are continuously replenished by monomer molecules which diffuse through the aqueous phase from big monomer droplets. Therefore, after the initial nucleation stage, the polymerization proceeds inside the hydrophobic polymer particles. When conducting RDRP techniques in an ab initio emulsion system, the polymerization catalyst or control agent, as well as the initiating system, must be water-soluble to generate radicals in the aqueous phase. However, as particles are nucleated, the catalyst or the control agent should effectively control the growth of polymer chains, which occurs inside the hydrophobic particles.[1-2]

Recently, a catalytic system has been designed to perform atom transfer radical polymerization (ATRP) in dispersed media.[6] The hydrophilic ATRP catalyst $CuBr_2$/TPMA [TPMA: Tris(2-pyridylmethyl)amine] was used in the presence of an anionic surfactant, sodium dodecyl sulfate (SDS). Excellent control over polymerizations resulted from the strong interaction between $CuBr_2$/TPMA and SDS. Indeed, the majority of the catalyst resided at the interface of polymer particles surrounded by the surfactant, and a small amount entered inside the hydrophobic particles by forming neutral ion-pairs [Br-$CuTPMA^+$][DS^-]. The use of an anionic surfactant was crucial to allow the catalyst to transfer between the aqueous phase and the growing polymer particles. This approach has

been successfully applied to ATRP of hydrophobic (meth)acrylate monomers in emulsion[7-8] and miniemulsion[6, 8-9] environments.

Another approach toward ab initio emulsion ATRP employed tetrabutylammonium halide salts as phase transfer agents to shuttle the ATRP catalyst into the particles.[10] However, acetone was used to favor monomers diffusion into the aqueous phase and the solids content was typically < 10 vol%. Alternatively, a surfactant was functionalized with a ligand molecule that bound to the copper catalyst in the surface of the micelles.[11] However, control over polymerization was not efficient due to the catalyst residing only on the surface. Other RDRPs were also successfully implemented into emulsion systems. Emulsion tellurium-mediated radical polymerization was developed by using a hydrophilic organotellurium chain transfer agent and both thermal and photochemical stimuli.[12] Furthermore, polymerization induced self-assembly (PISA) has been developed in various RDRP techniques, by taking advantage of the self-assembly of block copolymers composed of monomers of opposing hydrophilicity, and formed by chain extension of a hydrophilic macroinitiator with a hydrophobic monomer.[13-17] Different morphologies of polymer particles can be achieved in PISA processes, whereas emulsion polymerizations generally give well-defined, size-uniform spherical particles of about 100-1000 nm.

Photochemistry enables polymerizations to be conducted under mild conditions and provides spatiotemporal control over the processes.[18-22] Photoinduced polymerizations have been adapted to dispersed media with high photoinitiation efficiency achieved.[23-30] In particular, we previously reported well-controlled photoinduced ATRP of various monomers in miniemulsion, by exploiting the interaction between $CuBr_2$/TPMA and SDS.[31] Herein, photoinduced ATRP was successfully applied to an ab initio emulsion system, which is the preferable environment for industrial polymerizations. Various homopolymers and block copolymers were prepared with pre-determined MW, narrow MW distributions, and homogeneous distribution of polymer particles. Moreover, the photoinduced emulsion ATRP was also conducted in a non-degassed solution using glucose oxidase (GOx) to enzymatically consume oxygen.[32] This process uses commercially available and inexpensive materials, such as SDS and GOx, to prepare well-defined (co)polymers under benign conditions.

5.3. Results and Discussion

In ab initio emulsion ATRP, catalyzed by $CuBr_2$/TPMA in the presence of SDS and a highly water-soluble ATRP initiator, particles are effectively nucleated in the water phase, then the catalyst is able to control the polymerization inside the particles thanks to its strong interaction with the anionic surfactant.[7] In our previous work, a water-soluble reducing agent was fed into the polymerization system to continuously reduce $CuBr_2$/TPMA to form the catalytically active Cu^I species. However, relatively high temperatures were used and therefore, we tested the possibility of using light to (re)generate the Cu^I species. The emulsion ATRP of butyl methacrylate (BMA, 20 vol%) was performed under UV irradiation (λ_{max} = 365 nm) by using previously optimized conditions, except for working at room temperature (**Figure 5-1**). Moreover, 6-fold excess of TPMA was used, which acted as an electron donor that was oxidized to promote the reduction of the Cu catalyst.[33] The polymerization was well-controlled, reaching 81% conversion in 8.5 h, giving a polymer with predicted MW and low dispersity, $Đ$ = 1.19 (**Table 5-1** and **Figure 5-2**).

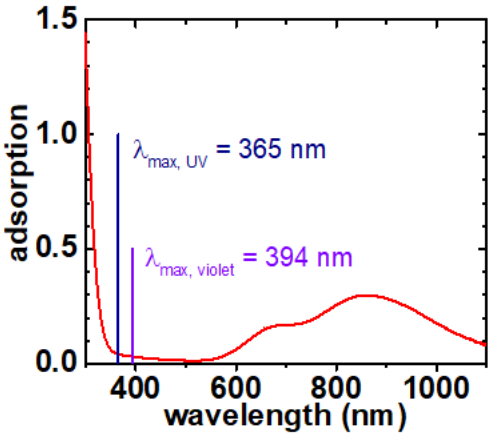

Figure 5-1. UV-Vis spectrum of $CuBr_2$/TPMA/TEA photocatalyst. [$CuBr_2$] = [TPMA] = 0.1 M; [TEA] = 0.5 M in water. The λ_{max} of two light sources (UV and violet) were labeled on the figure.

In order to work under milder conditions, the same emulsion polymerization of BMA was repeated by using a violet LED (λ_{max} = 394 nm) as a light source. The polymerization rate was similar to the case of UV irradiation, and the polymer showed MW matching the

theoretical value and low dispersity $Đ$ = 1.16 (**Table 5-1** and **Figure 5-2**). In both cases, polymer particles were homogeneously distributed with average size $d_{Z\text{-ave}}$ of about 97 and 70 nm, as revealed by dynamic light scattering (DLS) measurements. It should be noted that these systems employed a water-soluble ATRP initiator, 2-hydroxyethyl 2-bromophenylacetate (OH-BPA), and a low stirring rate, 250 rpm, which were both necessary to achieve an effective particle nucleation in the water phase.[7] Moreover, the monomer and the aqueous phase were not mixed prior to starting the polymerization (i.e. the light irradiation), to further prevent the radical generation inside the hydrophobic monomer phase.

Table 5-1. Effect of light source on the photoinduced ab initio emulsion ATRP of BMA.[a]

Entry	Light source	t (h)	Conv (%)	$M_{n,th}$ ($\times 10^{-3}$)	$M_{n,app}$ ($\times 10^{-3}$)	$Đ$	$d_{Z\text{-Ave}}$ (nm)
1	UV lamp (λ_{max} = 365 nm)	8.5	81	58.1	47.6	1.19	96.6 ± 1.5
2	Violet LED (λ_{max} = 394 nm)	8.5	70	49.8	46.1	1.16	70.8 ± 0.5

[a]Conditions: [BMA]/[OH-BPA]/[NaBr]/[$CuBr_2$]/[TPMA] = 500/1/20/0.2/1.2, BMA = 20 vol% in H_2O, 18.4 wt% SDS relative to BMA. V_{tot} = 10 mL. Stirring rate = 250 rpm.

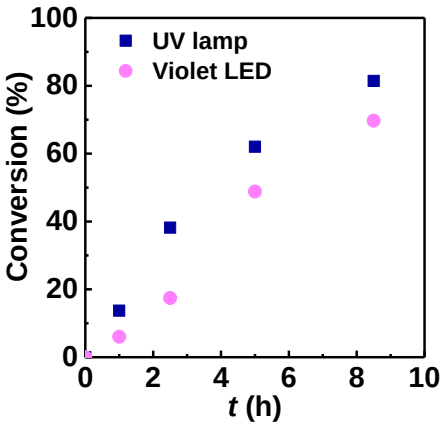

Figure 5-2. Semilogarithmic kinetic plot of the photoinduced emulsion ATRP of BMA 20 vol% in H_2O, by using an UV lamp (squares) or a violet LED (dots) as light source. Conditions as in **Table 5-1**.

Subsequently, the excess TPMA was replaced with triethylamine (TEA, **Figure 5-3**), which is frequently used as a low-cost electron donor in photo-ATRP.[33] However, a bimodal distribution of chains was observed in the samples collected during the polymerization and analyzed by gel permeation chromatography (GPC). Likely, this indicates that some chains were generated inside the hydrophobic phase.[7] By replacing the small molecule initiator OH-BPA with a water-soluble (macro)initiator with a long hydrophilic chain, poly(ethylene glycol) 2-bromophenylacetate (PEO_{2K}-BPA), the emulsion ATRP of BMA was again well-controlled. After 4 h, the monomer conversion was 40% and the polymer showed MW matching the theoretical value and very low dispersity $Đ$ = 1.09 (**Figure 5-3.** Semilogarithmic kinetic plot A), and MW and dispersity evolution with conversion B) in photoinduced emulsion ATRP of BMA 20 vol% in H_2O, [BMA]/[OH-BPA]/[NaBr]/[$CuBr_2$]/[TPMA]/[TEA] = 500/1/20/0.2/0.2/1, 18.4 wt % SDS relative to BMA. V_{tot} = 10 mL. Stirring rate = 250 rpm, violet LED.

Table 5-2, entry 3 and **Figure 5-4**).

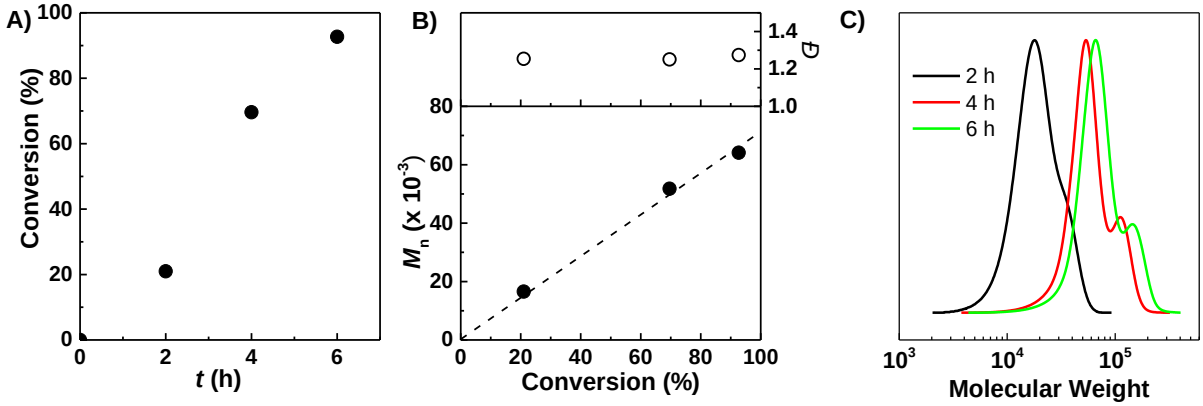

Figure 5-3. Semilogarithmic kinetic plot A), and MW and dispersity evolution with conversion B) in photoinduced emulsion ATRP of BMA 20 vol% in H_2O, [BMA]/[OH-

BPA]/[NaBr]/[$CuBr_2$]/[TPMA]/[TEA] = 500/1/20/0.2/0.2/1, 18.4 wt % SDS relative to BMA. V_{tot} = 10 mL. Stirring rate = 250 rpm, violet LED.

Table 5-2. Photoinduced ab initio emulsion ATRP of various (meth)acrylate monomers.[a]

Entry	M	Log P[b]	I	*t* (h)	Conv (%)	$M_{n,th}$ ($\times 10^{-3}$)	$M_{n,app}$ ($\times 10^{-3}$)	$Đ$	$d_{Z\text{-}Ave}$ (nm)
1	MMA	1.35	PEO_{2K}-BPA	3	94	52.2	32.9	1.79	30.7 ± 0.1
2	EMA	1.88	PEO_{2K}-BPA	4	84	50.0	46.6	1.24	22.3 ± 0.2
3	BMA	2.94	PEO_{2K}-BPA	4	40	28.6	33.6	1.09	70.8 ± 0.5
4	LMA	7.19	PEO_{2K}-BPA	25	6	-	-	-	-
5	BA	2.39-	PEO_{2K}-BiB	20	78	52.1	50.8	1.13	116.5 ± 1.3

[a]Conditions: [M]/[Initiator]/[NaBr]/[$CuBr_2$]/[TPMA]/[TEA] = 500/1/20/0.2/0.2/1, M = 20 vol% in H_2O, 18.4 wt% SDS relative to M. V_{tot} = 10 mL. Stirring rate = 250 rpm, violet LED. [b]Partition coefficients of M in a mixture of octanol/water 1/1. Log P values from chemspider.com, predicted from ACD/labs.

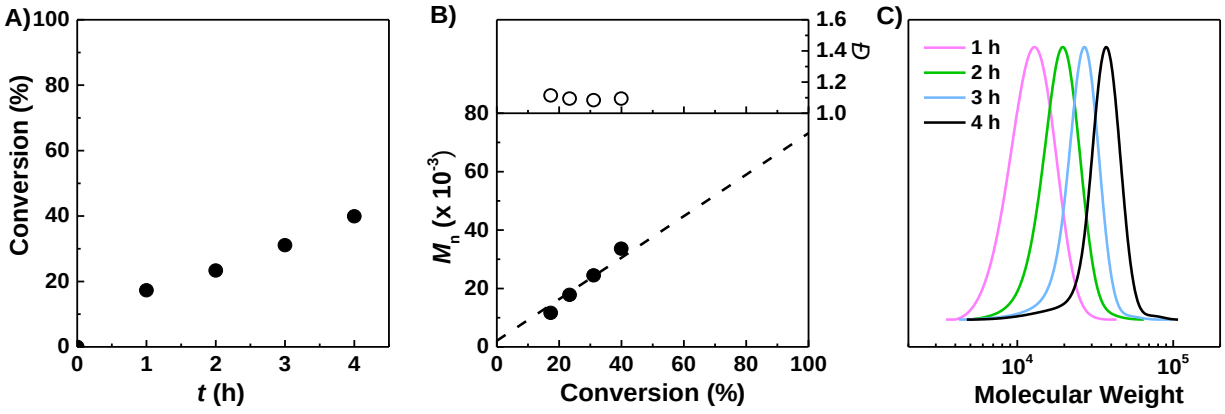

Figure 5-4. Semilogarithmic kinetic plot A), MW and dispersity evolution with conversion B), and GPC traces C) in photoinduced emulsion ATRP of BMA 20 vol% in

H_2O, [BMA]/[PEO_{2k}-BPA]/[NaBr]/[$CuBr_2$]/[TPMA]/[TEA] = 500/1/20/0.2/0.2/1, 18.4 wt% SDS to BMA. V_{tot} = 10 mL. Stirring rate = 250 rpm, violet LED.

Other methacrylate monomers were then tested under identical conditions (**Table 5-2, entries 1 and 2**). Ethyl methacrylate (EMA) showed a faster polymerization (84% conversion in 4h), and the polymer had expected MW and $Đ$ = 1.24 (**Figure 5-5**). Instead, the emulsion ATRP of methyl methacrylate (MMA) was even faster but less controlled (**Figure 5-6**). Interestingly, the polymerization rate increased with increasing the hydrophilicity of the monomer. Indeed, the partition coefficients of various monomers in an octanol-water mixture (log P) are reported in the literature and decrease in the order BMA > EMA > MMA: the monomer hydrophilicity increases according to the same trend. It is likely that more hydrophilic monomers can diffuse faster into the aqueous phase, therefore increasing the polymerization rate. In fact, when lauryl methacrylate was tested as monomer, negligible conversion was observed after 25h (**Table 5-2, entry 4**), due to the very high hydrophobicity of this compound. The increase of particle size with conversion during polymerization of EMA was shown in **Figure 5-7**.

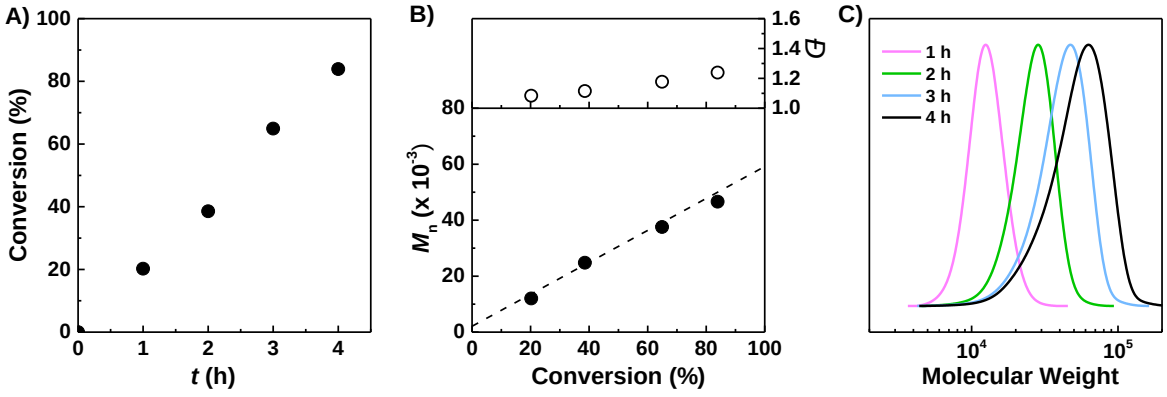

Figure 5-5. Semilogarithmic kinetic plot A), MW and dispersity evolution with conversion B), and GPC traces C) in photoinduced emulsion ATRP of EMA 20 vol% in H_2O, [EMA]/[PEO_{2k}-BPA]/[NaBr]/[$CuBr_2$]/[TPMA]/[TEA] = 500/1/20/0.2/0.2/1, 18.4 wt% SDS to EMA. V_{tot} = 10 mL. Stirring rate = 250 rpm, violet LED.

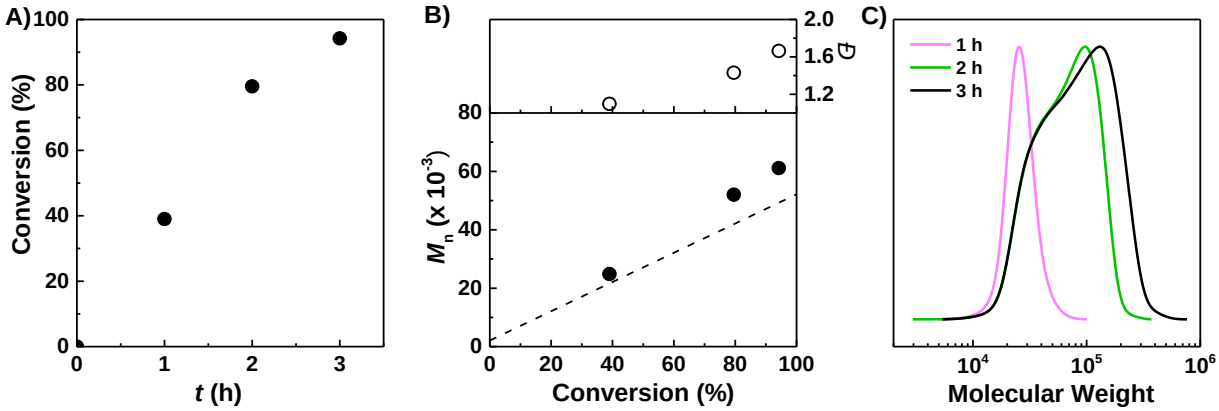

Figure 5-6. Semilogarithmic kinetic plot A), MW and dispersity evolution with conversion B), and GPC traces C) in photoinduced emulsion ATRP of MMA 20 vol% in H_2O, [MMA]/[PEO_{2k}-BPA]/[NaBr]/[$CuBr_2$]/[TPMA]/[TEA] = 500/1/20/0.2/0.2/1, 18.4 wt% SDS to MMA. V_{tot} = 10 mL. Stirring rate = 250 rpm, violet LED.

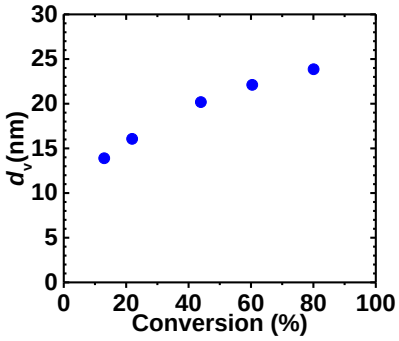

Figure 5-7. Evolution of volume-average diameter of polymer micelles in emulsion ATRP of EMA. See conditions in **Figure 5-9**.

The versatility of the process was confirmed by successfully polymerizing *n*-butyl acrylate (BA) by adopting the same conditions used for methacrylate monomers, except for employing poly(ethylene glyco) 2-bromoisobutyrate (PEO_{2K}-BiB) as a hydrophilic (marco)initiator. The polymerization was slower, reaching 78% conversion in 20 h (**Table 5-2, entry 5** and **Figure 5-8**), due to the lower ATRP reactivity of acrylates compared to methacrylates. Nevertheless, the process was well-controlled and the final polymer had MW matching the theoretical value, $Đ$ = 1.13, and a monomodal distribution of polymer particles, with average size $d_{Z\text{-}Ave}$ = 116.5 ± 1.3 nm.

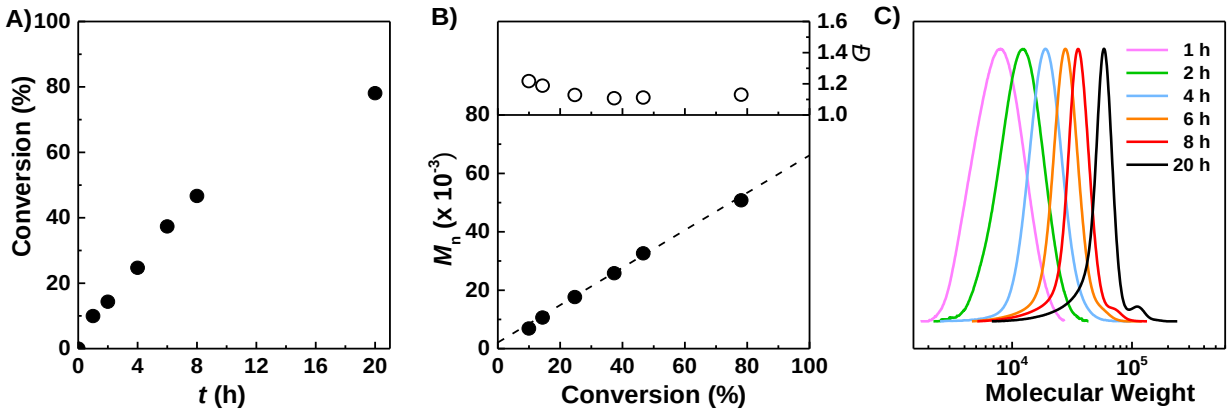

Figure 5-8. Semilogarithmic kinetic plot A), MW and dispersity evolution with conversion B), and GPC traces C) in photoinduced emulsion ATRP of BA 20 vol% in H_2O, [BA]/[PEO_{2k}-BiB]/[NaBr]/[$CuBr_2$]/[TPMA]/[TEA] = 500/1/20/0.2/0.2/1, 18.4 wt% SDS to MMA. V_{tot} = 10 mL. Stirring rate = 250 rpm, violet LED.

The preservation of chain end functionality during photoinduced emulsion ATRP was proved by performing a chain extension experiment (**Figure 5-9**). First, BA (12 vol%) was polymerized under previously described conditions, reaching 75 % conversion in 6 h. The second monomer, *tert*-butyl acrylate (*t*BA), was then fed into the system and incorporated into the growing PBA chains. Therefore, a block copolymer composed of a BA block and a block of randomly distributed BA and *t*BA units was obtained in situ, showing predetermined MW and low dispersity $Đ$ = 1.11.

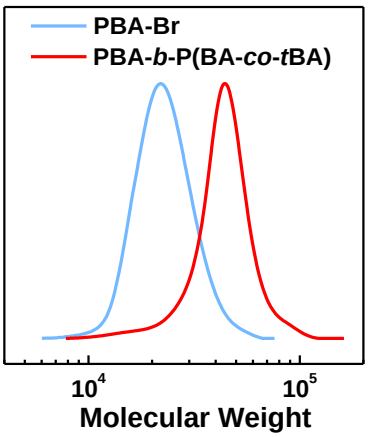

Figure 5-9. GPC traces of PBA-Br and PBA-b-P(BA-co-*t*BA) prepared by photoinduced emulsion ATRP. Conditions: [BA]/[PEO_{2k}-BPA]/[NaBr]/[$CuBr_2$]/[TPMA]/[TEA] = 300/1/20/0.2/0.2/1, 18.4 wt% SDS to BA. 0.8 mL *t*BA were fed to the emulsion system 6 h

after starting the polymerization of BA (feeding rate = 0.4 mL/h). V_{tot} = 10 mL. Stirring rate = 250 rpm, violet LED.

It was previously demonstrated that gradient copolymers can be easily prepared in situ in emulsion ATRP by using a mixture of two monomers with different hydrophilicity.[7] Indeed, the most hydrophilic monomer is initiated first and the most hydrophobic one will be gradually incorporated into the growing particles. Therefore, we envisioned that the polymerization in emulsion of very hydrophobic monomers, such as LMA, could be favored by mixing with a more hydrophilic monomer. Therefore, photoinduced emulsion ATRP of a mixture of LMA (10 vol%) and BMA (10 vol%) was tested. After 20 h, the system reached 36 % conversion, and the obtained copolymer P(BMA-*co*-LMA) contained about 85% BMA and 15% LMA, by weight, as calculated from NMR (**Figure 5-10**) and gravimetric measurements. This result confirms that more hydrophilic monomers can act as shuttle for very hydrophobic LMA units. Since very hydrophobic monomers have not been extensively investigated by RDRP techniques, further work will focus on combining more hydrophilic as well as more hydrophobic monomers and optimizing the operating conditions.

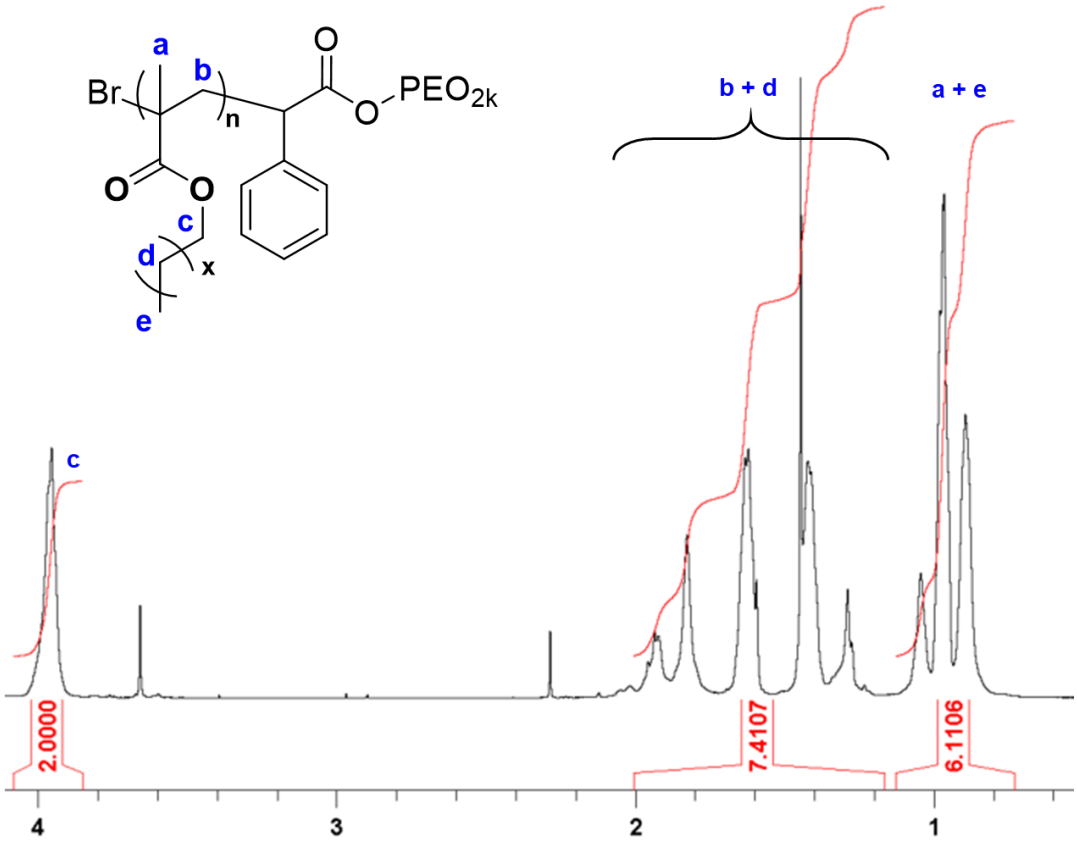

Figure 5-10. ^{1}H NMR of P(BMA-*co*-LMA) prepared by photoinduced emulsion ATRP of a mixture of BMA (10 vol%) and LMA (10 vol%) in H_2O. Conditions: [BMA]/[LMA]/[PEO_{2k}-BiB]/[NaBr]/[$CuBr_2$]/[TPMA]/[TEA] = 330/180/1/20/0.2/0.2/1, 18.4 wt% SDS to BMA+LMA. V_{tot} = 10 mL. Stirring rate = 250 rpm, violet LED. In the molecular structure x = 2 for BMA, and x = 10 for LMA.

Importantly, the photoinduced emulsion ATRP of BMA was also conducted in an open-to-air system, by using an enzymatic deoxygenation process. The use of a small amount of GOx in the presence of glucose to prevent oxygen inhibition was first adopted in free radical polymerization.[34] This technique was recently broadened to aqueous, miniemulsion and emulsion ATRP, with an additional agent, pyruvate, as radical scavenger.[8, 32] By employing GOx, glucose and sodium pyruvate to the emulsion photoATRP of BMA, conversion reached 65% in 4 h, with no detected induction period, and the polymer had MW matching the theoretical value and $Đ$ = 1.29 (**Figure 5-11**). This deoxygenation system greatly simplifies the reaction setup, decreases the cost, and suppresses monomer evaporation during traditional inert gas purging.[8]

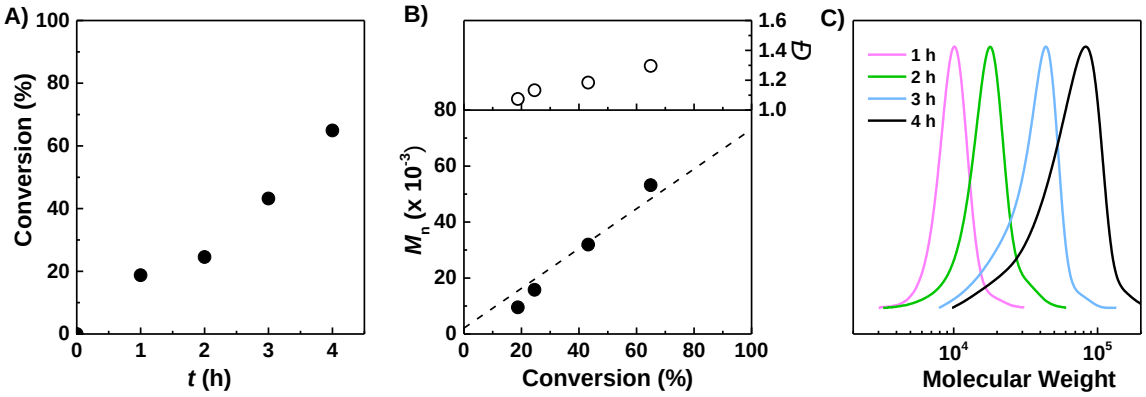

Figure 5-11. Enzymatically-degassed photoinduced ab initio emulsion ATRP of BMA. Semilogarithmic kinetic plot A), evolution of MW and dispersity with conversion B), and GPC traces C). Conditions: [BMA]/[PEO_{2k}BPA]/[NaBr]/[$CuBr_2$/TPMA]/[TEA] = 500/1/20/0.2/1, BMA 20 vol% in H_2O, 18.4 wt% SDS to BMA, [glucose] = 0.2 M, [GOx] = 2 μM, [sodium pyruvate] = 0.1 M. V_{total} = 10 mL. Stirring rate = 250 rpm, violet LED.

5.4. Conclusion

The photoinduced ab initio emulsion ATRP of acrylate and methacrylate monomers was investigated. The reported procedure employs inexpensive materials such as SDS as surfactant and TEA as electron donor, and a relatively low-energy light source (i.e. violet LED). Moreover, the ATRP catalyst loading was low, therefore reducing the metal contamination in the final latexes.

The polymerization rate was observed to increase with increasing the hydrophilicity of the monomer. More hydrophilic monomers could promote the polymerization of very hydrophobic monomers, and therefore copolymers could be obtained from mixtures of two monomers with very different hydrophilicity. Block copolymers were easily prepared by feeding in situ a second monomer.

This photoinduced emulsion ATRP technique allows for tuning the properties and the composition of the (co)polymers, and enables the preparation of polymer particles with homogeneous size distribution (varying between 22 and 116 nm). Further work will

investigate the possibility of tuning the size of the particles by changing the surfactant loading, as well as the preparation of polymers with more complex architectures.

Finally, the photoinduced emulsion ATRP of BMA was successfully conducted in an open-to-air system by adopting an enzymatic degassing process.

5.5. Experimental Section

Materials. Methyl methacrylate (MMA, 99%, Sigma-Aldrich), ethyl methacrylate (EMA, 995, Sigma-Aldrich), butyl methacrylate (BMA, 99% Sigma-Aldrich), lauryl methacrylate (LMA, 96%, Sigma-Aldrich), and butyl acrylate (BA, 99%, Sigma-Aldrich) were passed through a basic alumina column prior to use to remove polymerization inhibitors. Copper(II) bromide ($CuBr_2$, 99%), sodium dodecyl sulfate (SDS, 99%), sodium pyruvate (99%), glucose (96%) and glucose oxidase from *Aspergillus niger* (GOx, 100,000-250,000 units/g solid) were purchased from Sigma-Aldrich and used as received. Sodium bromide (NaBr, 99%) was purchased from Acros. Tris(2-pyridylmethyl)amine (TPMA) was received from KOEI Chemical. 2-Hydroxyethyl 2-bromophenylacetate (OH-BPA), poly(ethylene oxide) 2-bromophenylacetate (PEO_{2K}-BPA), and poly(ethylene glycol) 2-bromoisobutyrate (PEO_{2K}-BiB) were prepared according to literature report.[1]

Instruments. Polymerizations were conducted under either a UV lamp (λ_{max} = 365 nm, 4.9 mW/cm^2, MelodySusie®) or violet LEDs (λ_{max} = 394 nm, 2.6 mW/cm^2). Molecular weight and dispersity were determined by Gel Permeation Chromatography (GPC) equipped with Polymer Standards Services (PSS) columns (guard, 10^5, 10^3, and 10^2 Å) and a differential refractive index detector (Waters, 2410), with THF as eluent at a flow rate of 1.00 mL/min (T = 35 °C). GPC traces were processed by WinGPC 8.0 software (PSS) using a calibration based on linear poly(methyl methacrylate) standards. Monomer conversion was determined by gravimetric analysis, evaporating the samples at 110 °C for at least 30

min. Particle size and size distribution were determined by using a Zetasizer Nano from Malvern Instruments, Ltd.

General procedure for emulsion photo ATRP of BMA. In a 10-mL Schlenk flask was added water (8 mL), PEO_{2K}-BPA (52.81 mg, 0.025 mmol, 1 equiv.), $CuBr_2$/TPMA (0.005 mmol, 0.2 equiv.), SDS (328 mg, 18.4 wt% relative to monomer), NaBr (51.7 mg, 0.50 mmol), and TEA (4 µL, 0.025 mmol). The solution was degassed with nitrogen for 30 min. BMA was degassed in a separate vial and was slowly added to the aqueous solution (2.0 mL, 12.57 mmol, 500 equiv.) The reaction was irradiated under a light source with a stirring rate of 250 rpm. Samples were taken for monomer conversion and GPC analysis.

Procedure for emulsion photo ATRP of BMA using GOx deoxygenation agent. PEO_{2K}-BPA (52.81 mg, 0.025 mmol, 1 equiv.), $CuBr_2$/TPMA (0.005 mmol, 0.2 equiv.), SDS (328 mg, 18.4 wt% relative to monomer), NaBr (51.7 mg, 0.50 mmol), TEA (4 µL, 0.025 mmol), glucose (0.36 g, 2 mmol) and Na pyruvate (0.11 g, 1 mmol) were dissolved into 8 mL water in a 10 mL Schlenk flask. GOx (0.0032 g, 2×10^{-5} mmol) was added to the solution before the flask was capped by a rubber septum. After 3 min stirring, BMA (2.0 mL, 12.57 mmol, 500 equiv., no need to degas) was slowly added to the aqueous solution. The reaction was irradiated under violet light with a stirring rate of 250 rpm. Samples were taken for monomer conversion and GPC analysis.

5.6. References

(1) Cunningham, M. F., Controlled/Living Radical Polymerization in Aqueous Dispersed Systems. *Prog. Polym. Sci.* **2008,** *33* (4), 365-398.
(2) Zetterlund, P. B.; Thickett, S. C.; Perrier, S.; Bourgeat-Lami, E.; Lansalot, M., Controlled/Living Radical Polymerization in Dispersed Systems: An Update. *Chem. Rev.* **2015,** *115* (18), 9745-9800.
(3) Eslami, H.; Zhu, S., Emulsion Atom Transfer Radical Polymerization of 2-Ethylhexyl Methacrylate. *Polymer* **2005,** *46* (15), 5484-5493.

(4) Qiu, J.; Charleux, B.; Matyjaszewski, K., Controlled/Living Radical Polymerization in Aqueous Media: Homogeneous and Heterogeneous Systems. *Prog Polym Sci* **2001,** *26* (10), 2083-2134.
(5) Min, K.; Matyjaszewski, K., Atom Transfer Radical Polymerization in Aqueous Dispersed Media. *Cent Eur J Chem* **2009,** *7* (4), 657-674.
(6) Fantin, M.; Chmielarz, P.; Wang, Y.; Lorandi, F.; Isse, A. A.; Gennaro, A.; Matyjaszewski, K., Harnessing the Interaction between Surfactant and Hydrophilic Catalyst To Control eATRP in Miniemulsion. *Macromolecules* **2017,** *50* (9), 3726-3732.
(7) Lorandi, F.; Wang, Y.; Fantin, M.; Matyjaszewski, K., Ab Initio Emulsion Atom-Transfer Radical Polymerization. *Angewandte Chemie International Edition* **2018,** *57* (27), 8270-8274.
(8) Wang, Y.; Fu, L.; Matyjaszewski, K., Enzyme-Deoxygenated Low Parts per Million Atom Transfer Radical Polymerization in Miniemulsion and Ab Initio Emulsion. *Acs Macro Lett* **2018,** *7* (11), 1317-1321.
(9) Wang, Y.; Lorandi, F.; Fantin, M.; Chmielarz, P.; Isse, A. A.; Gennaro, A.; Matyjaszewski, K., Miniemulsion ARGET ATRP via Interfacial and Ion-Pair Catalysis: From ppm to ppb of Residual Copper. *Macromolecules* **2017,** *50* (21), 8417-8425.
(10) Cordero, R.; Jawaid, A.; Hsiao, M.-S.; Lequeux, Z.; Vaia, R. A.; Ober, C. K., Mini Monomer Encapsulated Emulsion Polymerization of PMMA Using Aqueous ARGET ATRP. *Acs Macro Lett* **2018,** *7* (4), 459-463.
(11) Wei, Y.; Jia, Y.; Wang, W.-J.; Li, B.-G.; Zhu, S., Surfactant–Ligand Design for ab Initio Emulsion Atom Transfer Radical Polymerization. *Macromolecules* **2014,** *47* (22), 7701-7706.
(12) Fan, W.; Tosaka, M.; Yamago, S.; Cunningham, M. F., Living Ab Initio Emulsion Polymerization of Methyl Methacrylate in Water Using a Water-Soluble Organotellurium Chain Transfer Agent under Thermal and Photochemical Conditions. *Angewandte Chemie International Edition* **2018,** *57* (4), 962-966.
(13) Canning, S. L.; Smith, G. N.; Armes, S. P., A Critical Appraisal of RAFT-Mediated Polymerization-Induced Self-Assembly. *Macromolecules* **2016,** *49* (6), 1985-2001.
(14) Wang, G.; Wang, Z.; Lee, B.; Yuan, R.; Lu, Z.; Yan, J.; Pan, X.; Song, Y.; Bockstaller, M. R.; Matyjaszewski, K., Polymerization-Induced Self-Assembly of Acrylonitrile via ICAR ATRP. *Polymer* **2017,** *129*, 57-67.
(15) Wang, J.; Wu, Z.; Wang, G.; Matyjaszewski, K., In Situ Crosslinking of Nanoparticles in Polymerization‐Induced Self‐Assembly via ARGET ATRP of Glycidyl Methacrylate. *Macromol Rapid Comm* **2018**, 1800332.
(16) Darabi, A.; Shirin-Abadi, A. R.; Pinaud, J.; Jessop, P. G.; Cunningham, M. F., Nitroxide-Mediated Surfactant-Free Emulsion Copolymerization of Methyl Methacrylate and Styrene Using Poly (2-(diethyl) aminoethyl Methacrylate-co-Styrene) as a Stimuli-Responsive Macroalkoxyamine. *Polym Chem-Uk* **2014,** *5* (21), 6163-6170.
(17) Derry, M. J.; Fielding, L. A.; Armes, S. P., Polymerization-Induced Self-Assembly of Block Copolymer Nanoparticles via RAFT Non-Aqueous Dispersion Polymerization. *Prog. Polym. Sci.* **2016,** *52*, 1-18.
(18) Dadashi-Silab, S.; Doran, S.; Yagci, Y., Photoinduced Electron Transfer Reactions for Macromolecular Syntheses. *Chem Rev* **2016,** *116* (17), 10212-10275.
(19) Pan, X.; Tasdelen, M. A.; Laun, J.; Junkers, T.; Yagci, Y.; Matyjaszewski, K., Photomediated Controlled Radical Polymerization. *Prog Polym Sci* **2016,** *62*, 73-125.

(20) Yagci, Y.; Jockusch, S.; Turro, N. J., Photoinitiated Polymerization: Advances, Challenges, and Opportunities. *Macromolecules* **2010,** *43* (15), 6245-6260.
(21) Corrigan, N.; Shanmugam, S.; Xu, J.; Boyer, C., Photocatalysis in Organic and Polymer Synthesis. *Chem Soc Rev* **2016,** *45* (22), 6165-6212.
(22) Dadashi-Silab, S.; Atilla Tasdelen, M.; Yagci, Y., Photoinitiated Atom Transfer Radical Polymerization: Current Status and Ruture Perspectives. *Journal of Polymer Science Part A: Polymer Chemistry* **2014,** *52* (20), 2878-2888.
(23) Jasinski, F.; Zetterlund, P. B.; Braun, A. M.; Chemtob, A., Photopolymerization in Dispersed Systems. *Prog Polym Sci* **2018,** *84*, 47-88.
(24) Krüger, K.; Tauer, K.; Yagci, Y.; Moszner, N., Photoinitiated Bulk and Emulsion Polymerization of Styrene – Evidence for Photo-Controlled Radical Polymerization. *Macromolecules* **2011,** *44* (24), 9539-9549.
(25) Ciftci, M.; Tasdelen, M. A.; Li, W.; Matyjaszewski, K.; Yagci, Y., Photoinitiated ATRP in Inverse Microemulsion. *Macromolecules* **2013,** *46* (24), 9537-9543.
(26) Tan, J.; Sun, H.; Yu, M.; Sumerlin, B. S.; Zhang, L., Photo-PISA: Shedding Light on Polymerization-Induced Self-Assembly. *Acs Macro Lett* **2015,** *4* (11), 1249-1253.
(27) Jung, K.; Xu, J.; Zetterlund, P. B.; Boyer, C., Visible-Light-Regulated Controlled/Living Radical Polymerization in Miniemulsion. *Acs Macro Lett* **2015,** *4* (10), 1139-1143.
(28) Yeow, J.; Boyer, C., Photoinitiated Polymerization-Induced Self-Assembly (Photo-PISA): New Insights and Opportunities. *Advanced Science* **2017,** *4* (7), 1700137.
(29) Jung, K.; Boyer, C.; Zetterlund, P. B., RAFT Iniferter Polymerization in Miniemulsion Using Visible Light. *Polym. Chem.* **2017,** *8* (27), 3965-3970.
(30) Yeow, J.; Xu, J.; Boyer, C., Polymerization-Induced Self-Assembly Using Visible Light Mediated Photoinduced Electron Transfer–Reversible Addition–Fragmentation Chain Transfer Polymerization. *Acs Macro Lett* **2015,** *4* (9), 984-990.
(31) Wang, Y.; Dadashi-Silab, S.; Matyjaszewski, K., Photoinduced Miniemulsion Atom Transfer Radical Polymerization. *Acs Macro Lett* **2018,** *7* (6), 720-725.
(32) Enciso, A. E.; Fu, L.; Russell, A. J.; Matyjaszewski, K., A Breathing Atom‐Transfer Radical Polymerization: Fully Oxygen‐Tolerant Polymerization Inspired by Aerobic Respiration of Cells. *Angewandte Chemie International Edition* **2018,** *57* (4), 933-936.
(33) Ribelli, T. G.; Konkolewicz, D.; Bernhard, S.; Matyjaszewski, K., How are Radicals (Re) Generated in Photochemical ATRP? *J Am Chem Soc* **2014,** *136* (38), 13303-13312.
(34) Oytun, F.; Kahveci, M. U.; Yagci, Y., Sugar Overcomes Oxygen Inhibition in Photoinitiated Free Radical Polymerization. *J Polym Sci Pol Chem* **2013,** *51* (8), 1685-1689.

Chapter 6 Oxygen Tolerant Atom Transfer Radical Polymerization in Miniemulsion and Emulsion

6.1. Preface

This content of this chapter was published in ACS Macro Letters (**Y. Wang**, Liye Fu, K. Matyjaszewski, "Enzyme-Deoxygenated Low ppm ATRP in Miniemulsion and *Ab Initio* Emulsion" *ACS Macro Letters*, **2018**, 7, 1317-1321.)

The work in this chapter is a continuation of results presented in previous chapters. All the experiments in previous chapters required oxygen exclusion since oxygen quenches the propagating radical and oxidizes the activator. In 2018, our group developed a glucose oxidase (GOx) deoxygenation system composed of glucose, GOx and pyruvate (Enciso, A. E.; Fu, L. Y.; Russell, A. J.; Matyjaszewski, K., *Angew. Chem. Int. Ed.* **2018,** *57* (4), 933-936.). This system transforms oxygen into inert species and achieves oxygen tolerance in homogeneous aqueous ATRP.

The idea to use the GOx system in miniemulsion and emulsion ATRP came from a discussion between Liye Fu and me. We conducted the polymer synthesis and characterization together. I contributed in most synthetic part and Liye analyzed the stability of the enzyme by circular dichroism (CD).

The financial support from NSF CHE 170749 and NIH (R01DE020843) is acknowledged.

6.2. Introduction

Reversible deactivation radical polymerization (RDRP) techniques have been widely studied and utilized to synthesize polymers with predetermined molecular weight and low dispersity. RDRP methods are compatible with a broad range of functional groups and solvents, and permit the synthesis of polymers with well-defined molecular architecture.[1] Atom transfer radical polymerization (ATRP)[2-5] and reversible addition-fragmentation (RAFT) polymerization[6-7] are among the most often used RDRP techniques, where the fraction of terminated chains is suppressed and chains grow concurrently.

Miniemulsion and emulsion procedures, used in dispersed aqueous media, are characterized by efficient heat transfer, low viscosity, and lack of volatile organic solvents.[8] Thus, polymerization in dispersed media is increasingly favored in both laboratory and industry. Indeed, many polymer emulsions are commercial products. RDRP in dispersed media can be more efficient than in homogeneous media for the synthesis of star, brush and multiblock polymers, as the compartmentalization effect further suppresses radical termination.[9]

Oxygen inhibits radical polymerizations.[10] O_2 reacts with C-based radicals to form low reactivity peroxy-radicals. Also, it oxidizes the ATRP activator, typically a $Cu^{I}L$ species to form the $Cu^{II}L$ deactivator species), thus gradually quenching the polymerization. Commonly used laboratory degassing techniques include freeze-pump-thaw cycles, purging with inert gas, and working in a glove box or Schlenk line. These methods are time consuming, difficult to scale up, challenging for non-experts, and may lead to significant evaporation of some volatile reagents. It would therefore be advantageous to design a chemical degassing procedure that is orthogonal to RDRP.

In recent years, four types of oxygen tolerant RDRP systems have been developed.[10] One is polymerizing "through oxygen", wherein a limited amount of O_2 is consumed by the propagating radicals and peroxides are incorporated in the polymer chain. This happens with a relatively high flux of radicals[11] and with a small headspace in the reaction vessel.[12] Another method used for both ATRP and RAFT is enzyme-degassing, where the oxidation of glucose catalyzed by GOx consumes oxygen rapidly and generates H_2O_2. The high activity and high stability of GOx makes this system attractive for radical polymerization.[13-18] However, in ATRP, H_2O_2 could interact with Cu(I) species via Fenton-like reaction and generate excess radicals, leading to unexpected new chains. This problem could be addressed by addition of sodium pyruvate to transforms H_2O_2 to inert species.[18] A third method is based on activator regeneration (ARGET ATRP), where reducing agents, such as ascorbic acid (AsAc) or tin (II)) scavenge oxygen.[12, 19-20] Lastly, photochemical RAFT systems, including photoinduced electron/energy transfer (PET)-RAFT, photoinduced RAFT and photoiniferter RAFT polymerizations also exhibit oxygen tolerance.[21-24] In PET-RAFT, triplet oxygen is rapidly transformed to singlet oxygen in the presence of singlet oxygen quenchers. [21-22, 25-26]

Most of the methods mentioned above have been reported in both organic and aqueous media. However the enzyme-degassing system in the presence of GOx has so far required aqueous media (or water/highly polar solvent mixture) to retain activity,[27-28] and this method has only been used for preparation of water-soluble polymers. The oxygen tolerant RDRP in dispersed media was only once reported. The activators generated by electron transfer (AGET) ATRP was conducted by the addition of excess ascorbic acid to consume the oxygen.[20] However, evaluating the appropriate dosage of AsAc for the

polymerization is challenging. The required amount depends not only on polymerization kinetics, but also on the flask size, reaction volume, and head space.

In this Chapter, we report the application of GOx-deoxygenated ATRP in miniemulsion and emulsion. The polymerizations were controlled by a Cu/TPMA/DS^- (tris(2-pyridylmethyl)amine)/dodecyl sulfate) ion-pair catalyst.[29-32] The reaction conditions were adapted from nitrogen-degassed systems. This enzyme-assisted deoxygenation was applied to various ATRP techniques and it was tested for polymerization of acrylates and methacrylates. The scalability was also investigated.

6.3. Results and Discussion

Table 6-1 shows the composition of miniemulsion and emulsion ARGET ATRP using the GOx-degassing method in the presence of glucose and pyruvate.[18] The procedure used for oxygen tolerant miniemulsion ATRP utilizing an ion-pair catalyst was straightforward. Glucose and sodium pyruvate were dissolved in the aqueous solution of NaBr and SDS. The aqueous solution was mixed with the organic solution and homogenized by ultrasonication to form a white miniemulsion. Finally, GOx was added to the miniemulsion, and the flask was capped with a rubber stopper, and stirred for 3 min. Polymerization was then triggered by feeding AsAc aqueous solution to the reaction (**Scheme 6-1**).

Table 6-1. Composition of organic and aqueous phases in miniemulsion and emulsion ARGET ATRP of BMA.

component[a]	weight (g)	comments
organic phase		
BMA	1.79	20 vol% (18 wt%) to total

EBPA	0.015	Initiator in miniemulsion ATRP, [BMA]/[EBPA] = 280/1
Hexadecane (HD)	0.19	10.8 wt% to BMA (ONLY used for miniemulsion）
aqueous phase		
Water	8	Distilled water
PEO_{2k}-BPA	0.053	Initiator in emulsion ATRP, [BMA]/[PEO_{2k}-BPA] = 500/1
SDS	0.082	4.6 wt% to BMA
NaBr	0.10	[NaBr] = 0.1 M
$Cu^{II}Br_2$	2.2×10^{-3}	1 mM with respect to V_{total}
TPMA	2.9×10^{-3}	[$Cu^{II}Br_2$]/[TPMA] = 1/1
Glucose	0.36	[Glucose] = 0.2 M
Sodium pyruvate	0.11	[Sodium pyruvate] = 0.1 M
GOx	3.2×10^{-3}	2 μM, added 3 minutes before reaction
AsAc		Fed at 6.5×10^{-4} g/h

[a]Conditions: T = 45 °C. V_{total} = 10 mL. The miniemulsion was prepared by ultrasonication, and the emulsion formed during polymerization. See details in the Supporting Information.

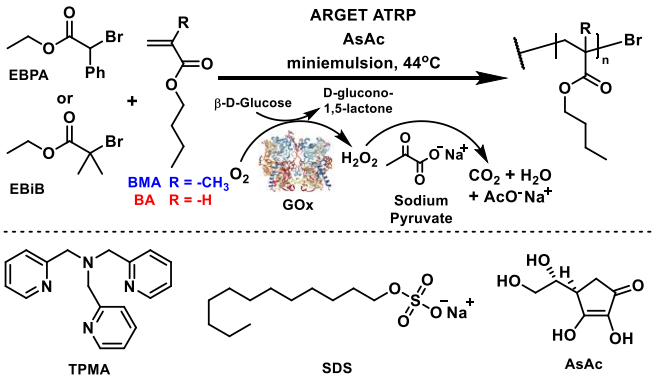

Scheme 6-1. Miniemulsion ARGET ATRP of BMA and BA using GOx deoxygenating system.

Miniemulsion ARGET ATRP of *n*-butyl methacrylate (BMA) and *n*-butyl acrylate (BA) were carried out using the GOx deoxygenating system, **Figure 6-1**. The molar ratio was [M]/[I]/[$CuBr_2$]/[TPMA] = 280/1/0.22/0.22 (I = ethyl α-bromophenylacetate (EBPA) for BMA and ethyl α-bromoisobutyrate (EBiB) for BA). The feeding rate of AsAc was 3.7 μmol/h. Well-controlled polymers were synthesized in a few hours. For BMA, 89% conversion was reached after 6.5 h, yielding polymers with $M_{n,exp}$ = 32,400 (vs. $M_{n,th}$ = 35,600) and low dispersity, 1.16. The polymerization of BA reached 71% conversion after 20 h. The M_n =25,300 of the final polymer was very close to its theoretical value (25,700) with a low dispersity, 1.24. The Zeta-average PBA particle size was 114.6 ± 0.8 nm, which was not influenced by addition of GOx, glucose and sodium pyruvate.[30] The chain-end functionality of PBA was demonstrated by successful chain extension by *tert*-butyl acrylate (*t*BA) (**Figure 6-2**). Thus, enzyme deoxygenated miniemulsion ARGET ATRP was successf ully applied to polymerization of both acrylates and methacrylates.

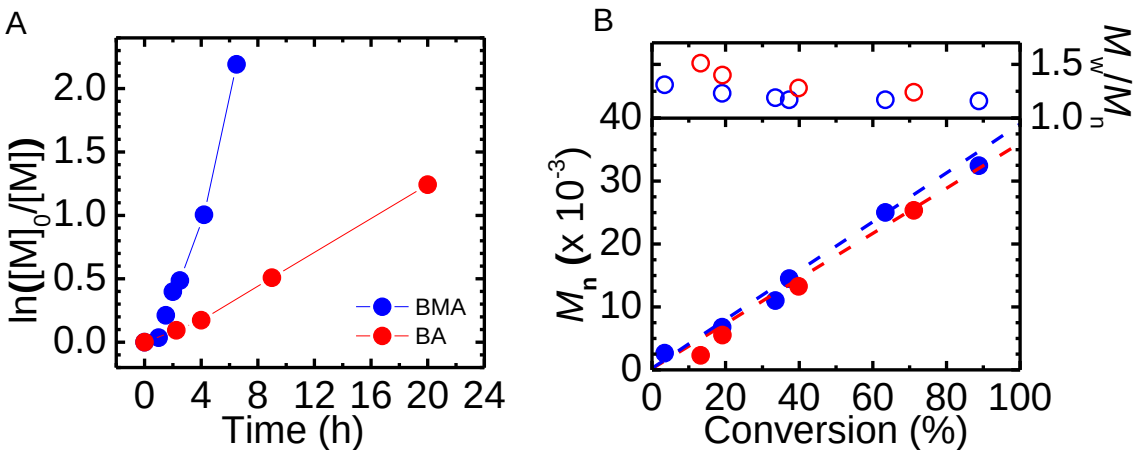

Figure 6-1. GOx degassed miniemulsion ARGET ATRP of BMA and BA. (A) Kinetics; (B) Evolution of M_n and Đ. Reaction conditions: BMA or BA (monomer, M) 2 mL (20 vol %), [M]/[I]/[$CuBr_2$/TPMA]= 280/1/0.2, [HD] = 10 wt % relative to M, [SDS] = 4.6 wt % relative to M, [NaBr] = 0.1 M, [glucose] = 0.2 M, [GOx] = 2 μM, [sodium pyruvate] = 0.1 M, T = 44 °C. AsAc was fed at a rate of 3.7 μmol/h.

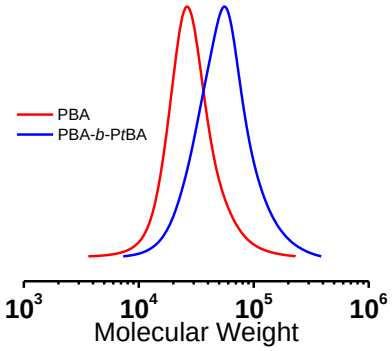

Figure 6-2. Chain extension of PBA-MI with *t*BA in miniemulsion. Reaction condition: *t*BA 1.67mL, [*t*BA]/[PBA MI]/[$CuBr_2$]/[TPMA] = 500/1/0.02/0.02, [SDS] = 4.6 wt% relative to *t*BA, [NaBr] = 0.1 M, [AsAc] = 2.5 mM. [glucose] = 0.2 M, [GOx] = 2 μM, [sodium pyruvate] = 0.1 M.

In addition to the enzyme-assisted degassing, traditional nitrogen bubbling and polymerization without any deoxygenation were also conducted (**Figure 6-3**). Nitrogen purging is an efficient method to remove oxygen prior to polymerization and is commonly

used in RDRP. The rate of polymerization using GOx was higher than with nitrogen purging due to a more thorough deoxygenation. As continuous injection of AsAc could facilitate consumption of oxygen, a control experiment without any degassing was carried out. After more than 6 hours induction period, 10% conversion was observed after next 12 h, but the molecular weight was twice higher than the theoretical value and the dispersity was high (1.44), indicating poor initiation efficiency and inefficient control. Thus GOx-degassing system increased rate of polymerization and provided superior control compared to other methods.

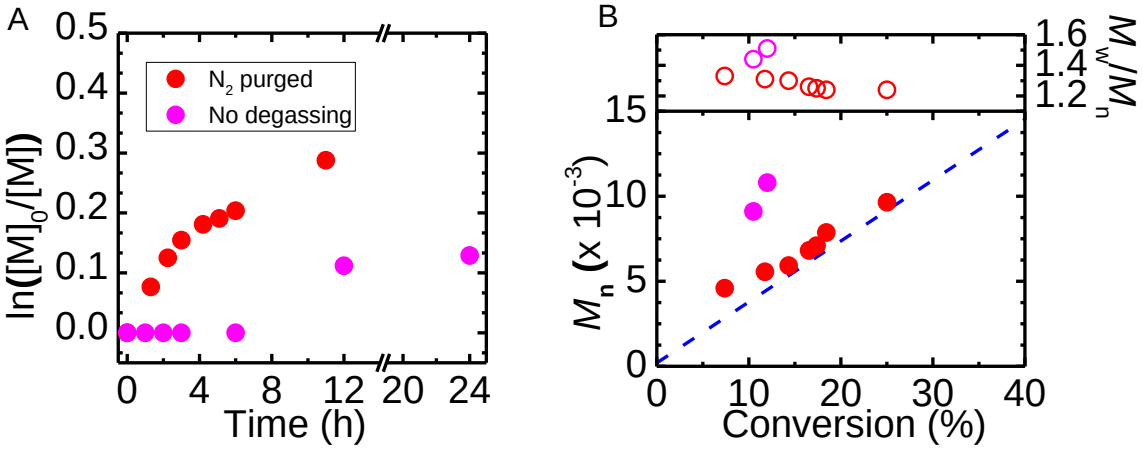

Figure 6-3. GOx degassed miniemulsion ARGET ATRP of BMA using (●) 30 min mild nitrogen bubbling; (●) no deoxygenation. (A) Kinetic plots; (B) Evolution of M_n and $Đ$ vs conversion. Reaction conditions: BMA 2 mL (20 vol %), [BMA]/[EBPA]/[$CuBr_2$/TPMA] = 280/1/0.2, [HD] = 10 wt % relative to BMA, [SDS] = 4.6 wt % relative to BMA, [NaBr] = 0.1 M, T = 44 °C. AsAc was fed at a rate of 3.7 μmol/h.

The ion-pair catalysis involving the Cu/TPMA/DS^- was applied to electrochemically mediated ATRP (*e*ATRP) and photoinduced ATRP (photo-ATRP), respectively (**Figure 6-4**). Using the same conditions as in original reports,[29, 32] well-controlled polymerizations were successfully carried out without nitrogen purging by

simple addition of glucose, GOx and sodium pyruvate. All miniemulsion polymerizations were triggered without significant induction period, and led to polymers with low dispersity.

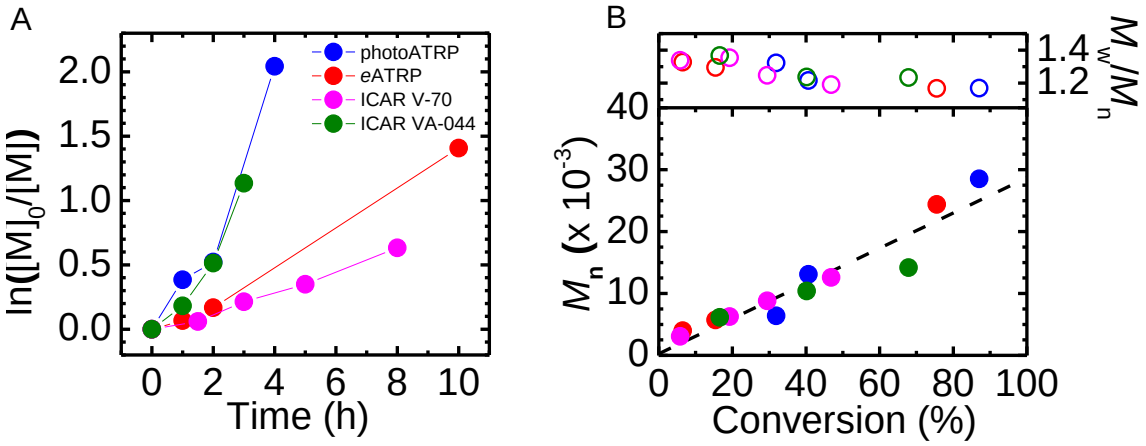

Figure 6-4. GOx degassed miniemulsion photoATRP, eATRP and ICAR ATRP of BMA. (A) Kinetics; (B) Evolution of M_n and Đ. Reaction conditions: BMA 2 mL (20 vol %), [BMA]/[EBPA]/[$CuBr_2$] = 200/1/0.16, [HD] = 10 wt % relative to BMA, [SDS] = 4.6 wt % relative to BMA, [NaBr] = 0.1 M, [glucose] = 0.2 M, [GOx] = 2 μM, [sodium pyruvate] = 0.1 M, T = 44 °C (except ICAR ATRP using V-70 at 30 °C). photoATRP--[$CuBr_2$]/[TPMA] = 1/3, λ_{max} = 365 nm, intensity = 5 mW/cm^2; eATRP--[$CuBr_2$]/[TPMA] = 1/1, $E_{app} = E_{pc, CuTPMA}$, working electrode = Pt mesh; ICAR ATRP--[$CuBr_2$]/EBPA = 1/1, TI/EBPA = 0.3/1, TI = VA-044 or V-70.

ICAR ATRP with thermal radical initiators (TI) with different water solubility was then investigated. According to previous reports,[29] over 95% of Cu resides on the surface of the oil drop lets, thus both hydrophilic and hydrophobic radicals could access the Cu catalysts and trigger polymerization. The water-soluble VA-044 and oil-soluble V-70 had $t_{1/2}$ = 10 h at 44 and 30 °C, respectively. To ensure the similar rate of initiator dissociation, the ratio of [EBPA]/[TI] was fixed at 1/0.3, and the two ICAR ATRP reactions were carried out at these temperatures. The polymerization induced by V-70 was slower because rate of activation (k_{act}),[33] ATRP equilibrium constant (K_{ATRP}), and rate of propagation (k_p) of BMA

all increase with temperature.[34] Yet in all aforementioned ATRP systems, the obtained polymers had predetermined molecular weights and low dispersities (**Figure 6-4**).

The GOx deoxygenated system was then applied to a standard emulsion. Conducting emulsion polymerization does not require high sheer forces, and thus is more energy efficient. The key to synthesize polymers with predetermined molecular weight is to avoid pre-emulsification and maintain a low stirring rate.[31] Previously, the aqueous solution, monomer, and AsAc solution had to be degassed separately. Employing the GOx deoxygenation system avoided this problem. The aqueous solution of initiator PEG_{2k}-BPA, SDS, NaBr, glucose, and sodium pyruvate was mixed with GOx, and then BMA was slowly injected to the flask without stirring. AsAc was fed into the flask at a stirring rate of 250 rpm. The monomer slowly diffused to the formed polymer micelles and the organic layer disappeared after one hour. The conversion reached 60% after 4 h, and the molecular weight matched the theoretical value with dispersity as low as 1.15 (**Figure 6-5**). The final Zeta-average particle size was 184.6 ± 1.8 nm.

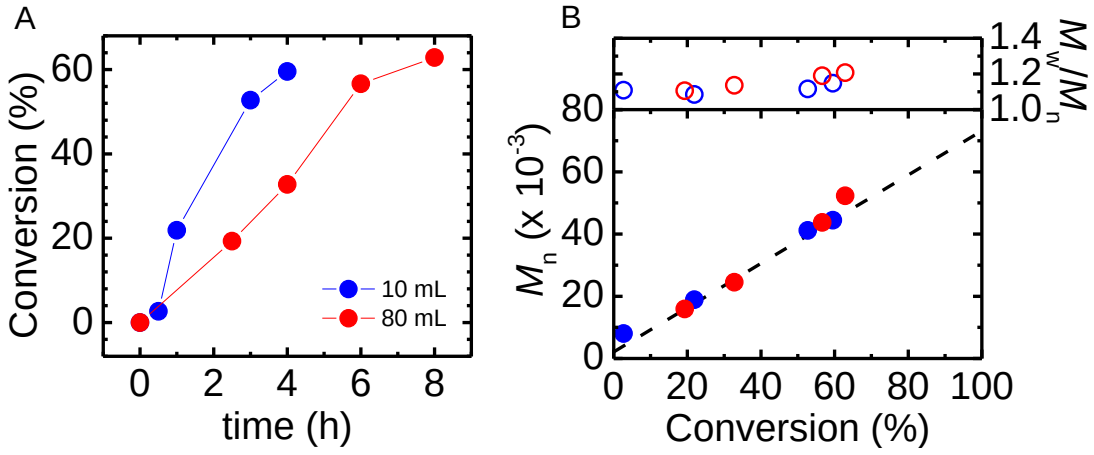

Figure 6-5. GOx degassed *ab initio* emulsion ARGET ATRP of BMA using different total volumes. (A) Kinetics; (B) Evolution of M_n and $Đ$. Conditions: [BMA]/[PEO_{2k}BPA]/[NaBr]/[$CuBr_2$/TPMA] = 500/1/20/0.2, BMA 20% (v/v) in H_2O,

SDS was 18.4 wt% to BMA. [glucose] = 0.2 M, [GOx] = 2 μM, [sodium pyruvate] = 0.1 M. V_{total} = 10 mL or 80 mL. T = 44 °C. (10 mL) 0.8; (80 mL) 6.4 μmol AsAc injected at t = 0, then AsAc was fed with a syringe pump, feeding rate = (10 mL) 0.8; (80 mL) 6.4 μmol /h. Stirring rate = 250 rpm.

Since emulsion polymerization is widely used in industrial applications, the feasibility of scaling up the GOx-deoxygenated emulsion ATRP was tested. The total volume was increased to 80 mL using identical molar ratios of reagents (**Figure 6-5**). The rate of polymerization slightly decreased due to less efficient stirring in the larger volume flask. Nevertheless, over 60% conversion was reached in 8 h, and the molecular weight of the final polymer agreed perfectly with the theoretical value and had low dispersity. Since glucose, GOx, and sodium pyruvate are very inexpensive, this system can be attractive for industry.

SDS is a commonly used surfactant, but it is also often used to denature proteins by disrupting non-covalent peptide bonds. Thus, SDS could destroy enzymes. Therefore, circular dichroism (CD) measurements were carried out to examine the viability of the enzyme. In all of the ATRP experiments, 4.6 wt % SDS vs. monomer was used, i.e. 28.5 mM. The same concentration of SDS was used with GOx in deionized water for 2 hours and compared to a control group, without added SDS, and another experiment in which SDS was added just before the measurement.

In the CD spectra (**Figure 6-6**), signals of all samples perfectly overlapped, indicating the unchanged secondary structure of GOx. This is in agreement with a previous report,[35] where SDS did not show any rapid effects on the stability of GOx.

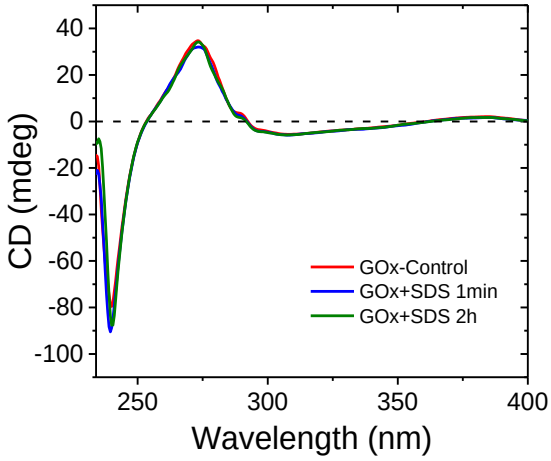

Figure 6-6. CD spectra of GOx solution in the absence and presence of SDS. [GOx] = 2 μM, [SDS] = 28.5 mM, T = 44 ºC.

6.4. Conclusion

In conclusion, oxygen tolerant ATRP using GOx as oxygen scavenger was conducted in miniemulsion and emulsion ATRP using various low ppm ATRP techniques. The GOx deoxygenation process is greener than nitrogen purging, as monomer evaporation is suppressed. The compatibility of the GOx deoxygenation system with several ATRP methods and monomers was confirmed. The stability of GOx in miniemulsion was demonstrated both by polymerization results and CD analysis. The application of GOx was expanded to dispersed media and constitutes the first report of GOx-assisted synthesis of hydrophobic polymers with industrial potentials.

6.5. Experimental Section

Materials. Copper(II) bromide (CuBr2, 99%), sodium dodecyl sulfate (SDS, 99%), hexadecane (HD, 99%), tetrahydrofuran (THF, > 99%), ethyl α-bromoisobutyrate (EBiB, 98%), ethyl α-bromophenylacetate (EBPA, 97%), sodium pyruvate (99%), glucose (96%), glucose oxidase from Aspergillus niger (GOx, 100,000-250,000 units/g solid) and ascorbic acid (AsAc) were purchased from Sigma-Aldrich. Sodium bromide (NaBr, 99%) was purchased from Fisher Scientific. Tetraethylammonium hexafluorophosphate (Et4NPF6, 98%) was purchased from Alfa Aesar. 2,2'-Azobis[2-(2-imidazolin-2-yl)propane]dihydrochloride (VA-044, 98%) and 2,2'-azobis(4-methoxy-2,4-dimethylvaleronitrile) (V-70, 98%) were purchased from Wako Chemical Corporation. Tris(2-pyridylmethyl)amine (TPMA) and poly(ethylene glycol) bromophenylacetate (PEO2k-BPA) were prepared according to published procedures.1 n-Butyl methacrylate (BMA, 99%, Aldrich), n-butyl acrylate (BA, 99%, Aldrich) and tert-butyl acrylate (tBA, 99%, Aldrich) were passed through a column filled with basic alumina prior to use to remove polymerization inhibitors.

Apparatus configuration and characterization.

Ultrasound treatment was carried out using Sonics & Materials VCX500 ultrasonicator.

Mn and Mw/Mn were determined by GPC equipped with Polymer Standards Services (PSS) columns (SDV, 105, 103, and 102 Å) and a differential refractive index detector (Waters, 2410), with THF as eluent at a flow rate 1.00 mL/min (T = 35 °C). GPC traces were processed by WinGPC 8.0 software (PSS) using a calibration based on linear polystyrene (PS) standards.

Photo-mediated polymerization was conducted in a 4.9 mW/cm2 MelodySusie® UV lamp.

Cyclic voltammogram (CV) and electrolysis were conducted using Gamry REF 600 potentiostat.

Particle size and size distribution were determined by using a Zetasizer Nano from Malvern Instruments, Ltd.

Miniemulsion polymerization of BMA by ARGET ATRP. A stock solution of BMA (2 mL, 12.57 mmol), EBPA (7.86 μL, 0.045 mmol, to target degree of polymerization (DP) = 280), and HD (0.25 mL, 0.853 mmol) was prepared. $Cu^{II}Br_2$/TPMA stock solution (0.20 mL, 0.05 M in water), NaBr (0.129 g, 1.000 mmol), SDS (0.082 g, 0.285 mmol), glucose (0.36 g, 2 mmol) and Na pyruvate (0.11 g, 1 mmol) were dissolved in 8 mL of distilled water. The organic and aqueous solutions were mixed (total volume ≈ 10 mL), placed in an ice bath, and dispersed by a probe sonicator, amplitude = 20% for 20 min (application and rest time of 1 s each). The miniemulsion and GOx (0.0032 g, 2× 10-5 mmol) was added to a vial. The vial was immersed to 44 °C oil bath after 3 min stirring and AsAc solution was injected to start the reaction. Samples were withdrawn periodically to follow the monomer conversion by gravimetric analysis, while Mn and Mw/Mn were determined by GPC.

Synthesis of PBA-*b*-P*t*BA. A PBA-Br macroinitiator (MI) ARGET ATRP polymerization was conducted following the same procedure for BMA polymerization as mentioned above using the GOx-degassing method. After 20 h, the polymerization solution was transferred to a 50 mL centrifuge tube. 20 mL of water and 20 mL of MeOH were

added and then the tubes were placed in the centrifuge for 20 min at 5000 rpm. About 90% of the polymer was recovered after precipitation. The PBA-MI was re-dissolved in THF, passed through neutral alumina column and dried in vacuum.

A solution of *t*BA (1.67 mL, 11.40 mmol), PBA-MI (0.57 g, 0.023 mmol) to target DP = 500 was prepared. CuIIBr2/TPMA stock solution (0.20 mL, 0.01 mmol), NaBr (0.103 g, 1 mmol), SDS (0.082 g, 0.28 mmol), glucose (0.36 g, 2 mmol) and Na pyruvate (0.11 g, 1 mmol) were dissolved in 8 mL of distilled water. The organic and aqueous solutions were mixed (total volume ≈ 10 mL), placed in an ice-water bath, and dispersed by a probe sonicator, amplitude = 20% for 20 min (application and rest time of 1 s each). The miniemulsion and GOx (0.0032 g, 2× 10-5 mmol) was added to a vial. The vial was immersed to 44 °C oil bath after 3 min stirring to start the reaction. Samples were withdrawn periodically to follow the monomer conversion by gravimetric analysis, while Mn and Mw/Mn were determined by GPC.

Miniemulsion polymerization of BMA by photoATRP. A stock solution of BMA (2 mL, 12.57 mmol), EBPA (11.0 μL, 0.063 mmol, to target DP = 200), and HD (0.25 mL, 0.853 mmol) was prepared. CuIIBr2/3TPMA stock solution (0.20 mL, 0.05 M in water), NaBr (0.129 g, 1.000 mmol), SDS (0.082 g, 0.285 mmol), glucose (0.36 g, 2 mmol) and Na pyruvate (0.11 g, 1 mmol) were dissolved in 8 mL of distilled water. The organic and aqueous solutions were mixed (total volume ≈ 10 mL), placed in an ice bath, and dispersed by a probe sonicator, amplitude = 20% for 20 min (application and rest time of 1 s each). The miniemulsion and GOx (0.0032 g, 2× 10-5 mmol) was added to a vial. The UV lamp was placed on a stir plate with a stir rate = 500 rpm. The vial was inserted into the cavity of the UV lamp. The lamp was turned on to start the reaction. Samples were withdrawn

periodically to follow the monomer conversion by gravimetric analysis, while Mn and Mw/Mn were determined by GPC.

Miniemulsion polymerization of BMA by eATRP. A stock solution of BMA (2 mL, 12.57 mmol), EBPA (11.0 μL, 0.063 mmol, to target DP = 200) and HD (0.25 mL, 0.853 mmol) was prepared. CuIIBr2/TPMA stock solution (0.20 mL, 0.05 M in water), NaBr (0.129 g, 1.000 mmol), SDS (0.082 g, 0.285 mmol), glucose (0.36 g, 2 mmol) and Na pyruvate (0.11 g, 1 mmol) were dissolved in 8 mL of distilled water. The organic and aqueous solutions were mixed (total volume ≈ 10 mL), placed in an ice bath, and dispersed by a probe sonicator, amplitude = 20% for 20 min (application and rest time of 1 s each). The miniemulsion and GOx (0.0032 g, 2× 10-5 mmol) was added to a five-neck electrochemical cell. The vial was immersed to 44 °C oil bath after 3 min stirring. Samples were withdrawn periodically to follow the monomer conversion by gravimetric analysis, while Mn and Mw/Mn were determined by GPC.

Miniemulsion polymerization of BMA by ICAR ATRP (taking hydrophobic initiator, V-70 as example). A stock solution of BMA (2 mL, 12.57 mmol), EBPA (11.0 μL, 0.063 mmol, to target DP = 200), V-70 (0.058 g, 0.019 mmol, [V-70]/[EBPA] = 0.3/1) and HD (0.25 mL, 0.853 mmol) was prepared. CuIIBr2/TPMA stock solution (0.20 mL, 0.05 M in water), NaBr (0.129 g, 1.000 mmol), SDS (0.082 g, 0.285 mmol), glucose (0.36 g, 2 mmol) and Na pyruvate (0.11 g, 1 mmol) were dissolved in 8 mL of distilled water. The organic and aqueous solutions were mixed (total volume ≈ 10 mL), placed in an ice bath, and dispersed by a probe sonicator, amplitude = 20% for 20 min (application and rest time of 1 s each). The miniemulsion and GOx (0.0032 g, 2× 10-5 mmol) was added to a vial. The vial was immersed to 44 °C oil bath after 3 min stirring to start the reaction.

Samples were withdrawn periodically to follow the monomer conversion by gravimetric analysis, while Mn and Mw/Mn were determined by GPC.

Ab initio emulsion polymerization of BMA by ARGET ATRP. CuIIBr2/TPMA stock solution (0.20 mL, 0.05 M in water), PEG2k-BPA (0.053 g, 0.025 mmol, to target DP = 500), NaBr (0.129 g, 1.000 mmol), SDS (0.082 g, 0.285 mmol), glucose (0.36 g, 2 mmol) and Na pyruvate (0.11 g, 1 mmol) were dissolved in 8 mL of distilled water. The aqueous solution and GOx (0.0032 g, 2× 10-5 mmol) was added to a Schlenk flask. BMA (2 mL, 12.57 mmol) was slowly injected to the flask. The vial was immersed to 44 °C oil bath after 3 min stirring and AsAc solution was injected to start the reaction. Samples were withdrawn periodically to follow the monomer conversion by gravimetric analysis, while Mn and Mw/Mn were determined by GPC.

6.6. References

(1) Braunecker, W. A.; Matyjaszewski, K., Controlled/Living Radical Polymerization: Features, Developments, and Perspectives. *Prog Polym Sci* **2007,** *32* (1), 93-146.
(2) Matyjaszewski, K.; Xia, J. H., Atom Transfer Radical Polymerization. *Chem Rev* **2001,** *101* (9), 2921-2990.
(3) Matyjaszewski, K., Atom Transfer Radical Polymerization (ATRP): Current Status and Future Perspectives. *Macromolecules* **2012,** *45* (10), 4015-4039.
(4) Matyjaszewski, K.; Tsarevsky, N. V., Macromolecular Engineering by Atom Transfer Radical Polymerization. *J Am Chem Soc* **2014,** *136* (18), 6513-6533.
(5) Matyjaszewski, K., Advanced Materials by Atom Transfer Radical Polymerization. *Advanced Materials* **2018,** *30*, 1706441.
(6) Chiefari, J.; Chong, Y. K.; Ercole, F.; Krstina, J.; Jeffery, J.; Le, T. P. T.; Mayadunne, R. T. A.; Meijs, G. F.; Moad, C. L.; Moad, G.; Rizzardo, E.; Thang, S. H., Living Free-Radical Polymerization by Reversible Addition-Fragmentation Chain Transfer: The RAFT Process. *Macromolecules* **1998,** *31* (16), 5559-5562.
(7) Moad, G.; Chiefari, J.; Chong, Y. K.; Krstina, J.; Mayadunne, R. T. A.; Postma, A.; Rizzardo, E.; Thang, S. H., Living Free Radical Polymerization with Reversible Addition-Fragmentation Chain Transfer (the life of RAFT). *Polym Int* **2000,** *49* (9), 993-1001.
(8) Asua, J. M., Miniemulsion Polymerization. *Prog Polym Sci* **2002,** *27* (7), 1283-1346.
(9) Zetterlund, P. B.; Kagawa, Y.; Okubo, M., Controlled/Living Radical Polymerization in Dispersed Systems. *Chem Rev* **2008,** *108* (9), 3747-3794.

(10) Yeow, J.; Chapman, R.; Gormley, A. J.; Boyer, C., Up in the Air: Oxygen Tolerance in Controlled/Living Radical Polymerisation. *Chem Soc Rev* **2018,** *47* (12), 4357-4387.
(11) Calitz, F. M.; Tonge, M. P.; Sanderson, R. D., Kinetic and Electron Spin Resonance Analysis of RAFT Polymerization of Styrene. *Macromolecules* **2003,** *36* (1), 5-8.
(12) Liarou, E.; Whitfield, R.; Anastasaki, A.; Engelis, N. G.; Jones, G. R.; Velonia, K.; Haddleton, D. M., Copper-Mediated Polymerization without External Deoxygenation or Oxygen Scavengers. *Angewandte Chemie International Edition* **2018,** *57* (29), 8998-9002.
(13) O'malley, J. J., Ulmer, R. W., Thermal Stability of Glucose Oxidase and its Admixtures with Synthetic Polymers. *Biotechnology and Bioengineering* **1973,** *15*, 917-925.
(14) Iwata, H.; Hata, Y.; Matsuda, T.; Ikada, Y., Initiation Of Radical Polymerization by Glucose-Oxidase Utilizing Dissolved-Oxygen. *Journal of Polymer Science Part A: Polymer Chemistry* **1991,** *29* (8), 1217-1218.
(15) Oytun, F.; Kahveci, M. U.; Yagci, Y., Sugar overcomes oxygen inhibition in photoinitiated free radical polymerization. *J. Polym. Sci., Part A: Polym. Chem.* **2013,** *51* (8), 1685-1689.
(16) Lv, Y.; Liu, Z. F.; Zhu, A. Q.; An, Z. S., Glucose Oxidase Deoxygenation-Redox Initiation for RAFT Polymerization in Air. *Journal of Polymer Science Part A: Polymer Chemistry* **2017,** *55* (1), 164-174.
(17) Liu, Z. F.; Lv, Y.; An, Z. S., Enzymatic Cascade Catalysis for the Synthesis of Multiblock and Ultrahigh-Molecular-Weight Polymers with Oxygen Tolerance. *Angew. Chem. Int. Ed.* **2017,** *56* (44), 13852-13856.
(18) Enciso, A. E.; Fu, L. Y.; Russell, A. J.; Matyjaszewski, K., A Breathing Atom-Transfer Radical Polymerization: Fully Oxygen-Tolerant Polymerization Inspired by Aerobic Respiration of Cells. *Angewandte Chemie International Edition* **2018,** *57* (4), 933-936.
(19) Min, K.; Gao, H. F.; Matyjaszewski, K., Preparation of Homopolymers and Block Copolymers in Miniemulsion by ATRP using Activators Generated by Electron Transfer (AGET). *J Am Chem Soc* **2005,** *127* (11), 3825-3830.
(20) Min, K.; Jakubowski, W.; Matyjaszewski, K., AGET ATRP in the presence of air in miniemulsion and in bulk. *Macromol. Rapid Commun.* **2006,** *27* (8), 594-598.
(21) Xu, J. T.; Jung, K.; Atme, A.; Shanmugam, S.; Boyer, C., A Robust and Versatile Photoinduced Living Polymerization of Conjugated and Unconjugated Monomers and Its Oxygen Tolerance. *J Am Chem Soc* **2014,** *136* (14), 5508-5519.
(22) Xu, J. T.; Jung, K.; Boyer, C., Oxygen Tolerance Study of Photoinduced Electron Transfer-Reversible Addition-Fragmentation Chain Transfer (PET-RAFT) Polymerization Mediated by Ru(bpy)(3)Cl-2. *Macromolecules* **2014,** *47* (13), 4217-4229.
(23) Corrigan, N.; Xu, J. T.; Boyer, C., A Photoinitiation System for Conventional and Controlled Radical Polymerization at Visible and NIR Wavelengths. *Macromolecules* **2016,** *49* (9), 3274-3285.
(24) Fu, Q.; Xie, K.; McKenzie, T. G.; Qiao, G. G., Trithiocarbonates as Intrinsic Photoredox Catalysts and RAFT Agents for Oxygen Tolerant Controlled Radical Polymerization. *Polym Chem-Uk* **2017,** *8* (9), 1519-1526.
(25) Shanmugam, S.; Xu, J. T.; Boyer, C., Exploiting Metalloporphyrins for Selective Living Radical Polymerization Tunable over Visible Wavelengths. *J Am Chem Soc* **2015,** *137* (28), 9174-9185.

(26) Corrigan, N.; Rosli, D.; Jones, J. W. J.; Xu, J. T.; Boyer, C., Oxygen Tolerance in Living Radical Polymerization: Investigation of Mechanism and Implementation in Continuous Flow Polymerization. *Macromolecules* **2016,** *49* (18), 6779-6789.
(27) Chapman, R.; Gormley, A. J.; Herpoldt, K. L.; Stevens, M. M., Highly Controlled Open Vessel RAFT Polymerizations by Enzyme Degassing. *Macromolecules* **2014,** *47* (24), 8541-8547.
(28) Schneiderman, D. K.; Ting, J. M.; Purchel, A. A.; Miranda, R.; Tirrell, M. V.; Reineke, T. M.; Rowan, S. J., Open-to-Air RAFT Polymerization in Complex Solvents: From Whisky to Fermentation Broth. *Acs Macro Lett* **2018,** *7* (4), 406-411.
(29) Fantin, M.; Chmielarz, P.; Wang, Y.; Lorandi, F.; Isse, A. A.; Gennaro, A.; Matyjaszewski, K., Harnessing the Interaction between Surfactant and Hydrophilic Catalyst to Control eATRP in Miniemulsion. *Macromolecules* **2017,** *50* (9), 3726-3732.
(30) Wang, Y.; Lorandi, F.; Fantin, M.; Chmielarz, P.; Isse, A. A.; Gennaro, A.; Matyjaszewski, K., Miniemulsion ARGET ATRP via Interfacial and Ion-Pair Catalysis: From ppm to ppb of Residual Copper. *Macromolecules* **2017,** *50* (21), 8417-8425.
(31) Lorandi, F.; Wang, Y.; Fantin, M.; Matyjaszewski, K., Ab Initio Emulsion Atom-Transfer Radical Polymerization. *Angew. Chem. Int. Ed.* **2018,** *57* (27), 8270-8274.
(32) Wang, Y.; Dadashi-Silab, S.; Matyjaszewski, K., Photoinduced miniemulsion atom transfer radical polymerization. *ACS Macro Lett.* **2018,** *7* (6), 720-725.
(33) Seeliger, F.; Matyjaszewski, K., Temperature Effect on Activation Rate Constants in ATRP: New Mechanistic Insights into the Activation Process. *Macromolecules* **2009,** *42* (16), 6050-6055.
(34) Krys, P.; Matyjaszewski, K., Kinetics of Atom Transfer Radical Polymerization. *Eur Polym J* **2017,** *89*, 482-523.
(35) Moosavimovahedi, A. A.; Housaindokht, M. R.; Moghaddasi, J., Thermodynamic Studies Of the Interaction Of Glucose-Oxidase with Anionic And Cationic Surfactants. *Thermochim Acta* **1993,** *219*, 143-150.

Chapter 7 Low ppm Halogen Exchange in Miniemulsion

7.1. Preface

The content of this chapter was submitted for publication in *Macromolecular Rapid Communications*.

Previously, block copolymers were prepared in miniemulsion by chain extending a more active macroinitiator with a less active monomer, for example, chain extending a polymethacrylate with acrylate monomer. However, chain extension from the less active macroinitiator with the more active monomer causes a mismatch of reactivity and consequently low initiation efficiency and copolymers with high dispersity.

Halogen exchange of the macroinitiator from the Br chain end to Cl is an alternative way to a successful chain extension with a more active monomer. The mismatch of the initiator and monomer activity is compensated by exchanging the more active Br chain-end to the less active Cl chain-end. Halogen exchange typically employs CuCl/L in the equimolar amount of the macroinitiator. In this work, addition of methacrylate monomers to polyacrylate macroinitiators was achieved by catalytic halogen exchange in miniemulsion ATRP. Ppm amount of catalyst and excess Cl^- lead to high initiation efficiency and polymers with low dispersity in model reactions. Well-defined poly(butyl acrylate)-*b*-poly(methyl methacrylate) was synthesized.

I explored the catalytic halogen exchange conditions in both model reactions and chain extension.

The support from the National Science Foundation (CHE 1707490) is acknowledged. I acknowledge the financial support from Kwolek Fellowship.

7.2. Introduction

Reversible-deactivation radical polymerizations (RDRPs) are prevalent in synthesizing (co)polymers from a wide range of monomers, leading to polymers with predetermined molecular weight and low dispersity.[1-2] Main techniques of RDRP include atom transfer radical polymerization (ATRP),[3-4] reversible addition-fragmentation chain-transfer (RAFT) polymerization,[5-6] and nitroxide-mediated polymerization (NMP).[7]

Block copolymers are comprised of two or more chemically distinct blocks, providing polymers with diversified structures and functions.[8] Block copolymers could be synthesized by RDRP methods, where the chain end functionalities are retained after the first polymerization step, and RDRP of the second monomer could be initiated from the macroinitiator (MI). In ATRP, the reactivity of monomers follows the order: acrylonitrile > methacrylates > styrene ≈ acrylates > acrylamides.[9-11] The monomer generating more active alkyl bromide chain ends should be used for the synthesis of the MI to provide efficient cross-propagation to the second block, resulting in concurrent growth of all polymer chains. Otherwise, the apparent rate constant of initiation from the MI is lower than that of the propagation of the second monomer ($K_{ATRP}^{initiator} \times k_i < K_{ATRP}^{monomer} \times k_p$; K_{ATRP}: equilibrium constant of ATRP; k_i: initiation rate constant; k_p: propagation rate constant)[12-15], and the initiation efficiency is low (错误!未找到引用源。A). This could be solved by decreasing the K_{ATRP} of the chain extension step, which slows down the initiation from newly formed extended dormant species, thus allowing fast initiation/extension from the original MI (错误!未找到引用源。B). This can be

accomplished by incorporation of a comonomer with lower K_{ATRP},[15] but a more universal method is halogen exchange from Br to a less active Cl chain end. [16-19]

Typically, halogen exchange takes part in normal ATRP, where the P−Br MI and CuCl are used in equimolar concentrations, raising issues related to solubility and catalyst removal. During the past two decades, a series of low ppm ATRP, including activators re-generated by electron transfer (ARGET) ATRP,[20-22] initiators for continuous activator regeneration (ICAR) ATRP,[23] supplemental activator and reducing agent (SARA) ATRP,[24-27] electrochemically mediated ATRP (*e*ATRP)[28-30], photoATRP, [31-32] and mechanoATRP[33-34], were developed and applied to various monomers, reaction media and polymer architectures. However, halogen exchange using ppm amount of Cu catalyst has not been often used, although addition of salts with common ions in aqueous ATRP at both higher and lower concentration of Cu catalysts significantly improved control. [21, 35-36] In ARGET ATRP catalytic amount of $CuCl_2$ did not improve chain extension as compared to $CuBr_2$.[37] However, if sufficient amount of Cl^- is available, even with a catalytic amount of Cu catalyst, C−Br chain ends can be successfully converted to C−Cl chain ends under catalytic halogen exchange (*c*HE) conditions.[38]

Scheme 7-1C shows the *c*HE, taking ATRP of methyl methacrylate (MMA) from poly(butyl acrylate)−Br (PBA−Br) as an example. PBA−Br chains could be initiated efficiently for MMA polymerization, due to reduced activation rate of PBA-*b*-PMMA−Cl species which are predominantly formed after the exchange process. A key step is reaction III, which relies on much larger chloridophilicity than bromidophilicity of Cu^{II}/L species.[18, 39]

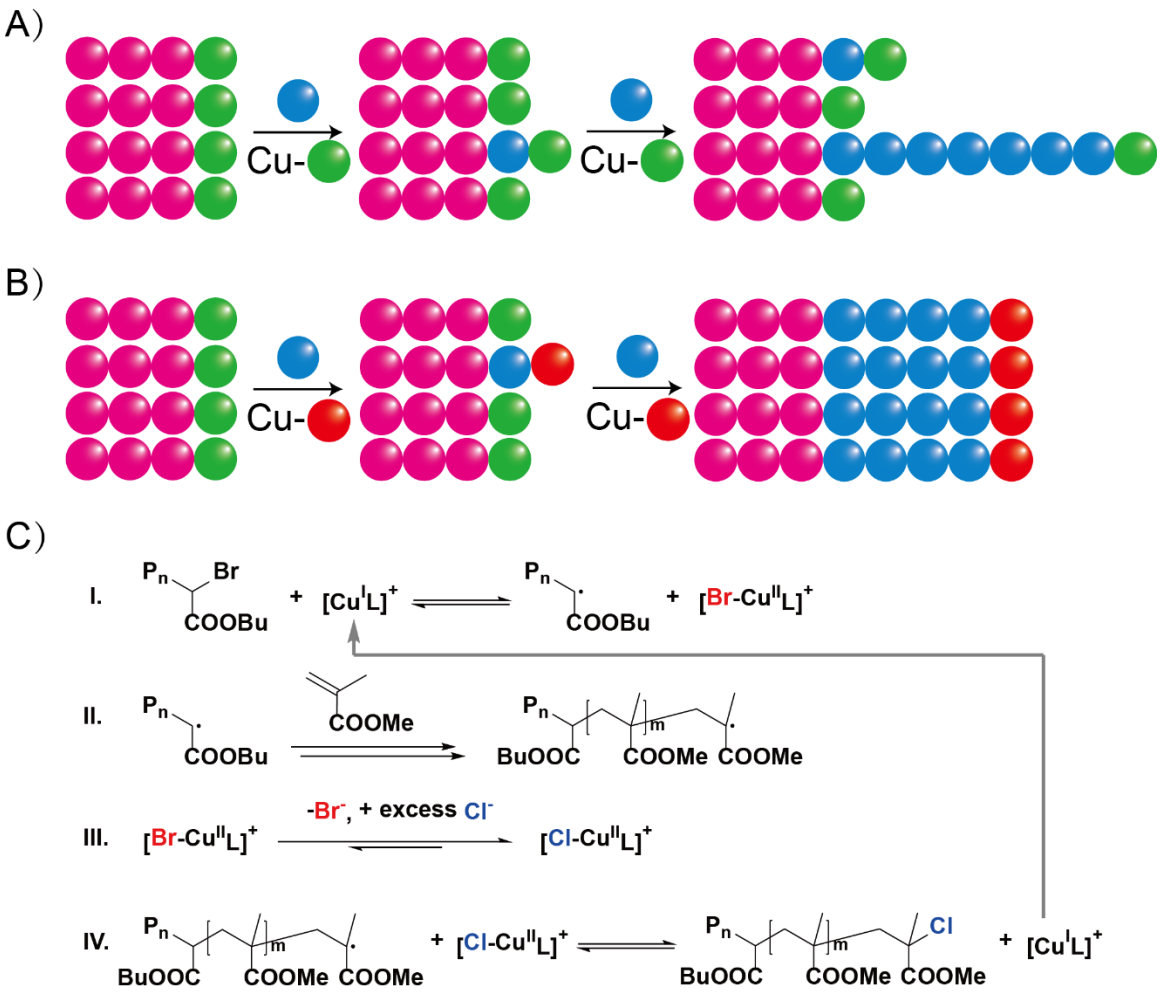

Scheme 7-1. Mechanism of halogen exchange. Chain extension from a less active MI-Br with A) CuBr; B) CuCl. monomer generating less active Br chain ends; monomer generating more active Br chain ends; Br; Cl. C)*c*HE in chain extension of PBA-Br with MMA in the presence of excess Cl^-.

Miniemulsion polymerization is beneficial in the synthesis of hydrophobic polymers with low catalyst loading, low viscosity, low termination reactions and low residual copper. [40-44] Our group has recently employed a combination of ATRP catalyst, CuTPMA (TPMA = tris(2-pyridylmethyl)amine), and an anionic surfactant, SDS (sodium dodecyl sulfate) as efficient ion-pair and interfacial catalyst, providing efficient control in miniemulsion and emulsion ATRP of acrylates and methacrylates.[45-48] The reaction

mixture could be precipitated into water/MeOH for facile removal of the catalyst, and the copper residual in the final polymer could be lower than 1 ppm.[45] Thus this system is very suitable for synthesis of hydrophobic linear, block, star and brush (co)polymers in a controlled manner using low catalyst content.

Herein, *c*HE in miniemulsion ARGET ATRP was studied to prepare PBA-*b*-PMMA. A series of model reactions were conducted, using methyl 2-bromopropionate (MBP) to mimic PBA−Br MI. Cu concentration, Cl^-/Cu ratio and halogen source have been varied to optimize the conditions. The optimal conditions were then used for chain extension of PBA−Br with MMA, and the clear shift of GPC traces demonstrated the feasibility of this system.

7.3. Results and Discussion

Model studies are often used to better understand the mechanisms of ATRP.[9-10, 49] Thus, a series of model studies were conducted in the *c*HE reaction in miniemulsion ARGET ATRP. A small molecular initiator, MBP, was used to mimic the PBA−Br MI. The secondary (2^o) C−Br structures in these two initiators should have similar reactivities in ATRP initiation.[50] Br^- anion was essential for controlling miniemulsion ATRP with the anionic surfactant SDS since it minimized the deactivator loss caused by the anion dissociation.[51] . 0.1 M NaBr was used in previous experiments in miniemulsion/emulsion ATRP using the Cu–TPMA/DS^- system.[45-48] We first used 0.1 M NaBr in the miniemulsion ARGET ATRP of MMA initiated from MBP (**Figure 7-1** and **Table 7-1**, entry 1).

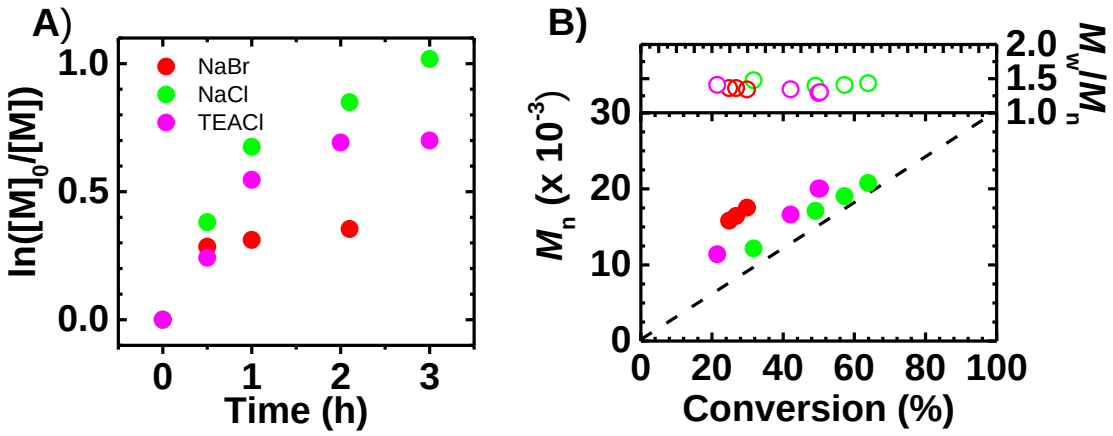

Figure 7-1. Miniemulsion ARGET ATRP of MMA from MBP using 0.1 M salt. (A) Kinetics and (B) evolution of M_n and $Đ$. See conditions in **Table 7-1**, entry 1, 2 and 6.

Table 7-1. Model reactions for halogen exchange under different conditions.

Entry a)	Salt	[X-]	[X-]/[MBP]	[X-]/[Cu]	*t* [h]	Conv [%]	k_{app}^{p} [h-1]	$M_{n,th}$ [×10-3]	$M_{n,app}$ [×10-3]	I_{eff} b)	*Đ*
1	NaBr	0.1	16	66	2.1	30	0.212	9.2	17.5	0.53	1.34
2	NaCl	0.1	16	66	3	64	0.389	19.4	20.8	0.93	1.43
3c)	NaCl	0.1	16	66	2	79	0.658	23.9	26.0	0.92	1.43
4	NaCl	0.05	8	33	2	87	1.025	26.3	28.8	0.91	1.39
5	NaCl	0.2	32	132	3	69	0.374	20.9	25.6	0.82	1.44
6	TEACl	0.1	16	66	3	50	0.391	15.2	20.0	0.76	1.30
7	TEACl	0.2	32	133		Coagulation after 1 h reaction					
8	TBACl	0.1	16	66		Cannot form a stable miniemulsion					
9	NaCl	0.1	16	132	3	39	0.279	11.9	18.4	0.65	1.64
10	NaCl	0.1	16	33	2	81	0.865	25.1	30.7	0.82	1.38

[a)]Conditions: [Oil] – [MMA]/[MBP] = 300/1 (20 vol% MMA), HD – 5.4 wt% (to MMA); [Water] – [$CuBr_2$] = [TPMA] = 1.5 mM (800 ppm vs. MMA, except for entry 9 and 10); SDS– 4.6 wt% (to MMA); [AsAc] = 0.5 *[CuTPMA] injected at the first 3 min; V_{tot} = 10 mL; T = 65 °C. [b)]AsAc was fed by syringe pump at 0.2 eq/h.

30% conversion was reached in 2 h, and the M_n of the resulting polymer was almost twice higher than the theoretical value. According to the rate law of ATRP under steady

state (Equation(1)), the slower rate of polymerization could be explained by the slower initiation of MBP.

$$R_p = k_p[M][P\cdot] = k_p K_{\mathrm{ATRP}}[M][P-X]\frac{[Cu^{I}/L]}{[X-Cu^{II}/L]} \quad (1)$$

The significantly higher molecular weight confirmed the low initiation efficiency caused by the activity mismatch of MBP and PMMA-Br dormant chains. Thus, it was essential to conduct *c*HE.

Because *c*HE required an excess amount of Cl^-, 0.1 M NaBr was substituted with 0.1 M NaCl (**Figure 7-1** and **Table 7-1**, entry 2). The ratio of Cl^-/MBP was 16/1. Though the ATRP equilibrium constant for Cl-based system is typically lower than Br-based system, the larger number of propagating chains resulted in faster polymerization. The initiation efficiency was almost 100%, confirmed by the perfect agreement of the M_n with predicted values. Similar results were observed using a slow feeding of the reducing agent, AsAc (**Table 7-1**, entry 3). Thus, in all subsequent experiments, AsAc was added at the beginning of the reaction.

Halogen exchange was fast and quantitative in homogeneous systems.[16, 38] However, in miniemulsion and *c*HE conditions, the biphasic nature made the exit of Br^- and entrance of Cl^- to the organic droplets in the presence of the anionic surfactant a more complex process and it was difficult to quantify the extent of halogen exchange. Therefore, the concentration of NaCl was varied to verify its impact on the polymerization. In **错误! 未找到引用源。**, entry 4, 2 and 5, [NaCl] was 0.05, 0.1 and 0.2 M, respectively. The rate of polymerization decreased at higher NaCl content, due to the high concentration of $Cl–Cu^{II}TPMA^+$, which agreed with previous reports.[21, 52] The molecular weights matched the

theoretical values using 0.05 and 0.1 M NaCl, but polymerization was slower with 0.2 M NaCl, possibly due to too high concentration of deactivators.[21] No significant difference was observed in dispersity (**Figure 7-2**). This indicated a NaCl concentration of 0.05 to 0.2 M allowed efficient *c*HE in miniemulsion.

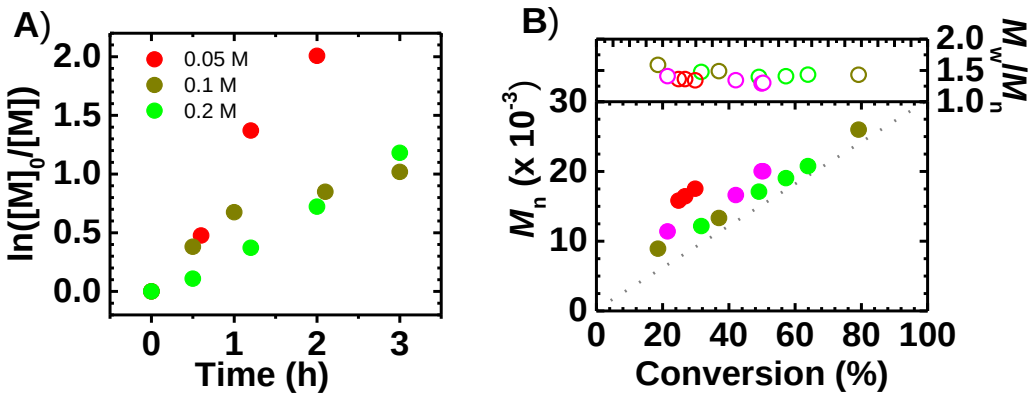

Figure 7-2. ARGET ATRP miniemulsion polymerization of MMA with different concentrations of NaCl. (A) Semi-logarithmic kinetic plots and (B) MW and *Đ* evolution vs. monomer conversion. See reaction conditions at **Table 7-1**, entry 4, 2, 5 for 0.05, 0.1 and 0.2 M, respectively.

To compare transport of Cl^- to the organic phase, tetraethylammonium chloride (TEACl) and tetrabutylammonium chloride (TBACl) were tested. The hydrophobic cations should promote a faster shuffling of Cl^- to the droplets. The model reaction using 0.1 M TEACl decreased the dispersity from 1.43 to 1.30 (**Table 7-1**, entry 6 and **Figure 7-1**). However, a more significant discrepancy of MW with theoretical value was observed in this entry. These observations confirmed that TEA^+ facilitated shuttling of Cl^- to the organic phase for halogen exchange reactions.

Organic cations could destabilize emulsions,[53] leading to larger particle sizes or even coagulation. DLS analysis showed Z-Ave size of MMA miniemulsion was 71.4, 77.9 and 84.6 nm for 0.1 M NaCl, 0.1 M TEACl and 0.2 M TEACl, respectively. Indeed, in the

presence of 0.2 M TEACl, noticeable coagulation was observed after 1 h polymerization (**Table 7-1**, entry 7). In the presence of 0.1 M TBACl, the probe ultrasonication failed to generate a miniemulsion, as TBA^+ was a strong destabilizer to anionic emulsions (**Table 7-1**, entry 8).

Effect of Cu concentration. Cu concentration was varied from 400 ppm to 800 and 1600 ppm (**Table 7-1**, entry 9, 2 and 10, respectively, and **Figure 7-3**). At 400 ppm, rate of polymerization was slow, and the polymerization was poorly controlled ($Đ$ = 1.64). This was consistent with basic rules in ARGET ATRP, where rate of polymerization was proportional to reduction rate of Cu^{II}, and a higher [Cu] was beneficial to prepare polymers with lower dispersity. Increasing the Cu concentration from 800 to 1600 ppm led to increased rate of polymerization, and slightly decreased $Đ$.

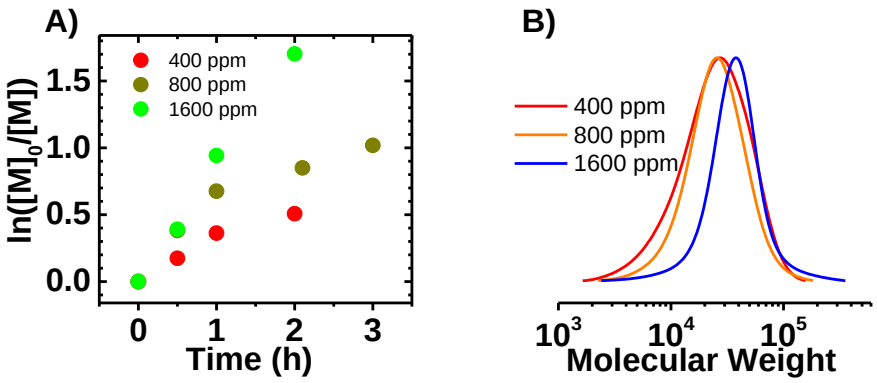

Figure 7-3. ARGET ATRP miniemulsion polymerization of MMA with different concentrations of catalyst. (A) Semi-logarithmic kinetic plots and (B) Final GPC traces. See reaction conditions at **Table 7-1**, entry 9, 2 and 10 for 400, 800 and 1600 ppm, respectively.

The model reactions show efficient *c*HE using 0.1 M NaCl or TEACl under 800 ppm of Cu. These conditions were then applied to the chain extension of PBA_{40k}−Br with MMA (**Figure 7-4**).

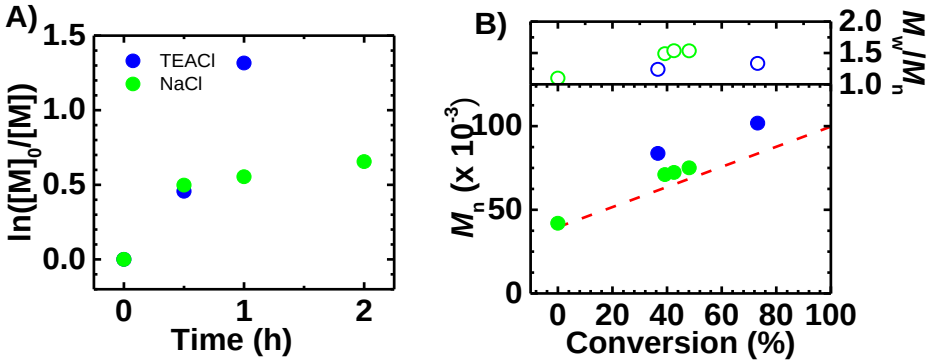

Figure 7-4. ARGET ATRP miniemulsion polymerization of MMA from PBA_{40k}−Br with NaCl or TEACl. A) Semi-logarithmic kinetic plots and (B) MW and $Đ$ evolution vs. monomer conversion. Reaction conditions: [MMA]/[PBA−Br]/[$CuBr_2$/TPMA] = 300/1/0.24, [$CuBr_2$/TPMA] = 1.00 mM, [NaCl or TEACl] = 0.1 M, [SDS] = 38 mM, [HD] = 85 mM, [AsAc] = 0.5 mM, T = 65 °C.

Although monomodal GPC curve was observed using NaCl, a large fraction of the PBA_{40k}−Br was not successfully extended (**Figure 7-5**A). The limited initiation efficiency could be caused by the lower concentration of salt and of Cl^- anions in the organic phase, as the presence of PBA-Br increased hydrophobicity of organic phase more than in the model reactions.

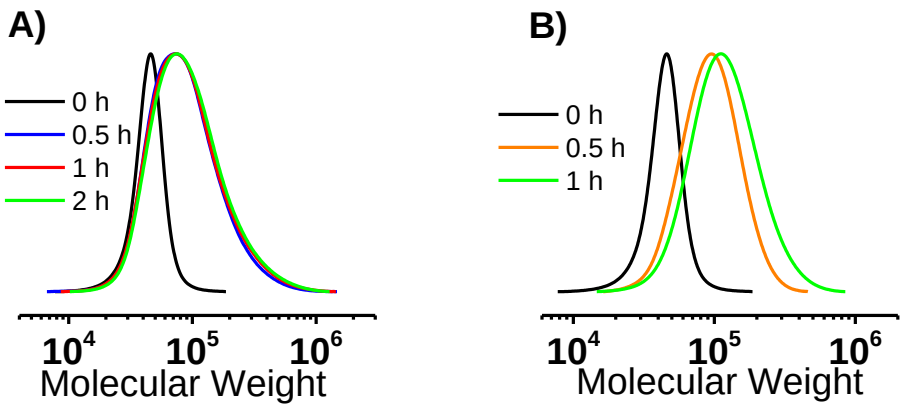

Figure 7-5. MMA polymerization from PBA_{40k}−Br using A) NaCl; B) TEACl. Reaction conditions: [MMA]/[PBA−Br]/[$CuBr_2$/TPMA] = 300/1/0.24, [salt] = 0.1 M, [SDS] = 38 mM, [HD] = 85 mM, [AsAc] = 0.5 mM, T = 65 °C.

Therefore, PBA-Br MI was next extended with MMA using 0.1 M TEACl. A clean shift of GPC traces was observed, yielding block copolymers with final dispersity of 1.3, showing a significant improvement from the NaCl system (**Figure 7-5**B). The more efficient chain extension using TEACl in comparison with NaCl could be explained by the ability of TEA^+ to "transport" more Cl^- to the organic phase.

7.4. Conclusion

In summary, *c*HE was applied under low ppm ATRP conditions in miniemulsion. In model reactions, the initiation efficiency of MBP in ATRP of MMA was greatly improved when using NaCl for halogen exchange in comparison with NaBr. The influence of various reagents was studied in detail. Both NaCl and TEACl were efficient Cl^- anion sources. Block copolymers were successfully synthesized via *c*HE in miniemulsion ARGET ATRP of MMA from PBA−Br. The initiation efficiency was higher using TEACl

instead of NaCl, as confirmed by the cleaner shift of the monomodal GPC trace. The synthesis of well-defined copolymers will be beneficial for various applications, including thermoplastic elastomers and pressure-sensitive adhesives. Such materials are currently being explored in our laboratory.

7.5. Experimental Section

Materials. Copper(II) bromide ($Cu^{II}Br_2$, 99%), sodium dodecyl sulfate (SDS, 99%), tetrahydrofuran (THF, > 99%), methyl 2-bromopropionate (MBP, 98%), ethyl α-bromoisobutyrate (EBiB, 98%), tris(2-pyridylmethyl)amine (TPMA, 98%), hexadecane (HD, 99%) and ascorbic acid (AsAc) were purchased from Sigma-Aldrich. Sodium bromide (NaBr, 99%) and sodium chloride (NaCl, 99%) were purchased from Acros. These chemicals were used as received. Tetraethylammonium chloride (TEACl, 98%) and tetrabutylammonium chloride (TBACl, 98%) were purchased from Sigma-Aldrich and recrystallized in ethanol. *n*-Butyl acrylate (BA, 99%, Aldrich) and methyl methacrylate (MMA, 99%, Aldrich) were passed through a column filled with basic alumina prior to use to remove polymerization inhibitors.

Instrumentation. Ultrasound treatment to prepare miniemulsion samples was carried out using Ultrasonics W-385 sonicator.

M_n and M_w/M_n were determined by GPC equipped with Polymer Standards Services (PSS) columns (guard, 10^5, 10^3, and 10^2 Å) and a differential refractive index detector (Waters, 2410), with THF as eluent at a flow rate of 1.00 mL/min (T = 35 °C). GPC traces

were processed by WinGPC 8.0 software (PSS) using a calibration based on linear polystyrene (PS) standards.

Monomer conversion was determined by gravimetric analysis, evaporating the samples at 110 °C for at least 30 min.

Particle size and size distribution were determined by using a Zetasizer Nano from Malvern Instruments, Ltd.

General procedure for miniemulsion ARGET ATRP of MMA using MBP as initiator. A solution of MMA (2 mL, 18.78 mmol), MBP (7.53 μL, 0.062 mmol) to target DP = 300, and HD (0.25 mL, 0.85 mmol) was prepared. $Cu^{II}Br_2$/TPMA stock solution (0.20 mL, 0.01 mmol), NaCl (0.058 g, 1 mmol), and SDS (0.082 g, 0.28 mmol) were dissolved in 8 mL of distilled water. The organic and aqueous solutions were mixed (total volume ≈ 10 mL), placed in an ice bath, and dispersed by a probe sonicator, amplitude = 70% for 15 min (application and rest time of 1 s each). Nitrogen was bubbled through the miniemulsion solution for 0.5 h. The flask was immersed in a 65 °C oil bath and then AsAc solution was slowly injected over 3 min to start the reaction. Samples were withdrawn periodically to follow the monomer conversion by gravimetric analysis, while M_n and M_w/M_n were determined by GPC.

Preparation of PBA-Br MI. A solution of BA (4 mL, 27.9 mmol), EBiB (6.8 μL, 0.046 mmol, to target DP = 600), and HD (0.50 mL, 1.71 mmol) was prepared. $Cu^{II}Br_2$/TPMA stock solution (0.40 mL, 0.02 mmol), NaBr (0.206 g, 2 mmol), and SDS (0.164 g, 0.57 mmol) were dissolved in 16 mL of distilled water. The organic solution was mixed with the aqueous solution, then the mixture was placed in an ice bath, and dispersed

by a probe sonicator, amplitude = 70% for 15 min (application and rest time of 1 s each). Nitrogen was bubbled through the miniemulsion solution for 0.5 h. The flask was immersed in a 65 °C oil bath and a degassed AsAc solution fed by a syringe pump at 0.2 mmol/h. Samples were withdrawn periodically to follow the monomer conversion by gravimetric analysis, while M_n and M_w/M_n were determined by GPC. The product was precipitated into MeOH/H_2O (1/1 by v/v), redissolved in THF, passed through neutral alumina column and dried in vacuum.

General procedure for chain extension from PBA-MI. A solution of MMA (1.2 mL, 11.3 mmol), PBA-MI (0.74 g, 0.018 mmol, M_n = 39,600) to target DP = 300, and HD (0.25 mL, 0.85 mmol) was prepared. $Cu^{II}Br_2$/TPMA stock solution (0.20 mL, 0.01 mmol), NaCl (0.058 g, 1 mmol), and SDS (0.082 g, 0.28 mmol) were dissolved in 8 mL of distilled water. The organic and aqueous solutions were mixed (total volume ≈ 10 mL), placed in an ice bath, and dispersed by a probe sonicator, amplitude = 70% for 15 min (application and rest time of 1 s each). Nitrogen was bubbled through the miniemulsion solution for 0.5 h. The flask was immersed in a 65 °C oil bath and then a degassed AsAc solution was added by a syringe pump at 0.2 mmol/h. Samples were withdrawn periodically to follow the monomer conversion by gravimetric analysis, while M_n and M_w/M_n were determined by GPC.

7.6. References

(1) Matyjaszewski, K.; Spanswick, J., Controlled/Living Radical Polymerization. *Mater Today* **2005,** *8* (3), 26-33.
(2) Braunecker, W. A.; Matyjaszewski, K., Controlled/Living Radical Polymerization: Features, Developments, and Perspectives. *Prog Polym Sci* **2007,** *32* (1), 93-146.

(3) Matyjaszewski, K.; Xia, J. H., Atom Transfer Radical Polymerization. *Chem Rev* **2001,** *101* (9), 2921-2990.
(4) Matyjaszewski, K., Advanced Materials by Atom Transfer Radical Polymerization. *Advanced Materials* **2018,** *30*, 1706441.
(5) Moad, G.; Rizzardo, E.; Thang, S. H., Living Radical Polymerization by the RAFT Process. *Aust J Chem* **2005,** *58* (6), 379-410.
(6) Moad, G.; Rizzardo, E.; Thang, S. H., Living Radical Polymerization by the RAFT Process - A third update. *Aust J Chem* **2012,** *65* (8), 985-1076.
(7) Nicolas, J.; Guillaneuf, Y.; Lefay, C.; Bertin, D.; Gigmes, D.; Charleux, B., Nitroxide-Mediated Polymerization. *Prog Polym Sci* **2013,** *38* (1), 63-235.
(8) Bates, F. S.; Fredrickson, G. H., Block Copolymers - Designer Soft Materials. *Phys. Today* **1999,** *52* (2), 32-38.
(9) Tang, W.; Matyjaszewski, K., Effects of Initiator Structure on Activation Rate Constants in ATRP. *Macromolecules* **2007,** *40* (6), 1858-1863.
(10) Tang, W.; Kwak, Y.; Braunecker, W.; Tsarevsky, N. V.; Coote, M. L.; Matyjaszewski, K., Understanding Atom Transfer Radical Polymerization: Effect of Ligand and Initiator Structures on the Equilibrium Constants. *J Am Chem Soc* **2008,** *130* (32), 10702-10713.
(11) Lin, C. Y.; Marque, S. R. A.; Matyjaszewski, K.; Coote, M. L., Linear-Free Energy Relationships for Modeling Structure-Reactivity Trends in Controlled Radical Polymerization. *Macromolecules* **2011,** *44* (19), 7568-7583.
(12) Matyjaszewski, K.; Shipp, D. A.; McMurtry, G. P.; Gaynor, S. G.; Pakula, T., Simple and Effective One-Pot Synthesis of (Meth)acrylic Block Copolymers through Atom Transfer Radical Polymerization. *J Polym Sci Pol Chem* **2000,** *38* (11), 2023-2031.
(13) Davis, K. A.; Charleux, B.; Matyjaszewski, K., Preparation of Block Copolymers of Polystyrene and Poly (t-butyl Acrylate) of Various Molecular Weights and Architectures by Atom Transfer Radical Polymerization. *J Polym Sci Pol Chem* **2000,** *38* (12), 2274-2283.
(14) Nicolay, R.; Kwak, Y.; Matyjaszewski, K., Synthesis of Poly(vinyl Acetate) Block Copolymers by Successive RAFT and ATRP with a Bromoxanthate Iniferter. *Chem Commun* **2008,** (42), 5336-5338.
(15) Mueller, L.; Jakubowski, W.; Tang, W.; Matyjaszewski, K., Successful Chain Extension of Polyacrylate and Polystyrene Macroinitiators with Methacrylates in an ARGET and ICAR ATRP. *Macromolecules* **2007,** *40* (18), 6464-6472.
(16) Matyjaszewski, K.; Shipp, D. A.; Wang, J. L.; Grimaud, T.; Patten, T. E., Utilizing Halide Exchange to Improve Control of Atom Transfer Radical Polymerization. *Macromolecules* **1998,** *31* (20), 6836-6840.
(17) Hong, S. C.; Pakula, T.; Matyjaszewski, K., Preparation of Polyisobutene-graft-poly(methyl methacrylate) and Polyisobutene-graft-polystyrene with Different Compositions and Side Chain Architectures through Atom Transfer Radical Polymerization (ATRP). *Macromol Chem Phys* **2001,** *202* (17), 3392-3402.
(18) Peng, C. H.; Kong, J.; Seeliger, F.; Matyjaszewski, K., Mechanism of Halogen Exchange in ATRP. *Macromolecules* **2011,** *44* (19), 7546-7557.
(19) Chuang, Y. M.; Wenn, B.; Gielen, S.; Ethirajan, A.; Junkers, T., Ligand Switch in Photoinduced Copper-Mediated Polymerization: Synthesis of Methacrylate-acrylate Block Copolymers. *Polym Chem-Uk* **2015,** *6* (36), 6488-6497.

(20) Jakubowski, W.; Min, K.; Matyjaszewski, K., Activators Regenerated by Electron Transfer for Atom Transfer Radical Polymerization of Styrene. *Macromolecules* **2006,** *39* (1), 39-45.
(21) Simakova, A.; Averick, S. E.; Konkolewicz, D.; Matyjaszewski, K., Aqueous ARGET ATRP. *Macromolecules* **2012,** *45* (16), 6371-6379.
(22) Payne, K. A.; D'hooge, D. R.; van Steenberge, P. H. M.; Reyniers, M. F.; Cunningham, M. F.; Hutchinson, R. A.; Marin, G. B., ARGET ATRP of Butyl Methacrylate: Utilizing Kinetic Modeling To Understand Experimental Trends. *Macromolecules* **2013,** *46* (10), 3828-3840.
(23) Matyjaszewski, K.; Jakubowski, W.; Min, K.; Tang, W.; Huang, J. Y.; Braunecker, W. A.; Tsarevsky, N. V., Diminishing Catalyst Concentration in Atom Transfer Radical Polymerization with Reducing Agents. *P Natl Acad Sci USA* **2006,** *103* (42), 15309-15314.
(24) Matyjaszewski, K.; Tsarevsky, N. V.; Braunecker, W. A.; Dong, H.; Huang, J.; Jakubowski, W.; Kwak, Y.; Nicolay, R.; Tang, W.; Yoon, J. A., Role of Cu0 in Controlled/"Living" Radical Polymerization. *Macromolecules* **2007,** *40* (22), 7795-7806.
(25) Zhang, Y.; Wang, Y.; Matyjaszewski, K., ATRP of Methyl Acrylate with Metallic Zinc, Magnesium, and Iron as Reducing Agents and Supplemental Activators. *Macromolecules* **2011,** *44* (4), 683-685.
(26) Konkolewicz, D.; Wang, Y.; Zhong, M. J.; Krys, P.; Isse, A. A.; Gennaro, A.; Matyjaszewski, K., Reversible-Deactivation Radical Polymerization in the Presence of Metallic Copper. A Critical Assessment of the SARA ATRP and SET-LRP Mechanisms. *Macromolecules* **2013,** *46* (22), 8749-8772.
(27) Konkolewicz, D.; Wang, Y.; Krys, P.; Zhong, M. J.; Isse, A. A.; Gennaro, A.; Matyjaszewski, K., SARA ATRP or SET-LRP. End of Controversy? *Polym Chem-Uk* **2014,** *5* (15), 4396-4417.
(28) Bortolamei, N.; Isse, A. A.; Magenau, A. J. D.; Gennaro, A.; Matyjaszewski, K., Controlled Aqueous Atom Transfer Radical Polymerization with Electrochemical Generation of the Active Catalyst. *Angew Chem Int Ed* **2011,** *50* (48), 11391-11394.
(29) Magenau, A. J. D.; Strandwitz, N. C.; Gennaro, A.; Matyjaszewski, K., Electrochemically Mediated Atom Transfer Radical Polymerization. *Science* **2011,** *332* (6025), 81-84.
(30) Chmielarz, P.; Fantin, M.; Park, S.; Isse, A. A.; Gennaro, A.; Magenau, A. J. D.; Sobkowiak, A.; Matyjaszewski, K., Electrochemically Mediated Atom Transfer Radical Polymerization (eATRP). *Prog Polym Sci* **2017,** *69*, 47-78.
(31) Konkolewicz, D.; Schroder, K.; Buback, J.; Bernhard, S.; Matyjaszewski, K., Visible Light and Sunlight Photoinduced ATRP with ppm of Cu Catalyst. *Acs Macro Lett* **2012,** *1* (10), 1219-1223.
(32) Pan, X. C.; Tasdelen, M. A.; Laun, J.; Junkers, T.; Yagci, Y.; Matyjaszewski, K., Photomediated Controlled Radical Polymerization. *Prog Polym Sci* **2016,** *62*, 73-125.
(33) Mohapatra, H.; Kleiman, M.; Esser-Kahn, A. P., Mechanically Controlled Radical Polymerization Initiated by Ultrasound. *Nat Chem* **2017,** *9* (2), 135-139.
(34) Wang, Z. H.; Pan, X. C.; Yan, J. J.; Dadashi-Silab, S.; Xie, G. J.; Zhang, J. N.; Wang, Z. H.; Xia, H. S.; Matyjaszewski, K., Temporal Control in Mechanically Controlled Atom Transfer Radical Polymerization Using Low ppm of Cu Catalyst. *Acs Macro Lett* **2017,** *6* (5), 546-549.

(35) Averick, S.; Simakova, A.; Park, S.; Konkolewicz, D.; Magenau, A. J. D.; Mehl, R. A.; Matyjaszewski, K., ATRP under Biologically Relevant Conditions: Grafting from a Protein. *Acs Macro Lett* **2012,** *1* (1), 6-10.
(36) Fu, L.; Wang, Z.; Lathwal, S.; Enciso, A. E.; Simakova, A.; Das, S. R.; Russell, A. J.; Matyjaszewski, K., Synthesis of Polymer Bioconjugates via Photoinduced Atom Transfer Radical Polymerization under Blue Light Irradiation. *Acs Macro Lett* **2018,** *7*, 1248-1253.
(37) Aitchison, T. J.; Ginic-Markovic, M.; Clarke, S.; Valiyaveettil, S., Polystyrene-block-poly(methyl methacrylate): Initiation Issues with Block Ccopolymer Formation using ARGET ATRP. *Macromol Chem Phys* **2012,** *213* (1), 79-86.
(38) De Bon, F.; Fantin, M.; Isse, A. A.; Gennaro, A., Electrochemically Mediated ATRP in Ionic Liquids: Controlled Polymerization of Methyl Acrylate in [BMIm][OTf]. *Polym Chem-Uk* **2018,** *9* (5), 646-655.
(39) Fang, C.; Fantin, M.; Pan, X. C.; de Fiebre, K.; Coote, M. L.; Matyjaszewski, K.; Liu, P., Mechanistically Guided Predictive Models for Ligand and Initiator Effects in Copper-Catalyzed Atom Transfer Radical Polymerization (Cu-ATRP). *J Am Chem Soc* **2019,** *141* (18), 7486-7497.
(40) Qiu, J.; Charleux, B.; Matyjaszewski, K., Controlled/living radical polymerization in aqueous media: homogeneous and heterogeneous systems. *Prog. Polym. Sci.* **2001,** *26* (10), 2083-2134.
(41) Asua, J. M., Miniemulsion Polymerization. *Prog Polym Sci* **2002,** *27* (7), 1283-1346.
(42) Min, K.; Matyjaszewski, K., Atom Transfer Radical Polymerization in Aqueous Dispersed Media. *Cent Eur J Chem* **2009,** *7* (4), 657-674.
(43) Zetterlund, P. B.; Kagawa, Y.; Okubo, M., Controlled/Living Radical Polymerization in Dispersed Systems. *Chem Rev* **2008,** *108* (9), 3747-3794.
(44) Zetterlund, P. B.; Thickett, S. C.; Perrier, S.; Bourgeat-Lami, E.; Lansalot, M., Controlled/Living Radical Polymerization in Dispersed Systems: An Update. *Chem Rev* **2015,** *115* (18), 9745-9800.
(45) Fantin, M.; Chmielarz, P.; Wang, Y.; Lorandi, F.; Isse, A. A.; Gennaro, A.; Matyjaszewski, K., Harnessing the Interaction between Surfactant and Hydrophilic Catalyst to Control eATRP in Miniemulsion. *Macromolecules* **2017,** *50* (9), 3726-3732.
(46) Lorandi, F.; Wang, Y.; Fantin, M.; Matyjaszewski, K., Ab initio emulsion atom-transfer radical polymerization. *Angew. Chem. Int. Ed.* **2018,** *57* (27), 8270-8274.
(47) Wang, Y.; Fu, L. Y.; Matyjaszewski, K., Enzyme-Deoxygenated Low Parts Per Million Atom Transfer Radical polymerization in Miniemulsion and Ab Initio Emulsion. *Acs Macro Lett* **2018,** *7* (11), 1317-1321.
(48) Wang, Y.; Dadashi-Silab, S.; Lorandi, F.; Matyjaszewski, K., Photoinduced atom transfer radical polymerization in ab initio emulsion. *Polymer* **2019,** *165*, 163-167.
(49) Ribelli, T. G.; Krys, P.; Cong, Y. D.; Matyjaszewski, K., Model studies of alkyl halide activation and comproportionation relevant to RDRP in the presence of Cu0. *Macromolecules* **2015,** *48* (23), 8428-8436.
(50) Lin, C. Y.; Coote, M. L.; Petit, A.; Richard, P.; Poli, R.; Matyjaszewski, K., Ab Initio Study of the Penultimate Effect for the ATRP Activation Step using Propylene, Methyl Acrylate, and Methyl Methacrylate Monomers. *Macromolecules* **2007,** *40* (16), 5985-5994.
(51) Teo, V. L.; Davis, B. J.; Tsarevsky, N. V.; Zetterlund, P. B., Successful Miniemulsion ATRP using an Anionic Surfactant: Minimization of Deactivator Loss by Addition of a Halide Salt. *Macromolecules* **2014,** *47* (18), 6230-6237.

(52) Bon, F. D.; Isse, A. A.; Gennaro, A., Electrochemically-Mediated ATRP of Methyl Methacrylate: the Importance of Catalytic Halogen Exchange. *ChemElectroChem* **2019,** *6*, 4257-4265.
(53) Jansson, M.; Eriksson, L.; Skagerlind, P., The Effect Of Tetraalkylammonium Ions on the Stability Of Dilute O/W Emulsions. *Colloid Surf.* **1991,** *53* (1-2), 157-167.

Chapter 8 Synthesis of Hairy Nanoparticles by Miniemulsion ATRP

8.1. Preface

The content of this chapter will be submitted for publication.

This research was a continuation of my work presented in Chapters II – VI. The ion-pair catalyst was demonstrated as an efficient catalytic system for miniemulsion ATRP using low ppm concentration of catalyst. Besides homopolymers and block copolymers, polymer stars and brushes were also prepared. In this project, the synthesis of core-crosslinked hairy nanoparticles in miniemulsion ATRP was conducted.

In miniemulsion polymerization, the mass transfer between monomer droplets and the continuous phase is negligible, and each droplet acts as a nanoreactor. Thus, nanoobjects with uniform size distribution could be prepared by miniemulsion ATRP in the presence of crosslinkers, and further modified with hydrophilic polymer chains from the surface, forming hairy nanoparticles.

I designed this project and carried out most of the experiments. I want to thank Julia Cuthbert for providing 2-((2-bromo-2-methylpropanoyl)oxy)ethyl methacrylate (HEMA-iBBr) and Tong Liu for assistance in electron microscopy.

This project was completed with a financial support from the NSF (CHE-2000391) and the Kwolek Fellowship.

8.2. Introduction

Miniemulsion polymerization is a robust pathway to synthesize nanoobjects, due to the avoided mass transfer between the particles and the dispersed media. Thus, miniemulsion droplets could behave as "nanoreactors". Various macromolecular structures were synthesized in miniemulsion by reversible deactivation radical polymerization (RDRP), especially atom transfer radical polymerization (ATRP). Using multifunctional initiators, polymer stars and brushes were synthesized up to high monomer conversion and minimal termination reactions.[1] Gradient copolymers were prepared thanks to the difference of reactivity of comonomers [2], feeding rate,[3] or solubility.[4] The segregation of polymerization media into numerous droplets resulted in suppression termination reactions, allowing the synthesis of bottlebrush and hyperbranched polymers without macroscopic gelation.[1, 5-6]

A Cu complex/anionic surfactant ion-pair catalyst was recently investigated in miniemulsion ATRP, allowing for synthesis of linear polymers and block copolymers. [5, 7-8] Despite the robust synthesis technique, the potential for incorporation of complex architectures, function groups and applications have not been heavily studied. Particles with hairy, core-shell, hollow and multilayered structures have been synthesized via polymerizations in dispersed media.[9-12] Potential applications include drug delivery or responsive materials.

Hydrophobic poly(methyl methacrylate/ethyleneglycol dimethacrylate)-poly-*n*-butyl acrylate (P(MMA/EGDMA)-PBA) hairy nanoparticles synthesized via a two-step approach. The P(MMA/EGDMA) crosslinked networks were prepared by microemulsion ATRP. *n*-Butyl acrylate BA was slowly added to the microemulsion and swelled the

P(MMA/EGDMA) crosslinked networks. PBA was grafted from initiation site both at the oil-water interface and inside the crosslinked networks, forming an enlarged network grafted with hydrophobic PBA chains.[13]

The addition of hydrophilic monomers to the crosslinked nanoparticles miniemulsion is a different story, since the crosslinked nanoparticles cannot swell. In this chapter, hydrophobic crosslinked nanoparticles were synthesized by miniemulsion ARGET ATRP, and modified with hydrophilic chains by successive chain extension at the oil-water interface (**Scheme 8-1**). The efficacy of chain extension was demonstrated, and the influence of surface initiator density was studied. The efficiency of chain extension was evaluated by degradation of a disulfide-based network.

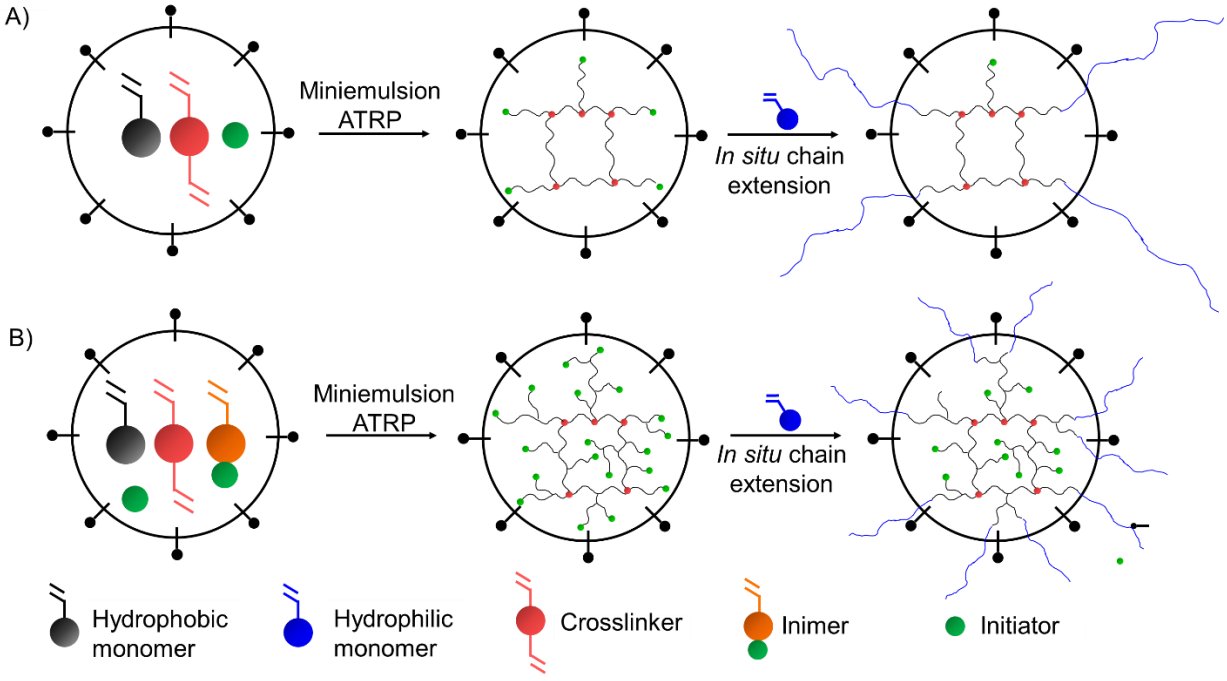

Scheme 8-1. Proposed procedures to synthesize functional polymer nanogels. A) without inimer; B) with inimer.

8.3. Results and Discussion

Hydrophobic P(BMA/EGDMA) network was synthesized in miniemulsion ARGET ATRP. The reaction conditions were adopted from previous reports,[5] and modified by the addition of 8 mol% of ethylene glycol dimethacrylate (EGDMA) (with respective to total monomer). The reaction was tracked by NMR. After 15 h of irradiation, the concentration of residual double bonds was negligible, indicating almost complete polymerization and full crosslinking.

A hydrophilic nonionic polymer, $POEOMA_{500}$, was grafted from the P(BMA/EGDMA) crosslinked nanoparticles. The degassed $OEOMA_{500}$ ($OEOMA_{500}$/Br = 20/1) was injected to the miniemulsion. The droplet sizes before and after addition of $OEOMA_{500}$ were 140 and 139 nm, respectively, demonstrating the hydrophilic $OEOMA_{500}$ dissolved in the aqueous phase, instead of swelling the P(BMA/EGDMA) crosslinked nanoparticles. AsAc was added to trigger the polymerization of $OEOMA_{500}$ from P(BMA/EGDMA). After 6 h polymerization, ^1H NMR showed the depletion of $OEOMA_{500}$, and the particle size significantly increased to 423 nm, indicating long $POEOMA_{500}$ chains. Due to the hydrophilicity of $OEOMA_{500}$, initiation only occurred from the active bromine sites at the surface of the network, and the inaccessible initiation sites buried inside the nanoparticles resulted in a high degree of polymerization. Grafting hydrophilic $POEOMA_{500}$ did not hamper the stability of the miniemulsion, despite increased viscosity.

The large increase of particle size after grafting a small amount of $OEOMA_{500}$ indicated the small number of accessible initiation sites on the surface of P(BMA/EGDMA). To increase the number of grafted $POEOMA_{500}$ chain, an inimer, HEMA-iBBr was added to the organic phase of the miniemulsion, forming P(BMA/EGDMA/HEMA-iBBr) network, with 10 times more ATRP initiation sites than P(BMA/EGDMA) network.

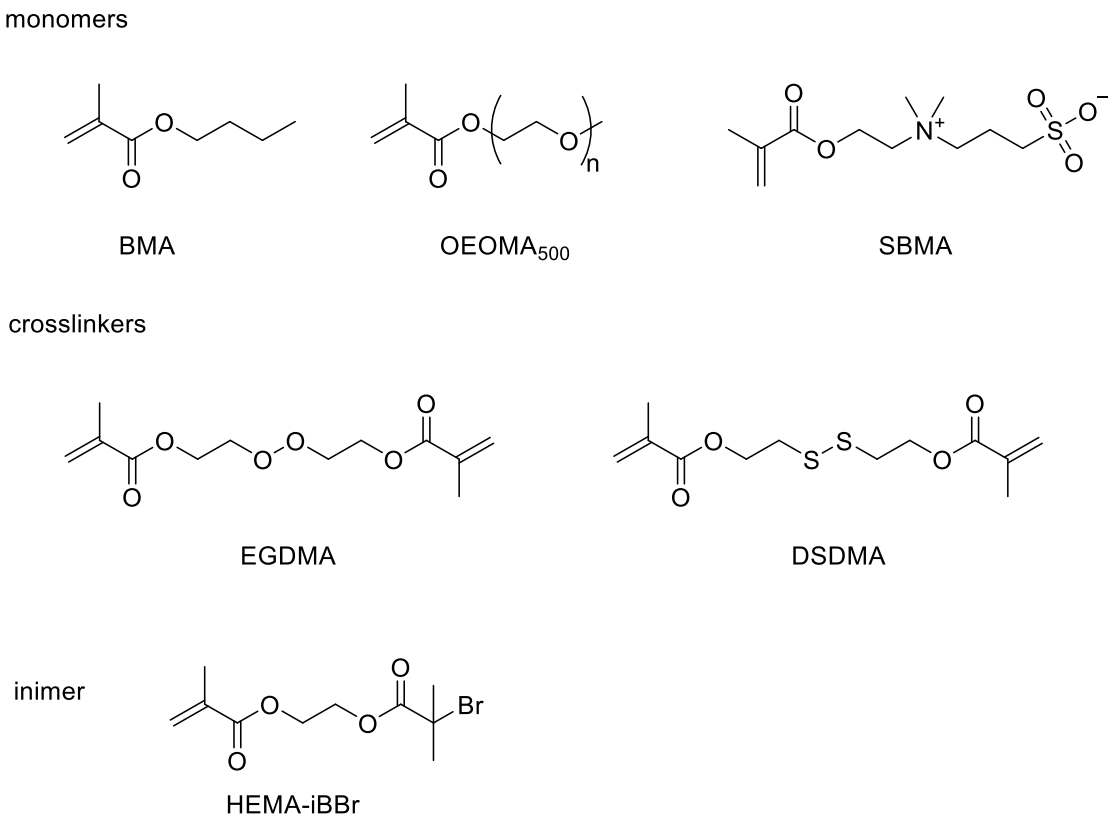

Scheme 8-2. Structure of monomers, crosslinkers and inimer.

P(BMA/EGDMA/HEMA-iBBr) crosslinked nanoparticles were also chain extended with $OEOMA_{500}$ *in situ*. Since the accessible initiation sites increased, under the same $OEOMA_{500}$ amount, the resulting $POEOMA_{500}$ had significantly shorter chains. This

was evidenced by the smaller size increase and confirmed by the particle size measured by DLS (**Table 8-1**) and SEM (**Figure 8-1**).

Table 8-1. Zeta-average size of polymer networks before and after grafting of OEOMA.

Sample	Before (nm)	After (nm)	Size increase (nm)
P(BMA/EGDMA)	139	423	284
P(BMA/EGDMA/HEMA-iBBr)	125	148	27

The difference of P(BMA/EGDMA) and P(BMA/EGDMA/HEMA-iBBr) in network structure strongly influences the initiation site density. To demonstrate the difference, a disulfide crosslinker, DSDMA was employed in PBMA NP synthesis in the presence and absence of HEMA-iBBr. The resulting networks were both chain extended with $OEOMA_{500}$, and the degradation products were analyzed by GPC (**Figure 8-2**). The GPC of degraded P(BMA/DSDMA) showed a M_n = 21,700, close to theoretical value (80% conversion of PBMA with target DP = 200), and with low dispersity. However, the complete degradation of P(BMA/DSDMA)-$POEOMA_{500}$ was not successful, and some degradation products were too large to be analyzed by GPC. The M_n of degraded P(BMA/DSDMA/HEMA-iBBr) was lower than that of P(BMA/DSDMA), because the branched structure caused by inimers could decrease the hydrodynamic volume. The MW increased upon grafting of $POEOMA_{500}$. I would add a schematic or both structures, linear and branched., also how much extension? You should get a bimodal distrib I think for both of them but % extension could be different

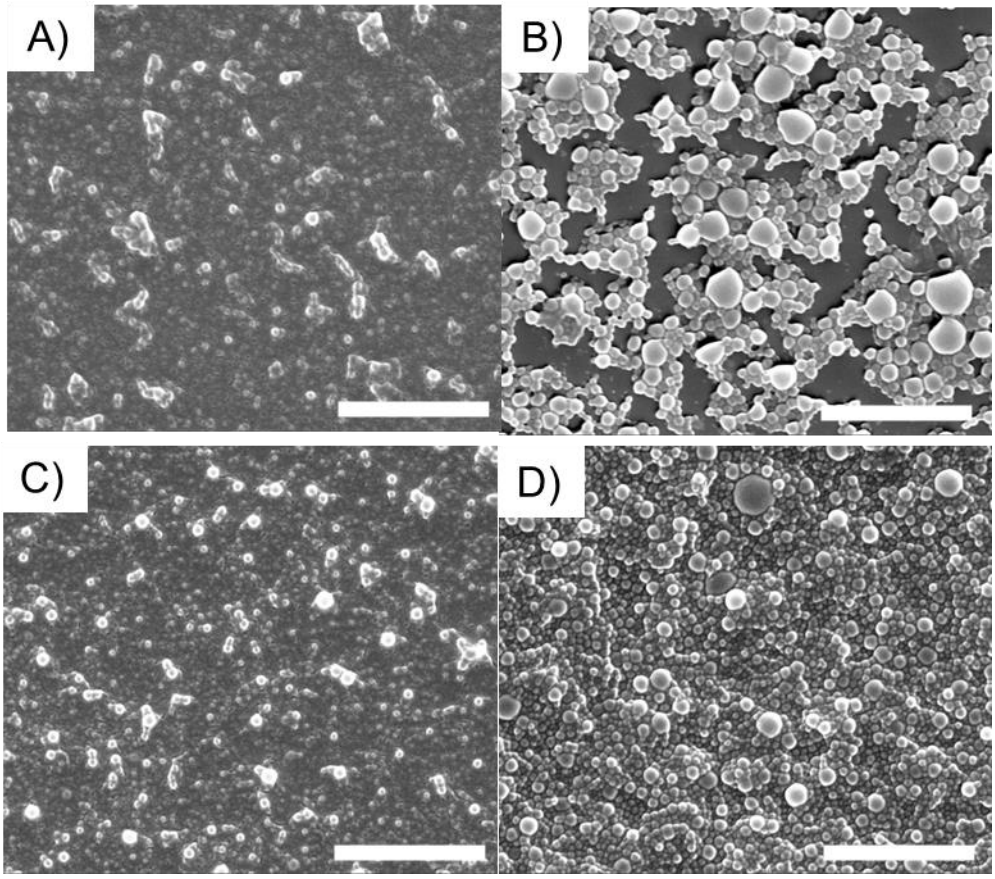

Figure 8-1. SEM image of A) P(BMA/EGDMA); B) P(BMA/EGDMA)-POEOMA$_{500}$; C) P(BMA/EGDMA/HEMA-iBBr); D) P(BMA/EGDMA/HEMA-iBBr)-POEOMA$_{500}$. Scale bar = 5 μm.

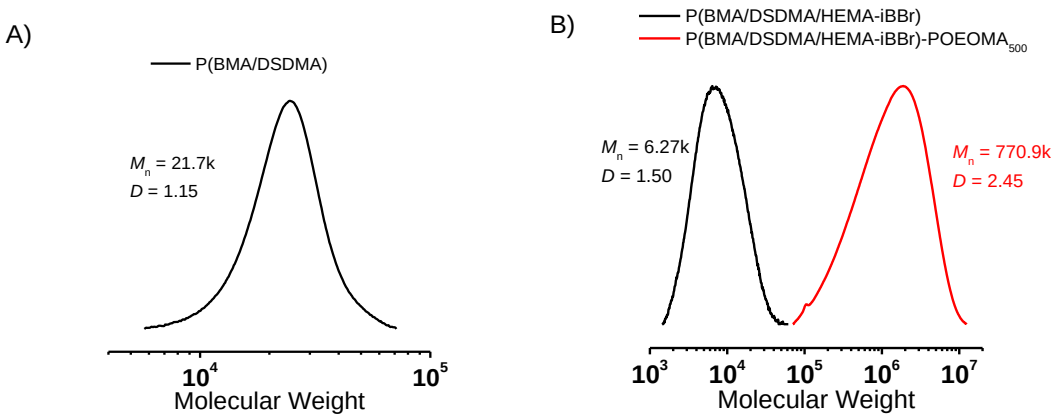

Figure 8-2. GPC traces of degraded (left) sample 1 before grafting of POEOMA; (right) sample 2 before and after grafting of POEOMA.

P(BMA/EGDMA) NPs had good stability after *in situ* chain extension of OEOMA$_{500}$. Therefore, PBMA NP-*g*-POEOMA were isolated as an aqueous dispersion, and then chain extended with functional monomers in water borne system (**Scheme 8-3**). By using this approach, the employed POEOMA could: 1) increase the stability of the NP in water; 2) bring Br chain ends further from the surface to facilitate chain extension is easier.

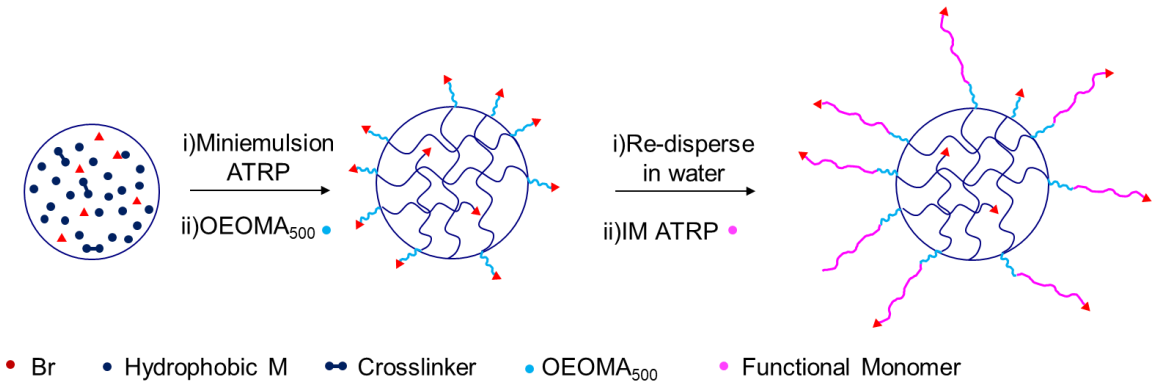

Scheme 8-3. Grafting functional aqueous monomers from PBMA NP-g-POEOMA.

Polyzwitterionic surfaces have good anti-fouling properties and low frictions. [14] Thus, a zwitterionic monomer, [2-(methacryloyloxy)ethyl]dimethyl-(3-sulfopropyl)ammonium hydroxide (SBMA) was grafted from the surface of the PBMA nanoparticles. Since ATRP of SBMA is poorly controlled in water, ATRP of SBMA is usually carried out in water/alcohol mixture. Methanol decreases the polarity, slows down the polymerization, and improves the control. Since the PBMA NPs precipitate in alcohol, SBMA was not successfully extended. Thus, Br atoms at the surface of P(BMA/EGDMA) NPs could not directly initiate ATRP of SBMA.

P(BMA/EGDMA)-$POEOMA_{500}$ and P(BMA/EGDMA/HEMA-iBBr)-$POEOMA_{500}$ were re-dispersed in water/methanol (**Figure 8-3**). The dispersion remained stable upon addition of SBMA. ATRP of SBMA from the nanoparticles was then conducted. P(BMA/EGDMA/HEMA-iBBr)-$POEOMA_{500}$ was successfully chain extended with SBMA, while very low conversion was observed from P(BMA/EGDMA)-$POEOMA_{500}$. The difference in efficiency of SBMA chain extension could be explained by the higher Br-initiation site concentration in P(BMA/EGDMA/HEMA-iBBr)-$POEOMA_{500}$.

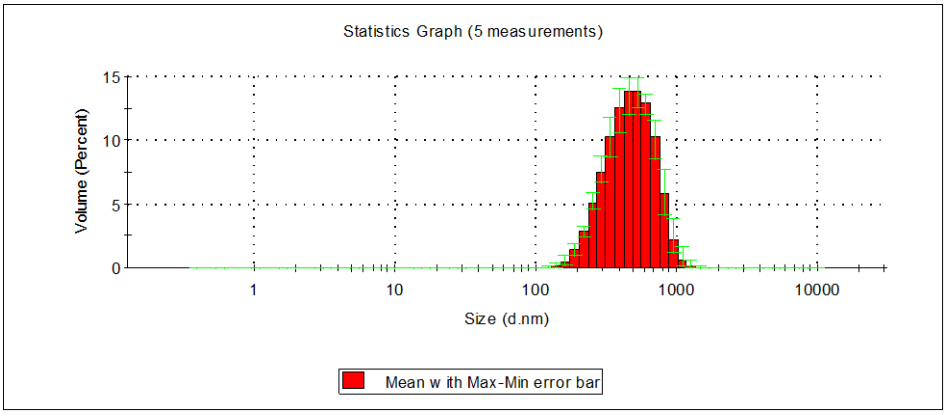

Figure 8-3. Volume-mean hydrodynamic size of NP in water/methanol at room temperature. d = 498 nm.

8.4. Conclusion

In summary, the synthesis polymer networks with hydrophobic core and hydrophilic "hair" was achieved by two-step miniemulsion ATRP. The Br chain end density could be increased by incorporation of inimers. The hydrophobic PBMA crosslinked nanoparticles could be chain extended by addition of a hydrophilic $OEOMA_{500}$ to the miniemulsion, forming amphiphilic hairy nanoparticles. The network structures were studied by degradation of the PBMA networks and the hairy nanoparticles. The P(BMA/EGDMA/HEMA-iBBr)-$POEOMA_{500}$ could be re-dispersed in water/methanol mixture, allowing the incorporation of a zwitterionic PSBMA block to the hairy nanoparticles. These results demonstrate the feasibility of miniemulsion ATRP in the synthesis of core-shell structures as well as functional copolymers.

8.5. Experimental Section

Materials. Copper(II) bromide ($Cu^{II}Br_2$, 99%), sodium dodecyl sulfate (SDS, 99%), hexadecane (HD, 99%), tetrahydrofuran (THF, > 99%), ethyl α-bromoisobutyrate (EBiB, 98%), ethyl α-bromophenylacetate (EBPA, 97%), and tri-*n*-butyl phosphine (Bu_3P) were purchased from Sigma-Aldrich. Sodium bromide (NaBr, 99%) was purchased from Acros. Tris(2-pyridylmethyl)amine (TPMA) was provided by KOEI Chemical. The reagents above were used as received. *n*-Butyl methacrylate (BMA, 99%, Sigma-Aldrich), poly(ethylene glycol) methyl ether methacrylate (average M_n = 500, $OEOMA_{500}$, Sigma-Aldrich) and bis(2-methacryloyl)oxyethyl disulfide (DSDMA, 99%, Sigma-Aldrich) were passed through a column filled with basic alumina prior to use to remove polymerization inhibitors. Poly(ethylene oxide) bromophenyl acetate (HEMA-iBBr) was prepared according to previously published procedures.[15]

Instrumentation. Ultrasound treatment to prepare miniemulsion samples was carried out using Autotune Series High Intensity Ultrasonic Processor, 1500 Watt Model.

M_n and $Đ$ were determined by GPC equipped with Polymer Standards Services (PSS) columns (guard, 10^5, 10^3, and 10^2 Å) and a differential refractive index detector (Waters, 2410), with THF as eluent at a flow rate of 1.00 mL/min (T = 35 °C). GPC traces were processed by WinGPC 8.0 software (PSS) using a calibration based on linear polystyrene (PS) standards.

Particle size and size distribution were determined by using a Zetasizer Nano from Malvern Instruments, Ltd.

General procedure for synthesis of P(BMA/EGDMA) crosslinked nanoparticles by miniemulsion ARGET ATRP. A solution of BMA (2.0 mL, 12.57 mmol), EGDMA (0.06 mL, 0.31 mmol), EBPA (11.0 μL, 0.063 mmol) to target DP = 200, and HD (0.25 mL, 0.85 mmol) was prepared. A stock solution of $Cu^{II}Br_2$/TPMA (0.20 mL, 0.01 mmol), NaBr (0.103 g, 1 mmol), and SDS (0.082 g, 4.6 wt% to BMA) was prepared in 8 mL of distilled water. The organic and aqueous solutions were mixed (total volume ≈ 10 mL), placed in an ice-water bath, and dispersed by a probe sonicator, amplitude = 20% for 20 min (application and rest time of 1 s each). Nitrogen was bubbled through the miniemulsion solution for 30 min. Polymerization was started by addition of AsAc (0.1 mL of 0.1 M solution, 0.01 mmol). Samples were withdrawn periodically to follow the monomer conversion by NMR analysis.

Procedure for grafting $OEOMA_{500}$ from P(BMA/EGDMA) miniemulsion. After the PBMA nanoparticle synthesis in miniemulsion reaches >90% conversion, $OEOMA_{500}$ (0.42 mL, 0.93 mmol) was degassed and injected into the miniemulsion. AsAc (0.1 mL of 0.1 M solution, 0.01 mmol) was added. Samples were withdrawn periodically to follow the monomer conversion by NMR analysis. The PBMA-$POEOMA_{500}$ nanoparticles were precipitated in methanol, collected by centrifuge, and re-dispersed in water.

Procedure for grafting SBMA from P(BMA/EGDMA)-$POEOMA_{500}$. SBMA (0.28 g, 1 mmol), bpy (0.0016 g, 0.01 mmol) and 5 mL methanol were dissolved in 5 mL aqueous dispersion of P(BMA/EGDMA)-$POEOMA_{500}$ (0.05 g/mL). The resulting dispersion was degassed by three freeze-pump-thaw cycles. CuBr (0.0014 g, 0.01 mmol) was added to the dispersion in N_2 atmosphere. The mixture was immersed to a 40 ^oC oil

bath. Samples were withdrawn periodically to follow the monomer conversion by NMR analysis.

Procedure for degradation of P(BMA/DSDMA)-POEOMA$_{500}$. Bu_3P was added to P(BMA/DSDMA)-POEOMA$_{500}$ dispersion in dichloromethane, and the mixture was stirred at 300 rpm at room temperature for 7 days.

8.6. References

(1) Min, K.; Yu, S.; Lee, H. I.; Mueller, L.; Sheiko, S. S.; Matyjaszewski, K., High Yield Synthesis of Molecular Brushes via ATRP in Miniemulsion. *Macromolecules* **2007,** *40* (18), 6557-6563.
(2) Min, K.; Li, M.; Matyjaszewski, K., Preparation of Gradient Copolymers via ATRP using a Simultaneous Reverse and Normal Initiation Process. I. Spontaneous Gradient. *J Polym Sci Pol Chem* **2005,** *43* (16), 3616-3622.
(3) Min, K.; Oh, J. K.; Matyjaszewski, K., Preparation of Gradient Copolymers via ATRP in Miniemulsion. II. Forced Gradient. *J Polym Sci Pol Chem* **2007,** *45* (8), 1413-1423.
(4) Wang, Y.; Dadashi-Silab, S.; Lorandi, F.; Matyjaszewski, K., Photoinduced atom transfer radical polymerization in ab initio emulsion. *Polymer* **2019,** *165*, 163-167.
(5) Wang, Y.; Lorandi, F.; Fantin, M.; Chmielarz, P.; Isse, A. A.; Gennaro, A.; Matyjaszewski, K., Miniemulsion ARGET ATRP via Interfacial and Ion-Pair Catalysis: From ppm to ppb of Residual Copper. *Macromolecules* **2017,** *50* (21), 8417-8425.
(6) Wang, X. F.; Graff, R. W.; Shi, Y.; Gao, H. F., One-Pot Synthesis of Hyperstar Polymers via Sequential ATRP of Inimers and Functional Monomers in Aqueous Dispersed Media. *Polym Chem-Uk* **2015,** *6* (37), 6739-6745.
(7) Fantin, M.; Chmielarz, P.; Wang, Y.; Lorandi, F.; Isse, A. A.; Gennaro, A.; Matyjaszewski, K., Harnessing the Interaction between Surfactant and Hydrophilic Catalyst to Control eATRP in Miniemulsion. *Macromolecules* **2017,** *50* (9), 3726-3732.
(8) Wang, Y.; Dadashi-Silab, S.; Matyjaszewski, K., Photoinduced miniemulsion atom transfer radical polymerization. *ACS Macro Lett.* **2018,** *7* (6), 720-725.
(9) Wang, W. Z.; Song, W. B.; Wang, R.; Liu, T. X., ATRP Synthesis of Poly(4-bromostyrene)-b-Poly(propylene glycol) Block Copolymer and Its Self-Assembly in Catalystic Emulsion Polymerization to Form Luminescent Nanospheres with Core-Shell Structure. *J Polym Sci Pol Chem* **2009,** *47* (5), 1478-1483.
(10) Kagawa, Y.; Minami, H.; Okubo, M.; Zhou, H., Preparation of Block Copolymer Particles by Two-Step Atom Transfer Radical Polymerization in Aqueous Media and its Unique Morphology. *Polymer* **2005,** *46* (4), 1045-1049.
(11) Kitayama, Y.; Kagawa, Y.; Minami, H.; Okubo, M., Preparation of Micrometer-Sized, Onionlike Multilayered Block Copolymer Particles by Two-Step AGET ATRP in Aqueous

Dispersed Systems: Effect of the Second-Step Polymerization Temperature. *Langmuir* **2010,** *26* (10), 7029-7034.
(12) Sasaki, Y.; Konishi, N.; Kasuya, M.; Kohri, M.; Taniguchi, T.; Kishikawa, K., Preparation of Size-Controlled Polymer Particles by Polymerization of O/W Emulsion Monomer Droplets Obtained through Phase Inversion Temperature Emulsification using Amphiphilic Comb-Like Block Polymers. *Colloid Surface A* **2015,** *482*, 68-78.
(13) Min, K.; Gao, H.; Yoon, J. A.; Wu, W.; Kowalewski, T.; Matyjaszewski, K., One-Pot Synthesis of Hairy Nanoparticles by Emulsion ATRP. *Macromolecules* **2009,** *42* (5), 1597-1603.
(14) Kotsuchibashi, Y.; Ebara, M.; Aoyagi, T.; Narain, R., Recent Advances in Dual Temperature Responsive Block Copolymers and Their Potential as Biomedical Applications. *Polymers-Basel* **2016,** *8* (11).
(15) Cuthbert, J.; Beziau, A.; Gottlieb, E.; Fu, L. Y.; Yuan, R.; Balazs, A. C.; Kowalewski, T.; Matyjaszewski, K., Transformable Materials: Structurally Tailored and Engineered Macromolecular (STEM) Gels by Controlled Radical Polymerization. *Macromolecules* **2018,** *51* (10), 3808-3817.

Chapter 9 Electrochemically Mediated Reversible Addition-Fragmentation Chain-Transfer Polymerization by Electroreduction of Diazonium Salt

9.1. Preface

The content of this chapter was published in Macromolecules (**Y. Wang**, M. Fantin, S. Park, E. Gottlieb, L. Fu, K. Matyjaszewski, *Macromolecules*, **2017**, *50*(20), 7872-7879.)

Reversible addition-fragmentation chain-transfer polymerization (RAFT) polymerization is an important method in reversible deactivation radical polymerization (RDRP) taking advantage of the degenerative transfer of the polymeric radical in the presence of RAFT chain-transfer agents (CTAs). RAFT is compatible with a broad range of monomers and reaction media. RAFT process typically involves thermal initiators which decompose at specific temperatures. The elevated temperature hinders the application of RAFT polymerization in the synthesis of some thermoresponsive polymers and bio-related systems. In addition, externally generated radicals initiate new chains and result in lower molecular weights, lower chain-end functionality and higher dispersity.

Electrochemistry can provide an external stimulus for tuning RAFT polymerization. The early success of electrochemically mediated atom transfer radical polymerization (*e*ATRP) triggered our interest to develop *e*RAFT. However, the direct electrochemical activation of CTAs was not efficient, as it resulted in irreversible reduction at very low potential, where the polymeric radicals were also reduced. Thus, some indirect pathways were investigated. Chapters IX – XI present a few pathways to achieve a successful *e*RAFT.

In chapter IX, benzoyl peroxide (BPO) and a diazonium salt, 4-bromobenzenediazonium tetrafluoroborate ($BrPhN_2^+$), were reduced by electrochemistry and provided radicals for RAFT polymerization.

I mainly contributed in the investigation of $BrPhN_2^+$ mediated *e*RAFT polymerization. Electrochemical analysis and preliminary eRAFT attempts showed a side reaction, electrodeposition of aryl compounds on the electrode. This significantly decreased the conductivity on the surface of the working electrode, leading to a very diminished current. I designed experiments to investigate the side reactions, and switched the electrolysis from a fixed potential to a fixed current to provide a sufficient amount of radicals. The chain extension from a macro-CTA was successfully conducted.

Previous group members, Dr. Marco Fantin and Dr. Sangwoo Park contributed to investigate initiator selection. Dr. Eric Gottlieb, helped us in X-ray Photoelectron Spectroscopy (XPS). Liye Fu aided in ^1H NMR study.

The support from the National Science Foundation (CHE 1707490) and the National Institutes of Health (R01DE020843) is acknowledged.

9.2. Introduction

Reversible deactivation radical polymerization (RDRP) methods have been employed to prepare polymers with pre-determined molecular weight (MW), low dispersity (*Đ*), controlled architecture, and preserved chain-end functionality.[1] Reversible radical trapping or degenerative chain-transfer assure concurrent growth of all polymer chains, and are employed to extend the lifetime of propagating chains from seconds to hours or even days.[1-2] Two most often used RDRP methods include atom transfer radical

polymerization (ATRP)[3-6] and reversible addition-fragmentation chain-transfer polymerization (RAFT) polymerization.[7-8]

ATRP is based on converting propagating radicals ($P_n^{\bullet}$) into dormant alkyl halide species (P_n-X) by transition metal complexes, usually X-Cu^{II}/L (L = ligand) (**Figure 9-1**A).[3, 5] The resulting Cu^{I}/L complex reactivates the dormant species, P_n-X. The dynamic exchange between active and dormant states enables the simultaneous and uniform growth of all chains with pre-determined molecular weights and high chain-end fidelity.

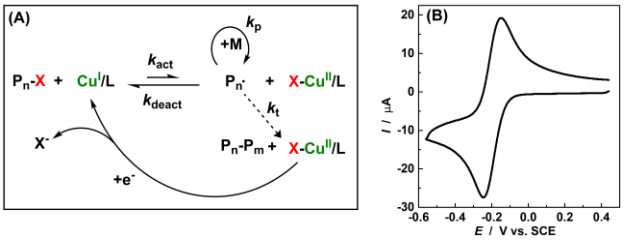

Figure 9-1 (A) Mechanism of *e*ATRP. (B) CV of 2×10^{-3} M [Br-Cu^{II}(tris(2-methylpyridyl)amine]$^{+}$ in DMSO + 0.1 Et_4NBF_4, at T = 25 °C and scan rate 0.2 V s^{-1}.

In ATRP, the active Cu^{I}/L catalyst can be (re)generated by (photo)chemical or electrochemical methods.[9-13] Electrochemically mediated ATRP (*e*ATRP) relies on the well-defined and reversible redox behavior of Cu/L complexes (**Figure 9-1**B), which allows for a precise control of the polymerization. For example, the [Cu^{I}]/[Cu^{II}] ratio can be set by adjusting the applied potential, which in turn determines the polymerization rate;[9, 14] *e*ATRP can be switched "on" and "off" by shifting the potential during polymerization.[9, 15] Moreover, Cu can be easily recycled by electroplating onto the working electrode (WE), and then oxidized back into solution and re-used multiple times.[14, 16] *e*ATRP has been applied to various monomers,[9, 15, 17] preparing copolymers with different architectures[18-19] in a range of reaction media.[20-21] Computational

simulations were also conducted for *e*ATRP, elucidating the key parameters.[22] The application of Fe-based catalyst broadened the application of *e*ATRP.[23]

Another important RDRP procedure is RAFT polymerization (**Figure 9-2**),[8, 24-27] which is based on degenerative transfer, and is mediated by chain transfer agents (CTAs) such as dithioesters, dithiocarbamates, trithiocarbonates, or xanthates.[25] RAFT polymerization is compatible with many vinyl monomers and solvents, including both homogeneous and heterogeneous conditions.[28]

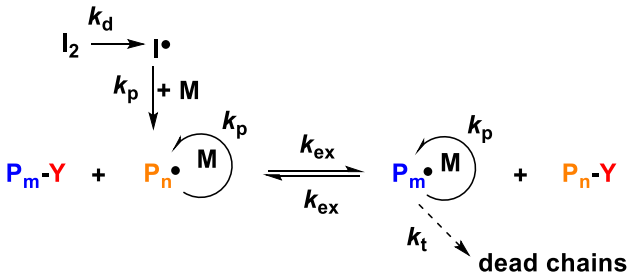

Figure 9-2. Mechanism of RAFT polymerization.

A continuous supply of radicals (i.e. "initiation") is essential in RAFT due to inevitable termination process. Initiation can be accomplished by thermal decomposition of radical sources such as azobisisobutyronitrile (AIBN) between 50 and 70 °C. However, such temperatures may be not suitable for some functional monomers[29] or for biological or thermo-responsive systems.[30] Thus, alternative radical generation methods were used for

RAFT at ambient temperature, including zerovalent metals,[31-33] redox reactions,[34-35] γ-rays,[36] and light via the iniferter[37] or the photoinduced electron transfer processes.[38-39]

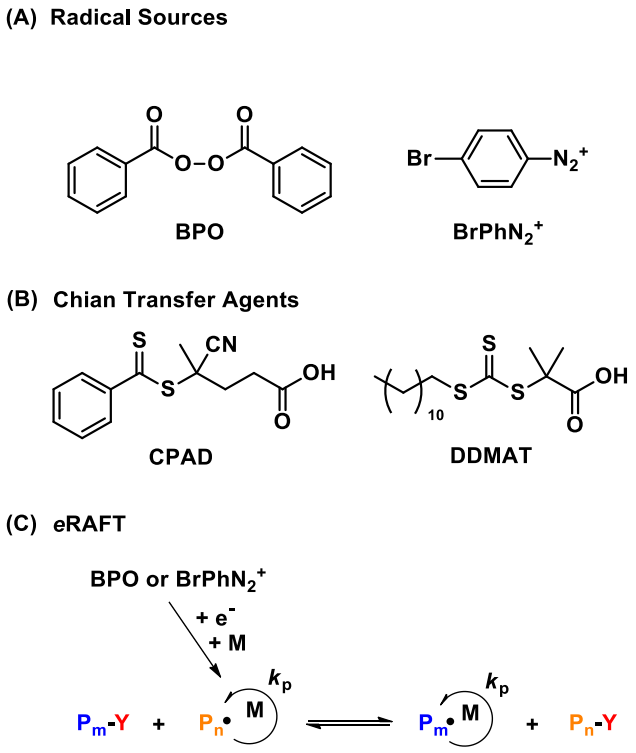

Figure 9-3. Structures of (A) radical sources and (B) CTAs used in this work. (C) Schematic representation of *e*RAFT polymerization, where Y is a chain-transfer moiety, M = monomer, k_p = propagation rate constant.

In this work, we investigated the use of electrical current for RAFT polymerization, inspired by successful *e*ATRP procedure and by modification of electrodes in the presence of RAFT agents.[40-42] However, an electrochemically mediated RAFT (*e*RAFT) is more challenging than *e*ATRP. Cu/L complexes for ATRP have a well-defined and reversible redox behavior,[43] whereas the electrochemical reactivity of RAFT agents is mostly unexplored, and could result in irreversible redox processes that cannot be exploited to generate radicals. Thus, we first studied the redox properties of common CTAs (**Figure**

9-3B), which were found to be unsuitable for the direct electrogeneration of radicals by reduction on common electrodes. To circumvent this limitation, we employed electroreduction of common radical initiators, such as benzoyl peroxide (BPO), or a diazonium salt, 4-bromobenzenediazonium tetrafluoroborate ($BrPhN_2^+$). As depicted in **Figure 9-3**A, reduction of both compounds generated radicals at ambient temperature, triggering controlled *e*RAFT polymerization of methyl methacrylate (MMA), *n*-butyl acrylate (BA), and *tert*-butyl acrylate (*t*BA).

Reduction of diazonium salts occurred at more positive potentials and was further investigated under both fixed potential and fixed current conditions. The rate of radical generation was controlled by electrical current or potential, providing well-defined polymers with variable degrees of polymerizations (DPs) and good retention of chain-end functionality.

9.3. Results and Discussion

Electrochemical properties of RAFT chain transfer agents. Cyclic voltammetry (CV) of CPAD (4-cyano-4-(phenylcarbonothioylthio)pentanoic acid) and DDMAT (2-(dodecylthiocarbonothioylthio)-2-methylpropionic acid) gave irreversible reduction peaks at –1.00 V and –1.25 V vs. saturated calomel electrode (SCE), **Figure 9-4**. These values are comparable to the ones obtained in a previous report.[44] Quantitative reduction of CPAD by electrolysis at –1.4 V vs. SCE required two electrons per CPAD molecule (**Figure 9-5**). Both CV and electrolysis suggested that the weak C–S bond was irreversibly cleaved, with reduction of both ensuing fragments to anions, without generating radicals (Eq. 1). A similar behavior was observed for the reduction of alkyl halides used as ATRP initiators, which are also characterized by a weak bond, C–Br.[45] This mechanism is fundamentally

different from the one-electron photoreduction in the photoinduced electron transfer (PET)-RAFT process.[39] Indeed, bulk electroreduction of the CTAs in the presence of monomer did not yield any polymer, confirming that the reduction process did not produce any long-lived free radicals. Therefore, electroreduction of radical initiators was tested in place of the electroreduction of CTAs.

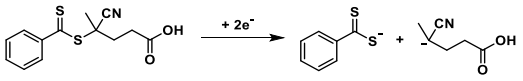

Eq. 1

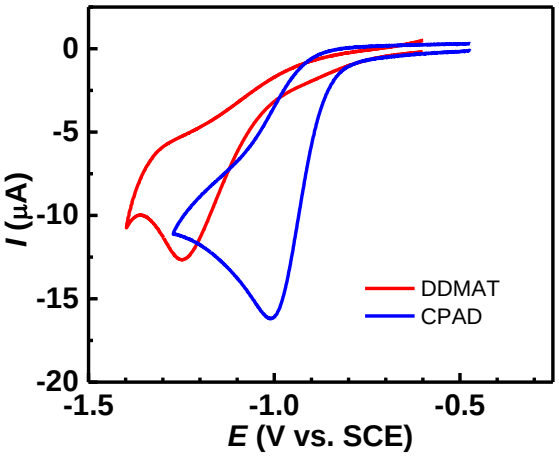

Figure 9-4. CV of 10^{-3} M CPAD and DDMAT in DMF + 0.1 M *n*-Bu_4NPF_6. T = 25 °C, v = 0.1 V s^{-1}.

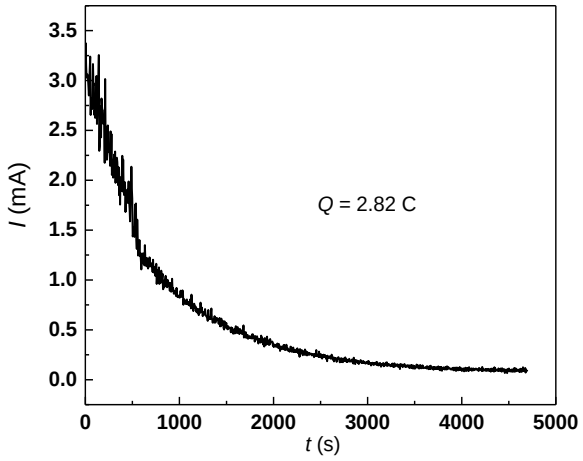

Figure 9-5. Electrolysis of CPAD. Conditions: [CPAD] = 0.93 mM in CH_3CN, [CH_3COOH] = 9.3 mM, [Et_4NPF_6] = 0.1 M, V_{tot} = 15 mL. WE = glassy carbon, CE = Pt wire separated from the reaction solution by the supporting electrolyte saturated tylose gel, RE = SCE, E_{app} = - 1.3V vs. RE. Excess acetic acid was added to avoid self-protonation reaction due to the formation of anions.

Electrochemical Properties of Benzoyl Peroxide. Benzoyl peroxide (BPO) is a thermal initiator with a half-life time of ~1 h at 90 °C.[46] However, BPO is essentially stable at ambient temperature and without application of any electrical current, giving < 1% of MMA conversion after 20 h (**Table 9-1**, entry 1). CV showed that BPO is irreversibly reduced at cathodic peak potential $E_{pc,BPO}$ = – 0.83 V vs. SCE (**Figure 9-6**). The peak significantly overlapped with the reduction of CPAD ($E_{pc,CPAD}$ = – 1.00 V vs. SCE), which could be problematic due to concurrent electroreduction of CTA.

Table 9-1. *e*RAFT by Electroreduction of BPO.[a]

Entry		[M]/[CPAD]/[BPO]	E_{app}	Time (h)	Conv (%)	k_p^{app} [b] (h^{-1})	$M_{n,th}$ [c] ($\times10^{-3}$)	$M_{n,app}$ ($\times10^{-3}$)	M_w/M_n
1	MMA	500/0/1	-	20	1	-	-	-	-
2	MMA	4670/0/1	$E_{pc,BPO}$ – 0.08 V	20	38	0.023	-	71.1	1.78
3	MMA	500/1/1	$E_{pc,BPO}$ – 0.17 V	20	<5	-	-	-	-
4	MMA	500/1/1	$E_{pc,BPO}$ – 0.05 V	20	22	0.013	10.9	7.2	1.17
5	MMA	500/1/1	$E_{pc,BPO}$ + 0.34 V	20	0	-	-	-	-

6[d]	BA	500/1/1	$E_{pc,BPO}$	20	25	0.015	10.0	7.6	1.16

[a][MMA] = 4.67 M (in DMF, 50% v/v), V_{tot} = 30 mL, [Et_4NPF_6] = 0.1 M, T = 25 ºC. [b]The slope of the ln([M]$_0$/[M]) vs. time plot. [c]$M_{n,th}$ = [M]/[I] × M_M × conversion + M_{CTA}. [d]BA and DDMAT replaced MMA and CPAD.

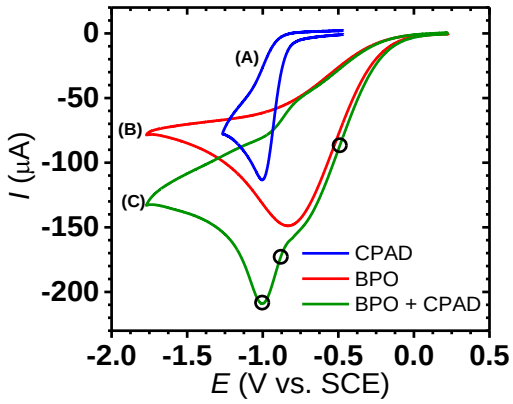

Figure 9-6. CV of (A) 7×10^{-3} M CPAD, (B) 10^{-2} M BPO, and (C) 7×10^{-3} M CPAD + 10^{-2} M BPO in DMF + 0.1 M Et_4NPF_6, T = 25 °C, v = 0.1 V s^{-1}. The circles represent E_{app} during polymerization.

The overall electro-reductive cleavage of BPO to two anionic fragments requires two electrons (Eq. 2-3). [47] However, it involves the formation of more stable radical intermediates, which could initiate a polymerization in the presence of monomer (Eq. 4). Indeed, electroreduction of BPO at E_{app} = $E_{pc,BPO}$ – 0.08 V in the presence of MMA gave polymers in good yield via free radical polymerization (FRP, **Figure 9-7** and **Table 9-1**, entry 2).

$$(RO)_2 + e^- = RO^\bullet + RO^- \quad \text{Eq. 2}$$

$$RO^\bullet + e^- = RO^- \quad \text{Eq. 3}$$

$RO^{\bullet} + M = P_n^{\bullet}$ Eq. 4

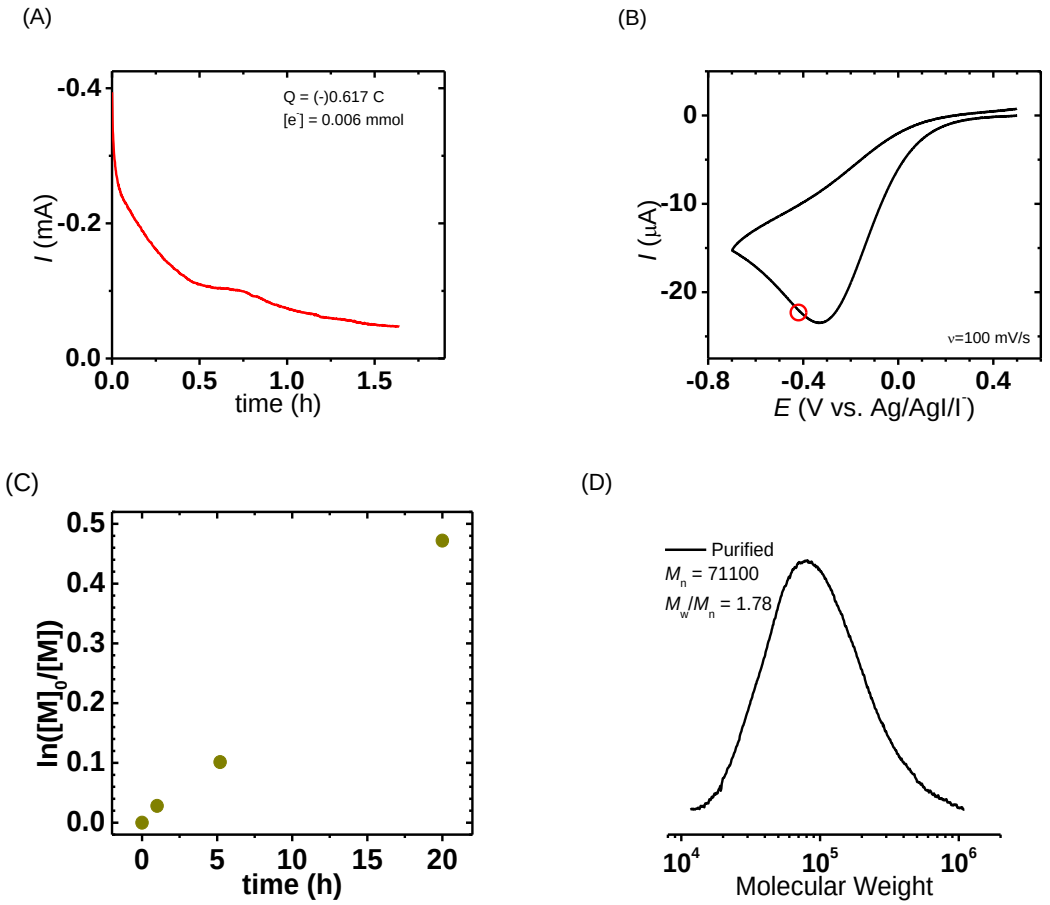

Figure 9-7. Electrochemical study of BPO. (A) Current profile vs. time. (B) CV of 1 mM BPO and applied potential (red circle). (C) Kinetic plot. (D) Final GPC trace. [MMA] = 4.67 M (in DMF, 50% by v), V_{tot} = 30 mL, [Et_4NPF_6] = 0.1 M, T = 25 °C, E_{app} = $E_{pc,BPO}$ - 0.08 V, WE = Pt mesh, CE = Pt wire separated from the reaction solution by the supporting electrolyte saturated tylose gel, RE = Ag/AgI/I^-.

***e*RAFT with BPO.** In the presence of CPAD and BPO, MMA was polymerized at three different applied potentials shown by the circles in Figure 9-6 (entries 3-5 in **Table 9-1**). At E_{app} = $E_{pc,BPO}$ – 0.17 V, < 5% conversion was detected. The potential was too negative, resulting in decomposition of the CTA. At E_{app} = $E_{pc,BPO}$ – 0.05 V, controlled polymerization with a linear semilogarithmic kinetics and low $Đ$ was observed (**Figure**

9-8), but M_n was 30% lower than theoretical value due to chains generated by BPO "electro-decomposition". At $E_{app} = E_{pc,BPO} + 0.34$ V, reduction of BPO was insufficient and no polymer was generated. The large overlap between the reduction waves of CPAD and BPO narrowed the useful potential window to conduct an *e*RAFT, thus only $E_{app} \approx E_{pc,BPO}$ could be successfully applied.

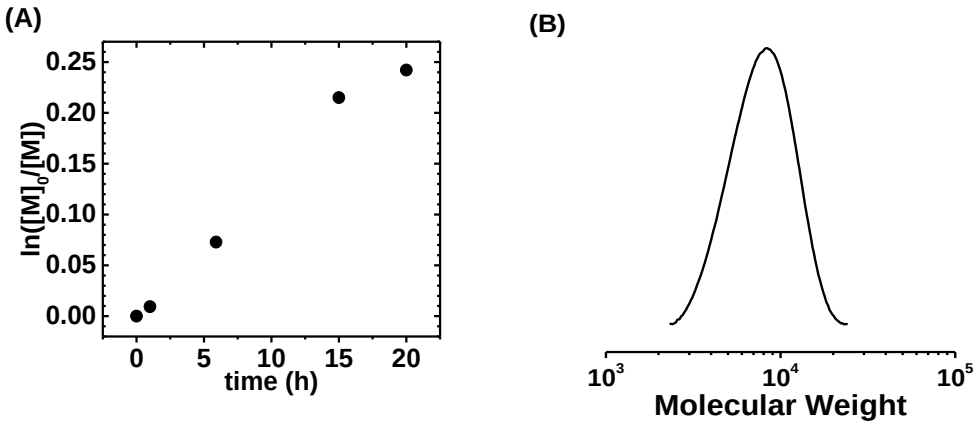

Figure 9-8. *e*RAFT of MMA by electroreduction of BPO. (A) Semilogarithmic kinetic plot and (B) gel permeation chromatography (GPC) of the obtained polymer, at $E_{app} = E_{pc,BPO}$ – 50 mV (**Table 9-1**, entry 4). Reaction conditions: [MMA] = 4.67 M (in DMF, 50% v/v), V_{tot} = 30 mL, [MMA]/[CPAD]/[BPO] = 500/1/1, [Et_4NPF_6] = 0.1 M, T = 25 ºC.

BA was also polymerized in the presence of DDMAT and BPO, at $E_{app} = E_{pc,BPO}$ (**Table 9-1**, entry 6). Despite the smaller overlap between the reduction waves of DDMAT and BPO, slow polymerization and M_n lower than theoretical values were observed. The limited potential window available with BPO prompted us to use a radical source with a more positive potential.

Electrochemical properties of $BrPhN_2^+$. Reduction of $BrPhN_2^+$ gave an irreversible reduction peak at about –0.1 V vs. SCE, which is ~ 1 V more positive than reduction of

CPAD (**Figure 9-9**). Therefore, $BrPhN_2^+$ could be reduced without affecting the CTAs. The reduction of $BrPhN_2^+$ is a well-known process that generates very reactive bromophenyl radicals ($BrPh^{\bullet}$). They are so reactive that they can quickly graft onto any electrode surface, forming a multi-layered coating of branched bromobenzenes.[48] However, some radicals can escape to solution to initiate and sustain the RAFT polymerization. Only a small amount of radicals is required to sustain the process because radical concentration is typically low (< 10^{-8} M). Therefore, we tested electrogeneration of radicals via reduction of $BrPhN_2^+$.

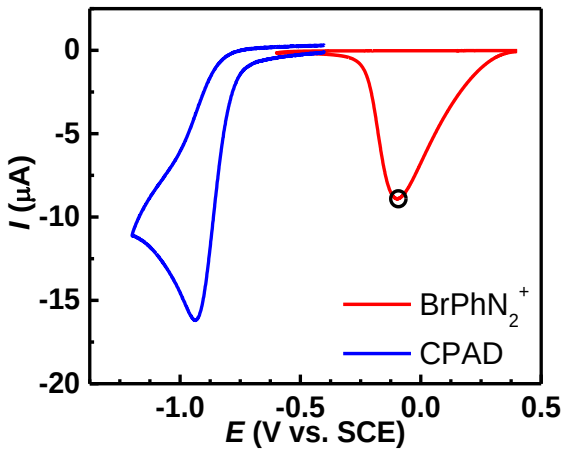

Figure 9-9. CV of 10^{-3} M $BrPhN_2^+$ and 10^{-3} M CPAD. The circle represent E_{app} during polymerization.

Electrogeneration of Radicals by $BrPhN_2^+$. FRP of BA was conducted by reducing $BrPhN_2^+$ at $E_{app} = E_{pc,BrPhN_2^+}$ on a Pt foil electrode (**Table 9-2**, entry 1). PBA was formed reaching 75% monomer conversion in 16 h and high molecular weight, M_n = 681,000, typical for FRP. This confirmed that electroreduction of $BrPhN_2^+$ generated aryl radicals that could initiate polymerization significantly faster than with BPO.

Table 9-2. *e*RAFT of BA and MMA by reduction of $BrPhN_2^+$ under potentiostatic conditions.[a]

Entry	M	Time (h)	[M]/[DDMAT]/[$BrPhN_2^+$]	Q[b] (C)	Conv (%)	k_p^{app} [c] (h^{-1})	$M_{n,th}$[d] ($\times10^{-3}$)	$M_{n,app}$ ($\times10^{-3}$)	M_w/M_n
1	BA	16	500/0/1	-0.5	75	0.087	----	681.0	1.44
2	BA	4	500/1/10	-11.6	60	0.248	38.9	18.9	6.23
3	BA	20	500/1/1	-7.0	48	0.183	31.1	24.4	1.27
4	BA	20	500/1/0.5	-6.0	25	0.079	16.3	13.8	1.15
5[e]	MMA	48	500/1/10	-0.5	40	0.017	20.0	19.8	1.20

[a][BA] = 3.49 M (in DMF, 50% by v/v), V_{tot} = 8 mL, WE = Pt mesh (except for entry 1: Pt foil), E_{app} = -0.1 V vs. SCE. E_{app} was close to E_{pc} of the irreversible reduction peak of $BrPhN_2^+$. [b]Consumed charge, calculated from cathodic current profile recorded during electrolysis. [c]The slope of the $\ln([M]_0/[M])$ vs. time plot. k_{app} for entries 2-4 was measured in the first 4 h. [d]$M_{n,th}$ = [M]/[CTA] × M_M × conversion + M_{CTA}. [e]MMA = 4.67 M in DMF (**Figure 9-10**).

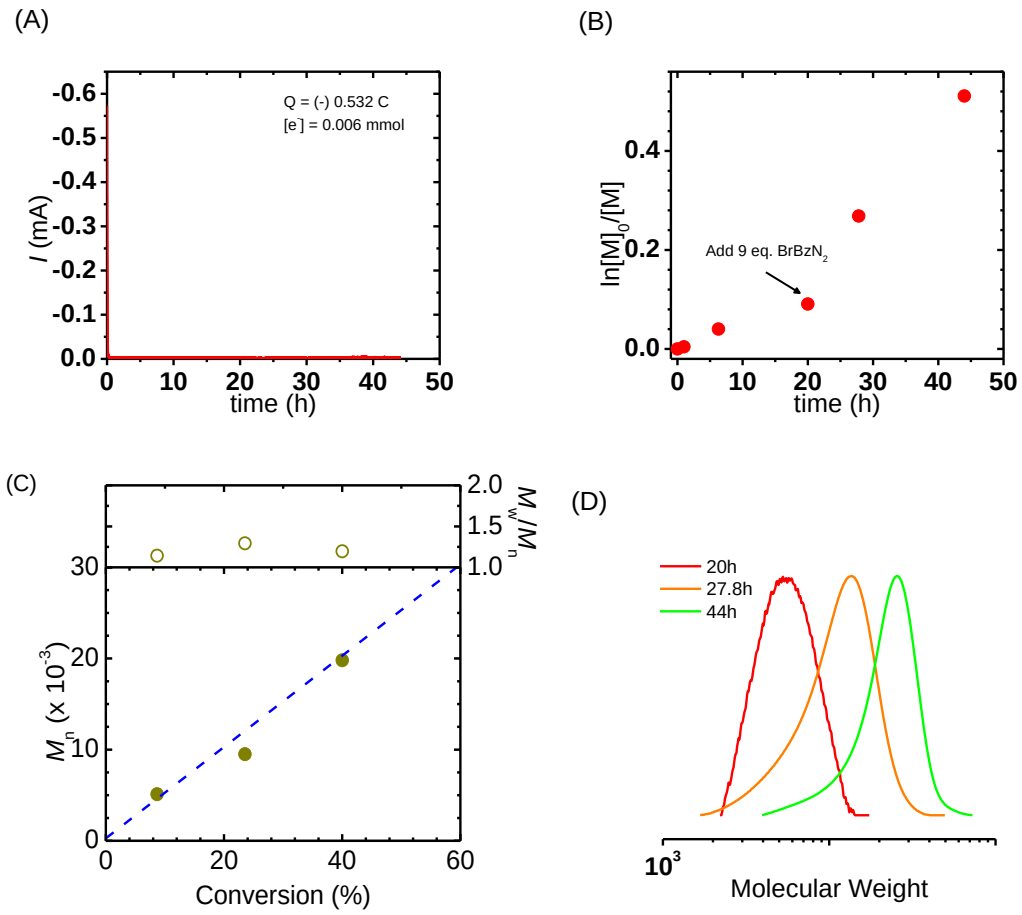

Figure 9-10 *e*RAFT of MMA under potentiostatic conditions. Reaction condition: [MMA] = 4.67 M (in DMF, 50% by v), V_{tot} = 30 mL, [MMA]/[CPAD]/[$BrPhN_2^+$] = 500/1/1, [Et_4NPF_6] = 0.1 M, T = 25 ºC, E_{app} = - 0.1 V vs. SCE, WE = Pt mesh, CE = Pt wire (separated from the reaction solution by the supporting electrolyte saturated tylose gel), RE = Ag/AgI/I^-. Further 9 equivalents of $BrPhN_2^+$ were added after 24 h. (A) Current profile. (B) Kinetic plot. (C) MW and dispersity. (D) GPC traces.

Potentiostatic *e*RAFT with $BrPhN_2^+$. Potentiostatic *e*RAFT was conducted under a fixed $E_{app} = E_{pc,BrPhN_2^+} \approx -0.1$ V vs. SCE, using DDMAT as chain transfer agent for BA polymerization. **Figure 9-11** shows the influence of the [DDMAT]/[$BrPhN_2^+$] ratio on *e*RAFT. The rate of polymerization increased with [$BrPhN_2^+$] due to faster reduction, which led to a higher concentration of radicals. However, the addition of too much diazonium salt was detrimental to polymerization control. The final M_w/M_n was 6.2 for

[DDMAT]/[$BrPhN_2^+$] = 1/10 (**Table 9-2**, entry 2), whereas M_w/M_n was 1.3 for [DDMAT]/[$BrPhN_2^+$] = 1/1.

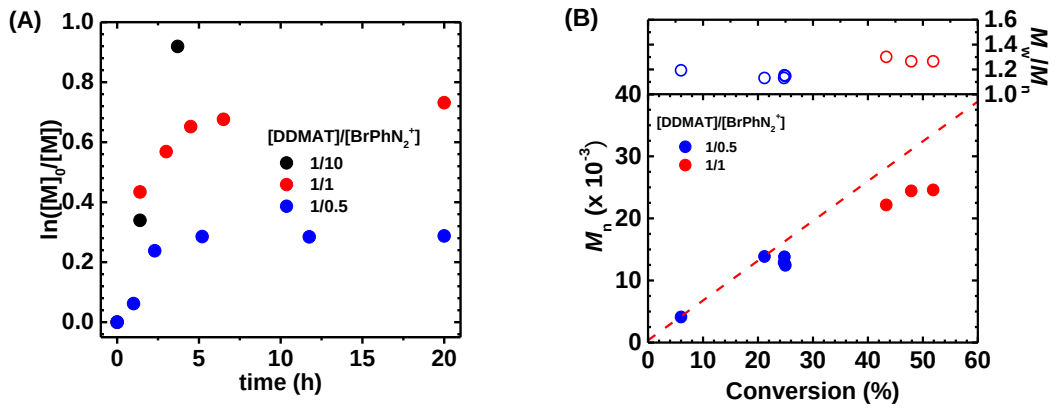

Figure 9-11. *e*RAFT of BA under potentiostatic conditions. (A) Polymerization kinetics; (B) MW and *Đ* evolution with conversion. Reaction conditions: [BA] = 3.49 M (in DMF, 50% by v), [BA]/[DDMAT] = 500/1, [Et_4NPF_6] = 0.1 M, T = 25 ºC, E_{app} = - 0.1 V vs. SCE.

Despite the better control over *Đ*, the final MW was 15% lower than the theoretical value, suggesting that reduction of $BrPhN_2^+$ generated more chains than defined by DDMAT. Continuous generation of new chains during polymerization caused some low MW tailing and higher dispersity. Decreasing the [DDMAT]/[$BrPhN_2^+$] to 0.5 improved control but polymerization was slower (**Figure 9-11**).

For [$BrPhN_2^+$]/[DDMAT] = 1/1 and 1/0.5, the reaction stopped after ca. 5 h at limited conversion (**Figure 9-11**A). This could be due to insufficient current flowing from the working electrode. Indeed, at fixed E_{app} the applied current quickly decayed (**Figure 9-12**A) due to electrografting of the insulating aryl compounds, as discussed in the next section.

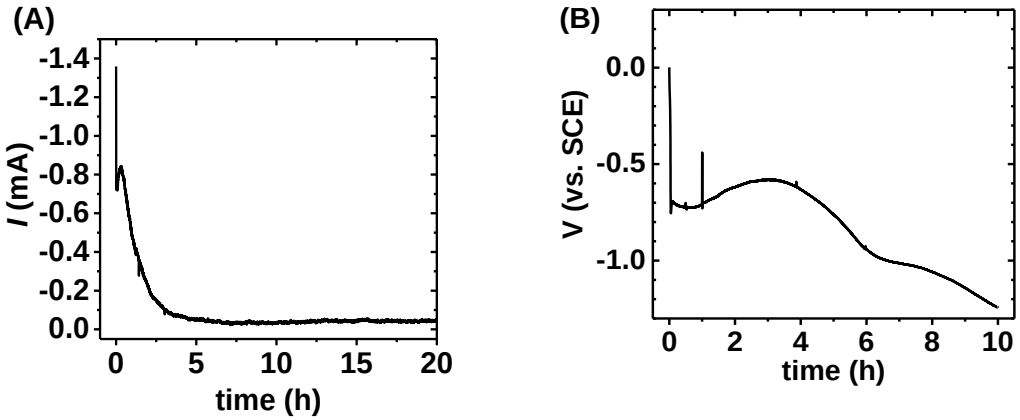

Figure 9-12. *e*RAFT by electroreduction of 7×10-3 M $BrPhN_2^+$; (A) current profile during chronoamperometry at $E_{app} = E_{pc,BrPhN_2^+}$ (**Table 9-2**, entry 3), and (B) potential between WE and CE during chronopotentiometry at I_{app} = -50 uA (**Table 9-4**, entry 3).

*e*RAFT of MMA was also examined at fixed E_{app} and in the presence of CPAD. Despite a slow polymerization rate, the MW of the resulting PMMA correlated well with theoretical values and *Đ* was 1.2 (**Table 9-2**, entry 5 and **Figure 9-10**). Interestingly, almost identical polymerization results were obtained for three different working electrodes, Pt, carbon felt, or graphite (**Figure 9-10**, **Figure 9-13** and **Figure 9-14**). Polymers with higher *Đ* were obtained when using a Cu electrode (**Figure 9-15**).

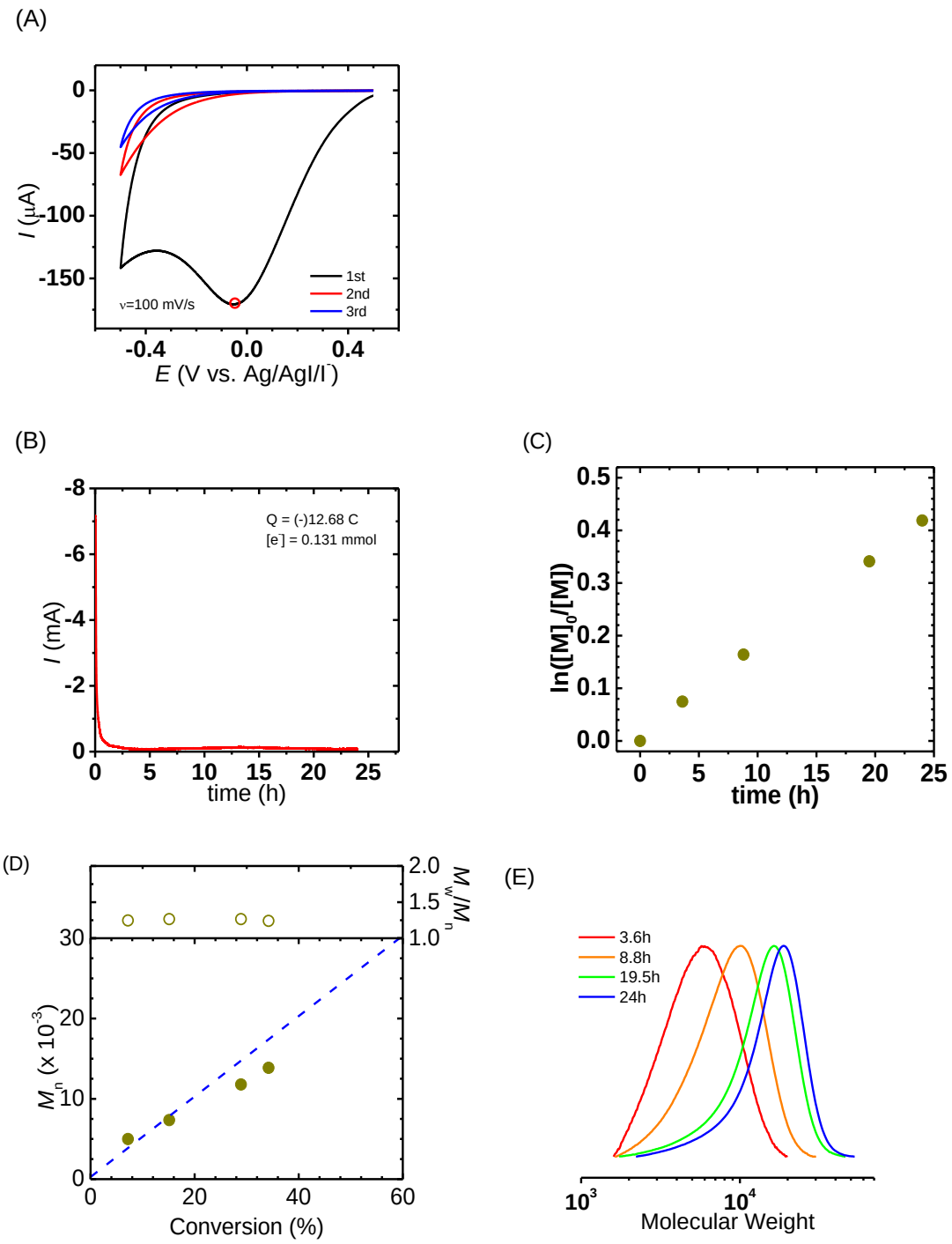

Figure 9-13 *e*RAFT of MMA with carbon felt WE under potentiostatic conditions. Reaction condition: [MMA] = 4.67 M (in DMF, 50% by v), V_{tot} = 30 mL, [MMA]/[CPAD]/[$BrPhN_2^+$] = 500/1/1, [Et_4NPF_6] = 0.1 M, T = 25 °C, E_{app} = $E_{pc,BrPhN_2^+}$, WE = carbon felt, CE = Pt wire (separated from the reaction solution by the supporting electrolyte saturated tylose gel), RE = Ag/AgI/I^-. (A) Cyclic voltammetry. (B) Current profile. (C) Kinetic plot. (D) MW and dispersity. (E) GPC traces.

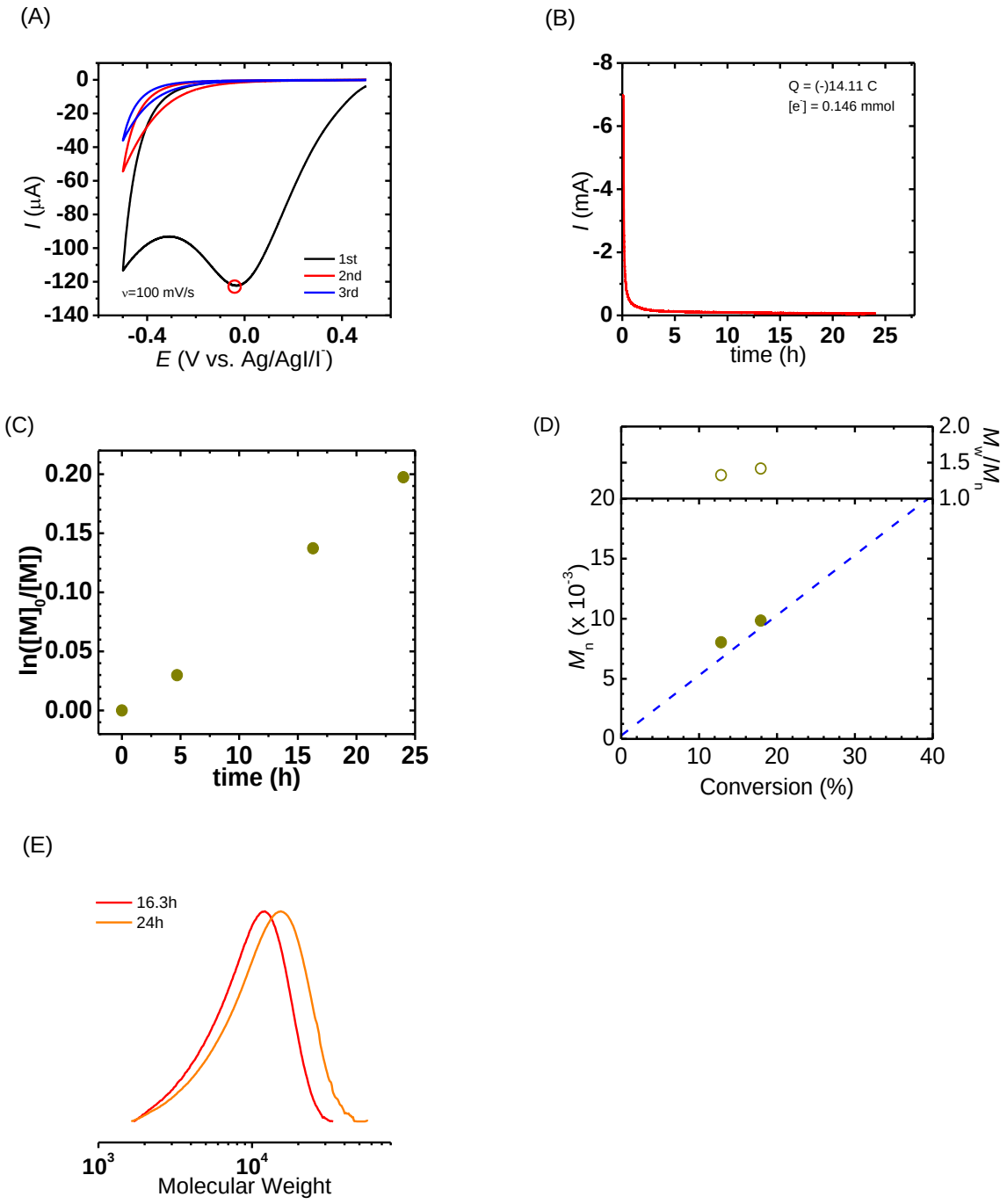

Figure 9-14. *e*RAFT of MMA with graphite WE under potentiostatic conditions. Reaction condition: [MMA] = 4.67 M (in DMF, 50% by v), V_{tot} = 30 mL, [MMA]/[CPAD]/[$BrPhN_2^+$] = 500/1/1, [Et_4NPF_6] = 0.1 M, T = 25 ºC, E_{app} = $E_{pc,BrPhN_2^+}$, WE = graphite, CE = Pt wire (separated from the reaction solution by the supporting electrolyte saturated tylose gel), RE = Ag/AgI/I^-. (A) Cyclic voltammetry. (B) Current profile. (C) Kinetic plot. (D) MW and dispersity. (E) GPC traces.

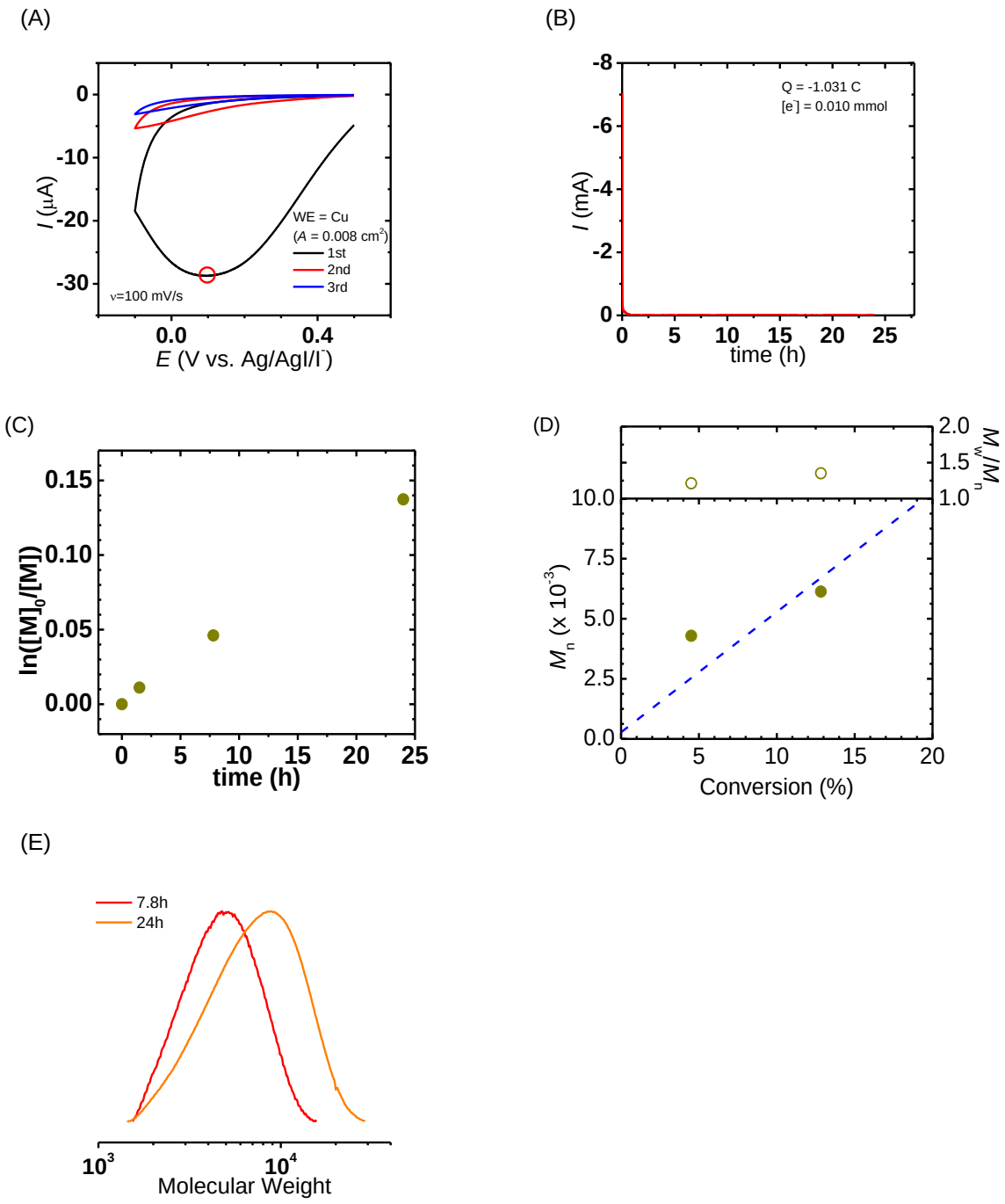

Figure 9-15. *e*RAFT of MMA with Cu wire working electrode under potentiostatic conditions. Reaction condition: [MMA] = 4.67 M (in DMF, 50% by v), V_{tot} = 30 mL, [MMA]/[CPAD]/[$BrPhN_2^+$] = 500/1/1, [Et_4NPF_6] = 0.1 M, T = 25 ºC, E_{app} = $E_{pc,BrPhN_2^+}$, WE = Cu wire, CE = Pt wire (separated from the reaction solution by the supporting electrolyte saturated tylose gel), RE = Ag/AgI/I^-. (A) Cyclic voltammetry. (B) Current profile. (C) Kinetic plot. (D) MW and dispersity. (E) GPC traces.

Electrografting of aryl compounds. The low current and slow polymerization rate observed under potentiostatic conditions prompted us to analyze the electrografting of $BrPhN_2^+$ on the surface of the WE. A variety of surfaces such as carbon, metals, and semiconductors can be grafted via a reduction of diazonium salts.[39,40] They are important agents for surface modification.[49-55] Even in the presence of monomer, a large fraction of aryl radicals was grafted onto the electrode, while some of them initiated polymerization. Although polymeric radicals cannot directly graft onto the electrode, they could covalently couple to the grafted aryl rings in the 3 or 5 position, thus increasing the thickness of organic layer.[50, 56]

The layer grafted during *e*FRP of BA (conditions as in **Table 9-3**, entry 1) was analyzed by X-ray photoelectron spectroscopy (XPS). XPS of the Pt WE showed an increase in the presence of C and Br, demonstrating grafting of an organic layer containing bromoaryl groups (**Table 9-3** and **Figure 9-16**). The Pt content on the surface strongly decreased, indicating almost complete coverage; about 3% of Pt remained exposed, allowing for continuous electroreduction throughout the process. The macroscopic appearance of the electrode did not change after polymerization, indicating the formation of a thin layer.

Table 9-3. XPS of Pt foil electrode before and after electrochemical reduction of $BrPhN_2^+$.[a]

Atom number %	O	C	Pt	Br
Before reaction	37.6	34.4	38.0	0
After 2 h reaction	20.7	74.9	2.8	1.6

[a]The large amount of adventitious O and C on the surface prior to deposition is due to the process employed to clean and activate the Pt electrode surface (see supporting information).

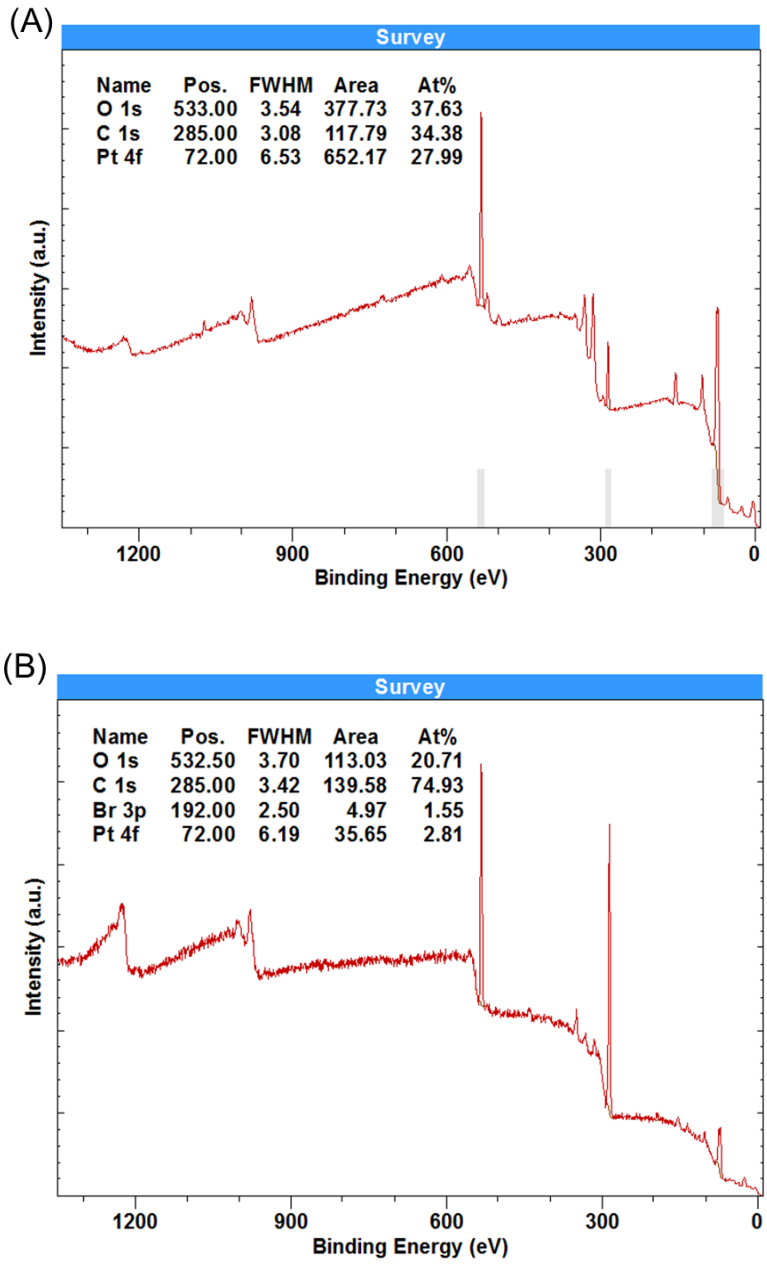

Figure 9-16. XPS pattern of the Pt foil WE in **Table 9-2**, Entry 1 (A) before; (B) after reaction.

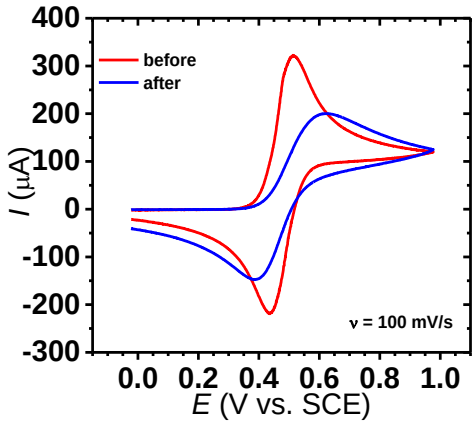

Figure 9-17. CV of 10^{-2} M ferrocene (red) before and (blue) after grafting of aryl compounds. The grafting was performed by CV of 7×10^{-3} M $BrPhN_2^+$ between +0.3 V and -0.3 V vs. SCE. WE = Pt disk in DMF + 0.1 M Et_4NPF_6 at 25 °C.

The Pt surface was also investigated by CV of a redox probe, ferrocene, which was analyzed before and after reduction of the diazonium salt (**Figure 9-17**). After deposition, ΔE_p, the difference between anodic and cathodic peak potentials increased. This indicated the presence of a layer that decreased the rate of electron transfer to ferrocene on the surface. The resistance caused by the organic layer dissipated some of the applied voltage, lowering the true applied potential in the polymerization, so that true potentiostatic conditions were not applied. This explains the decreasing polymerization rate in **Figure 9-11**A. In conclusion, the electrografting of a poorly-conductive layer on the electrode slowed $BrPhN_2^+$ reduction, leading to current decay and slower radical generation.

Galvanostatic *e*RAFT with $BrPhN_2^+$. Due to electrografting, potentiostatic condition for eRAFT resulted in limited conversion. Therefore, polymerizations under a

fixed current, *i.e.*, galvanostatic conditions, were tested to provide a continuous supply of radicals. The setup was simple, with application of a single current step during each polymerization (in comparison, a galvanostatic *e*ATRP requires a few different current steps).[19, 57] In *e*RAFT with $BrPhN_2^+$, however, the formation of a resistive organic layer required the application of a negative E_{app} to supply constant current during polymerization (**Figure 9-12B**). Despite the negative E_{app}, reduction of monomer or solvent is not significant (see **Figure 9-18** and **Figure 9-19**).

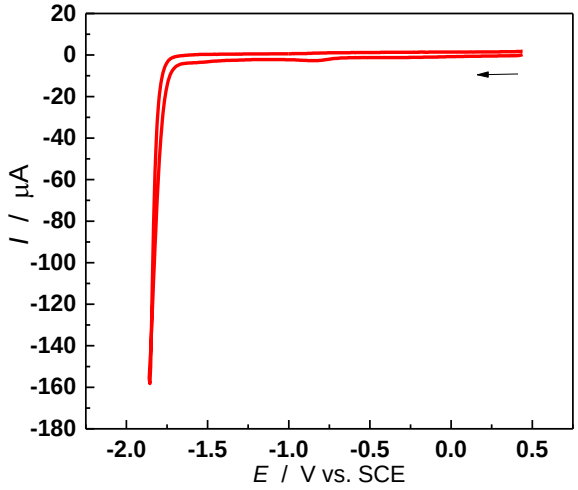

Figure 9-18. Reduction of MMA in MMA/DMF 1:1 + 0.1 M Et_4NPF_6. v = 0.2 V s^{-1}.

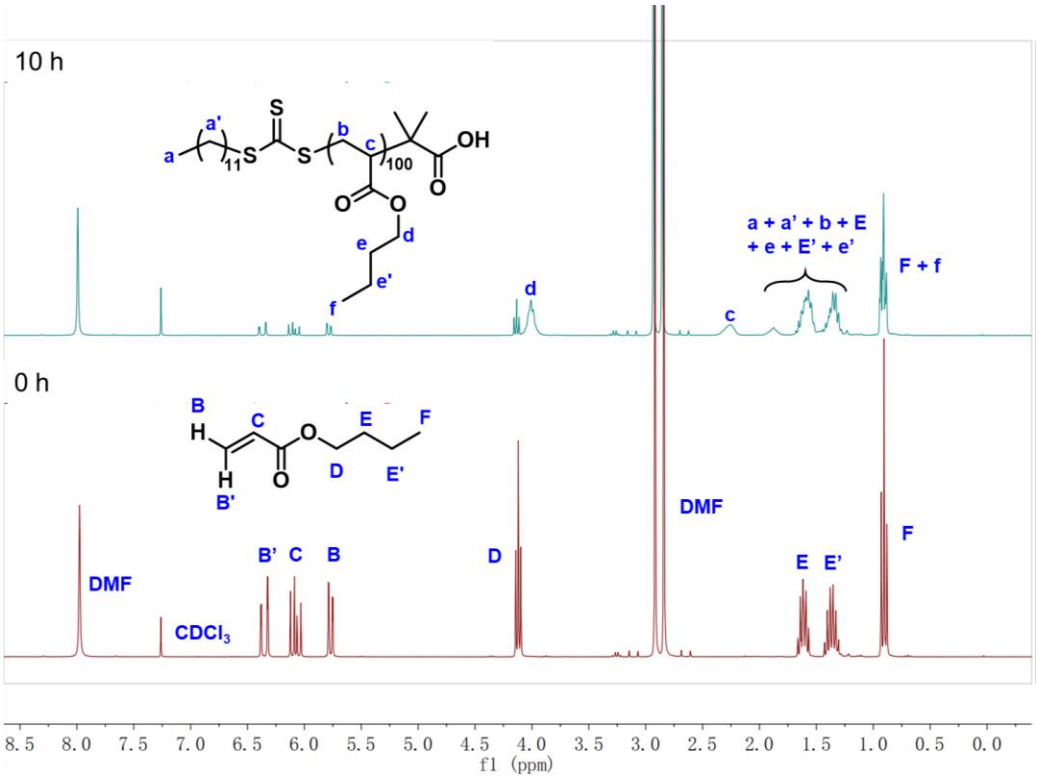

Figure 9-19. ^{1}H NMR spectrum of the reaction mixture. Detailed conditions in **Table 9-4**, entry 1 in the main text.

Table 9-4. Galvanostatic *e*RAFT with $BrPhN_2^+$.[a]

Entry	Time (h)	I_{app} (μA)	Q[b] (C)	Conv (%)	k_p^{app} [c] (h^{-1})	$M_{n,th}$[d] ($\times10^{-3}$)	$M_{n,app}$ ($\times10^{-3}$)	M_w/M_n
1	10	-200	-7.2	80	0.186	51.5	27.9	1.41
2	10	-100	-3.6	73	0.160	47.1	32.4	1.25
3	10	-50	-1.8	58	0.099	37.5	33.4	1.18

[a]General reaction conditions: [BA] = 3.49 M (in DMF, 50% by v/v), V_{tot} = 8 mL, [BA]/[DDMAT]/[$BrPhN_2^+$] = 500/1/1, [Et_4NPF_6] = 0.1 M, T = 25 °C, [b]Calculated from cathodic current profile recorded during electrolysis. [c]The slope of the ln([M]$_0$/[M]) vs. time plot. [d]$M_{n,th}$ = [M]/[CTA] × M_M × conversion + M_{CTA}.

Different applied currents (I_{app}s) were tested, which affected rate of radical generation (**Table 9-4**, entries 1-3 and **Figure 9-20**). Increasing I_{app} from –50, to –100, and to –200 μA gave more linear semilogarithmic kinetic plots, and conversion reached 80% in 10 h with the highest I_{app} (**Figure 9-21**). This is a noticeable improvement compared to *e*RAFT under potentiostatic conditions, indicating that a fixed current can provide a more efficient supply of radicals.

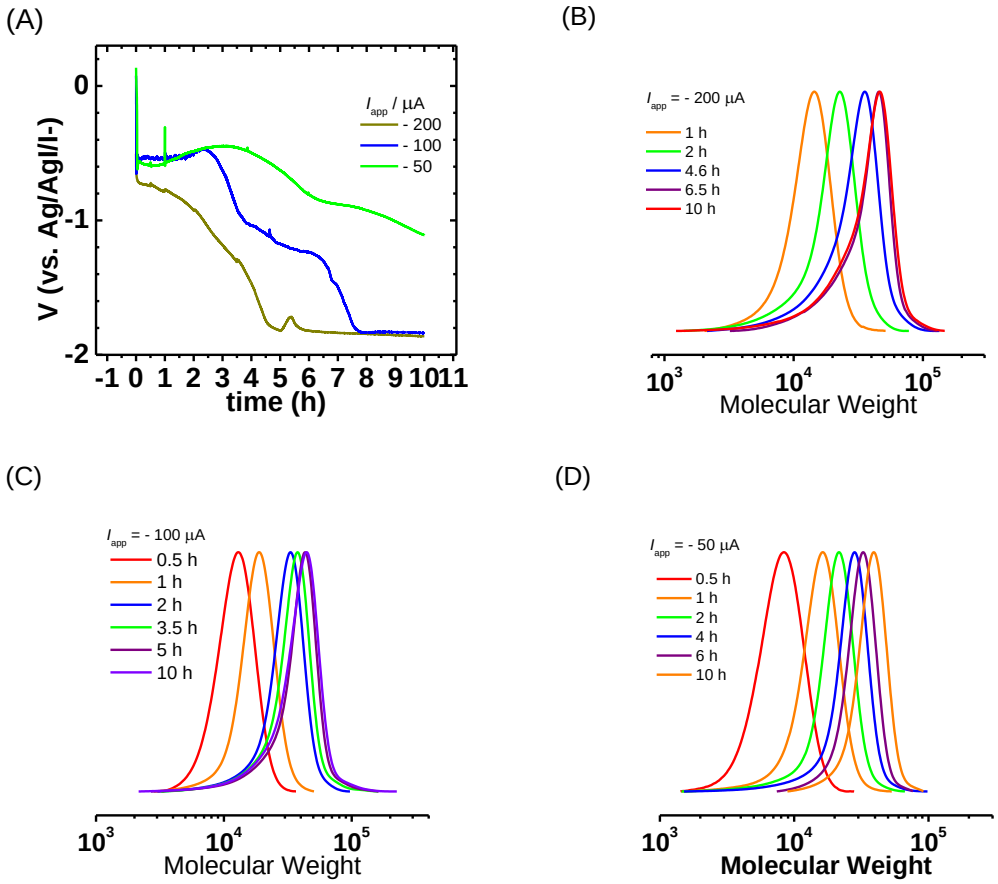

Figure 9-20. *e*RAFT of BA under galvanostatic conditions using different cathodic current. Reaction condition: [BA] = 3.49 M (in DMF, 50% by v), V_{tot} = 8 mL, [BA]/[DDMAT]/[$BrPhN_2$] = 500/1/1, [Et_4NPF_6] = 0.1 M, T = 25 ºC, I_{app} = -200, -100 and -50 μA, respectively, WE = Pt mesh, CE = Pt wire (separated from the reaction solution by the supporting electrolyte saturated tylose gel), RE = Ag/AgI/I^-. (A) Profile of applied potentials; (B-D) GPC traces.

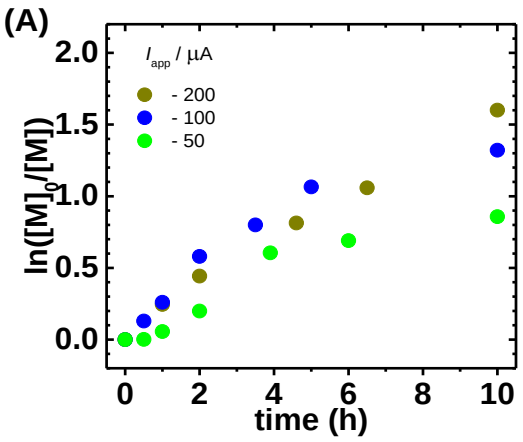
(A)
I_{app} / μA
- 200
- 100
- 50
ln([M]$_0$/[M])
time (h)

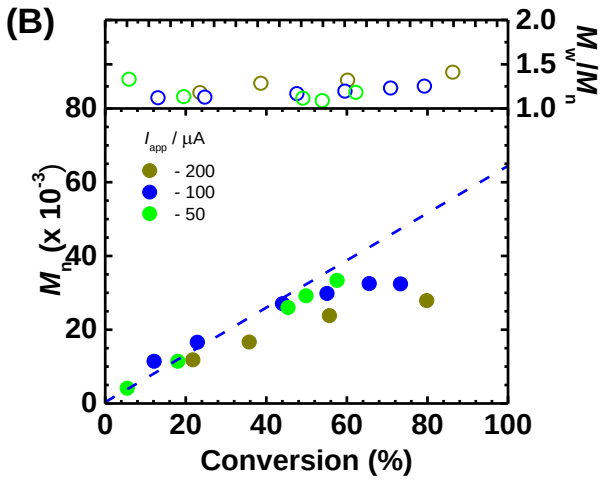
(B)
M_w/M_n
I_{app} / μA
- 200
- 100
- 50
M_n (x 10^{-3})
Conversion (%)

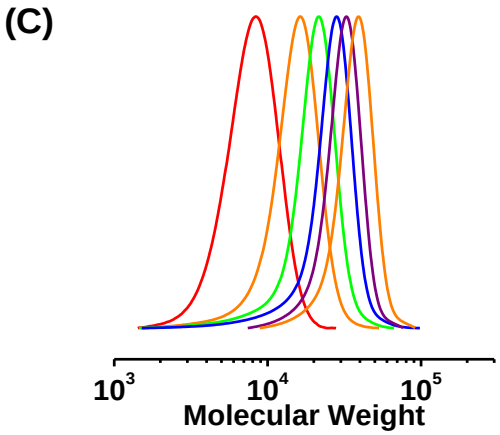
(C)
Molecular Weight

Figure 9-21. Galvanostatic *e*RAFT of BA with different I_{app}s. Reaction conditions: [BA] = 3.49 M (in DMF, 50% by v), [BA]/[DDMAT]/[$BrPhN_2^+$] = 500/1/1, [Et_4NPF_6] = 0.1 M, T = 25 ºC. (A) Kinetic plot, (B) evolution of MW and $Đ$, (C) GPC traces for I_{app} = - 50 μA.

I_{app} influenced also MW and $Đ$. At each applied current $M_{n,app} < M_{n,th}$, indicating the formation of new chains during polymerization. Higher I_{app} generated a larger numbers of chains compared to the number defined by the chain transfer agent, and thus resulted in lower $M_{n,app}$.[58] Nevertheless, polymers with different degrees of polymerization were successfully prepared, in the range 100 – 400, with < 30% deviation from theoretical DP and $M_w/M_n \approx 1.2$ (**Table 9-5**, **Figure 9-22** and **Figure 9-23**).

Table 9-5. *e*RAFT under at different DP_{target}.[a]

Entry	Time (h)	[BA]/[DDMAT]/[$BrPhN_2$]	I_{app} (μA)	Q[b] (C)	Conv[c] (%)	k_p^{app}[d] (h^{-1})	$M_{n,th}$[e] ($\times10^{-3}$)	$M_{n,app}$[f] ($\times10^{-3}$)	M_w/M_n[f]
1	10	1000/1/2	-200	-7.2	86	0.207	110.6	60.1	1.59
2	5	1000/1/2	-50	-0.9	50	0.141	64.4	52.4	1.21
3	10	500/1/1	-100	-3.6	73	0.160	47.1	32.4	1.25
4	10	250/1/0.5	-200	-7.2	56	0.174	18.3	16.0	1.22
5[g]	6	250/1/0.5	-500	-10.8	40	0.075	13.2	12.9	1.19

[a]General reaction conditions: [BA] = 3.5 M (in DMF, 50% by v/v), V_{tot} = 8 mL, [Et_4NPF_6] = 0.1 M, T = 25 °C, WE = Pt mesh, RE = Ag/AgI/I^-. [b]Calculated from cathodic current profile recorded during electrolysis. [c]The slope of the $\ln([M]_0/[M])$ vs. time plot. [d]A larger V_{tot} = 30 mL was used in this entry. Polymer was recovered and successively used for chain extension.

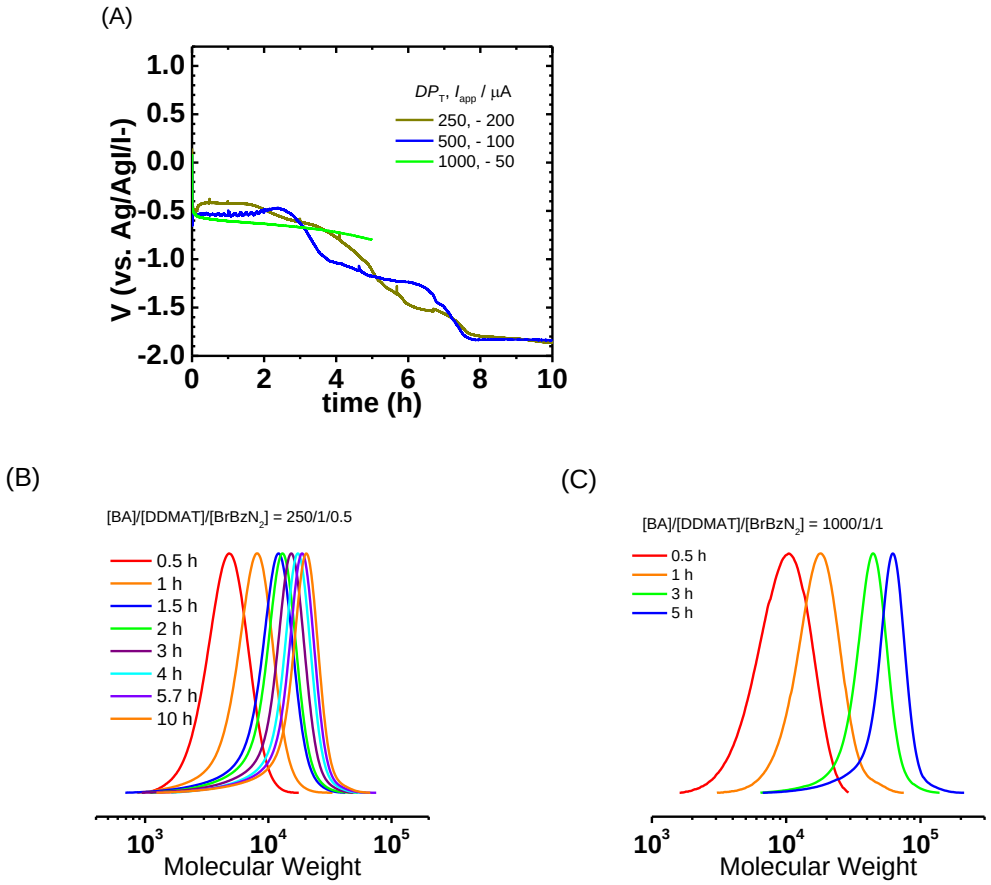

Figure 9-22. *e*RAFT of BA under potentiostatic conditions using different cathodic currents. Reaction condition: [BA] = 3.49 M (in DMF, 50% by v), V_{tot} = 8 mL, [BA]/[$BrPhN_2$] = 500/1, [Et_4NPF_6] = 0.1 M, T = 25 ºC, I_{app} = -200, -100 and -50 µA for DP 250, 500 and 1000, respectively, WE = Pt mesh, CE = Pt wire (separated from the reaction solution by the supporting electrolyte saturated tylose gel), RE = Ag/AgI/I^-. (A) Profile of applied potentials; (B-C) GPC traces.

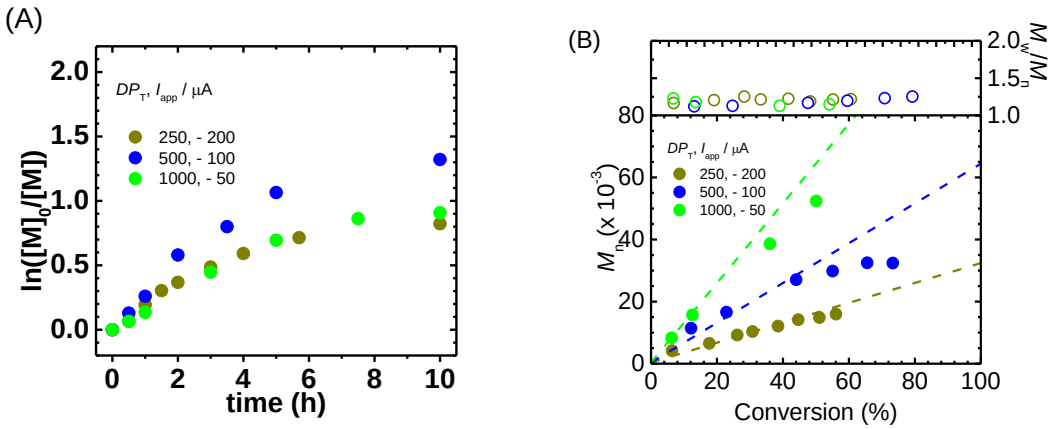

Figure 9-23. *e*RAFT of BA under potentiostatic conditions using different cathodic currents. Reaction conditions: [BA] = 3.49 M (in DMF, 50% by v), V_{tot} = 8 mL, [BA]/[DDMAT]/[$BrPhN_2$] = 500/1/1, [Et_4NPF_6] = 0.1 M, T = 25 ºC, I_{app} = - 200, - 100 and - 50 µA for DP 250, 500 and 1000, respectively. (A) Kinetic plot. (B) Evolution of MW and *Đ*.

Chain extension. To evaluate the chain-end functionality of the obtained PBA, a PBA-macroCTA was chain-extended with *t*BA (**Figure 9-24**). The PBA-macroCTA was prepared via galvanostatic *e*RAFT with $BrPhN_2^+$ and had $M_{n,app}$ = 12,900 ($M_{n,th}$ = 13,200) and M_w/M_n = 1.19. The chain extension was carried out by both *e*RAFT and traditional RAFT polymerization. In the latter case, a thermal initiator, AIBN, was used at 65 °C (**Table 9-6**).

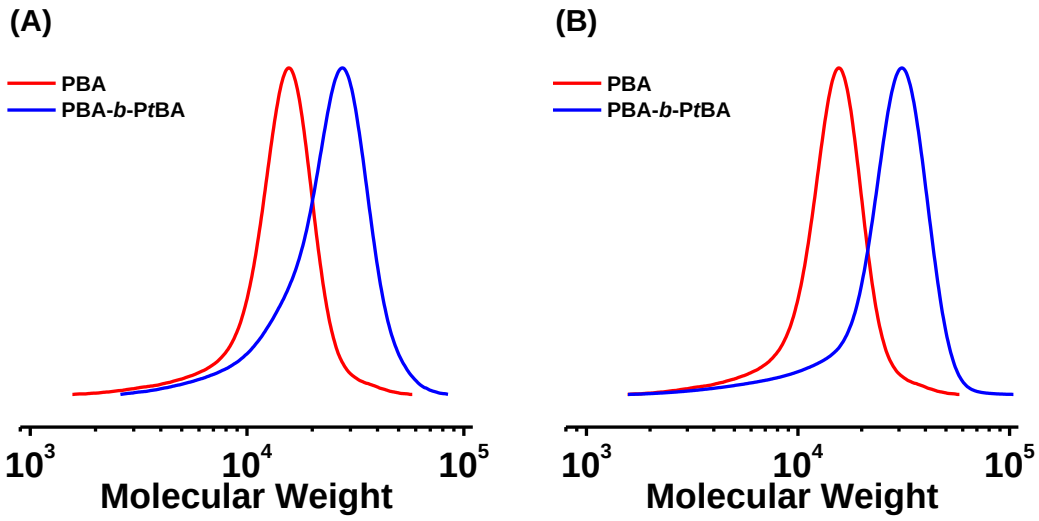

Figure 9-24. Chain extension of PBA-macroCTA with *t*BA by (A) *e*RAFT at room temperature and (B) RAFT polymerization initiated by AIBN at 65 °C.

Figure 9-24 shows the GPC traces of the macroCTA and the resulting block copolymers (PBA-*b*-P*t*BA). The block copolymer obtained from *e*RAFT had $M_{n,app}$ = 20,200 ($M_{n,th}$ = 26,800) and M_w/M_n = 1.27, while the product obtained by extension with conventional RAFT polymerization had $M_{n,app}$ = 22,400 ($M_{n,th}$ = 28,800) and M_w/M_n = 1.29. In both cases, a clean shift of MWD with conversion was observed. Chain extension by *e*RAFT showed a larger fraction of low-MW chains, further indicating that new chains were initiated during polymerization by the *e*RAFT process. Nevertheless, chain extension by traditional RAFT showed that the initiator prepared by *e*RAFT retained most of its chain-end functionality.

Table 9-6. Chain extension of PBA-macroCTA by *e*RAFT and conventional RAFT polymerization.

Entry	Time	[*t*BA]/[PBA-macroCTA]/[I]	I_{app}	Q^a	Conv	$k_p^{app\ b}$	$M_{n,th}^c$	$M_{n,app}$	M_w/M_n

	(h)		(μA)	(C)	(%)	(h^{-1})	($\times10^{-3}$)	($\times10^{-3}$)	
1[d]	5	500/1/1	-50	-0.9	22	0.040	26.8	20.2	1.27
2[e]	2	500/1/0.2	----	----	25	0.135	28.8	22.4	1.29

[a]Calculated from cathodic current profile recorded during electrolysis. [b]The slope of the $\ln([M]_0/[M])$ vs. time plot. [c]$M_{n,th} = [M]/[CTA] \times M_M \times$ conversion + M_{CTA}. [d]Reaction conditions: [*t*BA] = 3.4 M (in DMF, 50% by v/v), V_{tot} = 8 mL, I = $BrPhN_2^+$, [Et_4NPF_6] = 0.1 M, T = 25 °C, WE = Pt mesh, I_{app} = -100 μA. [e]Reaction conditions: [*t*BA] = 3.4 M (in DMF, 50% by v/v), V_{tot} = 8 mL, I = AIBN, T = 65 °C.

9.4. Conclusion

An *e*RAFT polymerization was mediated by reduction of BPO or $BrPhN_2^+$ at a Pt electrode. The two initiators had very different reduction peak potentials, -0.83 V and -0.10 V vs. SCE, respectively. The CTAs were irreversibly reduced at peak potential ~ -1 V vs. SCE via a two-electron reduction without formation of long-lived radical species; they could not be directly used to produce radicals by electroreduction.

Electroreduction of BPO initiated a conventional free radical polymerization, and was used for a successful but slow *e*RAFT at potentials $E_{app} \approx E_{pc,BPO}$. Reduction of BPO partially overlapped with reduction of the CTAs, limiting the use of the peroxide for *e*RAFT polymerization.

Reduction of $BrPhN_2^+$ occurred at much more positive potentials than reduction of the CTAs, resulting in a more effective generation of radicals to initiate a RAFT polymerization. An undesired electrografting of the aryl radicals on the electrode surface decreased its conductivity.

Well-defined polymers were prepared by applying either fixed potential or fixed current conditions. *e*RAFT with $BrPhN_2^+$ can be carried out under galvanostatic conditions at a single current value, utilizing a simple current generator at ambient temperature. The amount of new chains generated by reduction of $BrPhN_2^+$ was lowered by decreasing I_{app} or by decreasing the amount of diazonium salt relative to the CTA. Lower I_{app}s produced better controlled polymers but at slower rates. The chain-end functionality was well-maintained, as confirmed by synthesis of block copolymers with narrow molecular weight distribution.

9.5. Experimental Section

Materials. 4-Cyano-4-(phenylcarbonothioylthio)pentanoic acid (CPAD, 97%), 2-(dodecylthiocarbonothioylthio)-2-methylpropionic acid (DDMAT, 98%), ferrocene (Fc, 98%) and *N*,*N*-dimethylformamide (DMF, 99%) were purchased from Sigma-Aldrich and used as received. 4-Bromobenzenediazonium tetrafluoroborate ($BrPhN_2$, 96%) and tetraethylammonium hexafluorophosphate (Et_4NPF_6, 98%) were purchased from Alfa Aesar and used as received. 2,2'- Azobis(2-methylpropionitrile) (AIBN, 98%) was purchased from Sigma-Aldrich and recrystallized in methanol. Methyl methacrylate (MMA, 99%, Aldrich), butyl acrylate (BA, 99%, Aldrich) and *tert*-butyl acrylate (*t*BA, 98%, Aldrich) were passed through a column filled with basic alumina prior to use to remove polymerization inhibitors.

Apparatus configuration and characterization. Number-average molecular weight ($M_{n,app}$) and molecular weight distribution (M_w/M_n) were determined by GPC equipped with a Waters 515 pump and Wyatt r-Ex differential refractometer using Polymer Standards Services (PSS) columns (guard, 10^5, 10^3, and 500 Å), with THF as eluent at a flow rate 1.00 mL/min (T = 35 °C). GPC traces were processed by WinGPC 8.0 software (PSS) using a calibration based on linear PMMA standards for PMMA and polystyrene (PS) standards for PBA and P*t*BA, respectively. XPS experiments were run on a Thermo Fisher Scientific K-Alpha XPS instrument. Five analysis points were defined on each

sample and a survey scan was collected at each of the 50 points using the 400 micron Al-K-alpha X-ray spot.

Cyclic voltammetry (CV) analysis (taking $BrPhN_2^+$ as example). 7 mM (0.015 g, 0.06 mmol) $BrPhN_2^+$ was dissolved in 8 mL DMF. 0.1 M of Et_4NPF_6 (0.22 g, 0.8 mmol) was used as a supporting electrolyte. CV spectra were recorded at a Pt disk working electrode (WE) with a Pt wire counter electrode (CE) and Ag|AgI|0.1 M n-Bu_4NI in DMF reference electrode (RE). Scan rate (v) was 100 mV/s. The RE was calibrated against the saturated calomel electrode (SCE) scale by measuring ΔE between a SCE.

Electrochemical study of aryl compound deposition on Pt disk electrode. Et_4NPF_6 (0.22 g, 0.8 mmol) and Fc (0.009 g, 0.08 mmol) were added to a five-neck electrolysis cell with 8 mL DMF. CV spectra were recorded at a clean Pt disk WE with a Pt wire CE. v was 100 mV/s. The Pt disk electrode was polished with 0.25 μm diamond paste and then sonicated for 5 minutes and rinsed with methanol. It was then used in a CV of 7 mM $BrPhN_2^+$ DMF solution, between +0.3 and -0.3 V vs. SCE. The same electrode was rinsed with methanol but not polished, and CV of the aforementioned Fc solution was recorded.

RAFT polymerization of BA mediated by electroreduction of $BrPhN_2$. Et_4NPF_6 (0.220 g, 0.8 mmol), $BrPhN_2^+$ (0.015 g, 0.06 mmol) and DDMAT (0.020 g, 0.06 mmol) were placed in a five-neck electrolysis cell maintained at 25 °C under a slow N_2 purge. Then, 4 mL of N_2 purged BA (27.9 mmol) and 4 mL of N_2 purged DMF were added to the reaction. A CV was recorded at 100 mV/s with this electrode setup: a Pt disk WE; a Pt wire CE separated from polymerization mixture by a glass frit filled with tylose gel (saturated with Et_4NPF_6); a Ag/AgI/0.1 M *n*-Bu_4NI in DMF ($Ag/AgI/I^-$) RE. To ensure reproducible application of E_{app}, the potential of $Ag/AgI/I^-$ vs. saturated calomel electrode (SCE) was measured with a voltmeter before the beginning of the polymerization. The Pt mesh electrode was then used as the working electrode for the polymerization. Appropriate potential (or current) was applied. Samples were withdrawn periodically to follow the monomer conversion by ^1H NMR, while M_n and M_w/M_n were determined by GPC. The theoretical MW was calculated as $M_{n,th} = [M]/[DDMAT] \times MW_M \times \text{conversion} + MW_{DDMAT}$.

Synthesis and purification of the PBA macro chain transfer agent (macroCTA). Et_4NPF_6 (0.8258 g, 3 mmol), $BrPhN_2^+$ (0.057 g, 0.2 mmol) and DDMAT (0.153 g, 0.4 mmol) were placed in a five-neck electrolysis cell maintained at 25 °C under a slow N_2 purge. Then, 15 mL of N_2 purged BA (104.6 mmol) and 15 mL of N_2 purged DMF were added to the reaction. A CV was recorded at 100 mV/s with this electrode setup: a Pt disk WE; a Pt wire CE separated from polymerization mixture by a glass frit filled with tylose gel (saturated with Et_4NPF_6); a Ag/AgI/I^- RE. The potential of Ag/AgI/I^- vs. saturated calomel electrode (SCE) was measured. The Pt mesh electrode was then used as the working electrode for the polymerization. A current of -500 μA was applied. The current was increased to take into account the larger scale of this reaction. Samples were withdrawn periodically to follow the monomer conversion by ^{1}H NMR, while M_n and M_w/M_n were determined by GPC. The final product was precipitated by addition to a mixture of MeOH/H_2O (9/1 by v/v) three times and then dried under vacuum.

Chain extention of PBA macroCTA with *t*BA via *e*RAFT. Et_4NPF_6 (0.220 g, 0.8 mmol), $BrPhN_2^+$ (0.008 g, 0.03 mmol) and PBA macroCTA (0.700 g, 0.06 mmol) were placed in a five-neck electrolysis cell maintained at 25 °C under a slow N_2 purge. Then, 4 mL of N_2 purged *t*BA (27.9 mmol) and 4 mL of N_2 purged DMF were added to the reaction. A CV was recorded at 100 mV/s with this electrode setup: a Pt disk WE; a Pt wire CE separated from polymerization mixture by a glass frit filled with tylose gel (saturated with Et_4NPF_6); a Ag/AgI/I^- RE. The potential of Ag/AgI/I^- vs. saturated calomel electrode (SCE) was measured. The Pt mesh electrode was then used as the working electrode for the polymerization. A current of -50 μA was applied. Samples were withdrawn periodically to follow the monomer conversion by ^{1}H NMR, while M_n and M_w/M_n were determined by GPC.

Chain extention of PBA macroCTA with *t*BA via RAFT polymerization. AIBN (0.002 g, 0.01 mmol), PBA macroCTA (0.700 g, 0.06 mmol), *t*BA (4 mL, 27.9 mmol) and DMF (4 mL) were added in a schlenk flask and subjected 3 freez-pump-thaw cycles. The flask was backfilled with N_2 and placed in a 65 °C oil bath. Samples were withdrawn periodically to follow the monomer conversion by ^{1}H NMR, while M_n and M_w/M_n were determined by GPC.

9.6. References

(1) Braunecker, W. A.; Matyjaszewski, K., Controlled/Living Radical Polymerization: Features, Developments, and Perspectives. *Prog Polym Sci* **2007,** *32* (1), 93-146.
(2) Goto, A.; Fukuda, T., Kinetics of Living Radical Polymerization. *Prog Polym Sci* **2004,** *29* (4), 329-385.
(3) Wang, J. S.; Matyjaszewski, K., Controlled Living Radical Polymerization - Halogen Atom-Transfer Radical Polymerization Promoted by a Cu(I)/Cu(II) Redox Process. *Macromolecules* **1995,** *28* (23), 7901-7910.
(4) Wang, J. S.; Matyjaszewski, K., Controlled Living Radical Polymerization - Atom-Transfer Radical Polymerization In the Presence Of Transition-Metal Complexes. *J Am Chem Soc* **1995,** *117* (20), 5614-5615.
(5) Matyjaszewski, K., Atom Transfer Radical Polymerization (ATRP): Current Status and Future Perspectives. *Macromolecules* **2012,** *45* (10), 4015-4039.
(6) Matyjaszewski, K.; Xia, J. H., Atom Transfer Radical Polymerization. *Chem Rev* **2001,** *101* (9), 2921-2990.
(7) Chiefari, J.; Chong, Y. K.; Ercole, F.; Krstina, J.; Jeffery, J.; Le, T. P. T.; Mayadunne, R. T. A.; Meijs, G. F.; Moad, C. L.; Moad, G.; Rizzardo, E.; Thang, S. H., Living Free-Radical Polymerization by Reversible Addition-Fragmentation Chain Transfer: The RAFT Process. *Macromolecules* **1998,** *31* (16), 5559-5562.
(8) Moad, G.; Rizzardo, E.; Thang, S. H., Living Radical Polymerization by the RAFT Process - A third update. *Aust J Chem* **2012,** *65* (8), 985-1076.
(9) Magenau, A. J. D.; Strandwitz, N. C.; Gennaro, A.; Matyjaszewski, K., Electrochemically Mediated Atom Transfer Radical Polymerization. *Science* **2011,** *332* (6025), 81-84.
(10) Chmielarz, P.; Fantin, M.; Park, S.; Isse, A. A.; Gennaro, A.; Magenau, A. J. D.; Sobkowiak, A.; Matyjaszewski, K., Electrochemically Mediated Atom Transfer Radical Polymerization (eATRP). *Prog Polym Sci* **2017,** *69*, 47-78.
(11) Pan, X. C.; Tasdelen, M. A.; Laun, J.; Junkers, T.; Yagci, Y.; Matyjaszewski, K., Photomediated Controlled Radical Polymerization. *Prog Polym Sci* **2016,** *62*, 73-125.
(12) Wang, Z. H.; Pan, X. C.; Yan, J. J.; Dadashi-Silab, S.; Xie, G. J.; Zhang, J. N.; Wang, Z. H.; Xia, H. S.; Matyjaszewski, K., Temporal Control in Mechanically Controlled Atom Transfer Radical Polymerization Using Low ppm of Cu Catalyst. *Acs Macro Lett* **2017,** *6* (5), 546-549.
(13) Simakova, A.; Averick, S. E.; Konkolewicz, D.; Matyjaszewski, K., Aqueous ARGET ATRP. *Macromolecules* **2012,** *45* (16), 6371-6379.
(14) Magenau, A. J. D.; Bortolamei, N.; Frick, E.; Park, S.; Gennaro, A.; Matyjaszewski, K., Investigation of Electrochemically Mediated Atom Transfer Radical Polymerization. *Macromolecules* **2013,** *46* (11), 4346-4353.
(15) Fantin, M.; Isse, A. A.; Venzo, A.; Gennaro, A.; Matyjaszewski, K., Atom Transfer Radical Polymerization of Methacrylic Acid: A Won Challenge. *J Am Chem Soc* **2016,** *138* (23), 7216-7219.
(16) Jasinski, N.; Lauer, A.; Stals, P. J. M.; Behrens, S.; Essig, S.; Walther, A.; Godmann, A. S.; Barner-Kowollik, C., Cleaning the Click: A Simple Electrochemical Avenue for

Copper Removal from Strongly Coordinating Macromolecules. *Acs Macro Lett* **2015,** *4* (3), 298-301.
(17) Chmielarz, P.; Krys, P.; Park, S.; Matyjaszewski, K., PEO-b-PNIPAM Copolymers via SARA ATRP and eATRP in Aqueous Media. *Polymer* **2015,** *71*, 143-147.
(18) Park, S.; Cho, H. Y.; Wegner, K. B.; Burdynska, J.; Magenau, A. J. D.; Paik, H. J.; Jurga, S.; Matyjaszewski, K., Star Synthesis Using Macroinitiators via Electrochemically Mediated Atom Transfer Radical Polymerization. *Macromolecules* **2013,** *46* (15), 5856-5860.
(19) Chmielarz, P.; Park, S.; Sobkowiak, A.; Matyjaszewski, K., Synthesis of Beta-Cyclodextrin-Based Star Polymers via a Simplified Electrochemically Mediated ATRP. *Polymer* **2016,** *88*, 36-42.
(20) Fantin, M.; Isse, A. A.; Gennaro, A.; Matyjaszewski, K., Understanding the Fundamentals of Aqueous ATRP and Defining Conditions for Better Control. *Macromolecules* **2015,** *48* (19), 6862-6875.
(21) Fantin, M.; Park, S.; Wang, Y.; Matyjaszewski, K., Electrochemical Atom Transfer Radical Polymerization in Miniemulsion with a Dual Catalytic System. *Macromolecules* **2016,** *49* (23), 8838-8847.
(22) Guo, J. K.; Zhou, Y. N.; Luo, Z. H., Kinetic Insight into Electrochemically Mediated ATRP Gained through Modeling. *Aiche J* **2015,** *61* (12), 4347-4357.
(23) Guo, J. K.; Zhou, Y. N.; Luo, Z. H., Kinetic Insights into the Iron-Based Electrochemically Mediated Atom Transfer Radical Polymerization of Methyl Methacrylate. *Macromolecules* **2016,** *49* (11), 4038-4046.
(24) Moad, G.; Chiefari, J.; Chong, Y. K.; Krstina, J.; Mayadunne, R. T. A.; Postma, A.; Rizzardo, E.; Thang, S. H., Living Free Radical Polymerization with Reversible Addition-Fragmentation Chain Transfer (the life of RAFT). *Polym Int* **2000,** *49* (9), 993-1001.
(25) Moad, G.; Rizzardo, E.; Thang, S. H., Living Radical Polymerization by the RAFT Process. *Aust J Chem* **2005,** *58* (6), 379-410.
(26) Moad, G.; Rizzardo, E.; Thang, S. H., Living Radical Polymerization by the RAFT Process - A first update. *Aust J Chem* **2006,** *59* (10), 669-692.
(27) Moad, G.; Rizzardo, E.; Thang, S. H., Living Radical Polymerization by the RAFT Process - A second update. *Aust J Chem* **2009,** *62* (11), 1402-1472.
(28) Hill, M. R.; Carmean, R. N.; Sumerlin, B. S., Expanding the Scope of RAFT Polymerization: Recent Advances and New Horizons. *Macromolecules* **2015,** *48* (16), 5459-5469.
(29) Li, Y.; Yang, J.; Benicewicz, B. C., Well-controlled polymerization of 2-azidoethyl methacrylate at near room temperature and click functionalization Journal of Polymer Science Part A: Polymer Chemistry Volume 45, Issue 18. *J. Polym. Sci., Part A: Polym. Chem.* **2007,** *45* (18), 4300-4308.
(30) Convertine, A. J.; Lokitz, B. S.; Vasileva, Y.; Myrick, L. J.; Scales, C. W.; Lowe, A. B.; McCormick, C. L., Direct synthesis of Thermally Responsive DMA/NIPAM Diblock and DMA/NIPAM/DMA Triblock Copolymers via Aqueous, Room Temperature RAFT Polymerization. *Macromolecules* **2006,** *39* (5), 1724-1730.
(31) Kwak, Y.; Nicolay, R.; Matyjaszewski, K., Synergistic Interaction Between ATRP and RAFT: Taking the Best of Each World. *Aust J Chem* **2009,** *62* (11), 1384-1401.

(32) Nicolay, R.; Kwak, Y.; Matyjaszewski, K., A Green Route to Well-Defined High-Molecular-Weight (Co)polymers Using ARGET ATRP with Alkyl Pseudohalides and Copper Catalysis. *Angew Chem Int Ed* **2010,** *49* (3), 541-544.
(33) Gu, Y. W.; Zhao, J. F.; Liu, Q. Q.; Pan, X. Q.; Zhang, W.; Zhang, Z. B.; Zhu, X. L., Zero Valent Metal/RAFT Agent Mediated CRP of Functional Monomers at Room Temperature: a Promising Catalyst System for CRP. *Polym Chem-Uk* **2015,** *6* (3), 359-363.
(34) Martin, L.; Gody, G.; Perrier, S., Preparation of Complex Multiblock Copolymers via Aqueous RAFT Polymerization at Room Temperature. *Polym Chem-Uk* **2015,** *6* (27), 4875-4886.
(35) Vandenbergh, J.; Schweitzer-Chaput, B.; Klussmann, M.; Junkers, T., Acid-Induced Room Temperature RAFT Polymerization: Synthesis and Mechanistic Insights. *Macromolecules* **2016,** *49* (11), 4124-4135.
(36) Barner, L.; Quinn, J. F.; Barner-Kowollik, C.; Vana, P.; Davis, T. P., Reversible Addition-Fragmentation Chain Transfer Polymerization Initiated with Gamma-Radiation at Ambient Temperature: an Overview. *Eur Polym J* **2003,** *39* (3), 449-459.
(37) Otsu, T., Iniferter Concept and Living Radical Polymerization. *J Polym Sci Pol Chem* **2000,** *38* (12), 2121-2136.
(38) Shanmugam, S.; Xu, J. T.; Boyer, C., Photoinduced Electron Transfer-Reversible Addition-Fragmentation Chain Transfer (PET-RAFT) Polymerization of Vinyl Acetate and N-Vinylpyrrolidinone: Kinetic and Oxygen Tolerance Study. *Macromolecules* **2014,** *47* (15), 4930-4942.
(39) Xu, J. T.; Jung, K.; Atme, A.; Shanmugam, S.; Boyer, C., A Robust and Versatile Photoinduced Living Polymerization of Conjugated and Unconjugated Monomers and Its Oxygen Tolerance. *J Am Chem Soc* **2014,** *136* (14), 5508-5519.
(40) Tria, M. C. R.; Grande, C. D. T.; Ponnapati, R. R.; Advincula, R. C., Electrochemical Deposition and Surface-Initiated RAFT Polymerization: Protein and Cell-Resistant PPEGMEMA Polymer Brushes. *Biomacromolecules* **2010,** *11* (12), 3422-3431.
(41) Grande, C. D.; Tria, M. C.; Jiang, G. Q.; Ponnapati, R.; Advincula, R., Surface-Grafted Polymers from Electropolymerized Polythiophene RAFT Agent. *Macromolecules* **2011,** *44* (4), 966-975.
(42) Bunsow, J.; Manz, M.; Vana, P.; Johannsmann, D., Electrochemically Induced RAFT Polymerization of Thermoresponsive Hydrogel Films: Impact on Film Thickness and Surface Morphology. *Macromol Chem Phys* **2010,** *211* (7), 761-767.
(43) Fantin, M.; Lorandi, F.; Gennaro, A.; Isse, A. A.; Matyjaszewski, K., Electron Transfer Reactions in Atom Transfer Radical Polymerization. *Synthesis-Stuttgart* **2017,** *49* (15), 3311-3322.
(44) Christmann, J.; Ibrahim, A.; Charlot, V.; Croutxe-Barghorn, C.; Ley, C.; Allonas, X., Elucidation of the Key Role of [Ru(bpy)(3)](2+) in Photocatalyzed RAFT Polymerization. *Chemphyschem* **2016,** *17* (15), 2309-2314.
(45) Isse, A. A.; Mussini, P. R.; Gennaro, A., New Insights into Electrocatalysis and Dissociative Electron Transfer Mechanisms: The Case of Aromatic Bromides. *J Phys Chem C* **2009,** *113* (33), 14983-14992.
(46) Odian, G. G., *Principles of Polymerization*. 4th ed.; Wiley-Interscience: Hoboken, N.J., 2004; p xxiv, 812 p.

(47) Antonello, S.; Musumeci, M.; Wayner, D. D. M.; Maran, F., Electroreduction of Dialkyl Pperoxides. Activation-Driving Force Rrelationships and Bond Dissociation Free Energies. *J Am Chem Soc* **1997,** *119* (40), 9541-9549.
(48) Menanteau, T.; Dias, M.; Levillain, E.; Downard, A. J.; Breton, T., Electrografting via Diazonium Chemistry: The Key Role of the Aryl Substituent in the Layer Growth Mechanism. *J Phys Chem C* **2016,** *120* (8), 4423-4429.
(49) Mahouche-Chergui, S.; Gam-Derouich, S.; Mangeney, C.; Chehimi, M. M., Aryl Diazonium Salts: a New Class of Coupling Agents for Bonding Polymers, Biomacromolecules and Nanoparticles to Surfaces. *Chem Soc Rev* **2011,** *40* (7), 4143-4166.
(50) Deniau, G.; Azoulay, L.; Bougerolles, L.; Palacin, S., Surface Electroinitiated Emulsion Polymerization: Grafted Organic Coatings From aqueous solutions. *Chem Mater* **2006,** *18* (23), 5421-5428.
(51) Belanger, D.; Pinson, J., Electrografting: a Powerful Method for Surface Modification. *Chem Soc Rev* **2011,** *40* (7), 3995-4048.
(52) Bernard, M. C.; Chausse, A.; Cabet-Deliry, E.; Chehimi, M. M.; Pinson, J.; Podvorica, F.; Vautrin-Ul, C., Organic Layers Bonded to Industrial, Coinage, and Noble Metals Through Electrochemical Reduction of Aryldiazonium Salts. *Chem Mater* **2003,** *15* (18), 3450-3462.
(53) Boukerma, K.; Chehimi, M. M.; Pinson, J.; Blomfield, C., X-Ray Photoelectron Spectroscopy Evidence for the Covalent Bond Between an Iron Surface and Aryl Groups Attached by the Electrochemical Reduction of Diazonium Salts. *Langmuir* **2003,** *19* (15), 6333-6335.
(54) Chausse, A.; Chehimi, M. M.; Karsi, N.; Pinson, J.; Podvorica, F.; Vautrin-Ul, C., The Electrochemical Reduction of Diazonium Salts on iron Electrodes. The Formation of Covalently Bonded Organic Layers and their Effect on Corrosion. *Chem Mater* **2002,** *14* (1), 392-400.
(55) Matrab, T.; Chehimi, M. M.; Perruchot, C.; Adenier, A.; Guillez, A.; Save, M.; Charleux, B.; Cabet-Deliry, E.; Pinson, J., Novel Approach for Metallic Surface-Initiated Atom Transfer radical Polymerization using Electrografted Initiators Based on Aryl Diazonium Salts. *Langmuir* **2005,** *21* (10), 4686-4694.
(56) Tessier, L.; Deniau, G.; Charleux, B.; Palacin, S., Surface Electroinitiated Emulsion Polymerization (SEEP): A Mechanistic Approach. *Chem Mater* **2009,** *21* (18), 4261-4274.
(57) Fantin, M.; Lorandi, F.; Isse, A. A.; Gennaro, A., Sustainable Electrochemically-Mediated Atom Transfer Radical Polymerization with Inexpensive Non-Platinum Electrodes. *Macromol Rapid Comm* **2016,** *37* (16), 1318-1322.
(58) Keddie, D. J., A Guide to the Synthesis of Block Copolymers using Reversible-Addition Fragmentation Chain Transfer (RAFT) Polymerization. *Chem Soc Rev* **2014,** *43* (2), 496-505.

Chapter 10 Electrochemically Mediated Reversible Addition-Fragmentation Chain-Transfer Polymerization by Synergy with Electrochemically Mediated Atom Transfer Radical Polymerization

10.1. Preface

The content of this chapter was published in *Macromolecular Rapid Communications* (**Y. Wang**, M. Fantin, K. Matyjaszewski, *Macromolecular Rapid Communications*, **2018**, 39, 201800221.)

This chapter represents the second part of the series on electrochemically mediated RAFT polymerization (Chapters IX – XI).

The idea of coupling ATRP with RAFT was previously investigated in our group (Kwak, Y.; Nicolay, R.; Matyjaszewski, K., *Aust. J. Chem.* **2009,** *62* (11), 1384-1401). The radicals were solely generated via ATRP equilibrium, thus the molecular weight matches perfectly with the predicted value. The copper concentration could be decreased to a much lower level than that in pure ATRP because dispersity could be controlled by the degenerative exchange with RAFT reagents.

In this section, concurrent ATRP/RAFT was studied by electrochemical activation. Thorough electrochemical analysis was conducted to deeply understand the mechanism. The polymerization was controlled by tuning the applied potential. The advantage of concurrent *e*ATRP/RAFT over *e*ATRP was explored using very low Cu catalyst loading.

I designed this project and conducted all the experiments. Dr. Marco Fantin gave me many very useful suggestions. I also thank Dr. Sivaprakash Shanmugam for fruitful discussions. The support from the National Science Foundation (CHE 1707490) is acknowledged.

10.2. Introduction

Electrosynthesis and electrocatalysis are important synthetic methods that have experienced a renaissance in the past two decades.[1] They are fundamental tools for chemical transformations, switchable catalysis,[2-3] and external regulation of controlled polymerizations.[4] By shifting the applied potential, the valence of the metal center in the catalyst complexes can be readily tuned, thus shifting the reactivity and stereoselectivity *in situ*.

One of the most robust applications of electrocatalysis in polymer science is electrochemically mediated atom transfer radical polymerization (*e*ATRP),[5-6] which was applied to various monomers,[6-8] reaction media,[9-11] and electrode materials for the preparation of functional polymers, surfaces, and biosensors.[12-17] *e*ATRP is regulated by the reversible reduction of copper or iron complexes, which allows for temporal control by simply shifting the applied potential during polymerization.

Another controlled radical process that can be triggered electrochemically is reversible addition-fragmentation chain-transfer (RAFT) polymerization. Similar to atom transfer radical polymerization (ATRP), RAFT is a robust approach to fabricate well-defined polymers, based on the reversible radical exchange to a chain transfer agent (CTA).[18-19]

Electrochemical initiation is different in ATRP and RAFT. Direct reduction of RAFT CTAs was unsuccessful because the generated radicals were further reduced to carbanions or decomposed at the electrode.[20-21] Therefore, *e*RAFT was achieved by reduction of external radical sources, such as a diazonium salt (4-bromobenzenediazonium tetrafluoroborate, $BrPhN_2^+$) or a traditional radical initiator (benzoyl peroxide, BPO).[21] The diazonium salt had a reduction potential 1 V more positive than that of the CTA, which was not affected during electrolysis. Reduction of the diazonium salt, however, generated phenyl radicals that grafted on the electrode, significantly reducing its conductivity and slowing down the polymerization. Electroreduction of BPO also provided slow polymerization accompanied by some termination of the ensuing radicals next to the surface of the electrode.[21-22]

Instead of using reductive conditions and radical intermediates, a RAFT cationic polymerization was successfully triggered by either direct or mediated oxidation of a dithiocarbamate CTA,[23-24] resulting in well-defined polyvinyl ethers with a temporal control over the polymerization. However, under such oxidative conditions monomer propagated via cationic intermediates, instead of radical species.

An efficient approach to activate CTAs and generate radicals have been a dual-concurrent ATRP/RAFT system, in which both a RAFT CTA and an ATRP initiator (RX) were present.[25-28] The RX initiator was activated by copper catalysts, releasing radicals that propagated in a controlled manner under simultaneous ATRP and RAFT. This initiation approach is general and can be applied to virtually any monomer polymerizable by ATRP or RAFT. For a dual concurrent ATRP/RAFT system, the targeted degree of polymerization was defined as follows:

$$DP_T = [M]_0/([RX]_0 + [CTA]_0) \quad (1)$$

No additional chains are generated during reaction, giving good control of MW and retention of chain-end functionality. Concurrent ATRP/RAFT was conducted with only 0.33 ppm of Cu,[29] a very low Cu concentration that gave insufficient deactivation in a pure ATRP process. However, in concurrent ATRP/RAFT, the fast dynamic of ATRP activation-deactivation was no longer essential, as fast RAFT with equimolar CTA/RX ratio allowed synthesis of well-defined polymers. [30]

In this contribution, we propose dual-concurrent *e*ATRP/RAFT as a new pathway to electrochemically initiate RAFT polymerization (**Scheme 10-1**). First, relevant redox properties of Cu/L catalysts and RAFT agents were analyzed and discussed. Then, polymerization of *n*-butyl acrylate (BA) was triggered by reducing copper complexes in the presence of both R−X initiators and CTAs. Temporal polymerization control was achieved simply by shifting the applied potential to reduce or oxidize Cu complexes. The RAFT and ATRP processes complemented each other, whereby a small amount of CTA (1-2% with respect to ATRP initiator R−X) was sufficient to control polymerization with only 10 ppm of Cu.

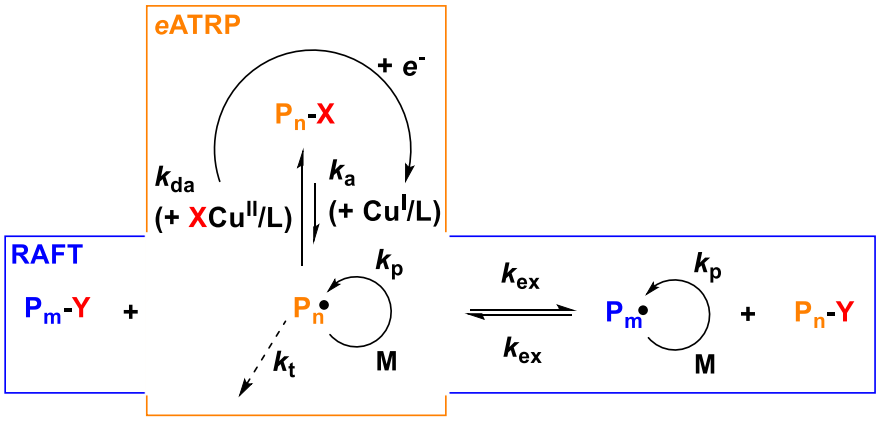

Scheme 10-1. Proposed mechanism of dual-concurrent *e*ATRP/RAFT polymerization.

10.3. Results and Discussion

Electrochemical ATRP/RAFT of BA. As discussed previously, direct reduction of CTAs such as 2-(dodecylthiocarbonothioylthio)-2-methylpropionic acid (DDMAT) did not initiate a radical polymerization.[21] Therefore, we investigated whether DDMAT could be electrochemically activated with a Cu catalyst mediator.

Figure 10-1A shows the cyclic voltammogram (CV) of Cu^{II}/tris(2-pyridylmethyl)amine (TPMA) in the presence and absence of DDMAT. As a typical ATRP catalyst, Cu^{II}/TPMA showed reversible redox behavior. The addition of DDMAT did not alter the shape of the voltammogram of Cu^{II}/TPMA, indicating that Cu^{I}/TPMA was not able to activate DDMAT. Thus, the ATRP initiator ethyl α-bromoisobutyrate (EBiB) was added as co-initiator, which could be catalytically activated by Cu/TPMA as shown in **Figure 10-1**B. The enhanced cathodic current arose from the occurrence of the ATRP process, whereby Cu^{II}/TPMA was continuously reformed during the CV scan by the reaction of Cu^{I}/TPMA with R−X. Therefore, the DDMAT/EBiB system was used for polymerization of BA in the presence of Cu/TPMA.

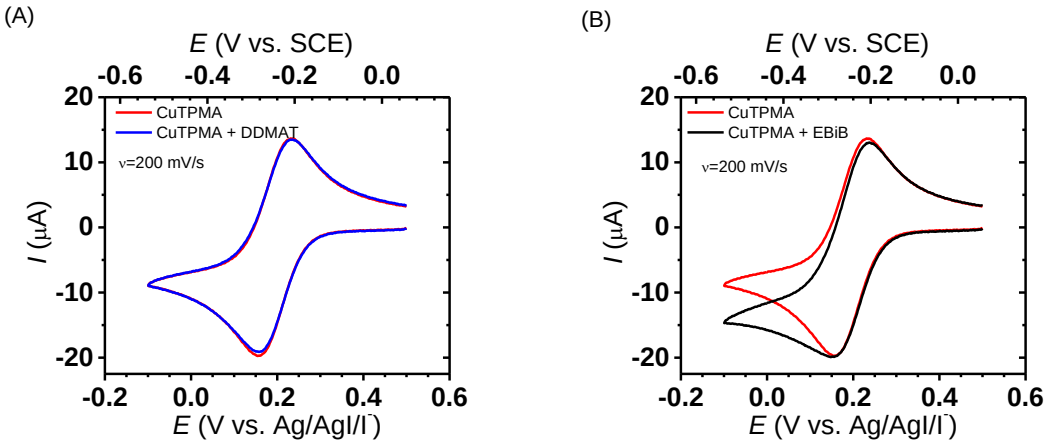

Figure 10-1. CV study of the dual-concurrent system. (A) $CuBr_2$/TPMA in the absence and in the presence of DDMAT; (B) $CuBr_2$/TPMA in the absence and the presence of EBiB. Conditions: [$CuBr_2$/2TPMA] =1.05 mM, [DDMAT] or [EBiB] = 3.5 mM, [$TEABF_4$] = 0.1 M in BA/DMF (1/1 by volume), T = 50 ºC, working electrode (WE) = glassy carbon.

As discussed above, Cu/TPMA was not able to activate DDMAT. The reduction of DDMAT was observed at peak potential ~ -1.25 V vs. SCE. The shift of the peak to more negative potential after addition of EBiB is associated to the change from tertiary to secondary leaving group in the CTA: After addition of EBiB, which was activated by Cu/TPMA, the radical initiating radicals propagated to form PBA oligomeric radicals. These secondary oligomeric radicals underwent transfer with DDMAT forming a new macro-chain transfer agent (macroCTA) different from DDMAT. Due to the higher bond dissociation energy of the new CTA, with a secondary carbon leaving group, the macroCTA showed a reduction potential more negative than that of DDMAT (**Figure 10-2**).

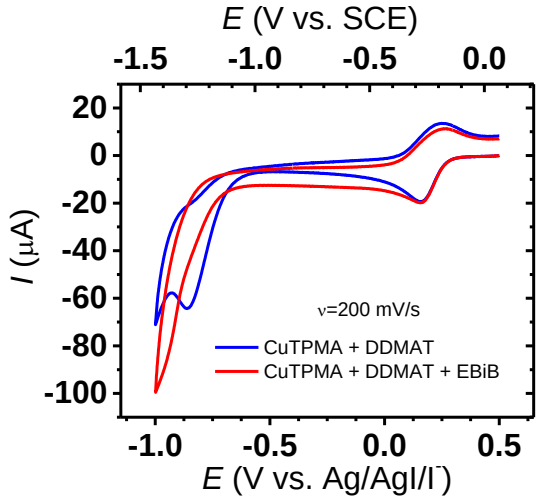

Figure 10-2. CV study of the dual concurrent system. $CuBr_2$/TPMA + DDMAT in the absence and presence of EBiB. Conditions: [$CuBr_2$/2TPMA] =1.05 mM, [DDMAT] = [EBiB] = 3.5 mM, [$TEABF_4$] = 0.1 M in BA/DMF (1/1 by volume), *T* = 50 ºC, WE = GC, CE = Pt mesh, RE = Ag/AgI/I^-.

The chain in structure of DDMAT was also probed by UV-Vis spectroscopy (**Figure 10-3**).

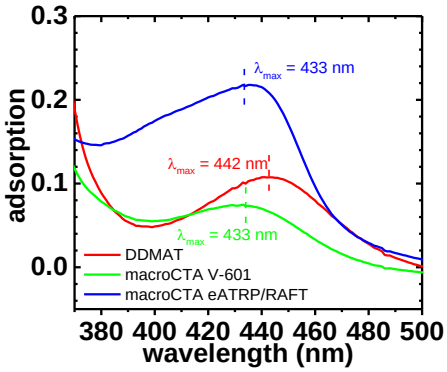

Figure 10-3. UV-Vis of DDMAT (red); PBA macroCTA (green) and test sample (blue).

The sample "macroCTA V-601" was prepared by traditional thermoinitiated RAFT polymerization. V-601 (0.006 g, 4.2 mM), DDMAT (0.015 g, 7 mM), BA (3 mL, 3.5 M) and DMF (3 mL) were added in a N_2 purged flask. The reaction mixture was placed in a 50 ºC oil bath for 8 h. The polymerization was quenched upon exposure to air. Then the mixture was exposed to vacuum in a Biotage V-10 evaporation system to remove DMF and remaining BA. The resulted yellow polymer, PBA macroCTA (M_n = 3.5×10^{-3}, $Đ$ = 1.22) was used for UV-Vis study.

The sample "macroCTA eATRP/RAFT" was obtained from the reaction mixture obtained as in Table 1, entry 5 (RBr/CTA = 30/70). The mixture was exposed to vacuum in Biotage V-10 evaporation system to remove DMF and remaining BA.

DDMAT showed λ_{max} = 442 nm, however, the macroCTA and test sample had λ_{max} = 433 nm. These observations show the complete transformation of DDMAT was into new macroCTAs during the dual-concurrent *e*ATRP/RAFT polymerization.

Polymerization of BA was initiated by application of a potential to reduce Cu^{II}/TPMA, E_{app} = E_{pc} (cathodic peak potential of the copper complex). Both ATRP initiator and RAFT agent were present, with [BA]/[DDMAT]/[EBiB] = 500/0.5/0.5 (**Table 1**, entry 1). The polymerization followed linear semilogarithmic kinetic plots (**Figure 10-4**). Molecular weight agreed with the theoretical value determined by **Equation (1)**, indicating that the propagating chains were controlled by both ATRP equilibrium and reversible chain transfer to (macro)CTA. The obtained polymer had dispersity of 1.19, indicating that efficient control was achieved by the dual-concurrent *e*ATRP/RAFT.

Table 10-1. Dual-concurrent *e*ATRP/RAFT of BA at different RBr/CTA ratios. [a)]

Entry	E_{app} [V vs. SCE]	Cu [ppm]	RBr/CTA	Q [b)] [C]	Conv[c)] [%]	k_p^{app} [d)] [h^{-1}]	$M_{n,th}$ [e)] [$\times 10^{-3}$]	$M_{n,th}$ [f)] [$\times 10^{-3}$]	$Đ$ [f)]
1	-0.29 (E_{pc})	300	50/50	-13.37	54	0.043	34.5	31.1	1.19
2	-0.70	300	50/50	-18.95	29	0.019	18.6	24.9	1.14
3	-1.00	300	50/50	-15.5	1	0.001	1.2	----	----
4	-0.29	300	0/100	-6.08	0	0	----	----	----
5	-0.29	300	30/70	-13.66	7	0.004	4.4	3.0	1.34
6[g)]	-0.29	300	30/70	-9.81	17	0.012	11.1	8.1	1.34
7	-0.29	300	70/30	-15.42	68	0.059	43.6	41.2	1.15
8	-0.29	300	90/10	-12.75	86	0.106	55.1	41.6	1.24
9[h)]	-0.29	300	100/0	-5.73	83	0.287	53.7	43.3	1.15
10	-0.29	10	100/0	-0.88	49	0.037	31.4	30.1	1.41
11	-0.29	10	99/1	-0.88	53	0.041	34.3	29.5	1.30
12	-0.29	10	98/2	-0.88	57	0.049	36.8	36.6	1.25

[a)]50 vol % BA in DMF ([BA] = 3.49 M), [BA]/([EBiB]+[DDMAT]) = 500/1, [$CuBr_2$]/[TPMA] = 1/2, [$TEABF_4$] = 0.1 M, T = 50 ºC, t = 20 h, WE = Pt mesh. [b)]Consumed charge determined from the chronoamperometry profile; [c)]Determined by ^{1}H NMR; [d)]The slope of the $\ln([M]_0/[M])$ vs. time plot; [e)]$M_{n,th}$ = [M]/([EBiB] + [DDMAT]) × M_M × conversion + (M_{EBiB} + M_{DDMAT})/2; [f)]Determined by THF GPC with polystyrene standards; [g)] T = 70 ºC; [h)]Polymerization time = 6 h;

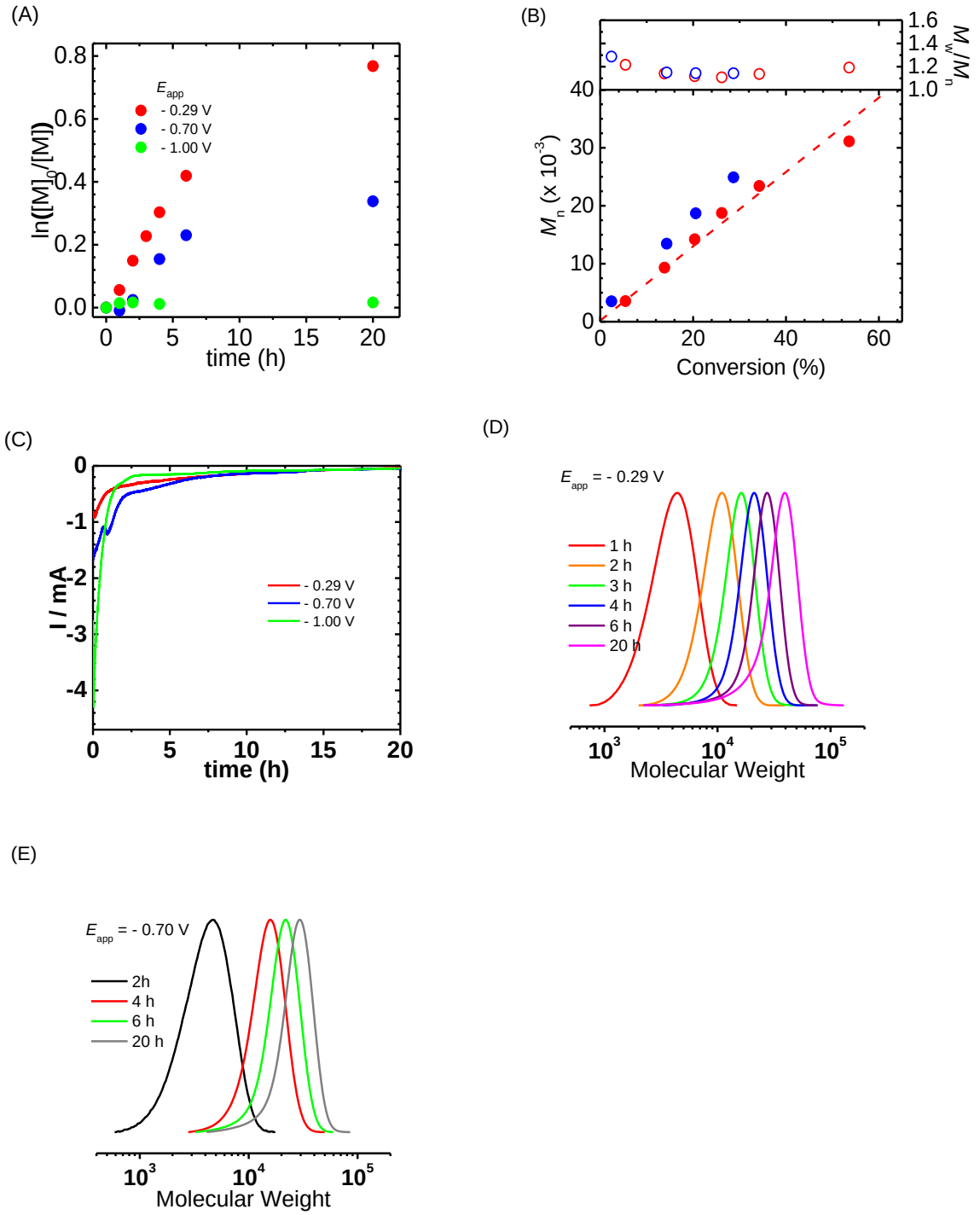

Figure 10-4. Dual concurrent *e*ATRP/RAFT under different applied potentials. (A) Polymerization kinetics; (B) MW and *Đ* evolution with conversion; (C) Current profile vs. time; GPC traces for (D) E_{app} = - 0.29 V; (E) E_{app} = - 0.70 V. Conditions: [BA] = 3.49 M (in DMF, 50% by v), [BA]/[DDMAT]/[EBiB]/[$CuBr_2$]/[TPMA] = 1000/1/1/0.3/0.6, [$CuBr_2$/2TPMA] = 300 ppm to BA, [$TEABF_4$] = 0.1 M, T = 50 ºC, t = 20 h, f = 900 rpm,

WE = Pt mesh, CE = Pt mesh (sep.), RE = Ag/AgI/I^-. The RE was calibrated against the saturated calomel electrode (SCE) scale by measuring ΔE between a SCE.

The presence of DDMAT decreased polymerization rate. A control *e*ATRP experiment in the absence of DDMAT ([BA]/[DDMAT]/[EBiB] = 500/0/0.5) showed faster polymerization rate, indicating that DDMAT caused rate retardation (**Table 10-2**, entry 2). This may be caused by slow fragmentation of the polymeric RAFT-adduct radical (**Figure 10-5**). Retardation by DDMAT was also observed in thermally initiated polymerization of glycidyl methacrylate and styrene,[31 32] as well as predicted by theoretical calculations.[33-34]

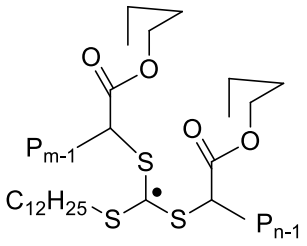

Figure 10-5. Proposed structure of the intermediate radical with high BDEs.

Table 10-2. *e*ATRP of BA in the presence and absence of DDMAT.[a]

Entry	[BA]/[DDMAT]/[EBiB]	*Time* (h)	*Q* (C)	Conv (%)	k_p^{app} (h^{-1})	$M_{n,th}$ ($\times10^{-3}$)	$M_{n,app}$ ($\times10^{-3}$)	*Đ*
1	500/0.5/0.5	20	-13.37	54	0.043	34.5	31.1	1.19
2	500/0/0.5	6	-4.255	64	0.174	82.5	58	1.19

[a][BA] = 3.49 M (in DMF, 50% by v), [$CuBr_2$/2TPMA] = 300 ppm to BA, [$TEABF_4$] = 0.1 M, T = 50 ºC, t = 20 h, stirring rate f = 900 rpm, WE = Pt mesh, CE = Pt mesh (sep.), RE = Ag/AgI/I^-. E_{app} = E_{pc} of $CuBr_2$/TPMA.

The reason for the slower polymerization rate can be evinced from the UV-Vis study in **Figure 10-3**, which showed the complete transformation of DDMAT into new macroCTAs during the dual-concurrent *e*ATRP/RAFT polymerization. Thus, slow initialization was not likely the reason for slow polymerization. The more possible reason is the relatively slow fragmentation of the RAFT adduct radical (**Figure 10-5**), because the higher BDE in secondary carbon-sulfur bond.

Influence of E_{app}. The applied potential (E_{app}) defines the [Cu^{II}]/[Cu^{I}] ratio close to the surface of the electrode according to the Nernst equation:

$$E_{app} = E^{o} + \frac{RT}{F} \ln \frac{[Cu^{II}]}{[Cu^{I}]} \quad (2)$$

where E^o is the standard reduction potential of the catalyst, R is the gas constant, and F is the Faraday constant. The [Cu^{II}]/[Cu^{I}] ratio influences the rate of polymerization, with more negative E_{app} generally giving faster polymerization.[14] Unexpectedly, an opposite trend was observed when applying relatively negative E_{app}. When E_{app} = -0.29 V vs. SCE (E_{app} = E_{pc} of Cu^{II}/TPMA), 54% conversion in 20 h was obtained (**Table 10-1**, entry 1). Polymerization was significantly slower, however, when E_{app} = -0.70 V vs. SCE was applied. No polymerization occurred at E_{app} = -1.0 V vs. SCE (**Table 10-1**, entry 2–3). Slower polymerization under negative potential was also observed in a pure *e*ATRP system (without CTA, **Table 10-3**). These unexpected results can be explained by considering the contribution of the organometallic mediated radical polymerization (OMRP).[35-36] Acrylate radicals can react with Cu^{I}/L forming relatively stable P_n–Cu^{II}/L organometallic complexes,

which are irreversibly reduced at cathodic peak potential ~ -0.65 V vs. SCE (**Figure 10-6**). In agreement with the mechanism in **Scheme 10-2**, reduction of P_n–Cu^{II}/L forms P_n–Cu^{I}/L, which then dissociated into $P_n^{\cdot}$ diminishing the radical propagation process.[36-37] Therefore, application of a potential more negative than ~ -0.65 V vs. SCE could cause decomposition of the organometallic species to carbanions with a loss of propagating chains, which slowed down or stopped the polymerization.

Table 10-3. *e*ATRP of BA under various applied potentials. [a]

Entry	E_{app} [V] (vs. SCE)	Q (C)	Conv (%)	k_p^{app} (h^{-1})	$M_{n,th}$ ($\times10^{-3}$)	$M_{n,app}$ ($\times10^{-3}$)	$Đ$
1	-0.29	-5.73	83	0.287	53.7	43.3	1.15
2	-0.70	-9.34	59	0.173	38.1	27.7	1.15

[a][BA] = 3.49 M (in DMF, 50% by v), [BA]/[EBiB]/[$CuBr_2$/2TPMA] = 500/1/0.15, [$CuBr_2$/2TPMA] = 300 ppm to BA, [$TEABF_4$] = 0.1 M, T = 50 ºC, t = 6 h, f = 900 rpm, WE = Pt mesh, CE = Pt mesh (sep.), RE = Ag/AgI/I^-. E_{app} = E_{pc} of $CuBr_2$/TPMA.

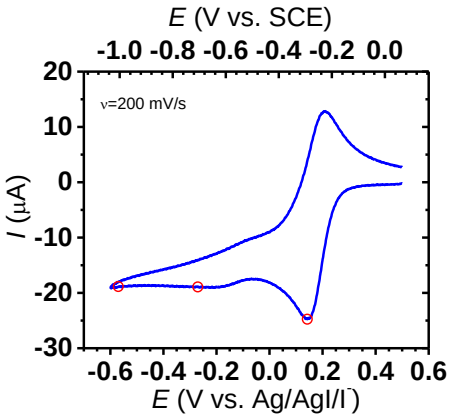

Figure 10-6. Model study of the organometallic species by CV. [$CuBr_2$/2TPMA] =1.05 mM, [EBP] = 10 mM, [$TEABF_4$] = 0.1 M in BA/DMF (1/1 by volume), T = 50 ºC, WE = GC, CE = Pt mesh, RE = Ag/AgI/I^-.

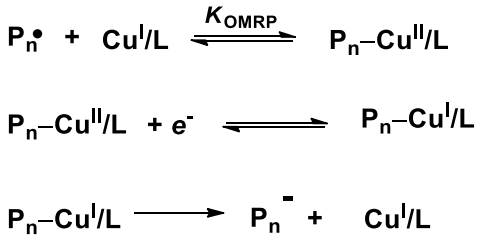

Scheme 10-2. Proposed mechanism for formation and reduction of organometallic species.

Application of a relatively positive potential caused oxidation of the catalyst, with the possibility to switch the reaction ON/OFF on demand. The "ON" potential was set at E_{pc}, and the "OFF" potential at E_{pc} + 0.6 V, under which most of the Cu catalyst shifted to $Br–Cu^{II}L^{+}$. The polymerization was switched off shortly after applying the "OFF" potential, due to fast oxidation of $Cu^{I}L^{+}$ activators, with negligible conversion during the "OFF" periods (**Figure 10-7**). By multiple-step electrolysis, the polymerization was stopped and restarted repeatedly. Molecular weight matched with the theoretical values, demonstrating that the chain-end functionality was retained during the polymerization.

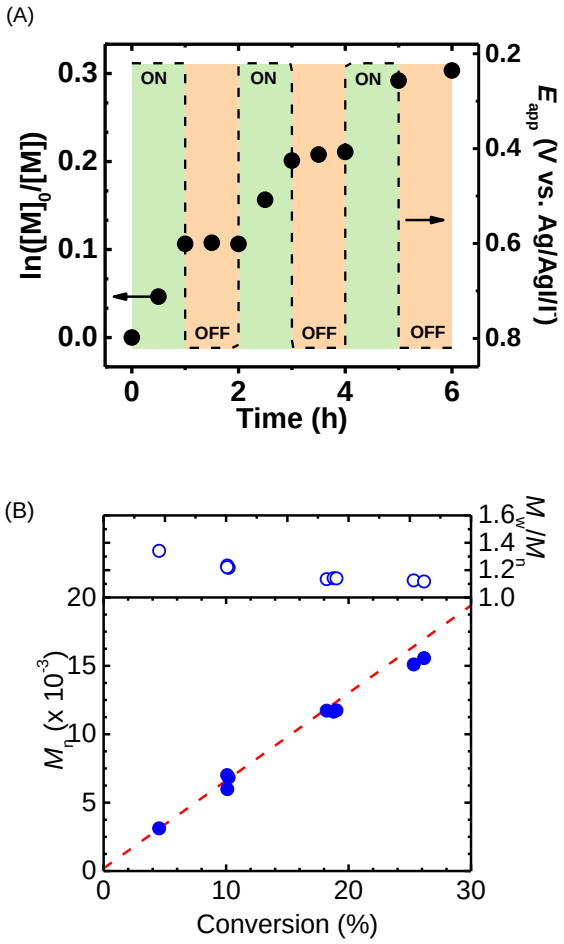

Figure 10-7. Temporal control in dual-concurrent *e*ATRP/RAFT polymerization of BA. (A) Polymerization kinetics; (B) MW and *Đ* evolution with conversion. Reaction conditions: [BA] = 3.49 M (in DMF, 50% by v), [BA]/[DDMAT]/[EBiB]/[$CuBr_2$]/[TPMA] = 500/0.5/0.5/0.015/0.03, [$CuBr_2$/2TPMA] = 30 ppm to BA, [$TEABF_4$] = 0.1 M, T = 50 ºC, "ON" potential = E_{pc}, "OFF" potential = E_{pc} + 0.6 V.

Influence of RBr/CTA Ratio. Targeting the same degree of polymerization (DP_T), i.e. $[M]_0/([RBr]_0 + [CTA]_0)$ = 500, polymerizations were conducted under various RBr/CTA ratios (**Table 10-1**, entry 1, 4–9). No polymerization was observed in the absence of RBr (**Table 10-1**, entry 4), because there was no pathway to generate radicals. A higher k_p^{app} was observed with increasing RBr/CTA, which was caused by two factors. First,

activation of a higher amount of RBr led to a higher radical concentration, thus giving faster polymerization. [14, 38] Second, a lower CTA content led to a smaller rate of retardation. Due to these two effects, polymerization was very slow for RBr/CTA = 30/70 (**Table 10-1**, entry 5). Increasing temperature from 50 ºC to 70 ºC accelerated the polymerization (**Table 10-1**, entry 6).

Table 10-4 summarizes the effect of Cu loading on the dual-concurrent and on the *e*ATRP systems. In *e*ATRP without DDMAT, a decrease in Cu concentration resulted in lower rate of polymerization and higher dispersity, in agreement with previous reports.[8] In the dual-concurrent system, however, polymerization did not slow down by decreasing copper concentration. Instead, the predominant factor influencing the rate of polymerization was the amount of RBr. At lower copper concentration, the dual-concurrent system gave polymer with lower dispersity due to the beneficial contribution of the RAFT process.

Table 10-4. Dual-concurrent *e*ATRP/RAFT and *e*ATRP of BA at different Cu concentrations.[a)]

Entry	[BA]/[EBiB]/[DDMAT]	Cu [ppm]	*t* [h]	*Q* [C]	Conv [%]	k_p^{app} [h^{-1}]	$M_{n,th}$ [$\times 10^{-3}$]	$M_{n,th}$ [$\times 10^{-3}$]	*Đ*
1	500/0.5/0.5	300	20	-13.37	54	0.043	34.5	31.1	1.19
2	500/0.5/0.5	30	20	-3.38	54	0.046	34.5	34.4	1.11
3	500/1/0	300	6	-5.73	83	0.287	53.7	43.3	1.15
4	500/1/0	30	6	-1.58	55	0.122	35.4	32.1	1.21

[a)]50 vol % BA in DMF ([BA] = 3.49 M), [BA]/([EBiB]+[DDMAT])/[$CuBr_2$]/[TPMA] = 500/1/0.15/0.3, [$CuBr_2$/2TPMA] = 300 ppm to BA, [$TEABF_4$] = 0.1 M, T = 50 ºC, E_{app} = $E_{pc,Cu/TPMA}$, WE = Pt mesh.

Cu concentration in *e*ATRP has been typically higher than 50 ppm to obtain good polymerization control. In fact, in **Table 10-1**, entry 10, *e*ATRP of BA was conducted with 10 ppm Cu^{II}/TPMA and EBiB initiator, resulting in a polymer with quite high $Đ$ = 1.41 at 49% conversion.

We envisioned that the synergic contribution of *e*ATRP and RAFT in the dual-concurrent system could improve polymerization control even at low concentration of CTA. In fact, dispersity markedly decreased from 1.41 to 1.30 when only 1% CTA with respect to RBr was added to the polymerization mixture (**Table 10-1**, entry 10 and 11). Dispersity further decreased to 1.25 when 2% CTA was added. Polymerization rate and molecular weight were not significantly influenced by increasing CTA content, which mostly affected dispersity. This approach could potentially be applied to other low ppm ATRP systems to accomplish ATRP/RAFT with very low amount of both Cu and CTA.

10.4. Conclusion

A dual-concurrent electrochemical ATRP/RAFT system was developed for the controlled polymerization of BA. Radicals were solely generated by Cu-catalyzed electrochemical activation of RBr, while propagating radicals and dormant species were shuffled via both ATRP and RAFT equilibria. CV analysis showed that DDMAT was not

activated by Cu^{I}/TPMA. E_{app} should not be too negative to prevent reduction of the organometallic species P_n–Cu^{II}/$TPMA^{+}$.

With 300 ppm of copper, polymerization was well controlled at each RBr/CTA ratio, but increasing RBr/CTA led to faster polymerizations. With RBr/CTA = 1/1 the polymerization was conducted with as low as 30 ppm of copper, and switched "ON" and "OFF" multiple times by shifting the electrolysis potential. Upon addition of 1% and 2% of CTA to RBr, dispersity of PBA prepared with 10 ppm of copper were 1.30 and 1.25, showing great improvement compared to traditional *e*ATRP without CTA, which gave PBA with dispersity = 1.41. These observations demonstrated that the synergistic interactions between *e*ATRP and RAFT gives well-controlled polymerization using low Cu and low CTA, employing alkyl halide initiators to generate radicals.

10.5. Experimental Section

Materials. Copper(II) bromide ($CuBr_2$, 99%), ethyl α-bromoisobutyrate (EBiB, 98%), 2-(dodecylthiocarbonothioylthio)-2-methylpropionic acid (DDMAT, 98%), ethyl 2-bromopropionate (EBP, 99%) and *N,N'*-dimethyl formaldehyde (DMF, 99%) were purchased from Sigma-Aldrich and used as received. Tetraethylammonium tetrafluoroborate ($TEABF_4$, 98%) was purchased from TCI and recrystallized from ethanol. Tris(2-pyridylmethyl)amine (TPMA) was prepared according to a published procedure.[1] *n*-Butyl acrylate (BA, 99%, Aldrich) was passed through a column filled with basic alumina prior to use to remove polymerization inhibitors. Dimethyl 2,2'-azobis(2-

methylproprionate) (V-601) was purchased from Wako Chemicals and was recrystallized from methanol and dried under high vacuum in the dark overnight at room temperature.

Procedures

General Procedure for Cyclic Voltammetry (CV) Measurement

CV was performed in 30 mL 1/1 (by volume) mixture of DMF and BA. 0.1 M of $TEABF_4$ (0.65 g, 3 mmol) was used as a supporting electrolyte in a seven-neck cell under N_2 flow at 50 ºC. CV spectra were recorded at a glassy carbon (GC) disk working electrode (WE) with a Pt wire counter electrode (CE) and a $Ag/AgI/I^-$ (AgI deposited on Ag, immersed in 0.1 M tetrabutylammonium tetrafluoroborate) reference electrode (RE) using a Gamry 600^{TM} Potentiostat. GC was chosen as WE because it is the most commonly used material for electrochemical analysis.[39] Both Pt CE and $Ag/AgI/I^-$ RE were separated from the solution by supporting electrolyte saturated tylose gel. Scan rate (ν) was 200 mV/s. The RE was calibrated against the saturated calomel electrode (SCE) scale by measuring ΔE between a SCE and $Ag/AgI/I^-$ at the beginning of each experiment.

General Procedure for Dual-Concurrent eATRP/RAFT Polymerization

$TEABF_4$ (0.65 g, 3 mmol), $CuBr_2$/2TPMA (0.63 mL of 0.05 M stock solution in DMF, 1.05 mM), EBiB (15.3 μL, 3.5 mM), DDMAT (0.038 g, 3.5 mM), BA (15 mL, 3.5 M) and DMF (15 mL) were added in a seven-neck cell under N_2 flow at 50 ºC. CV spectra were recorded at a GC disk WE with a Pt wire CE and a $Ag/AgI/I^-$ RE. Then a Pt mesh electrode (16 mm * 8 mm of Pt gauze, 52 mesh woven from 0.1 mm diameter wire) was used as WE for polymerization due to a higher surface area than the GC plate WE. The

polymerization was conducted under a stir rate of 900 rpm. Samples were withdrawn periodically for ^{1}H NMR and GPC analysis.

Apparatus Configuration and Characterization.

^{1}H NMR spectra in $CDCl_3$ used to calculate monomer conversion were measured with Bruker Avance 500 MHz spectrometer at 25 °C. Number-average molecular weight ($M_{n,app}$) and molecular weight distribution ($Đ = M_w/M_n$) were determined by GPC equipped with a Waters 515 pump and Wyatt r-Ex differential refractometer using Polymer Standards Services (PSS) columns (guard, 10^5, 10^3, and 500 Å), with THF as eluent at a flow rate 1.00 mL/min (T = 35 °C). GPC traces were processed by WinGPC 8.0 software (PSS) using a calibration based on linear polystyrene (PS) standards. UV-Vis spectra were recorded in Agilent 8453 with a glass cuvette (length = 1 cm).

10.6. References

(1) Yan, M.; Kawamata, Y.; Baran, P. S., Synthetic Organic Electrochemical Methods Since 2000: On the Verge of a Renaissance. *Chem Rev* **2017,** *117* (21), 13230-13319.
(2) Teator, A. J.; Lastovickova, D. N.; Bielawski, C. W., Switchable Polymerization Catalysts. *Chem Rev* **2016,** *116* (4), 1969-1992.
(3) Blanco, V.; Leigh, D. A.; Marcos, V., Artificial Switchable Catalysts. *Chem Soc Rev* **2015,** *44* (15), 5341-5370.
(4) Leibfarth, F. A.; Mattson, K. M.; Fors, B. P.; Collins, H. A.; Hawker, C. J., External Regulation of Controlled Polymerizations. *Angewandte Chemie International Edition* **2013,** *52* (1), 199-210.
(5) Magenau, A. J. D.; Strandwitz, N. C.; Gennaro, A.; Matyjaszewski, K., Electrochemically Mediated Atom Transfer Radical Polymerization. *Science* **2011,** *332* (6025), 81-84.
(6) Chmielarz, P.; Fantin, M.; Park, S.; Isse, A. A.; Gennaro, A.; Magenau, A. J. D.; Sobkowiak, A.; Matyjaszewski, K., Electrochemically Mediated Atom Transfer Radical Polymerization (eATRP). *Prog Polym Sci* **2017,** *69*, 47-78.
(7) Chmielarz, P.; Krys, P.; Park, S.; Matyjaszewski, K., PEO-b-PNIPAM Copolymers via SARA ATRP and eATRP in Aqueous Media. *Polymer* **2015,** *71*, 143-147.

(8) Fantin, M.; Isse, A. A.; Venzo, A.; Gennaro, A.; Matyjaszewski, K., Atom Transfer Radical Polymerization of Methacrylic Acid: A Won Challenge. *J Am Chem Soc* **2016,** *138* (23), 7216-7219.
(9) Chmielarz, P.; Park, S.; Simakova, A.; Matyjaszewski, K., Electrochemically Mediated ATRP of Acrylamides in Water. *Polymer* **2015,** *60*, 302-307.
(10) Fantin, M.; Park, S.; Wang, Y.; Matyjaszewski, K., Electrochemical Atom Transfer Radical Polymerization in Miniemulsion with a Dual Catalytic System. *Macromolecules* **2016,** *49* (23), 8838-8847.
(11) Fantin, M.; Chmielarz, P.; Wang, Y.; Lorandi, F.; Isse, A. A.; Gennaro, A.; Matyjaszewski, K., Harnessing the Interaction between Surfactant and Hydrophilic Catalyst to Control eATRP in Miniemulsion. *Macromolecules* **2017,** *50* (9), 3726-3732.
(12) Park, S.; Chmielarz, P.; Gennaro, A.; Matyjaszewski, K., Simplified Electrochemically Mediated Atom Transfer Radical Polymerization using a Sacrificial Anode. *Angewandte Chemie International Edition* **2015,** *54* (8), 2388-2392.
(13) Fantin, M.; Lorandi, F.; Isse, A. A.; Gennaro, A., Sustainable Electrochemically-Mediated Atom Transfer Radical Polymerization with Inexpensive Non-Platinum Electrodes. *Macromol Rapid Comm* **2016,** *37* (16), 1318-1322.
(14) Magenau, A. J. D.; Bortolamei, N.; Frick, E.; Park, S.; Gennaro, A.; Matyjaszewski, K., Investigation of Electrochemically Mediated Atom Transfer Radical Polymerization. *Macromolecules* **2013,** *46* (11), 4346-4353.
(15) Jin, G. P.; Fu, Y.; Bao, X. C.; Feng, X. S.; Wang, Y.; Liu, W. H., Electrochemically mediated atom transfer radical polymerization of iminodiacetic acid-functionalized poly(glycidyl methacrylate)grafted at carbon fibers for nano-nickel recovery from spent electroless nickel plating baths. *J. Appl. Electrochem.* **2014,** *44* (5), 621-629.
(16) Sun, Y.; Du, H. Y.; Lan, Y. T.; Wang, W. J.; Liang, Y. J.; Feng, C. L.; Yang, M., Preparation of Hemoglobin (Hb) Imprinted Polymer by Hb Catalyzed eATRP and its Application in Niosensor. *Biosens Bioelectron* **2016,** *77*, 894-900.
(17) Guo, J. K.; Zhou, Y. N.; Luo, Z. H., Kinetic Insights into the Iron-Based Electrochemically Mediated Atom Transfer Radical Polymerization of Methyl Methacrylate. *Macromolecules* **2016,** *49* (11), 4038-4046.
(18) Chiefari, J.; Chong, Y. K.; Ercole, F.; Krstina, J.; Jeffery, J.; Le, T. P. T.; Mayadunne, R. T. A.; Meijs, G. F.; Moad, C. L.; Moad, G.; Rizzardo, E.; Thang, S. H., Living Free-Radical Polymerization by Reversible Addition-Fragmentation Chain Transfer: The RAFT Process. *Macromolecules* **1998,** *31* (16), 5559-5562.
(19) Keddie, D. J.; Guerrero-Sanchez, C.; Moad, G.; Mulder, R. J.; Rizzardo, E.; Thang, S. H., Chain Transfer Kinetics of Acid/Base Switchable N-Aryl-N-Pyridyl Dithiocarbamate RAFT Agents in Methyl Acrylate, N-Vinylcarbazole and Vinyl Acetate Polymerization. *Macromolecules* **2012,** *45* (10), 4205-4215.
(20) Falsig, M.; Lund, H., Electrochemical Reduction Of Alkyl Aryl And Dialkyl Trithiocarbonates. *Acta Chem Scand B* **1980,** *34* (8), 545-549.
(21) Wang, Y.; Fantin, M.; Park, S.; Gottlieb, E.; Fu, L. Y.; Matyjaszewski, K., Electrochemically Mediated Reversible Addition-Fragmentation Chain-Transfer Polymerization. *Macromolecules* **2017,** *50* (20), 7872-7879.
(22) Antonello, S.; Musumeci, M.; Wayner, D. D. M.; Maran, F., Electroreduction of Dialkyl Pperoxides. Activation-Driving Force Rrelationships and Bond Dissociation Free Energies. *J Am Chem Soc* **1997,** *119* (40), 9541-9549.

(23) Peterson, B. M.; Lin, S.; Fors, B. P., Electrochemically Controlled Cationic Polymerization of Vinyl Ethers. *J Am Chem Soc* **2018,** *140* (6), 2076-2079.
(24) Wei, S.; Yan, Q., Electro-Controlled Living Cationic Polymerization. *Angewandte Chemie International Edition* **2018**.
(25) Kwak, Y.; Nicolay, R.; Matyjaszewski, K., Concurrent ATRP/RAFT of Styrene and Methyl Methacrylate with Dithioesters Catalyzed by Copper(I) Complexes. *Macromolecules* **2008,** *41* (18), 6602-6604.
(26) Nicolay, R.; Kwak, Y.; Matyjaszewski, K., Dibromotrithiocarbonate Iniferter for Concurrent ATRP and RAFT Polymerization. Effect of Monomer, Catalyst, and Chain Transfer Agent Structure on the Polymerization Mechanism. *Macromolecules* **2008,** *41* (13), 4585-4596.
(27) Kwak, Y.; Nicolay, R.; Matyjaszewski, K., Synergistic Interaction Between ATRP and RAFT: Taking the Best of Each World. *Aust J Chem* **2009,** *62* (11), 1384-1401.
(28) Elsen, A. M.; Nicolay, R.; Matyjaszewski, K., Dual Concurrent ATRP/RAFT of Methyl Acrylate Co-initiated by Alkyl Halides. *Macromolecules* **2011,** *44* (7), 1752-1754.
(29) Kwak, Y.; Yamamura, Y.; Matyjaszewski, K., ATRP of Styrene and Methyl Methacrylate with Less Efficient Catalysts and with Alkyl Pseudohalides as Initiators/Chain Transfer Agents. *Macromol Chem Phys* **2010,** *211* (5), 493-500.
(30) Nicolay, R.; Kwak, Y.; Matyjaszewski, K., A Green Route to Well-Defined High-Molecular-Weight (Co)polymers Using ARGET ATRP with Alkyl Pseudohalides and Copper Catalysis. *Angewandte Chemie International Edition* **2010,** *49* (3), 541-544.
(31) Tan, J. B.; Fu, L. L.; Zhang, X. C.; Bai, Y. H.; Zhang, L., Photosynthesis of Poly(glycidyl Methacrylate) Microspheres: a Component for making Covalently Cross-linked Colloidosomes and Organic/Inorganic Nanocomposites. *J Mater Sci* **2016,** *51* (20), 9455-9471.
(32) Gao, Y. G.; Lv, L.; Zou, G.; Zhang, Q. J., Dependence of Cross-Termination Rate on RAFT Agent Concentration in RAFT Polymerization. *Macromol Res* **2017,** *25* (9), 931-935.
(33) Coote, M. L.; Radom, L., Ab Initio Evidence for Slow Fragmentation in RAFT Polymerization. *J Am Chem Soc* **2003,** *125* (6), 1490-1491.
(34) Coote, M. L., Ab Initio Study of the Addition-Fragmentation Equilibrium in RAFT Polymerization: When is Polymerization Retarded? *Macromolecules* **2004,** *37* (13), 5023-5031.
(35) Schroder, K.; Konkolewicz, D.; Poli, R.; Matyjaszewski, K., Formation and Possible Reactions of Organometallic Intermediates with Active Copper(I) Catalysts in ATRP. *Organometallics* **2012,** *31* (22), 7994-7999.
(36) Ribelli, T. G.; Rahaman, S. M. W.; Daran, J. C.; Krys, P.; Matyjaszewski, K.; Poli, R., Effect of Ligand Structure on the Cu-II-R OMRP Dormant Species and Its Consequences for Catalytic Radical Termination in ATRP. *Macromolecules* **2016,** *49* (20), 7749-7757.
(37) Zerk, T. J.; Bernhardt, P. V., Organo-Copper(II) Complexes as Products of Radical Atom Transfer. *Inorg Chem* **2017,** *56* (10), 5784-5792.
(38) Krys, P.; Matyjaszewski, K., Kinetics of Atom Transfer Radical Polymerization. *Eur Polym J* **2017,** *89*, 482-523.
(39) Zoski, C., G., *Handbook of Electrochemistry*. Elsevier: 2007.

Chapter 11 Electrochemically Catalytic Activation of A Dithiocarbamate as A Pseudohalide

11.1. Preface

The content of this chapter was published in *Journal of Polymer Science, Part A: Polymer Chemistry* (**Y. Wang**, M. Fantin, K. Matyjaszewski, *Journal of Polymer Science, Part A: Polymer Chemistry*, **2019**, 57, 376-381.)

This is part 3 of the series on electrochemically mediated RAFT polymerization (Chapters IX – XI).

RAFT chain transfer agents (CTAs) are alkyl pseudohalides, which could potentially be activated by copper complexes in atom transfer radical polymerization (ATRP). In previous studies, a RAFT CTA, an alkyl dithiocarbamate, was employed in activation by ATRP catalysts. In this chapter, electrochemistry was applied to study the electrochemical activation of the alkyl dithiocarbamate in the presence of ATRP catalysts. Control experiments were conducted to identify the mechanism of the polymerization (ATRP, RAFT or concurrent ATRP/RAFT).

I conducted all the experiments and wrote the manuscript. Dr. Marco Fantin provided many helpful suggestions.

The authors acknowledge the financial support from NSF (CHE 1707490).

11.2. Introduction

Regulation of polymer chain length and dispersity is important in polymer chemistry. Synthesis of polymers with pre-determined molecular weight (MW) and low dispersity (*Đ*) allows to fine tune the physical properties of materials and to manufacture macromolecules with complex architectures. [1-2] Reversible deactivation radical polymerizations (RDRPs) are the tool of choice for such syntheses, taking advantage of reversible termination or chain-transfer. Atom transfer radical polymerization (ATRP) and reversible addition-fragmentation chain-transfer (RAFT) polymerization are the two most important RDRP techniques.[3-6]

ATRP depends on the reversible transfer of an atom (typically a halogen) between a transition metal complex (typically Cu-based) and a propagating radical. Most reports on ATRP focused on the activation of alkyl halides (RX, where X = F, Cl, Br, I).[7-8] Alkyl bromides and chlorides are the most efficient ATRP initiators, providing fast and well-controlled polymerization. Conversely, alkyl fluorides are very difficult to activate, despite the high affinity of $[Cu^{II}TPMA]^{2+}$ and $[Cu^{I}TPMA]^{+}$ to F, and the high stability of $[F–Cu^{II}TPMA]^{+}$ (TPMA = tris(2-pyridylmethyl) amine). The high C–F bond energy leads to slow activation and slow exchange between active and dormant species in ATRP. The C–Cl bond lies between C–F and C–Br and can be successfully activated; the higher bond energy of C-Cl is employed in chain extension procedures using a halogen exchange strategy,[9-10] or to minimize side reactions in the ATRP of acidic monomers.[11] The C–I bond is weak, thus RI is an effective initiator. However, light sensitivity of RI and the poor deactivation by $[I–Cu^{II}TPMA]^{+}$ obstructs the application of RI as initiators.[12]

Besides halogens, various pseudohalogens have been applied in ATRP, including dithiocarbamate (DC),[13-14] trithiocarbonate (TTC),[15] thiocyanate (SCN),[16] isothiocyanate (NCS),[16] isocyanate (NCO).[16-17] These terminal functional groups greatly expand the ATRP toolbox. The diversity of chain-ends facilitates post-modification, preparation of halogen-free polymers, and synthesis of various block copolymers.

RAFT is another RDRP technique, which takes advantage of the degenerative transfer between the propagating polymer chains and chain-transfer agents (CTAs). Most CTAs can be considered as pseudohalide compounds, with the leaving group (R) as the alkyl moiety and the sulfur-containing fraction as the pseudohalide moiety. RAFT agents can be added in small amounts to ATRP procedures to improve polymerization control,[18] and in some cases they can be directly activated by ATRP catalysts. Depending on the combination of monomer and alkyl pseudohalide, they could act as ATRP initiators,[13] CTAs,[19] or both.[20-21]

CTAs can be activated by traditional thermal initiation, or by redox,[22] radiative,[23] photochemical[24-25] and cationic[26-27] pathways. Recently, a RAFT polymerization was mediated electrochemically (*e*RAFT), but the intrinsic redox properties of the CTAs made electrochemical activation challenging.[28] Direct activation of the CTAs was not successful, because the reduction potentials of CTAs are so negative that the generated radical could be further reduced to anion; thus, no long-lived radicals are generated.[29] Alternatively, electrolysis of external initiators (benzoyl peroxide and 4-bromobenzenediazonium tetrafluoroborate) generated radicals, but with limited efficiency due to poor coulombic efficiency or electrodeposition of nonconductive layers on the working electrode.[28]

An alternative way to obtain an *e*RAFT polymerization is to activate RAFT agent by electroreduction of copper complexes, as in the electrochemically ATRP (*e*ATRP) procedure. *e*ATRP is one of the most robust approaches to electrochemically mediate an RDRP; it has been applied to different catalysts,[30-33] monomers,[11, 34] polymer architectures,[35-36] and polymer-inorganic hybrids.[37-40] *e*ATRP does not require external reagents, achieves temporal control,[41] and the copper catalyst can be electrodeposited and recycled.[42] Recently, *e*ATRP was conducted in the presence of RAFT agents as supplemental control agents; the control over MW and $Đ$ was efficient even with only 10 ppm of Cu catalyst.[43] However, the CTA contributed to improving polymerization control, but it was not directly activated by the ATRP catalyst due to too strong C-S bond of the employed CTA, 2-(dodecylthiocarbonothioylthio)-2-methylpropionic acid (DDMAT).

In this paper, the RAFT agent 1-cyano-1-methylethyldiethyl dithiocarbamate (MANDC), was directly activated by electrochemically-generated Cu^{I}, which led to well-defined polymers. The electrochemical properties of the catalytic system were analyzed, the key parameters in polymerization were examined, and the mechanism, kinetic features, and chain-end functionality were investigated.

11.3. Results and Discussion

Electrochemical studies. The cyclic voltammogram (CV) of the ATRP catalyst $Cu(DC)_2$/bpy showed good reversibility, as typical for ATRP catalysts (**错误!未找到引用源。**). The half-wave potential, $E_{1/2} = (E_{pc}+E_{pa})/2$, where E_{pc} and E_{pa} correspond to the cathodic and anodic peak potential, was −0.50 V vs. SCE. This value is more negative than

for traditional ATRP catalysts, [32] and suggests that DC binds strongly to Cu^{II} compared to Cu^{I}.[8] The bulky DC^- made a stable complex with Cu in the presence of only one equivalent of bpy ligand, i.e. when the coordination number was lower than 5.[8] Upon addition of MANDC, the cathodic peak increased due to the electrocatalytic activation of MANDC by Cu^{I}(DC)/bpy, which regenerated Cu^{II}. In the absence of Cu complexes, MANDC was reduced at the working electrode at a very negative potential, E_{pc} = -2.0 V vs SCE (**错误!未找到引用源。**); therefore, the Cu catalyst can be reduced without interference.

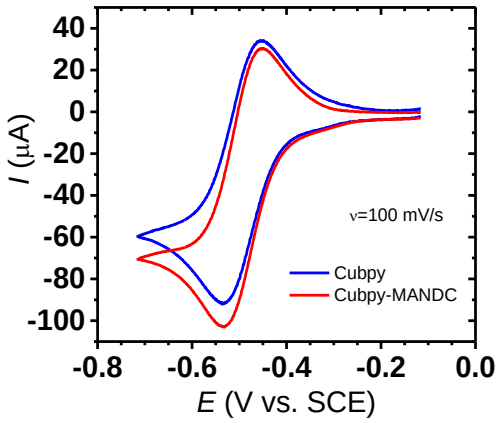

Figure 11-1. CV of the $Cu(DC)_2$ and MANDC. Conditions: [MMA]/[MANDC]/[$CuDC_2$]/[bpy] = 200/1/0.2/0.2; [MMA] = 4.67 M in DMF (50 % by volume); [*n*-Bu_4NClO_4] = 0.1 M, *T* = 80 ºC, WE = Pt disk, CE = Pt foil, RE = SCE.

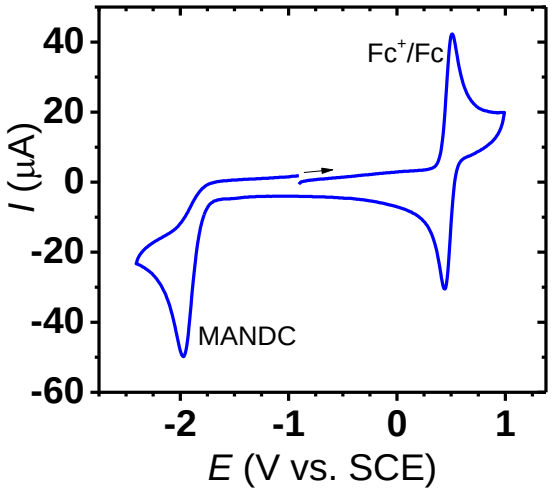

Figure 11-2. Cyclic voltammetry of 2 mM MANDC and 2 mM ferrocene in DMF + 0.1 M *n*-Bu_4NPF_6 at a Pt electrode at room temperature. Scan rate = 0.2 V s^{-1}. The potentials have been referred to SCE by using the conversion factor $E^o(Fc^+/Fc)$ = 0.475 V vs SCE.

Application of an electrolysis potential $E_{app} = E_{pc}$ of $Cu(DC)_2$/bpy in the presence of MMA and MANDC ([MMA]/[MANDC]/ $[Cu(DC)_2]$/[bpy] = 200/1/0.2/0.2) led to poly(methyl methacrylate) (PMMA) with low *Đ* (错误!未找到引用源。, entry 1). The MW of PMMA agreed with the theoretical value predicted by the ratio of consumed monomer to MANDC ($M_{n,th}$ = [MMA]/[MANDC] × conversion + M_{MANDC}).

However, dithiocarbamates can mediate an RDRP via multiple pathways, including photoiniferter polymerization,[14] RAFT polymerization,[44] or ATRP.[13] To understand the role of MANDC, two control experiments were conducted. First, the electrochemical activation of MANDC was repeated in the dark (错误!未找到引用源。). Nearly identical results were obtained, thus the contribution of the photoiniferter mechanism was excluded. Another experiment was the polymerization of MMA in the presence of azobisisobutyronitrile (AIBN) and MANDC (错误!未找到引用源。). The

polymerization resulted in low conversion, high MW, and high *Đ*, due to the low activity and slow chain transfer of the dithiocarbamate in the polymerization of MMA.[45] Therefore, the well-controlled polymerization of MMA, initiated by MANDC under electrolysis of copper complex, should be attributed to pseudohalide-based *e*ATRP (错误!未找到引用源。).

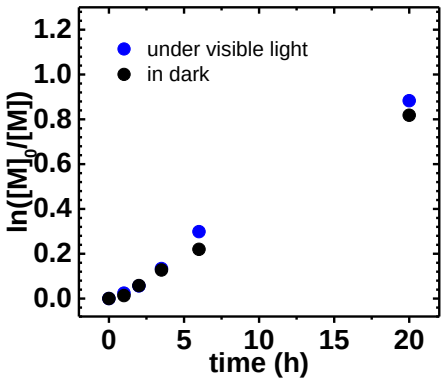

Figure 11-3. Semilogarithmic kinetic plots for *e*ATRP of MMA under ambient light (blue) and in dark (black, the whole system was covered with Al foil). [MMA]/[MANDC]/[$Cu(DC)_2$]/[bpy] = 200/1/0.2/0.2, [MMA] = 4.67 M in DMF (50 % by volume); [*n*-Bu_4NClO_4] = 0.1 M, *T* = 80 ºC, WE = Pt mesh, CE = Pt foil (separated), RE = Ag/AgI/I^-, $E_{app} = E_{pc}$ of $Cu(DC)_2$/bpy, *t* = 20 h.

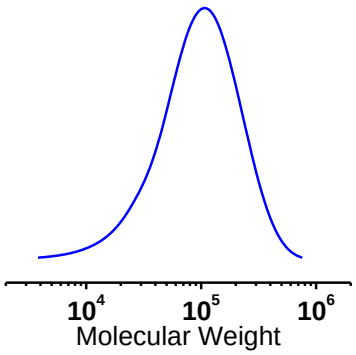

Figure 11-4. GPC trace for PMMA synthesized by thermoinitiated RAFT polymerization using MANDC as chain-transfer agent (CTA). [MMA]/[MANDC]/[AIBN] = 200/1/0.2, [MMA] = 4.67 M in DMF (50 % by volume); *T* = 80 ºC, *t* = 4 h.

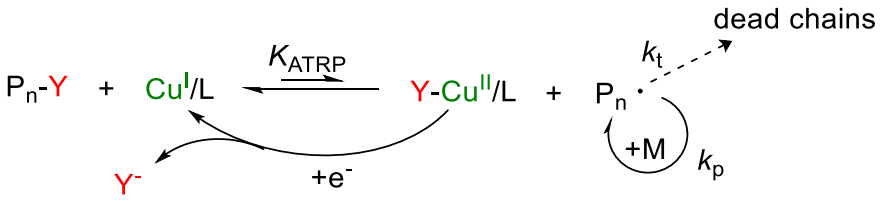

Scheme 11-1. Proposed mechanism of *e*ATRP with pseudohalides.

*e*ATRP of MMA using MANDC

Influence of applied potentials

Three different applied potentials were used for the electropolymerization of MMA/MANDC with $Cu(DC)_2$ (错误!未找到引用源。, entries 1-3 and 错误!未找到引用源。). Higher rates were observed at more negative potentials. The rate of polymerization in *e*ATRP is defined by the following equation:

$$R_p = k_p K_{ATRP}[RX][M]\frac{[Cu^IL^+]}{[XCu^{II}L^+]} \qquad (1)$$

where $[XCu^{II}L]/[XCu^IL]$ close to the surface of the working electrode is determined by Nernst equation:

$$E_{app} = E^o + \frac{RT}{F}\ln\frac{[XCu^{II}L]}{[XCu^IL]} \qquad (2)$$

where E^o is the standard reduction potential of the catalyst, R is the gas constant, and F is the Faraday constant. When a more negative potential was applied, the $[XCu^IL^+]/[XCu^{II}L^+]$ ratio was higher, leading to faster activation and higher radical concentration, and thus to faster polymerization. (XCu^IL quickly releases X^- generating the active Cu^IL^+ complex).

Table 11-1. *e*ATRP of MMA using MANDC as pseodohalide using various E_{app}s.

Entry[a]	Cu source	E_{app} (V vs. SCE)	*Time* (h)	Q[b] (C)	Conv.[c] (%)	k_p^{app} [d] (h^{-1})	$M_{n,th}$[e] ($\times 10^{-3}$)	$M_{n,app}$[f] ($\times 10^{-3}$)	$Đ$
1	$CuDC_2$	-0.50 ($E_{1/2}$)	20	-16.5	46	0.032	9.5	8.6	**1.29**
2	$CuDC_2$	-0.56 (E_{pc})	20	-30.2	59	0.044	12.0	11.9	**1.28**
3	$CuDC_2$	-0.60 (E_{pc} – 40 mV)	20	-69.8	70	0.061	14.3	14.6	**1.36**
4	$Cu(OTf)_2$	0.06 (E_{pc})	20	-14.9	46	0.039	9.4	8.2	**1.30**
5	$Cu(OTf)_2$	-0.56 (E_{pc})[f]	6	-24.5	93	0.446	18.8	13.0	**1.32**
6	$CuBr_2$	0.06 (E_{pc})	20	-12.8	<5	----	----	----	**----**
7	$CuBr_2$	-0.56 (E_{pc})[f]	5	-26.4	91	0.422	18.4	15.7	**1.40**
8	**$CuBr_2$**	**-0.96 ($E_{pc,2}$)[g]**	**5**	**-33.1**	**<5**	**----**	**----**	**----**	**----**

[a][MMA]/[MANDC]/[$Cu(DC)_2$]/[bpy] = 200/1/0.2/0.2, [MMA] = 4.67 M in DMF (50 % by volume); [*n*-Bu_4NClO_4] = 0.1 M, T = 80 ºC, WE = Pt mesh, CE = Pt foil (separated from the reaction solution by a glass frit filled with tylose gel), RE = Ag/AgI/I^-. The RE was calibrated against the saturated calomel electrode (SCE) scale by measuring ΔE between a SCE and Ag/AgI/I^- at the beginning of each experiment. [b]Consumed charge determined from the chronoamperometry profile; [c]Determined by ^{1}H NMR; [d]The slope of the $\ln([M]_0/[M])$ versus time plot; [e]$M_{n,th} = [M]/([MANDC]) \times M_M \times$ conversion + M_{MANDC}; [f]Determined by THF GPC with PMMA standards. [f]E_{pc} of $CuDC_2$/bpy. [g]E_{pc} of the most negative peak.

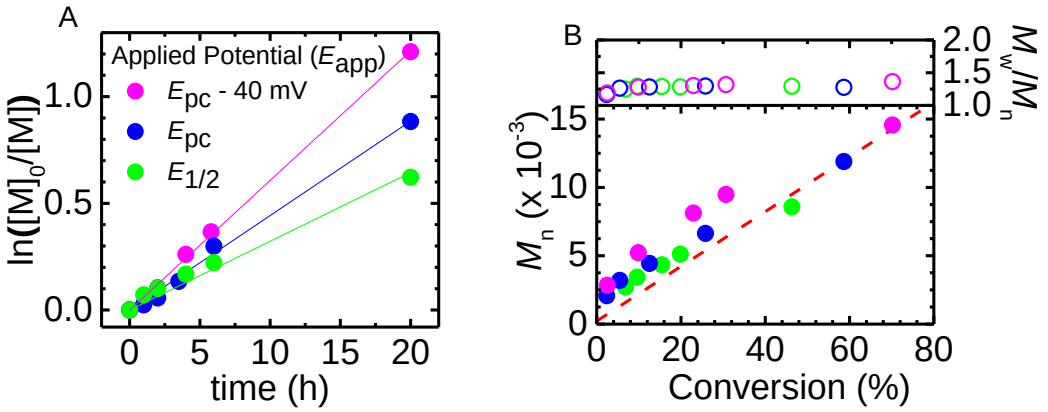

Figure 11-5. *e*ATRP of MMA with MANDC as initiator at various E_{app}s. Conditions: [MMA]/[MANDC]/ [$Cu(DC)_2$]/[bpy] = 200/1/0.2/0.2, [MMA] = 4.67 M in DMF (50 % by volume); [*n*-Bu_4NClO_4] = 0.1 M, T = 80 ºC, WE = Pt mesh, t = 20 h.

The MW of the final polymers agreed well with the theoretical prediction. However, the MW were slightly higher than expected at low conversion, especially when the most negative potential was used. Application of a negative potential led to lower [Cu^{II}], which gave slow deactivation and thus MW higher than expected. The low frequency of deactivation led also to higher *Đ*.

Influence of Type of Cu Source

The structure of the ternary Cu complex, $[X–Cu(bpy)]^+$, influences the polymerization greatly due to the different relative affinity of Cu to X^- and the different stability of the C-X chain end. The dithiocarbamate anion released by the activation of MANDC may substitute the original counterion of the Cu complex and form a new deactivator, $[DC–Cu(bpy)]^+$, which has a very negative reduction potential (**错误!未找到引用源。**A). As discussed above, the reduction of $CuDC_2$ was fully reversible, where $[DC–Cu(bpy)]^+$ is a well-defined and stable complex. The non-coordinating trifluoromethanesulfonate anion (OTf^-) generated the binary complex $[Cu(bpy)]^{2+}$, which was also reversible but rather ill-shaped (**错误!未找到引用源。**B). The system $CuBr_2$/bpy had a more complex redox behavior, with multiple peaks that could be due to the presence of multiple species in solution including [$Cu^{II}Br_2$/bpy], $[Cu^{II}Br/bpy]^+$, $[Cu^{II}/bpy]^{2+}$, etc (**错误!未找到引用源。**C).

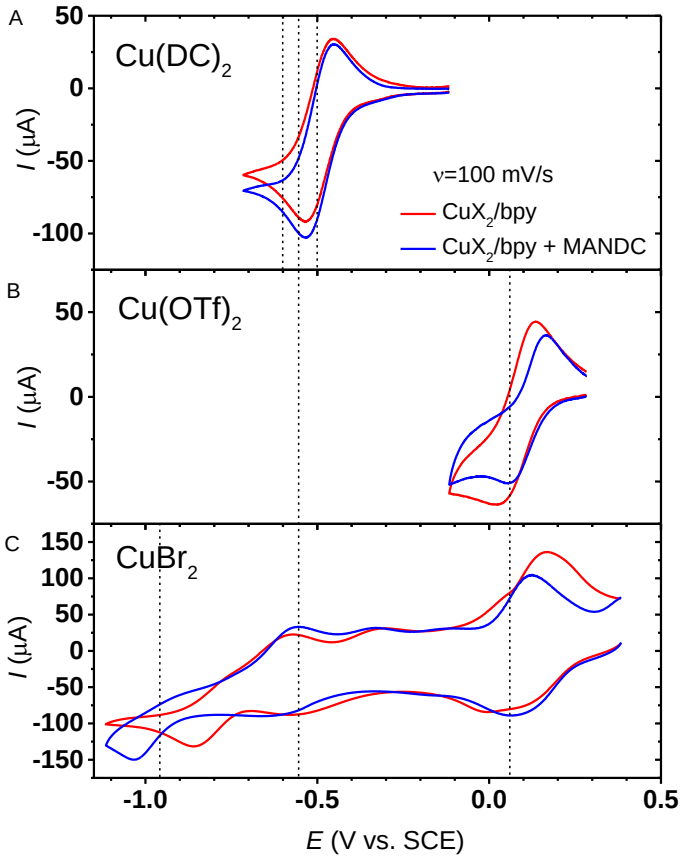

Figure 11-6. CV of various Cu salts and MANDC. A) $Cu(DC)_2$; B) $Cu(OTf)_2$; C) $CuBr_2$. Conditions: [MMA]/[MANDC]/[Cu salt]/[bpy] = 200/1/0.2/0.2; [MMA] = 4.67 M in DMF (50 % by volume); [*n*-Bu_4NClO_4] = 0.1 M, *T* = 80 ºC, WE = Pt disk. The vertical dashed lines represent the potentials applied during electrolysis.

错误!未找到引用源。 summarizes the results of a series of polymerizations using Cu/bpy complexes with different counterions and applied potentials. Using $Cu(DC)_2$ as the source of catalyst generated $[DC–Cu(bpy)]^+$ as the only deactivator. Polymerization gave linear kinetics as well as sufficiently low dispersity at each applied potential, as discussed above (**错误!未找到引用源。**, entries 1-3).

Then, the non-coordinating anion OTf^- was investigated (**错误!未找到引用源。**, entries 4-5). At $E_{app} = E_{pc}$ of the obtained $[Cu(bpy)]^{2+}$ complex (+0.06 V vs SCE), the polymerization gradually slowed down, reaching only 46% conversion in 20 h. During polymerization, some Cu species can be complexed by DC^-, generating a complex with a much more negative reduction potential, $[DC–Cu(bpy)]^+$, which is not reduced at +0.06 V vs SCE. On the other hand, at E_{app} = -0.56 V, all copper complexes present in solution could be reduced, and the much higher Cu^I/Cu^{II} ratio lead to faster polymerization, without sacrificing control over MW. Thus, application of a negative potential is an efficient approach to electrochemically synthesize polymers with pseudohalide chain end starting from $Cu(OTf)_2$/bpy.

Use of $CuBr_2$ as source of catalyst gave similar results to $Cu(OTf)_2$. Application of a positive $E_{app} = E_{pc}$ of the initially formed complex (+0.06 V vs SCE) gave little to no conversion after 20 h. The higher affinity of Cu to pseudohalogen than to bromine led to the transformation of $[Br–Cu(bpy)]^+$ to $[DC–Cu(bpy)]^+$, with a negative shift of reduction potential. Conversely, conducting polymerization at the E_{pc} of $[DC–Cu(bpy)]^+$ (-0.56 V vs SCE) led to almost full reduction of the complex. However, $Đ$ = 1.4 was relatively high, indicating that $CuBr_2$ is not a suitable source of copper, probably due to the complex speciation ensuing from the presence of both Br^- and pseudohalide counterions (**错误!未找到引用源。**C). When a more negative potential (-0.96 V vs SCE) was selected, no polymer was detected because methacrylate propagating radicals were directly reduced to anions at E = -0.91 V vs SCE.[29]

Influence of Cu Loading

*e*ATRP with dithiocarbamate chain end was conducted in the presence of various catalyst concentrations. The polymerization rate remained constant with decreasing copper concentrations, within experimental error (错误!未找到引用源。, entries 1-3, 错误!未找到引用源。). This indicated that under vigorous stirring, the electrolysis quickly reached the equilibrium $[Cu^{I}]/[Cu^{II}]$ ratio, according to Equation (2), and then proceed with roughly constant rate.

Table 11-2. *e*ATRP of MMA using MANDC as pseudohalide with various catalyst concentrations and targeted DPs.

Entry[a]	Cu (ppm)	[MMA]/[MANDC]	Q[b] (C)	Conv.[c] (%)	k_p^{app}[d] (h^{-1})	$M_{n,th}$[e] ($\times10^{-3}$)	$M_{n,app}$[f] ($\times10^{-3}$)	$Đ$
1	1000	200	-30.22	59	0.044	12.0	11.9	1.28
2	750	200	-56.06	66	0.055	13.5	13.8	1.33
3	500	200	-43.59	73	0.064	14.8	14.3	1.31
4	1000	100	-71.34	71	0.060	7.4	8.5	1.32
5	1000	400	-49.66	37	0.024	15.2	12.1	1.21

[a] [MMA] = 4.67 M in DMF (50 % by volume); $[Cu(DC)_2]/[bpy]$ = 1/1, $[n\text{-}Bu_4NClO_4]$ = 0.1 M, T = 80 ºC, WE = Pt mesh, $E_{app} = E_{pc}$, t = 20 h.

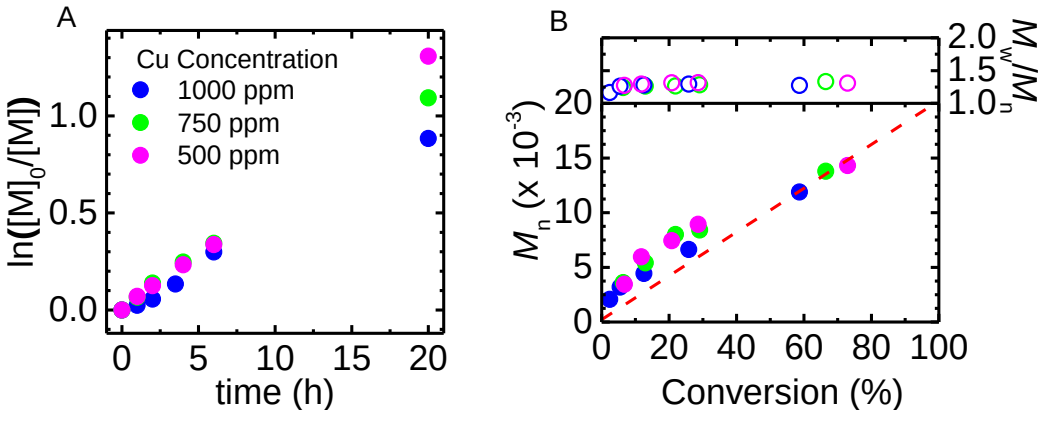

Figure 11-7. *e*ATRP of MMA using MANDC using various catalyst concentrations. (A) Semilogarithmic kinetics; (B) evolution of MW and dispersity with conversion. Conditions: [MMA]/[MANDC] = 200/1, [MMA] = 4.67 M in DMF (50 % by volume); $[Cu(DC)_2]/[bpy]$ = 1/1, $[n\text{-}Bu_4NClO_4]$ = 0.1 M, T = 80 ºC, WE = Pt mesh, $E_{app} = E_{pc}$, t = 20 h.

Influence of Targeted Degree of Polymerization (DP)

The amount of MANDC was varied to target different degrees of polymerization (DPs). Fixing the catalyst concentration at 1000 ppm with respect to monomer, and the applied potential at -0.56 V vs SCE, the conversion after 20 h was 71, 59 and 37% for DP = 100, 200 and 400, respectively (错误!未找到引用源。, entries 1, 4 and 5, 错误!未找到引用源。). For a lower targeted DP, i.e., higher MANDC amount, the overall rate of polymerization was higher as expected from Equation (1).

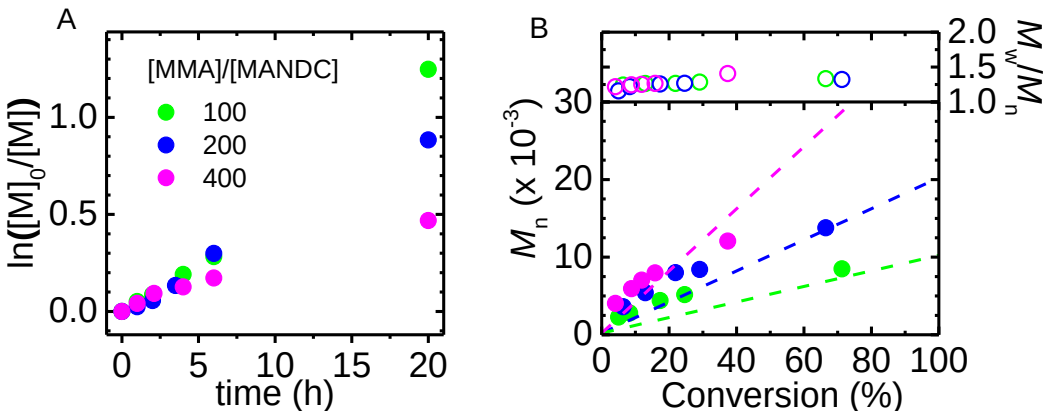

Figure 11-8. *e*ATRP of MMA using MANDC using various [MMA]/[MANDC] ratios. (A) Semilogarithmic kinetics; (B) evolution of MW and dispersity with conversion. Conditions: [MMA]/[$Cu(DC)_2$]/[bpy] = 1000/1/1, [MMA] = 4.67 M in DMF (50 % by volume); [*n*-Bu_4NClO_4] = 0.1 M, T = 80 ºC, WE = Pt mesh, $E_{app} = E_{pc}$, t = 20 h.

Chain Extension

The chain-end functionality of the obtained PMMA was investigated by extending it with different monomers. A PMMA-DC macroinitiator (M_n = 4,100, $Đ$ =1.28) was synthesized via *e*ATRP from MANDC, isolated, and chain-extended with *n*-butyl methacrylate (BMA).

A clean shift of GPC traces was observed (错误!未找到引用源。A), and the block copolymer had M_n = 15,700 and $Đ$ =1.28. Moreover, the macroinitiator was chain extended with styrene (Sty), obtaining a block copolymer with M_n = 10,800 and $Đ$ =1.24 (错误!未找到引用源。B). These experiments demonstrate that the PMMA synthesized by dithiocarbamate-based *e*ATRP had a high degree of chain-end functionality.

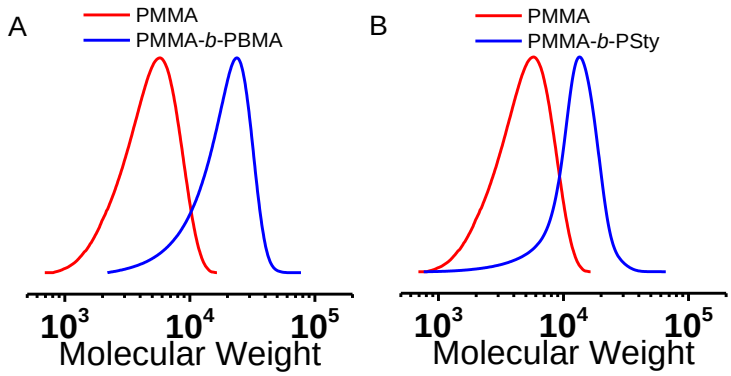

Figure 11-9. Chain extension from PMMA MI by ATRP. (A) *e*ATRP of BMA. [BMA]/[PMMA-DC]/[$Cu(DC)_2$]/[bpy] = 150/1/0.2/0.2, [BMA] = 3.14 M in DMF (50 % by volume); [*n*-Bu_4NClO_4] = 0.1 M, T = 80 ºC, WE = Pt mesh, CE = Pt foil (separated), RE = Ag/AgI/I^-, E_{app} = E_{pc}, t = 20 h. (B) Normal ATRP of Sty. [Sty]/[PMMA-DC]/[CuBr]/[PMDETA] = 200/1/1/1, [Sty] = 4.36 M in DMF (50 % by volume); T = 120 ºC, t = 4 h.

11.4. Conclusion

*e*ATRP of methacrylates was conducted *via* electrochemical activation of a dithiocarbamate with Cu catalysts. The rate of polymerization was tuned by varying the applied potentials and the nature of the employed Cu salt. Specifically, using non-coordinating anion OTf^- led to fast polymerization without sacrificing degree of control, while using Br^- required careful selection of applied potential and generally gave a less

controlled polymerization. Well-defined PMMA was synthesized with 500 ppm of catalyst and various targeted DPs. The PMMA macroinitiator was extended by methacrylates and styrene, demonstrating high chain-end fidelity.

Electrochemical activation of CTAs is challenging due to the high BDE and relatively negative reduction potential. Although this polymerization proceeded via an ATRP mechanism, instead of a RAFT mechanism, it opens the possibility for the electrochemical activation of RAFT agents, for new pathways to electrochemical control a RAFT reaction, and potentially to link *e*ATRP and *e*RAFT reactions in a one-pot approach. These topics are currently under investigation in our laboratory.

11.5. Experimental Section

Materials

Copper(II) bromide ($Cu^{II}Br_2$, 99%), copper(II) trifluoromethanesulfonate ($Cu^{II}(OTf)_2$, 98%), 2,2'-bipyridyne (bpy, 99%), *N*,*N*,*N*',*N*'',*N*''-pentamethyldiethylenetriamine (PMDETA, 99%) and *N,N'*-dimethylformamide (DMF, 99%) were purchased from Sigma-Aldrich. Copper(II) diethyldithiocarbamate ($Cu^{II}(DC)_2$, 98%) was purchased from TCI. Tetrabutylammonium perchlorate (*n*-Bu_4NClO_4, 99%) was purchased from Alfa Aesar. All the above mentioned chemicals were used as received. Copper (I) bromide ($Cu^{I}Br$, 98%) was purchased from Sigma-Aldrich and purified according to literature.[46] MANDC was synthesized following a published procedure.[13] Methyl methacrylate (MMA, 99%, Aldrich) was passed through a column filled with basic alumina prior to use to remove polymerization inhibitors.

Cyclic voltammetry (CV)

23 mM (0.152 g, 0.7 mmol) $Cu(DC)_2$ was dissolved in 30 mL of DMF/MMA 50:50 v/v under N_2 flow. 0.1 M of *n*-Bu_4NClO_4 (1.03 g, 3 mmol) was used as a supporting electrolyte. CV spectra were recorded at a Pt disk working electrode (WE) with a Pt wire counter electrode (CE) and a Ag/AgI/I^- reference electrode (RE). Scan rate (v) was 100 mV/s. The RE was calibrated against the saturated calomel electrode (SCE) scale by measuring ΔE between a SCE. or by using ferrocene as internal standard.

***e*ATRP of MMA**

n-Bu_4NClO_4 (1.03 g, 3 mmol), $Cu(DC)_2$ (0.015 g, 0.06 mmol) and bpy (0.020 g, 0.06 mmol) were placed in a five-neck electrolysis cell maintained at 80 °C under a slow N_2 purge. Then, 15 mL of N_2 purged MMA (140 mmol), 15 mL of N_2 purged DMF and 0.152 g of MANDC (0.7 mmol) were added to the reaction. A CV was recorded at 100 mV/s with this electrode setup: a Pt disk WE; a Pt wire CE separated from polymerization mixture by a glass frit filled with tylose gel (saturated with Et_4NPF_6); a Ag/AgI/I^- RE. To ensure the reproducible application of E_{app}, the potential of Ag/AgI/I^- vs. SCE was measured with a voltmeter before the beginning of the polymerization. The Pt mesh electrode was then used as the working electrode for the polymerization. Appropriate potential was applied. Samples were withdrawn periodically to follow the monomer conversion by ^{1}H NMR, while M_n and M_w/M_n were determined by GPC. The theoretical MW was calculated as $M_{n,th}$ = [M]/[MANDC] × MW_M × conversion + MW_{MANDC}.

Synthesis and Purification of PMMA Macroinitiator (PMMA-DC)

n-Bu_4NClO_4 (1.03 g, 3 mmol), $Cu(DC)_2$ (0.050 g, 0.14 mmol) and bpy (0.020 g, 0.14 mmol) were placed in a five-neck electrolysis cell maintained at 80 °C under a slow N_2 purge. Then, 15 mL of N_2 purged MMA (140 mmol), 15 mL of N_2 purged DMF and 0.30 g of MANDC (1.4 mmol) were added to the reaction. A CV was recorded at 100 mV/s with this electrode setup: a Pt disk WE; a Pt wire CE separated from polymerization mixture by a glass frit filled with tylose gel (saturated with Et_4NPF_6); a $Ag/AgI/I^-$ RE. To ensure reproducible application of E_{app}, the potential of $Ag/AgI/I^-$ vs. SCE was measured with a voltmeter before the beginning of the polymerization. The Pt mesh electrode was then used as the working electrode for the polymerization. The polymerization was conducted under the half-wave potential of $Cu(DC)_2$/bpy. Samples were withdrawn periodically to follow the monomer conversion by ^1H NMR, while M_n and M_w/M_n were determined by GPC. The theoretical MW was calculated as $M_{n,th} = [M]/[MANDC] \times MW_M \times \text{conversion} + MW_{MANDC}$. The reaction was quenched upon exposure to air. Then the reaction mixture was precipitated into hexane three times, and the PMMA-DC (M_n = 4,000, $Đ$ = 1.28) was dried under vacuum.

Chain Extension of PMMA-DC

Synthesis of PMMA-*b*-PBMA by *e*ATRP. *n*-Bu_4NClO_4 (0.27 g, 0.8 mmol), $Cu(DC)_2$ (0.012 g, 0.03 mmol), bpy (0.005 g, 0.03 mmol) and PMMA-DC (0.67 g, 0.17 mmol) were placed in a five-neck electrolysis cell maintained at 80 °C under a slow N_2 purge. Then, 4 mL of N_2 purged BMA (25.1 mmol) and 4 mL of N_2 purged DMF were added to the reaction. A CV was recorded at 100 mV/s with this electrode setup: a Pt disk WE; a Pt wire CE separated from polymerization mixture by a glass frit filled with tylose gel (saturated with Et_4NPF_6); a $Ag/AgI/I^-$ RE. To ensure reproducible application of E_{app},

the potential of Ag/AgI/I^- vs. SCE was measured with a voltmeter before the beginning of the polymerization. The Pt mesh electrode was then used as the working electrode for the polymerization. The polymerization was conducted under the half-wave potential of $Cu(DC)_2$/bpy.

Synthesis of PMMA-*b*-PSty by normal ATRP. CuBr (0.031 g, 0.09 mmol), PMDETA (0.018 mL, 0.09 mmol) and PMMA-DC (0.67 g, 0.17 mmol) were placed in Schlenk flask. Then, 2 mL of MMA (25.1 mmol) and 2 mL of DMF were added to the flask. A brown solution was obtained after stirring under room temperature. The mixture underwent three freeze-pump-thaw cycles to remove oxygen. Then the flask was sealed and immersed to 120 °C oil bath for 4 h, and the polymerization was quenched by exposure to the air.

Polymer Characterization

Conversion was calculated by detecting the decrease of the monomer peak area relative to the peak area of the internal standards. ^{1}H NMR spectroscopy for polymerization monitoring was performed using a Bruker Advance 300 MHz NMR spectroscope with $CDCl_3$ as a solvent. Number-average molecular weight ($M_{n,app}$) and molecular weight distribution ($Đ = M_w/M_n$) were determined by GPC equipped with a Waters 515 pump and Wyatt r-Ex differential refractometer using Polymer Standards Services (PSS) columns (guard, 10^5, 10^3, and 500 Å), with THF as eluent at a flow rate 1.00 mL/min (T = 35 °C). GPC traces were processed by WinGPC 8.0 software (PSS) using a calibration based on linear PMMA standards.

11.6. References

(1) Garcia-Valdez, O.; Champagne, P.; Cunningham, M. F., Graft Modification of Natural Polysaccharides via Reversible Deactivation Radical Polymerization. *Prog Polym Sci* **2018,** *76*, 151-173.
(2) Pearson, S.; St Thomas, C.; Guerrero-Santos, R.; D'Agosto, F., Opportunities for Dual RDRP Agents in Synthesizing Novel Polymeric Materials. *Polym Chem-Uk* **2017,** *8* (34), 4916-4946.
(3) Matyjaszewski, K., Atom Transfer Radical Polymerization (ATRP): Current Status and Future Perspectives. *Macromolecules* **2012,** *45* (10), 4015-4039.
(4) Moad, G.; Rizzardo, E.; Thang, S. H., Living Radical Polymerization by the RAFT Process - A third update. *Aust J Chem* **2012,** *65* (8), 985-1076.
(5) Matyjaszewski, K.; Tsarevsky, N. V., Macromolecular Engineering by Atom Transfer Radical Polymerization. *J Am Chem Soc* **2014,** *136* (18), 6513-6533.
(6) Matyjaszewski, K., Advanced Materials by Atom Transfer Radical Polymerization. *Advanced Materials* **2018,** *30*, 1706441.
(7) Lanzalaco, S.; Fantin, M.; Scialdone, O.; Galia, A.; Isse, A. A.; Gennaro, A.; Matyjaszewski, K., Atom Transfer Radical Polymerization with Different Halides (F, Cl, Br, and I): Is the Process "Living" in the Presence of Fluorinated Initiators? *Macromolecules* **2017,** *50* (1), 192-202.
(8) Fantin, M.; Lorandi, F.; Gennaro, A.; Isse, A. A.; Matyjaszewski, K., Electron Transfer Reactions in Atom Transfer Radical Polymerization. *Synthesis-Stuttgart* **2017,** *49* (15), 3311-3322.
(9) Shipp, D. A.; Wang, J. L.; Matyjaszewski, K., Synthesis of Acrylate and Methacrylate Block Copolymers using Atom Transfer Radical Polymerization. *Macromolecules* **1998,** *31* (23), 8005-8008.
(10) Peng, C. H.; Kong, J.; Seeliger, F.; Matyjaszewski, K., Mechanism of Halogen Exchange in ATRP. *Macromolecules* **2011,** *44* (19), 7546-7557.
(11) Fantin, M.; Isse, A. A.; Venzo, A.; Gennaro, A.; Matyjaszewski, K., Atom Transfer Radical Polymerization of Methacrylic Acid: A Won Challenge. *J Am Chem Soc* **2016,** *138* (23), 7216-7219.
(12) Matyjaszewski, K.; Xia, J. H., Atom Transfer Radical Polymerization. *Chem Rev* **2001,** *101* (9), 2921-2990.
(13) Kwak, Y.; Matyjaszewski, K., Effect of Initiator and Ligand Structures on ATRP of Styrene and Methyl Methacrylate Initiated by Alkyl Dithiocarbamate. *Macromolecules* **2008,** *41* (18), 6627-6635.
(14) Kwak, Y.; Matyjaszewski, K., Photoirradiated Atom Transfer Radical Polymerization with an Alkyl Dithiocarbamate at Ambient Temperature. *Macromolecules* **2010,** *43* (12), 5180-5183.
(15) Nicolay, R.; Kwak, Y.; Matyjaszewski, K., Dibromotrithiocarbonate Iniferter for Concurrent ATRP and RAFT Polymerization. Effect of Monomer, Catalyst, and Chain Transfer Agent Structure on the Polymerization Mechanism. *Macromolecules* **2008,** *41* (13), 4585-4596.

(16) Singha, N. K.; German, A. L., Pseudohalogens in Atom Transfer Radical Polymerization of Methyl Methacrylate. *J Appl Polym Sci* **2007,** *103* (6), 3857-3864.
(17) Davis, K. A.; Matyjaszewski, K., Effect of (Pseudo)halide Initiators and Copper Complexes with Non-Halogen Anions on the Atom Transfer Radical Polymerization. *J Macromol Sci Pure* **2004,** *A41* (5), 449-465.
(18) Kwak, Y.; Nicolay, R.; Matyjaszewski, K., Synergistic Interaction Between ATRP and RAFT: Taking the Best of Each World. *Aust J Chem* **2009,** *62* (11), 1384-1401.
(19) Elsen, A. M.; Nicolay, R.; Matyjaszewski, K., Dual Concurrent ATRP/RAFT of Methyl Acrylate Co-initiated by Alkyl Halides. *Macromolecules* **2011,** *44* (7), 1752-1754.
(20) Kwak, Y.; Nicolay, R.; Matyjaszewski, K., Concurrent ATRP/RAFT of Styrene and Methyl Methacrylate with Dithioesters Catalyzed by Copper(I) Complexes. *Macromolecules* **2008,** *41* (18), 6602-6604.
(21) Nicolay, R.; Kwak, Y.; Matyjaszewski, K., A Green Route to Well-Defined High-Molecular-Weight (Co)polymers Using ARGET ATRP with Alkyl Pseudohalides and Copper Catalysis. *Angew Chem Int Ed* **2010,** *49* (3), 541-544.
(22) Martin, L.; Gody, G.; Perrier, S., Preparation of Complex Multiblock Copolymers via Aqueous RAFT Polymerization at Room Temperature. *Polym Chem-Uk* **2015,** *6* (27), 4875-4886.
(23) Barner, L.; Quinn, J. F.; Barner-Kowollik, C.; Vana, P.; Davis, T. P., Reversible Addition-Fragmentation Chain Transfer Polymerization Initiated with Gamma-Radiation at Ambient Temperature: an Overview. *Eur Polym J* **2003,** *39* (3), 449-459.
(24) Tasdelen, M. A.; Durmaz, Y. Y.; Karagoz, B.; Bicak, N.; Yagci, Y., A New Photoiniferter/RAFT Agent for Ambient Temperature Rapid and Well-Controlled Radical Polymerization. *J Polym Sci Pol Chem* **2008,** *46* (10), 3387-3395.
(25) Xu, J. T.; Jung, K.; Atme, A.; Shanmugam, S.; Boyer, C., A Robust and Versatile Photoinduced Living Polymerization of Conjugated and Unconjugated Monomers and Its Oxygen Tolerance. *J Am Chem Soc* **2014,** *136* (14), 5508-5519.
(26) Peterson, B. M.; Lin, S.; Fors, B. P., Electrochemically Controlled Cationic Polymerization of Vinyl Ethers. *J Am Chem Soc* **2018,** *140* (6), 2076-2079.
(27) Uchiyama, M.; Satoh, K.; Kamigaito, M., Cationic RAFT Polymerization Using ppm Concentrations of Organic Acid. *Angew Chem Int Ed* **2015,** *54* (6), 1924-1928.
(28) Wang, Y.; Fantin, M.; Park, S.; Gottlieb, E.; Fu, L. Y.; Matyjaszewski, K., Electrochemically Mediated Reversible Addition-Fragmentation Chain-Transfer Polymerization. *Macromolecules* **2017,** *50* (20), 7872-7879.
(29) Lin, C. Y.; Coote, M. L.; Gennaro, A.; Matyjaszewski, K., Ab Initio Evaluation of the Thermodynamic and Electrochemical Properties of Alkyl Halides and Radicals and their Mechanistic Implications for Atom Transfer Radical Polymerization. *J Am Chem Soc* **2008,** *130* (38), 12762-12774.
(30) Magenau, A. J. D.; Strandwitz, N. C.; Gennaro, A.; Matyjaszewski, K., Electrochemically Mediated Atom Transfer Radical Polymerization. *Science* **2011,** *332* (6025), 81-84.
(31) Guo, J. K.; Zhou, Y. N.; Luo, Z. H., Kinetic Insights into the Iron-Based Electrochemically Mediated Atom Transfer Radical Polymerization of Methyl Methacrylate. *Macromolecules* **2016,** *49* (11), 4038-4046.

(32) Chmielarz, P.; Fantin, M.; Park, S.; Isse, A. A.; Gennaro, A.; Magenau, A. J. D.; Sobkowiak, A.; Matyjaszewski, K., Electrochemically Mediated Atom Transfer Radical Polymerization (eATRP). *Prog Polym Sci* **2017,** *69*, 47-78.
(33) Guo, J. K.; Zhou, Y. N.; Luo, Z. H., Iron-Based Electrochemically Mediated Atom Transfer Radical Polymerization with Tunable Catalytic Activity. *Aiche J* **2018,** *64* (3), 961-969.
(34) Chmielarz, P.; Park, S.; Simakova, A.; Matyjaszewski, K., Electrochemically Mediated ATRP of Acrylamides in Water. *Polymer* **2015,** *60*, 302-307.
(35) Park, S.; Cho, H. Y.; Wegner, K. B.; Burdynska, J.; Magenau, A. J. D.; Paik, H. J.; Jurga, S.; Matyjaszewski, K., Star Synthesis Using Macroinitiators via Electrochemically Mediated Atom Transfer Radical Polymerization. *Macromolecules* **2013,** *46* (15), 5856-5860.
(36) Chmielarz, P.; Park, S.; Sobkowiak, A.; Matyjaszewski, K., Synthesis of Beta-Cyclodextrin-Based Star Polymers via a Simplified Electrochemically Mediated ATRP. *Polymer* **2016,** *88*, 36-42.
(37) Li, B.; Yu, B.; Huck, W. T. S.; Zhou, F.; Liu, W. M., Electrochemically Induced Surface-Initiated Atom-Transfer Radical Polymerization. *Angew Chem Int Ed* **2012,** *51* (21), 5092-5095.
(38) Li, B.; Yu, B.; Huck, W. T. S.; Liu, W. M.; Zhou, F., Electrochemically Mediated Atom Transfer Radical Polymerization on Nonconducting Substrates: Controlled Brush Growth through Catalyst Diffusion. *J Am Chem Soc* **2013,** *135* (5), 1708-1710.
(39) Chmielarz, P.; Krys, P.; Wang, Z. Y.; Wang, Y.; Matyjaszewski, K., Synthesis of Well-Defined Polymer Brushes from Silicon Wafers via Surface-Initiated seATRP. *Macromol Chem Phys* **2017,** *218* (11).
(40) Chmielarz, P.; Yan, J. J.; Krys, P.; Wang, Y.; Wang, Z. Y.; Bockstaller, M. R.; Matyjaszewski, K., Synthesis of Nanoparticle Copolymer Brushes via Surface-Initiated seATRP. *Macromolecules* **2017,** *50* (11), 4151-4159.
(41) Pan, X.; Fantin, M.; Yuan, F.; Matyjaszewski, K., Externally Controlled Atom Transfer Radical Polymerization. *Chem Soc Rev* **2018**.
(42) Magenau, A. J. D.; Bortolamei, N.; Frick, E.; Park, S.; Gennaro, A.; Matyjaszewski, K., Investigation of Electrochemically Mediated Atom Transfer Radical Polymerization. *Macromolecules* **2013,** *46* (11), 4346-4353.
(43) Wang, Y.; Fantin, M.; Matyjaszewski, K., Synergy between Electrochemical ATRP and RAFT for Polymerization at Low Copper Loading. *Macromol Rapid Comm* **2018**.
(44) Mayadunne, R. T. A.; Rizzardo, E.; Chiefari, J.; Chong, Y. K.; Moad, G.; Thang, S. H., Living Radical Polymerization with Reversible Addition-Fragmentation Chain Transfer (RAFT Polymerization) using Dithiocarbamates as Chain Transfer Agents. *Macromolecules* **1999,** *32* (21), 6977-6980.
(45) Chiefari, J.; Mayadunne, R. T. A.; Moad, C. L.; Moad, G.; Rizzardo, E.; Postma, A.; Skidmore, M. A.; Thang, S. H., Thiocarbonylthio Compounds (S=C(Z)S-R) in Free Radical Polymerization with Reversible Addition-Fragmentation Chain Transfer (RAFT polymerization). Effect of the Activating Group Z. *Macromolecules* **2003,** *36* (7), 2273-2283.
(46) Grimaud, T.; Matyjaszewski, K., Controlled/"Living" Radical Polymerization of Methyl Methacrylate by Atom Transfer Radical Polymerization. *Macromolecules* **1997,** *30* (7), 2216-2218.

Chapter 12 Summary and Outlook

The goal of this dissertation was to explore the application of atom transfer radial polymerization (ATRP) in aqueous dispersed systems and the application of electrochemical stimulus to reversible addition-fragmentation chain-transfer (RAFT) polymerization. In Chapter I, an overview of deactivation radical polymerization (RDRP), focusing on ATRP and RAFT as important RDRP methods, was presented. Recent progress on ATRP with catalyst regeneration and in dispersed media were discussed. The initiation modes in RAFT polymerization and the renaissance of electrochemical synthesis were introduced. Therefore, there was a need for systematic mechanism and kinetic studies in ATRP in dispersed media and electrochemically mediated RAFT polymerization, which is addressed in the following chapters.

Mechanistic studies on ATRP in dispersed media were presented in Chapters II – VI and Appendix I. Previously, miniemulsion activator regenerated by electron transfer (ARGET) ATRP was conducted using hydrophobic catalysts. However, solely the hydrophobic catalyst cannot be used in electrochemically mediated atom transfer radical polymerization (*e*ATRP) due to the physical disconnection of the organic phase and the working electrode. This challenge was addressed using a dual catalyst system, composed of a hydrophilic catalyst to shuttle the electrochemical stimulus and a hydrophobic catalyst to control the polymerization in the organic phase. The synergy of the two catalysts facilitated well-controlled polymerization of poly(*n*-butyl acrylate) (PBA).[1] Further study demonstrated miniemulsion *e*ATRP was successful using a single catalyst setup (Appendix I). A hydrophilic catalyst, Cu/TPMA (TPMA = tris(2-pyridylmethyl)amine) and an anionic surfactant, dodecyl sulfate (DS^-) was able to form an ion-pair and interfacial catalyst,

providing efficient control in miniemulsion and emulsion ATRP of acrylates and methacrylates. Chapter II employed the CuTPMA/DS^- ion-pair catalyst to miniemulsion ARGET ATRP, demonstrated the efficacy in the control of methacrylates and acrylates polymerization, as well as the synthesis of block, star and brush copolymers. The resulting polymers were collected by precipitation, and the remaining Cu content was below 1 ppm. *Ab initio* emulsion ATRP had requirements for initiation loci and catalyst transport to micelles, and thus was more challenging than miniemulsion ATRP. Chapter III addressed the challenges by optimization of the key reaction conditions: start stirring only at the beginning of the polymerization, and employing water-soluble initiators. Chapters IV and V explored photomediated ATRP in miniemulsion and emulsion, respectively. The influence of particle size and solids content to the kinetics were analyzed, and temporal control was achieved by switching the light on and off. Block and gradient copolymers were prepared. Chapter VI applied an enzyme-deoxygenation system to miniemulsion and emulsion ATRP.

Chapters VII and VIII explored the preparation of materials by miniemulsion ARGET ATRP discussed in Chapter II. Synthesis of block copolymers with high initiation efficiency and low dispersity requires polymerization of monomers generating more active chain ends. To achieve successful chain extension of a less active macroinitiator with a high activity monomer, halogen exchange was employed using equimolar amounts of initiator and Cu catalyst. Chapter VII discussed halogen exchange using a catalytic amount of Cu complex and an access of Cl^-, allowing synthesis of poly(*n*-butyl acrylate)-*b*-poly(methyl methacrylate) (PBA-*b*-PMMA) and PBA-*b*-PMMA-*b*-PBA. Chapter VII explored the synthesis of amphiphilic hairy nanoparticles. The hydrophobic crosslinked

nanoparticles were prepared by miniemulsion ATRP of *n*-butyl methacrylate in the presence of crosslinkers. Direct addition of a hydrophilic monomer, poly(ethylene glycol) methyl ether methacrylate (average molecular weight = 500, $OEOMA_{500}$), allowed grafting of hydrophilic polymer chains from the network. The POEOMA-grafted crosslinked nanoparticles were re-dispersed in water/methanol mixture and further modified with polyzwitterionic chains.

Chapters IX – XI employed electrochemical stimulus to mediated reversible activation-fragmentation chain-transfer (*e*RAFT) polymerization. Direct electrochemical activation of RAFT agents was not capable for a well-controlled RAFT polymerization due to the irreversible reduction and low reduction potential of RAFT agents. Chapter IX presented electrochemical reduction of a diazonium salt to trigger *e*RAFT polymerization. The rate of polymerization was tuned by current, and the polymer chains could be chain extended to form block copolymers. Chapter X employed the synergy between electrochemically mediated ATRP (*e*ATRP) and RAFT polymerization. The radicals were generated by *e*ATRP equilibrium, and the reversibly deactivated by both ATRP and RAFT. The ratio of ATRP initiator to RAFT agent influenced the rate of polymerization, and the addition of 1% of RAFT agent significantly decreased the dispersity. Chapter XI studied the electrochemical activation of a dithiocarbamate type RAFT agent catalyzed by Cu complex. The dithiocarbamate acted as a pseudohalide in *e*ATRP.

The robust development of ATRP and RAFT polymerization mechanistic study facilitated the preparation of polymers with various architectures and functionalities, thus enables the synthesis of functional materials. The well-defined block copolymers regardless of sequence of monomer addition would be beneficial for preparation of

thermoplastic elastomers and pressure-sensitive adhesives. The additional benefits of segregation effect in dispersed media leads to decreased rate of termination, which is extremely beneficial for synthesis of brush polymers and hyperbranched polymers. Miniemulsion ATRP could be developed for polymer-inorganic nanoparticles with high conversion and low polymer molecular weight distribution. Hydrophobic molecules could be loaded into crosslinked nanoparticles and be released in proper conditions.

The various approaches for *e*RAFT polymerization facilitated RAFT polymerization with tunable polymerization rate, low catalyst concentration, temporal control and preparation of block copolymers. *e*RAFT polymerization could potentially be coupled with electrochemically mediated cationic RAFT polymerization and ring-opening polymerization to synthesis of diversified block copolymers. *e*RAFT could also be employed in surface-initiated polymerizations and potentially be used for anti-fouling surfaces and sensors.

(1) Fantin, M.; Park, S.; Wang, Y.; Matyjaszewski, K., Electrochemical Atom Transfer Radical Polymerization in Miniemulsion with a Dual Catalytic System. *Macromolecules* **2016,** *49* (23), 8838-8847.

Appendix 1 Miniemulsion Atom Transfer Radical Polymerization Using a Hydrophilic Catalyst

A1.1. Introduction

In an electrochemically mediated atom transfer radical polymerization (*e*ATRP, **Scheme A1-0-1**) the active Cu^{I} catalyst is (re)generated by electrochemical reduction at a working electrode (WE).[1] A successful ATRP in miniemulsion typically requires hydrophobic catalyst to be confined into the organic phase.[2-5] Thus, in a recently reported *e*ATRP miniemulsion procedure, a dual catalytic system was utilized, composed of one hydrophobic and one hydrophilic catalyst.[6] The presence of a second water-soluble catalyst was required to close the electrochemical circuit between the WE and the hydrophobic catalyst residing within monomer droplets. The WE was in contact with the aqueous phase, from which the water-soluble catalyst shuttled the electrochemical stimulus to the hydrophobic catalyst confined in the dispersed droplets.

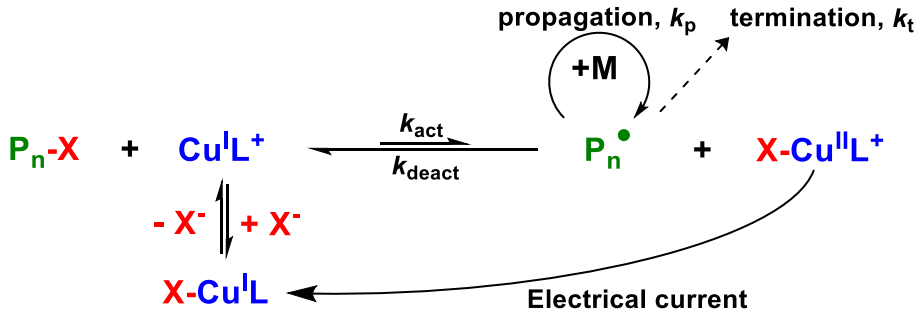

Scheme A1-0-1. Mechanism of *e*ATRP.

Unexpectedly, and in contrast with our previous results, we recently discovered that a single hydrophilic catalyst can control a miniemulsion *e*ATRP, if the cationic copper

complex is paired with an anionic surfactant. The catalyst/surfactant system then generates ion pairs that transport the catalyst into the hydrophobic monomer droplets, thus allowing a controlled polymerization.

Non-ionic surfactants are typically employed in miniemulsion ATRP.[7-8] Until recently, anionic surfactants such as sodium dodecyl sulfate (SDS) were considered a poison for ATRP catalysts.[9-10] Instead, in this work the interaction between SDS and Cu^{II}/L was exploited to concentrate the catalyst in the polymerization loci (L = amine ligand).

Different combinations of surfactant and hydrophilic Cu ligands were tested in the miniemulsion *e*ATRP of *n*-butyl acrylate (BA), relevant structures of the reagents are provided in **Scheme A1-0-2**. The $Br–Cu^{II}L^{+}$/SDS system was characterized by electrochemical and spectroscopic techniques in order to provide a detailed molecular description of the catalyst.

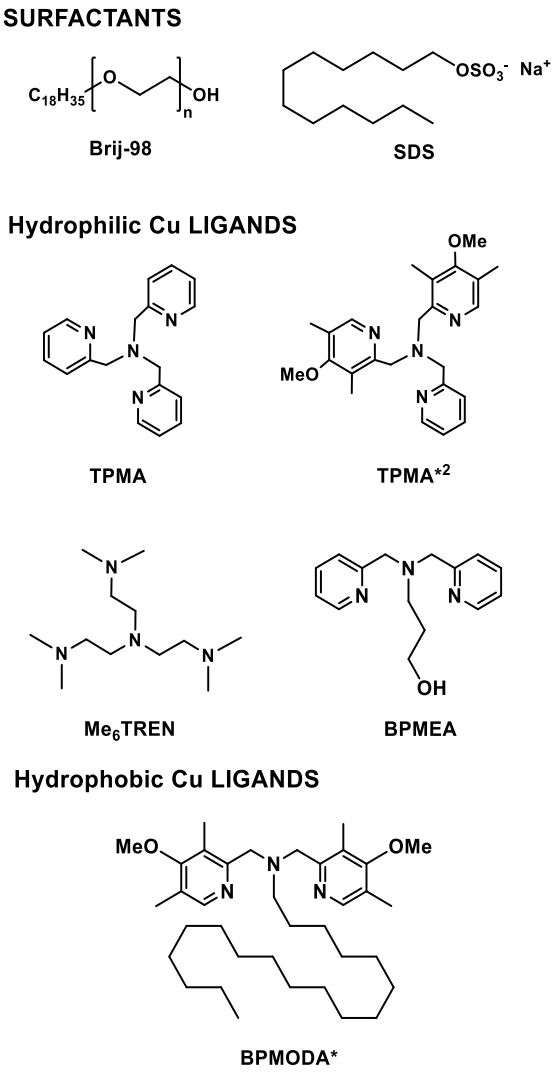

Scheme A1-0-2. Structures of the Investigated Surfactants and Copper Ligands.

A1.2. Results and Discussion

A typical list of reagents used in this miniemulsion *e*ATRP in the presence of hydrophilic catalyst and anionic surfactant is shown in **Table A1-0-1**. Since the surfactant (DS^- anion) can coordinate to $Cu^{II}L^{2+}$, displacing Br^- from the deactivator Br-$Cu^{II}L^{2+}$,[10] excess NaBr (0.1 M) was added to the reaction medium to avoid this undesired reaction.

Under such conditions, Br-$Cu^{II}L^{+}$ was stable and was therefore considered the main Cu^{II} species present in the aqueous phase.[11]

Table A1-0-1. Composition of Organic and Aqueous Phases in a Typical Miniemulsion Polymerization[a]

component	weight (g)	comments
organic phase		
BA	7.12	20 vol% (18 wt%) to total
Ethyl α-bromoisobutyrate (EBiB)	0.039[b]	[BA]/[EBiB] = 280/1
Hexadecane (HD)	0.77	10.8 wt% to BA
aqueous phase		
Water	32	Distilled water
SDS[c]	0.44	6.2 wt% to BA
NaBr	0.41	[NaBr] = 0.1 M
$Cu^{II}Br_2$	8.9×10^{-3}	1 mM with respect to V_{tot}
TPMA[c]	0.023	$[Cu^{II}Br_2]/[L] = 1/2$

[a]Polymerization conditions: T = 65 °C; working electrode = Pt mesh with area ≈ 6 cm^2; counter electrode = Pt mesh separated from reaction mixture by methylcellulose gel saturated with $(C_2H_5)_4NBF_4$; reference electrode = Ag/AgI/0.1 M $(n\text{-}C_4H_9)_4NI$; [b]Initiator concentration, [EBiB], was varied to target different degrees of polymerization (DP); [c]Other employed surfactants and copper ligands are listed in **Scheme A1-0-2**; tris(2-

pyridylmethyl)amine (TPMA), 1-(4-methoxy-3,5-dimethylpyridin-2-yl)-*N*-((4-methoxy-3,5-dimethylpyridin-2-yl)methyl)-*N*-(pyridin-2-ylmethyl)methanamine (TPMA*^{2}), tris[2-(dimethylamino)ethyl]amine (Me_6TREN), *N*,*N*-bis(2-pyridylmethyl)-2-hydroxyethylamine (BPMEA), and bis[2-(4-methoxy-3,5-dimethyl)pyridyl-methyl]octadecylamine (BPMODA*).

Table A1-0-2 shows the results of *e*ATRP of BA in miniemulsion with different surfactants and catalysts. In an *e*ATRP, the active $Cu^{I}L^{+}$ is (re)generated by electrochemical reduction of $Br–Cu^{II}L$ (**Scheme A1-0-1**). The appropriate potential (E_{app}) applied at the WE was chosen from the cyclic voltammetry (CV) of the catalyst in the polymerization mixture. $E_{app} \approx E_{pc}$ was chosen for each polymerization, in order to reduce $Br–Cu^{II}L^{+}$ with similar rates (E_{pc} = cathodic peak potential).

Table A1-0-2. *e*ATRP of BA in Miniemulsion with Different Surfactants and Catalysts, T = 65 °C[a]

entry	aq. phase ligand	org. phase ligand	surfactant	E_{app}	t (h)	Q[b] (C)	conv (%)	k_p^{app} [c] (h^{-1})	M_n	$M_{n,th}$	$Đ$
1	TPMA	-	Brij 98	E_{pc} – 0.03 V	7.5	16.2	90	0.60	27800	3200	4.77
2	TPMA	-	SDS	E_{pc} – 0.03 V	7.5	3.9	75	0.18	28400	27300	1.18
3	TPMA	BPMODA*	SDS	E_{pc}	24	6.6	13	0.01	12400	5100	1.32
4[d]	BPMEA	BPMODA*	SDS	E_{pc}	24	5.8	61	0.04	31800	22700	1.25
5	TPMA*^{2}	-	SDS	E_{pc} – 0.03 V	7.5	3.3	38	0.07	15900	14100	1.32
6	Me_6TREN	-	SDS	E_{pc} – 0.03 V	1.5	7.3	93	0.40	59500	33800	1.94

7	Me_6TREN	-	SDS	E_{pc} + 0.12 V	5	4.6	77	0.55	38700	27900	1.56
8[d]	BPMEA	-	SDS	E_{pc}	24	2.0	66	0.06	29100	24300	4.62

[a]Conditions as in **Table A1-0-1** unless otherwise stated. [b]Charge passed, determined from the chronoamperometry recorded during electrolysis. [c]The slope of the $\ln([M]_0/[M])$ vs time plot. [d]From reference [6].

Effect of Surfactant. *e*ATRP with a hydrophilic catalyst, such as Br-Cu^{II}TPMA$^+$, was strongly affected by the nature of the surfactant (**Table A1-0-2**, entry 1 vs. 2). The presence of non-ionic Brij-98 afforded an uncontrolled polymerization with very broad molecular weight dispersity, suggesting the presence of insufficient amount of deactivator in the polymerizing droplets (**Figure A1-0-1**). Conversely, the use of an anionic surfactant, SDS, provided good control (**Figure A1-0-2**). This indicated the presence of a specific interaction between Br-$Cu^{II}L^+$ and SDS that favored controlled polymerization within the dispersed monomer droplets, without requiring the presence of a dual hydrophilic/hydrophobic catalytic system.

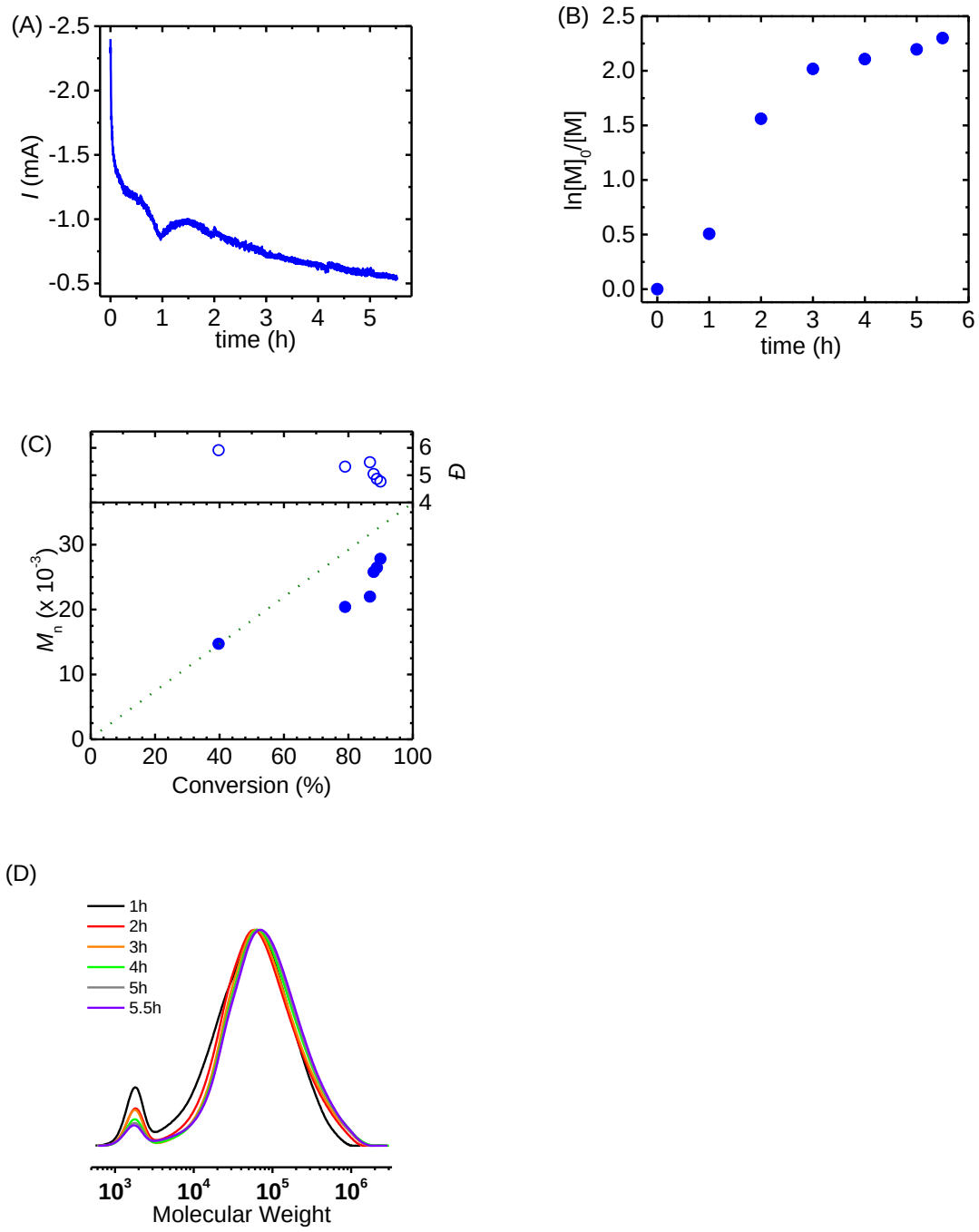

Figure A1-0-1. Miniemulsion *e*ATRP with $Cu^{II}Br_2$/2TPMA and non-ionic surfactant (Brij 98), **Table A1-0-2**, entry 1. (A) Current profile versus time, (B) first-order kinetic plot, (C) molecular weight (MW) and *Đ* evolution vs. monomer conversion and (D) GPC traces. Reaction conditions: [BA]/[EBiB]/[$Cu^{II}Br_2$/2TPMA] = 280/1/0.2, [BA] = 1.4 M, [$Cu^{II}Br_2$/2L] = 1.00 mM, T = 65 °C, [NaBr] = 0.1 M, [Brij 98] = 0.38 mM, [HD] = 85 mM, $E_{app} = E_{pc} - 0.03$ V.

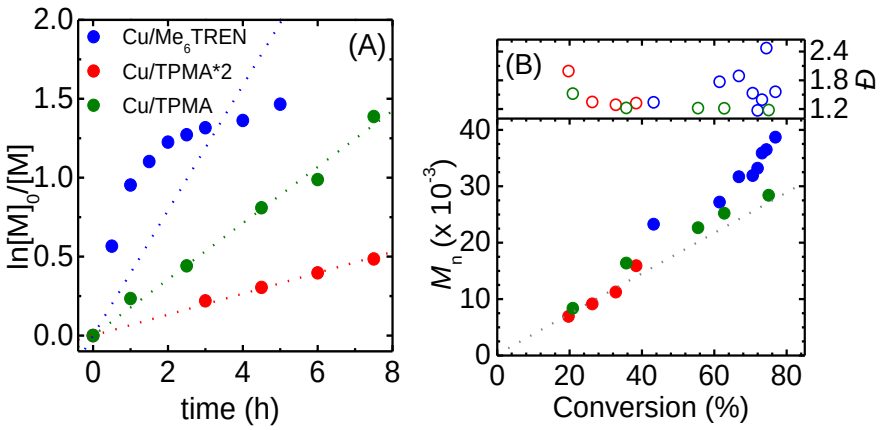

Figure A1-0-2. Miniemulsion *e*ATRP of BA with different copper ligands (L = TPMA, TPMA*[2], and Me_6TREN; **Table A1-0-2**, entries 2, 5, 6). (A) Logarithmic kinetic plot and (B) molecular weight (MW) and *Đ* evolution vs. monomer conversion. Reaction conditions as in **Table A1-0-1**.

In fact, *e*ATRP with the Br-Cu^{II}TPMA$^+$/SDS system was much faster, and somewhat better controlled in terms of molecular weight and dispersity, than *e*ATRP with the dual catalysts Br-Cu^{II}TPMA$^+$/Br-Cu^{II}(BPMODA*)$^+$ or Br-Cu^{II}BPMEA$^+$/Br-Cu^{II}(BPMODA*)$^+$ (**Table A1-0-2**, entries 3-4).

Effect of Catalyst Hydrophilicity. With the single Br-Cu^{II}TPMA$^+$ catalyst and SDS as surfactant, polymerization control increased with increasing hydrophilicity of the catalyst. Molecular-weight dispersity, sharply decreased, as shown in **Table A1-0-3**. Hydrophilicity was quantified from the distribution of the catalyst between water and BA, *i.e*. partition experiments in the absence of SDS. The catalyst Br-Cu^{II}TPMA$^+$, completely distributed in the aqueous phase, provided very well defined poly(*n*-butyl acrylate), PBA (**Figure A1-0-2**). Unexpectedly, the super-active catalyst Br-Cu^{II}(TPMA*[2])$^+$ provided

slower polymerization rate and poorer control, indicating that catalyst distribution and interfacial dynamics may play a more important role than the thermodynamics of RX activation.[12]

Table A1-0-3. Partition of $Cu^{II}Br_2$/L Catalysts between Water and BA[a]

L	$[Cu^{II}Br_2/L]_{water}/[Cu^{II}Br_2/L]_{tot}$		I_{eff}[b]	$Đ$[b]
	15 vol% BA[c]	30 vol% BA[d]		
TPMA[e,f]	1.00	1.00	0.96	1.18
TPMA*[2]	1.00	0.99	0.89	1.32
Me_6TREN	0.94	0.94	0.57	1.94
BPMEA[f]	0.54	0.73	0.84	4.62

[a]$[Cu^{II}Br_2/L]_{tot}$ = 2.5 mM at room temperature in water. Ratios of $[Cu^{II}Br_2/L]_{water}/[Cu^{II}Br_2/L]_{tot}$ were determined by calibration curve in water; [b]Initiation efficiency ($I_{eff} = M_{n,th}/M_n$), from **Table A1-0-2** (at $E_{app} = E_{pc} - 0.03$ V or $E_{app} = E_{pc}$). [c]13.5 wt% of BA; [d]27.8 wt% of BA. [e]No Cu complex was detected in the Vis-NIR spectrum of the organic phase. [f]From reference [6].

Overall, hydrophilicity of the catalyst or nature of the surfactant affected *e*ATRP much more than the rate and amount of Cu^I generation. For example, control only partially improved by decreasing the rate of regeneration of $Cu^IMe_6TREN^+$ (**Table A1-0-2**, entry 6 vs. 7). Cu^{II} reduction rate was diminished by applying a 0.15 V more positive E_{app}, which

resulted in ~300 times lower Cu^{I}/Cu^{II} ratio on the surface of the working electrode.[13] This drastic decrease in Cu^{II} reduction could not guarantee full control of *e*ATRP, lowering *Đ* from 1.94 to 1.56. Cu^{I} generation rate was also varied in the case of $Br–Cu^{II}TPMA^{+}$, with even smaller effects on polymerization control, which was always good. These results confirmed that the specific catalyst/surfactant interaction was the most important parameter affecting control.

The best performing system, $Br\text{-}Cu^{II}TPMA^{+}$/SDS, was also used to produce very well defined PBA (*Đ* = 1.1) in a much simplified *e*ATRP system (*se*ATRP), *i.e.* a two-electrode system with a sacrificial Al anode under fixed current conditions.[14] This setup requires a simpler instrumentation, a current generator instead of a potentiostat.[15]

Effect of Catalyst Loading. The efficiency of the $Br\text{-}Cu^{II}TPMA^{+}$/SDS complex catalyst was tested over the range of 1200 to 300 ppm of Cu (**Table A1-0-4**, entries 1-3). Controlled *e*ATRP was obtained in each case, with linear increase of MW with conversion. However, polymerization rate tended to slow down at high conversion with lower catalyst concentration. Higher catalyst loadings provided higher rates of polymerization and higher conversions with narrower *Đ*.

Table A1-0-4. *e*ATRP of BA in Miniemulsion at Different Copper Concentrations and Degree of Polymerization[a]

Entry	[M]/[EBiB]/ $[Cu^{II}Br_2]$	Q^b (C)	Conv (%)	$k_p^{app\ c}$ (h^{-1})	M_n	$M_{n,th}$	*Đ*	$d_{v,final}{}^d$ (nm)
1	280/1/0.09	2.6	60	0.14	24600	21800	1.19	105±1
2	280/1/0.20	3.9	75	0.18	28400	27300	1.18	126±2

3	280/1/0.34	4.8	87	0.27	33700	31900	1.16	174±1
4	100/1/0.07	4.9	80	0.22	10700	10600	1.26	117±1
5	500/1/0.36	1.8	47	0.09	31600	30200	1.09	100±1

[a]Conditions as in **Table A1-0-1** unless otherwise stated; $E_{app} = E_{pc} - 0.03$ V, selected from CV response; reaction time = 7.5 h. [b]Charge passed, determined from the chronoamperometry recorded during electrolysis. [c]The slope of the ln([M]$_0$/[M]) vs time plot. [d]Final average particle diameter, calculated from volume, determined by dynamic light scattering (DLS).

Targeted Degree of Polymerization (DP). Polymerizations of BA were also performed at three different [M]$_0$/[EBiB]$_0$ ratios, targeting DP = 100, 280, and 500 (**错误!未找到引用源。**). Polymerizations were well controlled with linear first-order kinetics (**Figure A1-0-3**a), M_n matching the theoretical values, and low $Đ$ (**Figure A1-0-3**b). Dispersity and polymerization rate decreased with increasing [M]$_0$/[EBiB]$_0$.[13, 16]

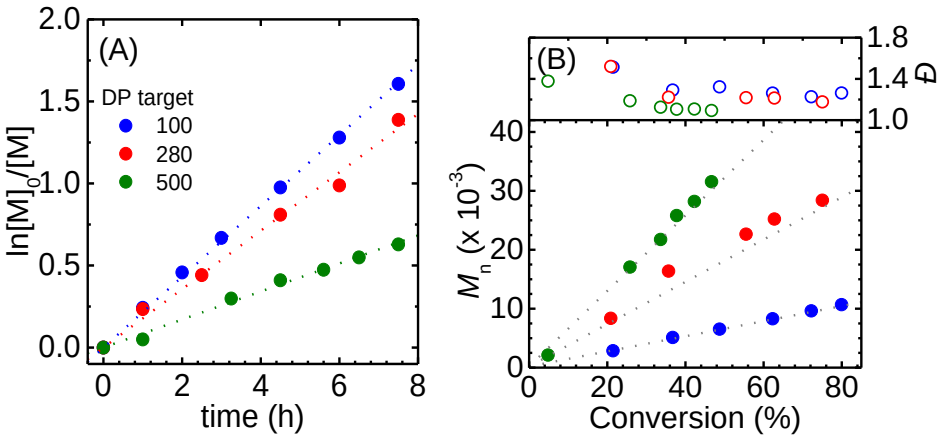

Figure A1-0-3. Miniemulsion *e*ATRP of BA with different target DP (100, 280, and 500). (A) Kinetic plot and (B) MW and $Đ$ vs. monomer conversion. Reaction conditions as in **Table A1-0-1**.

Chain-End Functionality. Chain-end functionality was completely retained, within the GPC detection limit, which was proven by chain extension of a PBA_{78}-Br macroinitiator prepared by miniemulsion *e*ATRP with Br-Cu^{II}TPMA^{+}/SDS (DP = 78, **Figure A1-0-4**). PBA_{78}-Br was seamlessly extended with *tert*-butyl acrylate (*t*BA) *in situ*, generating PBA_{78}-*b*-P(*t*BA_{67}-*stat*-BA_{18}), where *stat* indicates the formation of a statistical copolymer with composition *t*BA/BA 67/18. PBA_{78}-Br was also chain extended after purification of the macroinitiator and re-emulsification, generating PBA_{78}-*b*-P(*t*$BA)_{67}$. In each case, linear first-order kinetics, predetermined MWs, and low dispersities were obtained.

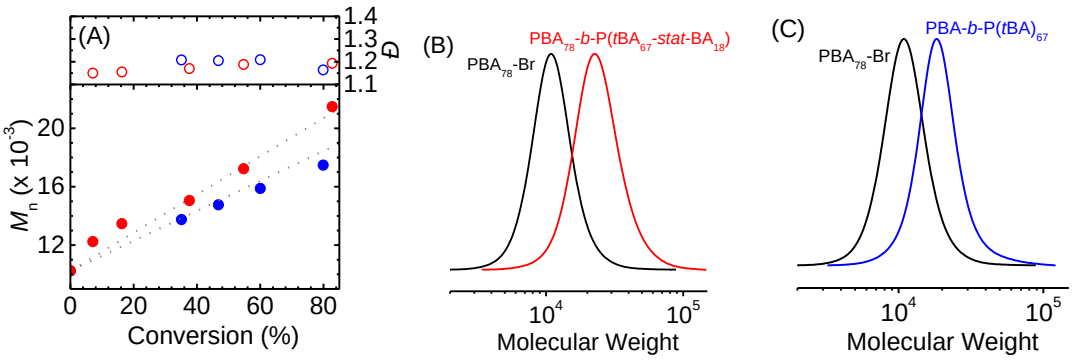

Figure A1-0-4. Chain extension of PBA_{78}-Br by simplified electrochemically mediated ATRP (*se*ATRP) in miniemulsion (red = in situ chain extension, blue = chain extension after purification of the PBA-Br macroinitiator). (A) MW and *Đ* vs. monomer conversion. (B-C) GPC traces. Reaction conditions as in **Table A1-0-1**, with [*t*BA]/[PBA_{78}-Br]/[Cu^{II}] = 80/1/0.06, 20% v/v *t*BA.

By recording the total consumed charge (*Q*) during *e*ATRP, it was determined that ⩽1% of chains terminated by radical−radical reactions.

The strongly hydrophilic Br−Cu^{II}TPMA$^+$ catalyst complex efficiently controlled a miniemulsion *e*ATRP inside the dispersed hydrophobic BA droplets stabilized with an anionic surfactant. This suggested that the catalyst could associate with the anionic surfactant present at the droplets' surface, realizing an "interfacial catalysis" procedure similar in nature to heterogeneous catalysis. The interaction between surfactant and catalyst at the interface was studied by CV.

Interfacial Catalysis and Interaction between Br-Cu^{II}TPMA$^+$ and SDS. CV was first applied to a model heterogeneous system, composed of catalyst and surfactant, but without monomer. In this medium, micelles with diameter ca. 2 nm were formed, as compared to larger miniemulsion droplets with diameter ca. 100 nm. The CV of Br-Cu^{II}TPMA$^+$ transition metal complex in water drastically changed after addition of SDS (**Figure A1-0-5**). The lower current indicated that the diffusion coefficient (*D*) of Br-Cu^{II}TPMA$^+$ diminished, because the catalyst was bound to the much larger micelles, which diffused slowly throughout the solution.[17] A similar behavior was observed for other Cu^{II} complexes.[18-19] Another feature of the CV in the presence of SDS is a –0.03 V shift of the half-wave potential ($E_{1/2}$). This indicated that the Cu^{II} complex (deactivator) had ca. 3 times more affinity for the micellar environment than the Cu^{I} complex (activator). This is an important aspect of the disclosed procedure that can enhance deactivation and control in ATRP conducted within the distributed micelles.[20] Indeed, the poor polymerization control obtained with Br-$Cu^{II}Me_6$TREN$^+$ could be due to its weaker interaction with SDS, which favored activation over deactivation. Br-$Cu^{II}Me_6$TREN$^+$ could also be partially reduced to Cu^0, subtracting catalyst from the polymerization environment thus reducing its efficiency.

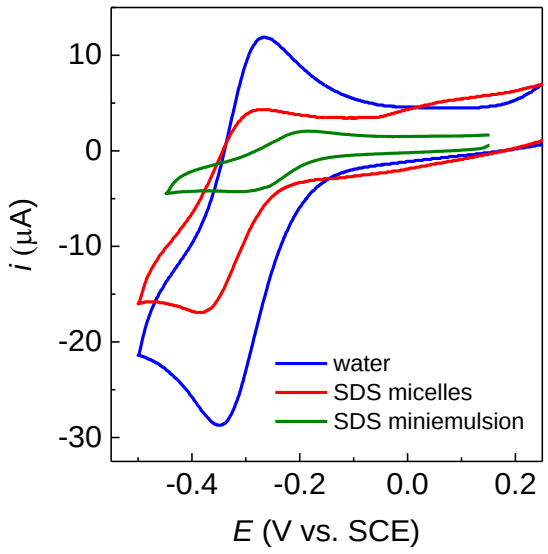

Figure A1-0-5. CV of Br-Cu^{II}TPMA^{+} in (—) water + 0.1 M NaBr; (—) water + 0.1 NaBr + 0.028 M SDS; (—) miniemulsion as described in **Table A1-0-1**, but without initiator EBiB. v = 0.1 V s^{-1}, T = 65 °C.

The CV pattern of Br-Cu^{II}TPMA^{+} in miniemulsion was similar to that in the micellar environment. In the miniemulsion, much lower current was observed because of the bigger size, and thus smaller D, of droplets compared to micelles. In this case, $E_{1/2}$ was influenced by the presence of both SDS and BA.

The fraction of Br-Cu^{II}TPMA^{+} bound to SDS micelles (f_{bound}) was determined by comparing D of Br-Cu^{II}TPMA^{+} in pure water to its D in the presence of micelles, according to a literature procedure.[21-22] A similar procedure was applied for the first time to estimate the fraction of catalyst bound to the droplets' interface in a polymerization environment, *i.e.* in the SDS miniemulsion. The detailed procedure is described in the SI, while results are summarized in **Table A1-0-5**; f_{bound} of Br-Cu^{II}TPMA^{+} was similar in micellar and in miniemulsion environments: ≥79% of the catalyst was bound to the interface, confirming

the strong interaction between Br-Cu^{II}TPMA$^+$ and SDS. Conversely, the less effective Br-$Cu^{II}Me_6$TREN$^+$ and Br-Cu^{II}BPMEA$^+$ exhibited weak bonding to the droplets' interface.

Table A1-0-5. Fraction of Br-$Cu^{II}L^+$ Bound to SDS Interfaces in Micellar Systems or in Miniemulsions, T = 65 °C.

catalyst	environment	f_{bound}
Br-Cu^{II}TPMA$^+$	micelles[a]	0.79
Br-Cu^{II}TPMA$^+$	miniemulsion[b]	0.95
Br-$Cu^{II}Me_6$TREN$^+$	miniemulsion[b]	<0.50
Br-Cu^{II}BPMEA$^+$	miniemulsion[b]	0.64

[a]Water + 0.1 M NaBr + 10^{-3} M $Cu^{II}Br_2$/TPMA + 0.028 M SDS. [b]$C_{n\text{-BuA}}/C_{NaBr}/C_{Cu^{II}Br_2}/C_L$= 280/20/0.2/0.4, 20% v/v BA in water, SDS = 28 mM = 4.6 wt % relative to BA, HD = 10.8 wt % relative to BA.

The strong interaction between catalyst and droplets did not destabilize the miniemulsion during polymerization; a roughly one-to-one copy of the original dispersion was obtained after each *e*ATRP, as determined by dynamic light scattering.

In conclusion, a large fraction of Br-Cu^{II}TPMA$^+$ was present at the droplets' surface, from where it could activate and deactivate the growing chains by an interfacial catalysis procedure. However, such heterogeneous catalysts are typically inefficient deactivators which would lead to broad $Đ$.[23-24] Therefore, we investigated if, in the presence of SDS, some of the catalyst could be transported inside the monomer droplets, acting as a traditional homogenous catalyst and supplementing the interfacial catalysis.

Ion pairing between Br-Cu^{II}TPMA^{+} and DS^{-}. In the absence of surfactant, no Cu^{II} complexes were detected in the Vis-NIR spectrum of the organic phase (**Figure A1-0-6**), indicating that Br-Cu^{II}TPMA^{+} was completely distributed in the aqueous phase (**Table A1-0-3**). The same was observed in the presence of Brij-98. Conversely, partition experiment in the presence of SDS (**Figure A1-0-6**) showed that 0.4% of the catalyst was present in the organic phase (*i.e.* ca. 3 ppm of Cu, out of a total 700 ppm Cu). This indicated that Br–Cu^{II}TPMA^{+} and DS^{-} formed hydrophobic ion pairs that transported some deactivator molecules into the organic phase, enhancing deactivation. Indeed, less than 10 ppm of deactivators were found to be sufficient for the controlled polymerization of acrylic monomers.[25] The neutral Br–Cu^{II}TPMA^{+}/DS^{-} ion pair, containing the long SDS alkyl chain, was significantly more hydrophobic than the cationic Br-Cu^{II} TPMA^{+} complex. However, when Br–Cu^{II}TPMA^{+} and DS^{-} are mixed in water, no precipitate was observed, because in polar media Br–Cu^{II}TPMA^{+} and DS^{-} interact forming soluble aggregates at the droplet surface.

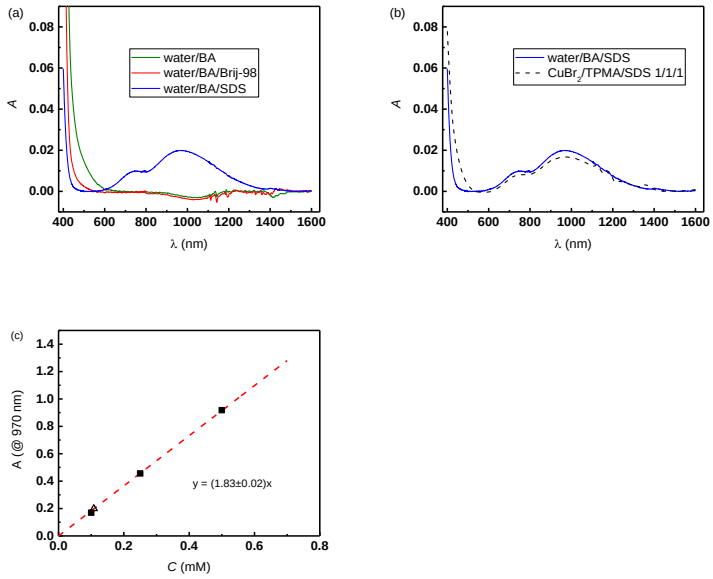

Figure A1-0-6. (a) Vis-NIR spectra of BA phase (20% BA in water + 0.1 M NaBr) with different surfactants (or in the absence of surfactants). (b) Comparison of Vis-NIR spectra of Cu^{II} complexes in the organic phase after partition experiment and after addition of $CuBr_2$/TPMA/SDS 1:1:1. (b) Calibration curve with different concentration of $CuBr_2$/TPMA/SDS 1:1:1 in BA, reporting the absorbance at 970 nm (full squares: experimental points; dashed line: linear regression). The hollow triangle indicates Br-$Cu^{II}TPMA^+$ concentration at the end of the partition experiment.

ICP-MS of the obtained polymer, before any purification procedure, showed the presence of a small amount (<20 ppm) of copper, which can also improve the stability of the latex. [26-27] Polymers obtained with Br–$Cu^{II}TPMA^+$/SDS were perfectly clear and transparent (**Figure A1-0-7**); in comparison, samples obtained with similar amounts of hydrophobic complexes contained >400 ppm of residual Cu and were intensely colored.

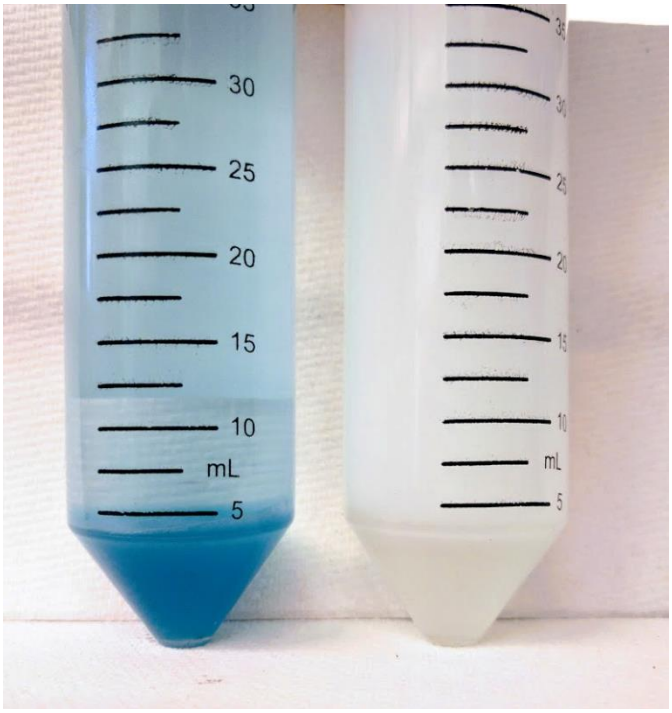

Figure A1-0-7. Comparison between polymer produced with dual catalytic system (left, ca. 1000 ppm of hydrophobic catalyst $CuBr_2$/BPMODA*) and single hydrophilic catalytic system (right, ca. 700 ppm of $Cu^{II}Br_2$/TPMA).

Regarding the activator complex, the ion pair [$Cu^{I}L^{+}/DS^{-}$] or the neutral complex Br–Cu^{I}L could enter the organic phase at concentrations slightly higher than that of [Br–$Cu^{II}L^{+}/DS^{-}$]. Indeed, we estimated a Cu^{I}/Cu^{II} ratio of ca. 4 in the monomer droplets.

Overall Mechanism of Interfacial and Ion-Pair Catalysis. Scheme A1-0-3 presents the proposed mechanism of miniemulsion *e*ATRP with X-$Cu^{II}TPMA^{+}$/SDS catalytic system. Atom transfer was carried out both by catalyst bound to the droplets' surface, "interfacial catalysis", and by ion-pairs distributed in the monomer droplets, "ion-pair catalysis". Electrochemical regeneration of the catalyst involved both a small amount of X-$Cu^{II}L^{+}$ dissolved in the aqueous phase and X-$Cu^{II}L^{+}$ bound to the droplets' interface.

The same catalyst could be reduced at the WE and then control polymerization in the monomer droplets, without the need of a dual (hydrophilic + hydrophobic) catalytic system.

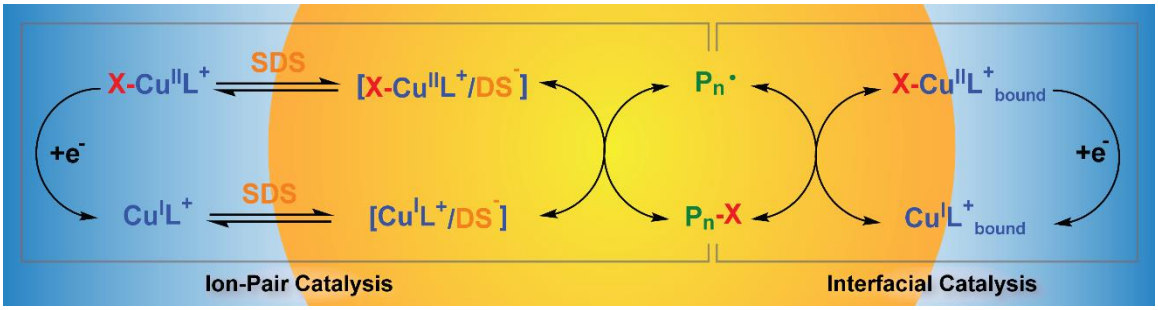

Scheme A1-0-3. Mechanism of Ion-Pair and Interfacial Catalysis in Miniemulsion *e*ATRP.

Table A1-0-6 presents a molecular description of the ATRP catalytic system in a single miniemulsion droplet, which can be considered an individual *mini-bulk* polymerization reactor. For a reaction volume of 40 mL, the number of droplets was determined as 7.6×10^{15}, considering each droplet as a sphere with diameter 126 nm (measured by DLS). The amount of reagents in each droplet was computed by determining the number of particles (*N*) of each species and dividing it by the number of droplets. The amount of catalyst inside each droplet was derived from the average 14 ppm of residual copper as determined by ICP-MS. Finally, the catalyst at the interface was calculated as 95% of the total catalyst concentration (**Table A1-0-5**).

Table A1-0-6. Molecular Description of the Br-Cu^{II}TPMA$^+$/SDS System in a Single Miniemulsion Droplet[a]

species	concentration (M)[b]	*N*[c]	ratio[d]
SDS[e]	-	9.2×10^4	1.5×10^3

Hexadecane	-	2.7×10^{5}	4.4×10^{3}
Br-$Cu^{II}TPMA^{+}_{bound}$	-	3.0×10^{3}	48
[Br-$Cu^{II}TPMA^{+}$/DS^{-}]	9.9×10^{-5}	62	1
BA	7.0	4.4×10^{6}	7.1×10^{5}
EBiB	2.5×10^{-2}	1.6×10^{4}	2.6×10^{2}
$P_n^{\bullet}$ [f]	$0/11.7\times10^{-6}$	0/1	$0/2.9\times10^{-2}$
	(1.3×10^{-9})	(8.2×10^{-4})	(2.3×10^{-5})

[a]Conditions as in **Table A1-0-1**. [b]Concentration of the species in the organic phase (V = 8 mL). [c]Average number of particles of each species in a single droplet. [d]$N/N_{catalyst}$. [e]The surfactant available to stabilize the droplets was considered as C_{SDS} – cmc (critical micellar concentration, see SI). [f]Two different values are reported, considering that during polymerization in most droplets the number of radicals is either 0 or 1. In parentheses the average of the whole organic phase.

With 700 ppm of total copper present in the miniemulsion, each ion-pair catalyst was responsible for the activation/deactivation of 260 chain ends. Conversely, each catalyst bound to the interface activated and deactivated an average of 5 chains. On the surface, one catalyst molecule (Br-$Cu^{II}TPMA^{+}_{bound}$) was present every ~30 surfactant molecules. Interestingly, during polymerization only 1 in 1200 droplets was active (*i.e.* contained an active radical) at any given moment, which suggests that radical-radical termination events could be limited.[28-30]

The concentration of residual copper determined by ICP (average 14 ppm) was higher than the concentration determined from the partition experiments (3 ppm). The concentration of Cu^{II} can increase during polymerization due to some radical termination reactions. Moreover, excess activator $Cu^{I}L^{+}$ can access the monomer droplets, resulting in overall higher catalyst loading in the organic phase during polymerization.

A1.3. Conclusion

In contrast to our previous report, it is now described that miniemulsion *e*ATRP can be carried out with an anionic surfactant and a single, strongly hydrophilic catalyst. The obtained PBA was well defined, with MWs matching theoretical values and low *Đ*. Chain extension experiments confirmed that chain-end functionality was very well retained. These results are in contrast with a previous paradigm that super-hydrophobic catalysts are required for ATRP in dispersed media.

In this work, the catalytic system was generated *in situ* by mixing commercially available reagents (NaBr, SDS, traditional copper catalysts). Only a few ppm of catalyst were present inside the monomer droplets. Polymer purification was simplified, because, after crashing the miniemulsion, >99% of the hydrophilic catalyst was present in the aqueous phase.

Controlled polymerization was favored by the strong interaction between copper complexes and an anionic surfactant, SDS. This interaction, once considered a poison for the ATRP catalyst, generated hydrophobic ion pairs [Br-Cu^{II}TPMA^{+}/DS^{-}] at the droplet surface that transported a fraction of the catalyst into the monomer droplets, enabling

controlled polymerization *via* “ion-pair catalysis”. Control was further enhanced by catalyst bound to the droplets’ surface *via* “interfacial catalysis”.

The ideal Cu catalyst has the following characteristics: (i) high activity, (ii) ability to form ion pairs with SDS, and (iii) stronger affinity for the surfactant when present in its Cu^{II} oxidation state.

A1.4. Experimental Section

Materials. Tetrabutylammonium hexafluorophosphate ($TBAPF_6$, 98%), copper(II) bromide ($CuBr_2$, 99%), methylated cellulose (Tylose, MH = 300), sodium dodecyl sulfate (SDS, 99%), hexadecane (HD, 99%), tetrahydrofuran (THF, > 99%), and ethyl α-bromoisobutyrate (EBiB, 98%) were purchased from Sigma-Aldrich. *N*,*N*-Dimethylformamide (DMF), sodium bromide (NaBr, 99%) and polyoxyethylene (20) oleyl ether (Brij 98) were purchased from Acros. Platinum (Pt) wire, Pt gauge mesh and Pt disk (3 mm diameter, Gamry) were purchased from Alfa Aesar. Tris(2-pyridylmethyl)amine (TPMA) was prepared according to a published procedure.[31] Bis(4-methoxy-3,5-dimethyl-pyridin-2-ylmethyl)-pyridin-2-ylmethyl-amine (TPMA*^{2}) was prepared according to a previously published procedure.[32] Tris(2-(dimethylamino)ethyl)amine (Me_6TREN) was synthesized according to literature procedures and stored under nitrogen prior to use.[31, 33] Bis(2-pyridylmethyl)octadecylamine (BPMODA) and bis[2-(4-methoxy-3,5-dimethyl)pyridylmethyl]octadecylamine (BPMODA*) were prepared as previously described.[6] *n*-Butyl acrylate (BA, 99%, Aldrich) was passed through a column filled with basic alumina prior to use to remove polymerization inhibitors.

Typical Procedure of a Partition Experiment. Aqueous solutions of $Cu^{II}Br_2$/TPMA, $Cu^{II}Br_2$/TPMA*^{2} and $Cu^{II}Br_2$/Me_6TREN (1/2 by mole) were prepared at

various concentrations, *i.e.*, 0.1, 1, 2.5, 5 and 10 mM. Catalyst absorbance was recorded by UV-Vis spectroscopy (maximum wavelength, λ_{max}, 867 nm). A linear calibration was obtained from the correlation between absorbance and catalyst concentration. Solutions of copper complex in water were prepared at various concentrations and then mixed with BA to obtain 70/30 and 85/15 water/BA ratios (by v/v). The mixtures were vigorously stirred using a Vortex Mixer at either RT or 60 °C. The aqueous phase was collected and absorbance at λ_{max} was recorded by UV-Vis spectrometer. Percentage of copper complex remaining in the aqueous phase was then calculated.

Procedure of a Partition Experiment in the Presence of Surfactant. In this case, the organic layer was analyzed in order to detect the minimum amount of hydrophilic catalyst distributed in the organic phase. Also, a higher quantity of $Cu^{II}Br_2$/L was used to detect more accurately the small amount of catalyst in the organic phase. The linear calibration was obtained as before, but using $Cu^{II}Br_2$/TPMA/SDS 1:1:1 in BA + a few drops of H_2O. This allowed to saturate the BA phase in water, as occurs during a miniemulsion experiment.

In the presence of surfactant, the analyzed solution was not vigorously mixed, in order to avoid formation of a dispersion. Therefore, aqueous and organic phase were put carefully in the same vial to form a macroscopic two-phase system. Then, the mixture was let to equilibrate for three days under gentle rocking on a platform rocker. After three days the mixture was still macroscopically well separated, but was centrifuged at 5000 rpm for 15 minutes to obtain a cleaner separation between the two phases. Finally, the organic top layer was withdrawn and analyzed by Vis-NIR spectroscopy.

Cyclic Voltammetry (CV) Analysis of Catalysts in Micellar Environment. Electrochemical investigations were conducted in a 6-neck electrochemical cell connected to a potentiostat (Gamry Ref-600) through a three-electrode system. The working electrode, WE, was a Pt disk, polished by means of a 0.25-μm diamond paste prior to each experiment, then rinsed with ethanol and sonicated for 5 minutes. The area of the WE was electrochemically determined as $A = 0.0665$ cm^2, , applied to CVs at different scan rates of the couple ferrocenium/ferrocene in MeCN at RT, for which the diffusion coefficient is reported in literature.[34] The reference electrode (RE) was a saturated calomel electrode (SCE), while the counter electrode was a Pt ring. The working solution was always deoxygenated for at least 30 minutes and maintained under a nitrogen atmosphere. An oil bath was used to keep the temperature constant at T = 65 °C. To measure the diffusion coefficients of each species, the baseline was corrected in every voltammograms. A literature procedure was followed to determine the fraction of catalyst bound to micelles[21]. In this experiment, probe and surfactant concentrations (C_p and C_{SDS} respectively) were both varied to maintain a constant ratio $C_p/C_{mic} \approx 1$, where $C_{mic} = (C_{SDS} - cmc)/N$. N is the aggregation number of SDS, which depends on the operating conditions. In literature, N = 82 was measured for ca. 0.038 M SDS in water + 0.1 M NaBr, at T = 40 °C.[35] Considering that N varies with T in pure water as: $N = 520 - 1.52*T(K)$, we assumed that a similar trend is valid also in the presence of 0.1 M NaBr, that is the slope of the curve N vs. T is the same. From N = 82 for T = 40 °C a new intercept was determined as 558, thus N = 44 for T = 65 °C.[36] CVs of the catalytic system were recorded at different scan rates, for 5 C_{SDS}.

Miniemulsion Preparation and Polymer Characterization. Ultrasound treatment was carried out using Ultrasonics W-385 sonicator. UV-Vis spectra were

recorded by Agilent 8453 spectrometer with a glass cuvette (length = 1 cm). Number-average molecular weight (M_n) and molecular-weight dispersity ($Đ$) were determined by GPC equipped with Polymer Standards Services (PSS) columns (guard, 10^5, 10^3, and 10^2 Å) and a differential refractive index detector (Waters, 2410), with THF as eluent at a flow rate 1.00 mL/min (T = 35 °C). GPC traces were processed by WinGPC 8.0 software (PSS) using a calibration based on linear polystyrene (PSty) standards. Electrolysis experiments were carried out under N_2 atmosphere using a Pt mesh as working and counter electrodes. The counter electrode was prepared using a glass frit and a salt bridge made of Tylose gel saturated with $TBAPF_6$ to separate the cathodic and anodic compartments. CVs were recorded at a scan rate (v) of 100 mV/s at a Pt disk WE with a Pt mesh CE and a $Ag/AgI/I^-$ RE. During preparative electrolysis, a condenser was connected to the reaction cell and maintained at -10 °C using a circulating chiller (NESLAB Inc., RTE-111). Particle size and size distribution were determined by using a Zetasizer Nano from Malvern Instruments, Ltd. Samples for inductively coupled plasma−mass spectrometry (ICP–MS) were prepared by digesting the samples in aqua regia at 95 °C for two hours, followed by dilution in 10 mL of 2% HNO_3 matrix. Acid with >99.999% purity (metal basis) were used. The concentration of copper (Cu) in purified polymers was determined using Thermo-Finnigan Element XR ICP-MS. The instrument was calibrated with standard Cu solutions before each element. The samples were analyzed immediately after the calibration, and the elemental results were within the calibration range.

Dynamic Light Scattering (DLS). A Malvern Zetasizer Nano ZS at 25 °C with water as dispersant was employed to determine number-average hydrodynamic diameter

(d_n) and volume-average hydrodynamic diameter (d_v). Samples were diluted prior to the measurement (3 drops of solution in *ca.* 1.5 mL of water).

Miniemulsion Polymerization by *e*ATRP with Single Catalyst and Non-ionic Surfactant under Potentiostatic Conditions. A stock solution of BA (8 mL, 55.55 mmol), EBiB (29 μL, 1.98×10^{-1} mmol, to target DP = 280; the amount of EBiB was adjusted for different targeted DPs), and HD (1 mL, 3.40 mmol) was prepared. $Cu^{II}Br_2$ (8.9 mg, 0.04 mmol), TPMA (23.1 mg, 0.08 mmol), NaBr (412 mg, 4 mmol), and Brij 98 (440 mg, 0.38 mmol) were dissolved in 32 mL of distilled water. The organic and aqueous solutions were mixed (total volume ≈ 40 mL), placed in an ice bath, and dispersed by a probe sonicator, amplitude = 70% for 15 min; (application and rest time of 1 s each). Nitrogen was bubbled through the miniemulsion solution for 40 min, prior to recording a CV at 100 mV/s. The CV allowed for accurate selection of the applied potential ($E_{app} = E_{pc} - 0.03$ V). A Pt mesh (geometrical area ca. 6 cm^2) WE was used for electrolysis under proper E_{app}. Samples were withdrawn periodically to follow the monomer conversion by gravimetric analysis, while M_n and $Đ$ were determined by GPC.

Miniemulsion Polymerization by *e*ATRP with Single Catalyst and Ionic Surfactant under Potentiostatic Conditions. A stock solution of BA (8 mL, 55.55 mmol), EBiB (29 μL, 1.98×10^{-1} mmol, to target degree of polymerization (DP) = 280; the amount of EBiB was adjusted for different targeted DPs), and HD (1 mL, 3.40 mmol) was prepared. $Cu^{II}Br_2$ (8.9 mg, 0.04 mmol; the amount of $Cu^{II}Br_2$ was adjusted for different catalyst concentrations), TPMA (23.1 mg, 0.08 mmol; experiments with TPMA*[2] and Me_6TREN were also performed), NaBr (412 mg, 4 mmol), and SDS (440 mg, 1.53 mmol) were dissolved in 32 mL of distilled water. The organic and aqueous solutions were mixed (total

volume ≈ 40 mL), placed in an ice bath, and dispersed by a probe sonicator, amplitude = 70% for 15 min; (application and rest time of 1 s each). Nitrogen was bubbled through the miniemulsion solution for 40 min, prior to recording a CV at 100 mV/. The CV allowed for accurate selection of the applied potential ($E_{app} = E_{pc} - 0.09$ V, $E_{pc} - 0.03$ V or $E_{pc} - 0.015$ V). A Pt mesh (geometrical area ca. 6 cm^2) WE was used for electrolysis under proper E_{app}. Samples were withdrawn periodically to follow the monomer conversion by gravimetric analysis, while M_n and $Đ$ were determined by GPC.

Miniemulsion Polymerization by Simplified Electrochemically Mediated ATRP (*se*ATRP) with Single Catalyst under Galvanostatic Conditions. The first *se*ATRP polymerization was carried out under potentiostatic conditions and the passed charge (Q) was determined by utilizing the Gamry Echem Analysis program. An identical reaction mixture was prepared and *se*ATRP was carried out under multiple applied currents ((-) 0.32 mA, (-) 0.16 mA, (-) 0.13 mA, and (-) 0.11 mA). Samples were withdrawn periodically to follow the monomer conversion by gravimetric analysis, while M_n and $Đ$ were determined by GPC.

Chain Extension of *t*BA from PBA. The PBA-Br macroinitiator was prepared *via* *se*ATRP method as described above (procedure for *se*ATRP with single catalyst under potentiostatic conditions). Polymerization conditions: [BA]/[EBiB]/[$Cu^{II}Br_2$/2TPMA] = 100/1/0.07, [BA] = 1.4 M, [$Cu^{II}Br_2$/2L] = 1.00 mM, T = 65 °C, [NaBr] = 0.1 M, [SDS] = 38 mM, [HD] = 85 mM, $E_{app} = E_{pc} - 0.03$ V, WE = Pt mesh, CE = Al wire, and RE = Ag/AgI/I^-. The polymerization was stopped after 7.5 h of reaction, and the reaction mixture was divided into 2 parts. The first one was used for *in situ* chain extension with *t*BA, whereas from the second part the macroinitiator was obtained after purification (*dried at*

100 °C for 1 day, dissolved in THF, precipitated in methanol/water mixture three times, *passed through* a *neutral alumina* column in order to remove catalyst, and *dried under* vacuum for 2 days) and then was used for chain extension with *t*BA.

For the *in situ* chain extension experiment, the macroinitiator and *t*BA solutions were mixed (total volume ≈ 40 mL), placed in an ice bath, and dispersed by a probe sonicator, amplitude = 70% for 15 min; (application and rest time of 1 s each). Nitrogen was bubbled through the miniemulsion solution for 40 min. The chain extension with *t*BA was carried out under the following reaction conditions: [*t*BA]/[PBA-Br]/[$Cu^{II}Br_2$/2TPMA] = 80/1/0.06, [*t*BA] = 0.7 M, [$Cu^{II}Br_2$/2L] = 1.00 mM, T = 65 °C, [NaBr] = 0.1 M, [SDS] = 38 mM, [HD] = 85 mM, $E_{app} = E_{pc} - 0.03$ V, WE = Pt mesh, CE = Al wire, and RE = Ag/AgI/I^-. The polymerization was continued for 7.5 h. Samples were withdrawn periodically to follow the monomer conversion by gravimetric analysis, while M_n and $Đ$ were determined by GPC.

For the second chain extension experiment, polymerization was carried out *via* *se*ATRP method as described above (procedure for *se*ATRP with single catalyst under potentiostatic conditions) under the following reaction conditions: [BA]/[PBA-Br]/[$Cu^{II}Br_2$/2TPMA] = 80/1/0.06, [*t*BA] = 1.1 M, [$Cu^{II}Br_2$/2L] = 1.00 mM, T = 65 °C, [NaBr] = 0.1 M, [SDS] = 38 mM, [HD] = 85 mM, $E_{app} = E_{pc} - 0.03$ V, WE = Pt mesh, CE = Al wire, and RE = Ag/AgI/I^-. The polymerization was stopped after 7.5 h. Samples were withdrawn periodically to follow the monomer conversion by gravimetric analysis, while M_n and $Đ$ were determined by GPC.

Miniemulsion Polymerization by *e*ATRP with Dual Catalyst under Potentiostatic Conditions. A stock solution of BA (50 mL, 348.76 mmol), $Cu^{II}Br_2$ (78 mg,

0.35 mmol), and BPMODA* (198 mg, 0.35 mmol) was prepared. HD (0.50 mL, 1.71 mmol), EBiB (29 μL, 1.97×10^{-1} mmol, to target DP = 283) were added to 8 mL of the BA containing stock solution (the amount of EBiB was adjusted for different targeted DPs). SDS (329 mg, 1.14 mmol), NaBr (411 mg, 4 mmol), $Cu^{II}Br_2$ (9 mg, 0.04 mmol), and BPMEA (10 mg, 0.04 mmol) were dissolved in 32 mL of distilled water. The organic and aqueous solutions were mixed (total volume ≈ 40 mL), placed in an ice bath, and dispersed by a probe sonicator, amplitude = 70% for 15 min; (application and rest time of 1 s each). Nitrogen was bubbled through the miniemulsion solution for 30 min, prior to recording a CV at 100 mV/s. The CV allowed for accurate selection of the applied potential (E_{pc} – 80 mV). A Pt mesh (geometrical area ca. 6 cm^2) WE was used for electrolysis under proper E_{app}. Samples were withdrawn periodically to follow the monomer conversion by gravimetric analysis, while M_n and $Đ$ were determined by GPC.

A1.5. References

(1) Chmielarz, P.; Fantin, M.; Park, S.; Isse, A. A.; Gennaro, A.; Magenau, A. J. D.; Sobkowiak, A.; Matyjaszewski, K., Electrochemically Mediated Atom Transfer Radical Polymerization (*e*ATRP). *Prog Polym Sci*, DOI: 10.1016/j.progpolymsci.2017.1002.1005.
(2) Qiu, J.; Charleux, B.; Matyjaszewski, K., Controlled/Living Radical Polymerization in Aqueous Media: Homogeneous and Heterogeneous Systems. *Prog Polym Sci* **2001,** *26* (10), 2083-2134.
(3) Cunningham, M. F., Controlled/Living Radical Polymerization in Aqueous Dispersed Systems. *Prog Polym Sci* **2008,** *33* (4), 365-398.
(4) Zetterlund, P. B.; Kagawa, Y.; Okubo, M., Controlled/Living Radical Polymerization in Dispersed Systems. *Chem Rev* **2008,** *108* (9), 3747-3794.
(5) Elsen, A. M.; Burdynska, J.; Park, S.; Matyjaszewski, K., Active Ligand for Low PPM Miniemulsion Atom Transfer Radical Polymerization. *Macromolecules* **2012,** *45* (18), 7356-7363.
(6) Fantin, M.; Park, S.; Wang, Y.; Matyjaszewski, K., Electrochemical Atom Transfer Radical Polymerization in Miniemulsion with a Dual Catalytic System. *Macromolecules* **2016,** *49* (23), 8838-8847.

(7) Simms, R. W.; Cunningham, M. F., High Molecular Weight Poly(butyl Methacrylate) by Reverse Atom Transfer Radical Polymerization in Miniemulsion Initiated by a Redox System. *Macromolecules* **2007,** *40* (4), 860-866.
(8) Kitayama, Y.; Yorizane, M.; Kagawa, Y.; Minami, H.; Zetterlund, P. B.; Okubo, M., Preparation of Onion-Like Multilayered Particles Comprising Mainly Poly(iso-butyl Methacrylate)-block-polystyrene by Two-Step AGET ATRP. *Polymer* **2009,** *50* (14), 3182-3187.
(9) Gaynor, S. G.; Qiu, J.; Matyjaszewski, K., Controlled/"Living" Radical Polymerization Applied to Water-Borne Systems. *Macromolecules* **1998,** *31* (17), 5951-5954.
(10) Teo, V. L.; Davis, B. J.; Tsarevsky, N. V.; Zetterlund, P. B., Successful Miniemulsion ATRP Using an Anionic Surfactant: Minimization of Deactivator Loss by Addition of a Halide Salt. *Macromolecules* **2014,** *47* (18), 6230-6237.
(11) Fantin, M.; Isse, A. A.; Gennaro, A.; Matyjaszewski, K., Understanding the Fundamentals of Aqueous ATRP and Defining Conditions for Better Control. *Macromolecules* **2015,** *48* (19), 6862-6875.
(12) Kaur, A.; Ribelli, T. G.; Schröder, K.; Matyjaszewski, K.; Pintauer, T., Properties and ATRP Activity of Copper Complexes with Substituted Tris(2-pyridylmethyl)amine-Based Ligands. *Inorg Chem* **2015,** *54* (4), 1474-1486.
(13) Magenau, A. J. D.; Bortolamei, N.; Frick, E.; Park, S.; Gennaro, A.; Matyjaszewski, K., Investigation of Electrochemically Mediated Atom Transfer Radical Polymerization. *Macromolecules* **2013,** *46* (11), 4346-4353.
(14) Park, S.; Chmielarz, P.; Gennaro, A.; Matyjaszewski, K., Simplified electrochemically mediated atom transfer radical polymerization using a sacrificial anode. *Angew. Chem. Int. Ed.* **2015,** *54* (8), 2388-2392.
(15) Fantin, M.; Lorandi, F.; Isse, A. A.; Gennaro, A., Sustainable Electrochemically‐Mediated Atom Transfer Radical Polymerization with Inexpensive Non‐Platinum Electrodes. *Macromol Rapid Comm* **2016,** *37* (16), 1318-1322.
(16) Chmielarz, P.; Sobkowiak, A.; Matyjaszewski, K., A simplified Electrochemically Mediated ATRP Synthesis of PEO-b-PMMA Copolymers. *Polymer* **2015,** *77*, 266-271.
(17) Harwell, J. H.; Hoskins, J. C.; Schechter, R. S.; Wade, W. H., Pseudophase Separation Model for Surfactant Adsorption: Isomerically Pure Surfactants. *Langmuir* **1985,** *1* (2), 251-262.
(18) Sivagnanam, U.; Palaniandavar, M., Electrochemical Behaviour of Certain Biomimetic Copper(II) Complexes in Aqueous and Aqueous Micellar Solutions. *Journal of Electroanalytical Chemistry* **1996,** *410* (1), 43-53.
(19) Anitha, N.; Balamurugan, R.; Palaniandavar, M., Spectral and Electrochemical Studies of Bis(diimine)copper(II) Complexes in Anionic, Cationic and Nonionic Micelles. *J Colloid Interf Sci* **2011,** *362* (2), 243-252.
(20) Lanzalaco, S.; Fantin, M.; Scialdone, O.; Galia, A.; Isse, A. A.; Gennaro, A.; Matyjaszewski, K., Atom Transfer Radical Polymerization with Different Halides (F, Cl, Br, and I): Is the Process "Living" in the Presence of Fluorinated Initiators? *Macromolecules* **2017,** *50* (1), 192-202.
(21) Mandal, A. B.; Nair, B. U.; Ramaswamy, D., Determination of the Critical Micelle Concentration of Surfactants and the Partition Coefficient of an Electrochemical Probe by using Cyclic Voltammetry. *Langmuir* **1988,** *4* (3), 736-739.

(22) Mandal, A. B.; Nair, B. U., Cyclic Voltammetric Technique for the Determination of the Critical Micelle Concentration of Surfactants, Self-Diffusion Coefficient of micelles, and Partition Coefficient of an Electrochemical Probe. *The Journal of Physical Chemistry* **1991,** *95* (22), 9008-9013.
(23) Hong, S. C.; Paik, H.-j.; Matyjaszewski, K., An Immobilized/Soluble Hybrid Catalyst System for Atom Transfer Radical Polymerization. *Macromolecules* **2001,** *34* (15), 5099-5102.
(24) Wei, Y.; Jia, Y.; Wang, W.-J.; Li, B.-G.; Zhu, S., Surfactant–Ligand Design for ab Initio Emulsion Atom Transfer Radical Polymerization. *Macromolecules* **2014,** *47* (22), 7701-7706.
(25) Williams, V. A.; Ribelli, T. G.; Chmielarz, P.; Park, S.; Matyjaszewski, K., A Silver Bullet: Elemental Silver as an Efficient Reducing Agent for Atom Transfer Radical Polymerization of Acrylates. *J Am Chem Soc* **2015,** *137* (4), 1428-1431.
(26) Wei, Y.; Liu, P.; Wang, W.-J.; Li, B.-G.; Zhu, S., Well-Controlled and Stable Emulsion ATRP of MMA with Low Surfactant Concentration using Surfactant-Ligand Design as the Copper Capture Agent. *Polym Chem-Uk* **2015,** *6* (15), 2837-2843.
(27) Wei, Y.; Zhang, Q.; Wang, W. J.; Li, B. G.; Zhu, S., Improvement on Stability of Polymeric Latexes Prepared by Emulsion ATRP through Copper Removal using Electrolysis. *Polymer* **2016,** *106*, 261-266.
(28) Kagawa, Y.; Zetterlund, P. B.; Minami, H.; Okubo, M., Compartmentalization in Atom Transfer Radical Polymerization (ATRP) in Dispersed Systems. *Macromol. Theory Simul.* **2006,** *15* (8), 608-613.
(29) Zetterlund, P. B.; Kagawa, Y.; Okubo, M., Compartmentalization in Atom Transfer Radical Polymerization of Styrene in Dispersed Systems: Effects of Target Molecular Weight and Halide End Group. *Macromolecules* **2009,** *42* (7), 2488-2496.
(30) Thomson, M. E.; Cunningham, M. F., Compartmentalization Effects on the Rate of Polymerization and the Degree of Control in ATRP Aqueous Dispersed Phase Polymerization. *Macromolecules* **2010,** *43* (6), 2772-2779.
(31) Xia, J.; Matyjaszewski, K., Controlled/"Living" Radical Polymerization. Atom Transfer Radical Polymerization Catalyzed by Copper(I) and Picolylamine Complexes. *Macromolecules* **1999,** *32* (8), 2434-2437.
(32) Schröder, K.; Mathers, R. T.; Buback, J.; Konkolewicz, D.; Magenau, A. J. D.; Matyjaszewski, K., Substituted Tris(2-pyridylmethyl)amine Ligands for Highly Active ATRP Catalysts. *Acs Macro Lett* **2012,** *1* (8), 1037-1040.
(33) Queffelec, J.; Gaynor, S. G.; Matyjaszewski, K., Optimization of Atom Transfer Radical Polymerization Using Cu(I)/Tris(2-(dimethylamino)ethyl)amine as a Catalyst. *Macromolecules* **2000,** *33* (23), 8629-8639.
(34) Martin, R. D.; Unwin, P. R., Theory and Experiment for the Substrate Generation/Tip Collection Mode of the Scanning Electrochemical Microscope: Application as an Approach for Measuring the Diffusion Coefficient Ratio of a Redox Couple. *Analytical Chemistry* **1998,** *70* (2), 276-284.
(35) Bergstrom, M.; Skov Pedersen, J., Structure of Pure SDS and DTAB Micelles in Brine Determined by Small-Angle Neutron Scattering (SANS). *Physical Chemistry Chemical Physics* **1999,** *1* (18), 4437-4446.
(36) Shah, S. S.; Jamroz, N. U.; Sharif, Q. M., Micellization Parameters and Electrostatic Interactions in Micellar Solution of Sodium Dodecyl Sulfate (SDS) at Different

Temperatures. *Colloids and Surfaces A: Physicochemical and Engineering Aspects* **2001,** *178* (1–3), 199-206.

Appendix 2 Synthesis of Nanoparticle Copolymer Brushes via Surface-Initiated *se*ATRP

A2.1. Introduction

Various silica nanoparticles (NPs) are commercially available and are used in industrial applications, such as catalysis, pigments, electronics, thin film substrates, electric and thermal insulators, humidity sensors, pharmacy, and biomedical approaches, such as drug delivery, bioimaging, sensing, and therapeutics.[1-8] Tethering polymeric chains to the surface of nano-sized inorganic particles has emerged as a powerful approach to stabilize NPs dispersions, "engineer" the physicochemical properties of particles but also as a route towards the synthesis of nanocomposite materials with new functionalities.[9-15] Preparation of stable inorganic-organic hybrid materials involves covalent binding of the polymer chains to the nanoparticles. This can be achieved e.g. *via* a *grafting-onto* approach, where polymer chains containing end-functional groups are synthesized and subsequently attached to the surface of the nanoparticles modified with complementary functional groups. This method is typically limited by the slow diffusion of polymer chains to the surface of the substrate and by the steric hindrance of the tethering sites arising from formation of random coils by the attached polymer chains.[10, 16] Another technique, *grafting-through*, utilizes tethering units of a polymerizable monomer to the surface of the nanoparticle. Subsequently, the covalently attached monomer is copolymerized with a low molecular weight monomer present in the contacting solution, yielding tethered polymers.[15] This method is less common, since it typically results in lower grafting

densities. Finally, the *grafting-from* method involves two steps: binding low molecular weight initiating groups to the surface of the particle and subsequent formation of polymers.[16] This is commonly achieved *via* a reversible-deactivation radical polymerization (RDRP) methods,[11, 15, 17] although anionic polymerization,[18] ring opening metathesis polymerization (ROMP),[19] or conventional radical polymerization[20-21] can also be used. RDRP allows for simultaneous growth of all chains affording high grafting densities and good control over the physicochemical properties of polymer-tethered particles.[22-23]

RDRP methods most commonly used for *grafting-from* include reversible addition-fragmentation chain transfer (RAFT) polymerization,[24] nitroxide-mediated polymerization (NMP),[25] and atom transfer radical polymerization (ATRP).[11, 15, 26] Surface-initiated ATRP (SI-ATRP) is one of the most established approaches to form hybrid particles.[10-11, 15, 17] It provides excellent control over architecture and wide range of accessible chemistries and compositions of the grafted polymer chains.[11, 15, 17, 27] The hybrid nanoparticle radius can be adjusted via fine-tuning of the grafting density (σ) and degree of polymerization (N) of the tethered chains. SI-ATRP allows one to synthesize well-defined polymer brushes with high grafting densities.[10-11, 15, 17, 22-23, 28-29] A wide variety of organic-inorganic hybrid materials, including matrix-free nanocomposites,[26, 30-31] compatibilizing fillers,[32] functional additives,[33-35] responsive particles,[36-37] functional surfaces,[38-39] and membranes[40-43] were successfully prepared *via* SI-ATRP in the past decade.

Recently several ATRP techniques utilizing low ppm of catalyst complex have emerged that possess broad capabilities in preparation of polymeric materials.[44-45] This includes activators regenerated by electron transfer (ARGET) ATRP,[46-48] supplemental

activator and reducing agent (SARA) ATRP,[49-51] initiators for continuous activator regeneration (ICAR) ATRP,[52-53] photochemically mediated ATRP (photoATRP),[54-55] electrochemically mediated ATRP (*e*ATRP),[56-58] and metal-free ATRP.[59-60] Most of these ATRP techniques were successfully applied to grafting polymer brushes from a range of surfaces of different shapes and compositions.[30, 61-67] The opportunity to harness the high level of structural and compositional control that ist facilitated by ATRP at reduced Cu concentrations offers intriguing possibilities for the synthesis of hybrid materials. This is because the presence of even small amounts of Cu impurities will could generallybe detrimental to the physical properties of hybrid materials (such as optical transparency, dielectric properties, or photothermal stability) of hybrid materials which that are fundamental to their application in advanced material technologies.

*e*ATRP is of particular interest to the synthesis of functional materials because it does not require the addition of reducing agents (since electrons in this case are provided by an external source). Parameters such as the applied current, applied potential, and total charge passed can be defined in *e*ATRP to allow selection of the desired concentration of redox-active catalytic species, and therefore, enhancing the level of control during polymerization.[56] *e*ATRP can be even stopped and (re)initiated on demand by modulating the applied potential, offering temporal control over the polymerization.[56, 68] Moreover, the procedure is tolerant to small amounts of oxygen and allows a new approach to catalyst removal or recycle *via* electrodeposition.[58] *e*ATRP has shown versatility in synthesizing wide range of well-defined polymer architectures,[56, 58] although some limitations remain, especially associated with eATRP's the reaction setup. Conventional *e*ATRP requires a three-electrode system comprised of a working (WE), a counter (CE), and a reference

electrode (RE), resulting in a somewhat complex experimental setup. More recently, a simplified electrochemically mediated ATRP (*se*ATRP) procedure was developed. This procedure does not require the separation of cathodic and anodic compartments in the *e*ATRP reaction system and utilizes a sacrificial counter electrode, thereby significantly simplifying the reaction system.[57-58, 69-75] One of the potential advantages of applying *se*ATRP to particle systems is possibility to produce Cu-free hybrid materials for optical applications. Here we present for the first time grafting well-defined poly(*tert*-butyl acrylate) (P*t*BA), poly(*tert*-butyl acrylate)-*b*-poly(styrene) (P*t*BA-*b*-PS), and poly(*tert*-butyl acrylate)-*b*-poly(butyl acrylate) (P*t*BA-*b*-PBA) brushes from the surfaces of 15.8 nm silica nanoparticles *via se*ATRP (**Scheme A2-1**). The effect of applied potential on the polymerization behavior was examined in order to optimize preparation of (co)polymer brushes with low dispersity ($Đ = M_w/M_n$).

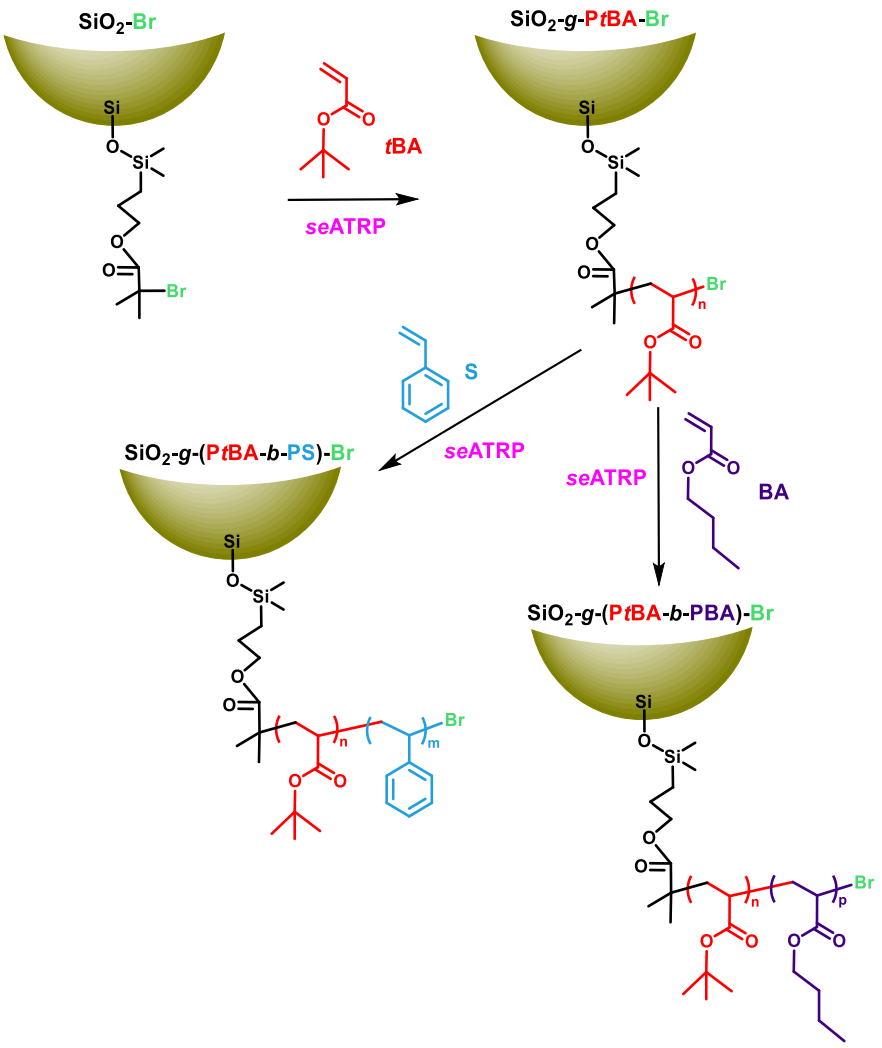

Scheme A2-1. Synthesis of P*t*BA-*b*-PS and P*t*BA-*b*-PBA brushes from silica nanoparticles by *se*ATRP.

A2.2. Results and Discussion

A Silica NPs with average diameter ⟨*d*⟩ = 15.8 nm were modified by tethering 3-(chlorodimethylsilyl)propyl 2-bromo-2-methylpropionate initiators to their surface, as

described in the literature.[76] The accessible initiator densities of the functionalized particles are typically ≈ 1 nm^{-2}, however grafting densities of polymers are usually smaller.[17, 23, 26, 30, 76-80] High targeted degrees of polymerization (1050 for homopolymer brushes and 4000 for block copolymer brushes) were selected to provide a sufficiently dilute reaction medium in order to avoid interparticle crosslinking.[11] The *se*ATRP procedure was used for the first time to graft well-defined (co)polymers composed of P*t*BA, P*t*BA-*b*-PS, or P*t*BA-*b*-PBA blocks from silica NPs (Table 1; Additional experimental data in Supporting Information). After the polymerizations were completed, silica cores were etched with HF to provide untethered polymer chains for size-exclusion chromatography (SEC) analysis. In all cases the experimental molecular weight (MW) correlated well with theoretical values and SEC traces showed well-defined, monomodal polymers with narrow molecular weight distributions (MWDs) ($Đ \leq 1.32$). Purified final products obtained by precipitation in methanol/water mixtures were studied by thermogravimetric analysis (TGA) to determine the fraction of the inorganic content and polymer graft densities (σ). The obtained hybrid materials were also characterized with dynamic light scattering (DLS), and transmission electron microscopy (TEM).

Table A2-1. Summary of homopolymer and block copolymer brushes grafted from silica NPs.

	Entry	Monomer	$[M]_0/[I]_0/[Cu^{II}Br_2]_0/[TPMA]_0$	E_{app}[a]	k_p^{app} (h^{-1})[b]	$M_{n,th}$ ($\times10^3$)[c]	$M_{n,app}$ ($\times10^3$)[d]	$Đ$[d]	$d_{Z\text{-}ave}$ (nm)[e]	σ (nm^{-2})[f]
Homopolymer brushes	1	*t*BA	1050/1[g]/0.105/0.21	–	0.239	51.2	49.8	1.18	126±1	0.92
	2	*t*BA	1050/1[g]/0.105/0.21	E_{pc} – 120 mV	0.348	58.7	64.5	1.29	147±1	0.93
	3	*t*BA	1050/1[g]/0.105/0.21	E_{pc} – 80 mV	0.286	54.9	60.3	1.21	137±1	0.89
	4	*t*BA	1050/1[g]/0.105/0.21	E_{pc} – 40 mV	0.236	48.5	57.4	1.32	135±1	0.88
	5	*t*BA	1050/1[g]/0.105/0.21	E_{pc}	0.177	38.6	36.0	1.32	86±1	0.71
Copolymer brushes	6	S	48000/1[h]/0.4/0.8	E_{pc} – 80 mV	0.014	92.9	86.5	1.20	155±1	0.88
	7	BA	4000/1[h]/0.4/0.8	E_{pc} – 80 mV	0.023	108.0	98.1	1.21	195±1	0.70

General reaction conditions: T = 55 °C; V_{tot} = 28.2 mL (except entry 1: V_{tot} = 10 mL); t = 1.73 h (except entry 6: t = 5 h, entry 7: t = 4 h); $[tBA]_0$ = 3.4 M (except entry 6: $[S]_0$ = 4.3 M and entry 7: $[BA]_0$ = 3.5 M); [I]: $[SiO_2\text{-Br}, \approx 1\ Br/nm^2]_0$ = 3.23 mM (except entry 6: $[SiO_2\text{-}g\text{-P}t\text{BA-Br}]_0$ = 1.08 M and entry 7: $[SiO_2\text{-}g\text{-P}t\text{BA-Br}]_0$ = 0.87 M); [TBAP] = 0.2 M (except entry 1: [TBAP] = 0.0 M). SARA ATRP (Cu^0 wire (l = 1 cm, d = 1 mm, S/V = 0.033 cm^{-1})): entry 1; *se*ATRP under constant potential electrolysis (WE = Pt mesh, CE = Al wire (l = 10 cm, d = 1 mm), RE = Ag/AgI/I^-): entries 2–7. [a]Applied potential (E_{app}) was selected based on cyclic voltammetry (CV) analysis of catalyst complex; [b]Monomer conversion was determined by ^{1}H NMR;[72] [c]$M_{n,th} = ([M]_0/[I]_0) \times \text{conversion} \times M_{monomer} +$

$M_{initiator}$; [d]Apparent M_n and $Đ$ were determined from untethered polymer chains untethered from NPs by HF etching using THF SEC with PS standards; [e]Particle size ($d_{Z\text{-}ave}$) was measured by DLS; [f]Grafting density (σ) was calculated from TGA inorganic fraction;[64] [g]I = SiO_2-Br (for entries 1–5); [h]I = SiO_2-*g*-P*t*BA-Br indicated as entry 3 in **Table A2-1** (for entries 6–7).

Synthesis of P*t*BA brushes from silica NPs by SARA ATRP. Homopolymerization of *t*BA was also conducted *via* SARA ATRP (**Table A2-1**, entry 1) as reference for the electrochemically mediated polymerizations. An induction period was observed, which can be attributed to the necessity to reduce a fraction of the added Cu^{II}/L complex to a sufficient amount of Cu^{I}/L activator. Afterwards, a linear first-order kinetic plot was obtained. The MW of polymers detached from the particles correlated well with theoretical expectation and MWDs remained narrow. Brushes with a grafting density of ≈ 0.92 nm^{-2} were obtained, which is comparable with those prepared by *se*ATRP (**Table A2-1**, entry 1 vs entries 2–5). SARA ATRP provides a viable route for synthesis of hybrid nanoparticles. However, it has a drawback of gradually introducing additional soluble Cu species into the reaction mixture *via* supplemental activation of alkyl halides by Cu^0 and comproportionation of Cu^{II} with Cu^0. It was reported that in aqueous SARA ATRP of oligo(ethylene oxide) methyl ether acrylate (M_n = 480) the amount of soluble Cu complexes gradually increased from initially added 100 ppm up to ≈ 600 ppm.[81] Such an increase might require a more burdensome and costly purification of the desired hybrid material. In contrast, the total amount of soluble Cu species in *se*ATRP is constant and equivalent to the quantity initially introduced into the reaction medium.

Influence of the applied potential on silica NPs grafting density. The choice of a suitable applied potential (E_{app}) is crucial when using controlled potential preparative electrolysis.[58] The effect of the E_{app} (E_{pc} – 120 mV, E_{pc} – 80 mV, E_{pc} – 40 mV, and E_{pc}) on the polymerization of *t*BA was investigated (**Figure A2-0-1**a). Similar to our previous studies[58, 70-72] faster rates of reduction provided faster polymerizations (**Table A2-1**, entries 2–5). This was caused by the faster regeneration of the activator and resulting higher concentration of the radical species ($[P_n^{\bullet}]$).[58, 82-83] As the rate of polymerization is proportional to $[P_n^{\bullet}]$ and to the square root of $[X–Cu^{II}/L]$, it can be tuned by the choice of an appropriate E_{app}.[58, 82-83] In all cases a linear relationship was observed between experimental and theoretical MW, and the MWDs remained narrow (**Figure A2-0-1**b), demonstrating good control over the polymerization. Both the MW of the P*t*BA homopolymer brushes etched from the silica NPs (38,600 – 58,700) and the grafting density (0.71 – 0.93 nm^{-2}) of the polymers attached to the NPs correlated well with the applied reduction potential (**Figure A2-0-1**c).

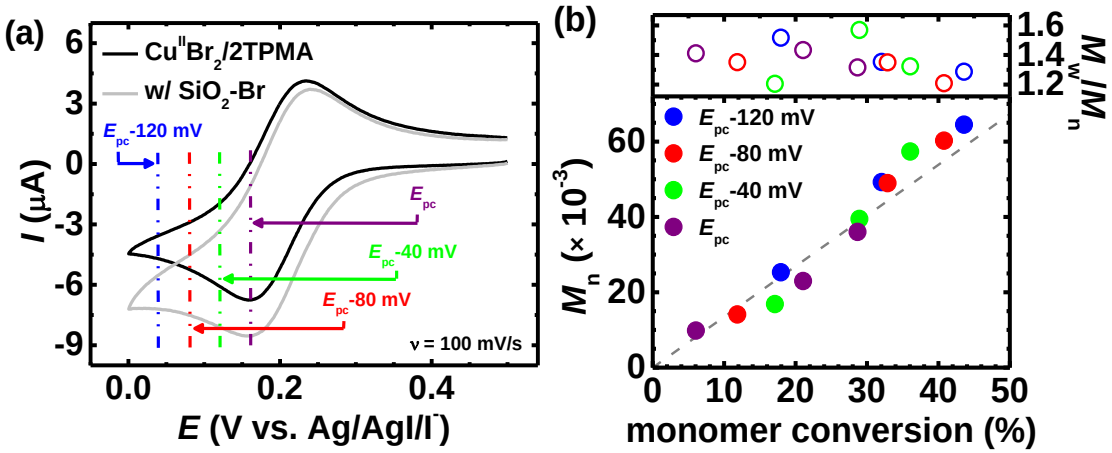

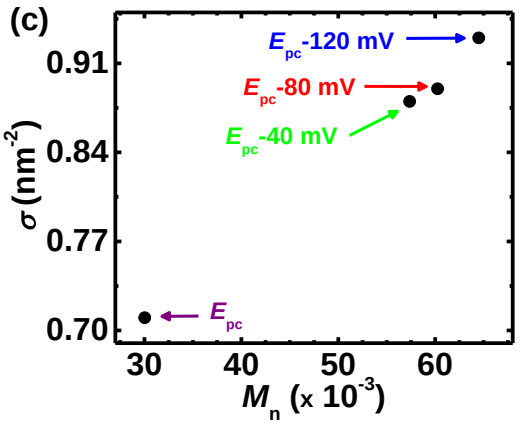

Figure A2-0-1. Synthesis of P*t*BA brushes from silica NPs as a function of applied potential. (a) Cyclic voltammetry of $Cu^{II}Br_2$/2TPMA with and without initiator (vertical lines indicate E_{app}), (b) M_n and M_w/M_n vs monomer conversion, and (c) grafting density (σ) vs M_n. Reaction conditions: [*t*BA]/[SiO_2-Br]/[$Cu^{II}Br_2$]/[TPMA] = 1050/1/0.105/0.21, $[tBA]_0$ = 3.4 M, T = 55 °C, [TBAP] = 0.2 M, V_{tot} = 28.2 mL. **Table A2-1**, entries 2–5.

Temporal control over polymerization. Application of external stimuli offers an exclusive possibility of temporal control, i.e. stopping and restarting the polymerization by switching the stimuli "off" and "on", respectively.[84] Despite multiple on/off cycles, high chain end functionality can be retained without compromising MW and MWD. This was previously demonstrated for *e*ATRP under homogeneous conditions by appropriately adjusting the applied potential.[56, 58] Similar effect was obtained by turning the light source on and off in photoATRP.[85] However, due to the use of nanoparticles in the current study, substantial light scattering could interfere or prevent efficient polymerization. Therefore, *e*ATRP offers a unique opportunity to synthesize well-defined hybrid nanoparticles with predefined size. To demonstrate the possibility of temporal control, *se*ATRP was carried out utilizing multiple-step potential electrolysis (**Figure A2-0-2**). When negative potential was applied ("ON" = E_{pc} – 80 mV) the reaction proceeded as expected. However, shortly upon applying more positive potential ("OFF" = E_{pc} + 720 mV) the reaction stopped. It

was efficiently restarted when the ON potential was reapplied. Such "pausing" of the reaction could be beneficial in preparation of hybrid nanoparticles with predictable molecular weights of the polymer grafts. After analysis, the reaction can easily be restarted, should longer grafts be required.

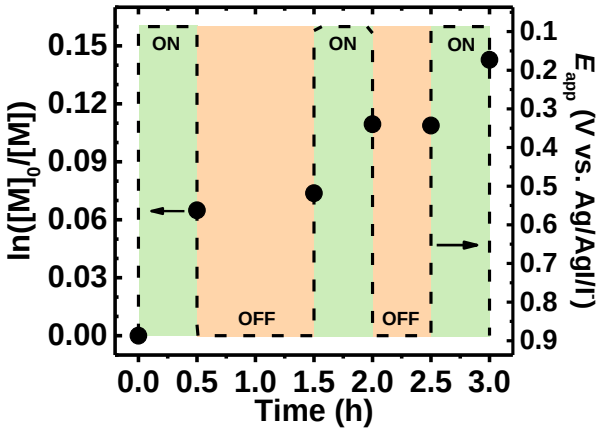

Figure A2-0-2. First-order kinetic plot of *se*ATRP with periodically applied different values of potential. Reaction conditions: [*t*BA]/[SiO_2-Br]/[$Cu^{II}Br_2$]/[TPMA] = 1050/1/0.021/0.042, $[tBA]_0$ = 3.4 M in DMF, T = 55 °C, [TBAP] = 0.2 M, V_{tot} = 28.2 mL. ON potential = E_{pc} – 80mV; OFF potential = E_{pc} + 720 mV.

Chain extension of SiO_2-*g*-P*t*BA brushes. The procedure to form diblock brushes was analogous to that of the homopolymer brushes, with the exception that a P*t*BA brush modified silica NPs were used instead of ATRP initiator modified NPs. This new SI–*se*ATRP technique offers some advantages in preparation of block copolymer tethered nanoparticles *e.g.* straightforward setup, enhanced control over polymerization rate, high achievable graft densities, and use of low amount of transition metal catalyst. The chain extension from P*t*BA brushes (**Table A2-1**, entry 3) with styrene (S) was conducted under constant potential preparative *electrolysis* conditions. A linear first-order kinetic plot was obtained (**Figure A2-0-3**a) and SEC traces demonstrated narrow MWD of the obtained

polymer (**Figure A2-0-3**b). High grafting density of ≈ 0.88 nm^{-2} was attained (**Table A2-1**). Grafting densities of ≈ 0.63 nm^{-2} were previously reported for PS-tethered SiO_2 particle brush materials prepared by SI–ATRP.[80]

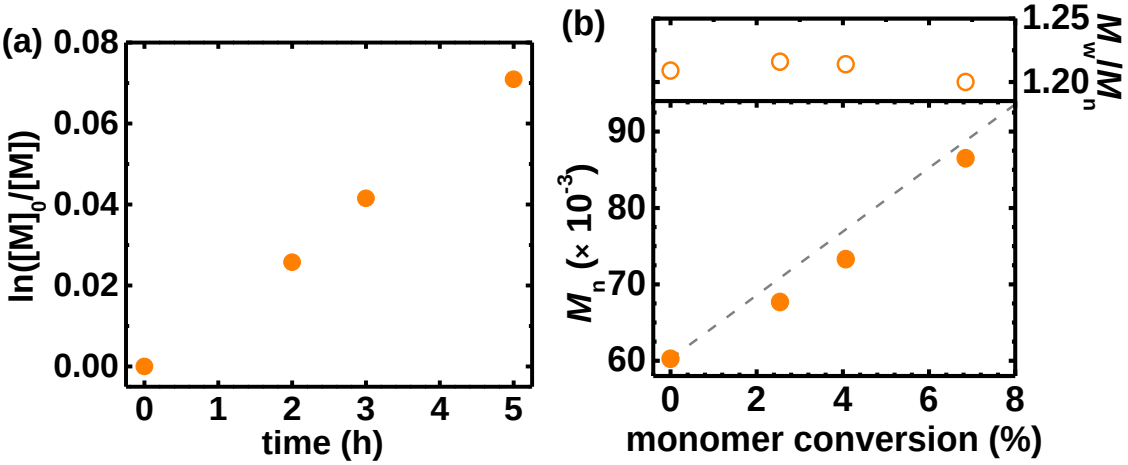

Figure A2-0-3. Chain extension of the P*t*BA-functionalized silica nanoparticles with styrene. (a) First-order kinetic plot of monomer conversion vs time, and (b) M_n and M_w/M_n vs monomer conversion. Reaction conditions: [S]/[SiO_2-*g*-P*t*BA-Br]/[$Cu^{II}Br_2$]/[TPMA] = 4000/1/0.4/0.8, $[S]_0$ = 4.3 M, T = 55 °C, [TBAP] = 0.2 M, V_{tot} = 28.2 mL. **Table A2-1**, entry 6.

Finally, chain extension of the P*t*BA brushes (**Table A2-1**, entry 3) with BA was conducted under constant potential electrolysis conditions. The polymerization was well-controlled with a linear first-order kinetic plot (**Figure A2-0-4**a). P*t*BA-*b*-PBA block copolymers etched from the silica NPs showed good correlation between experimental and theoretical MW and narrow MWD (**Figure A2-0-4**b). The reaction yielded brushes with a relatively high grafting density of ≈ 0.71 nm^{-2} that matches previously reported results for homopolymer grafted systems (**Table A2-1**, entry 7). For example, silica nanoparticles grafted with homopolymer PBA brushes with graft densities of around 0.80 nm^{-2} were reported.[86]

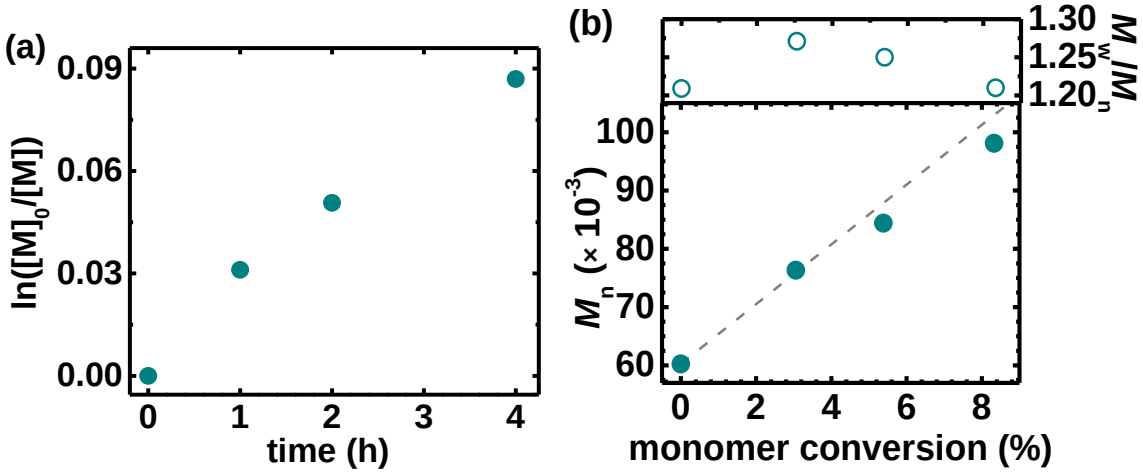

Figure A2-0-4. Chain extension of the P*t*BA-functionalized silica nanoparticles with BA. (a) First-order kinetic plot of monomer conversion vs time, and (b) M_n and M_w/M_n vs monomer conversion. Reaction conditions: [BA]/[SiO_2-*g*-P*t*BA-Br]/[$Cu^{II}Br_2$]/[TPMA] = 4000/1/0.4/0.8, $[BA]_0$ = 3.5 M, T = 55 °C, [TBAP] = 0.2 M, V_{tot} = 28.2 mL. **Table A2-1**, entry 7.

Material characterization. The silica hybrid materials were characterized with transmission electron microscopy (TEM), dynamic light scattering (DLS), and differential scanning calorimetry (DSC). Transmission electron microscopy (TEM) was carried out using a JEOL 2000 EX electron microscope operated at 200 kV. TEM images demonstrated successful grafting of P*t*BA from silica nanoparticles and showed no aggregated nanoparticles (**Figure A2-5**a) as compared to the unmodified silica NPs.

The breadth of the size distribution was inherited from the pristine NPs. Nonetheless, a relatively narrow size distribution of polymer-grafted nanoparticles was observed (**Figure A2-5**b). Increase of the degree of polymerization of P*t*BA brushes provided a linear increase of the particle size, *i. e.* $h \sim N$ where h denotes the 'brush height' that is equal to one half of the surface-to surface distance between neighboring particles. The

same relationship was observed for P*t*BA brushes prepared *via se*ATRP under on/off multiple-step potential electrolysis. This implied that the densely grafted polymer brushes were in the concentrated particle brush (CPB) regime.[26, 29] This is in agreement with theoretical predictions of the conformation of tethered chain in brush particles. For example, Fukuda and coworkers reported an extended Doud-Cotton model to predict the chain conformation of tethered chains.[23] Based on this model a transition from stretched chain conformations (CPB regime) to random-walk type conformation (semi-diluted polymer brush, SDPB, regime) is expected at $N_{crit} \approx 10^3$ for σ of 0.8–1.0 nm^{-2} when grafting from 15 nm NPs.[26, 87] Based on this estimate, we expected the transition to take place after chain extension as relatively smaller increase of particle brush sizes were observed, which agreed with the prediction. After chain extension (with either S or BA) excellent particle size uniformity was obtained and dispersions were stable without indication of aggregation (**Figure A2-5**c–f).

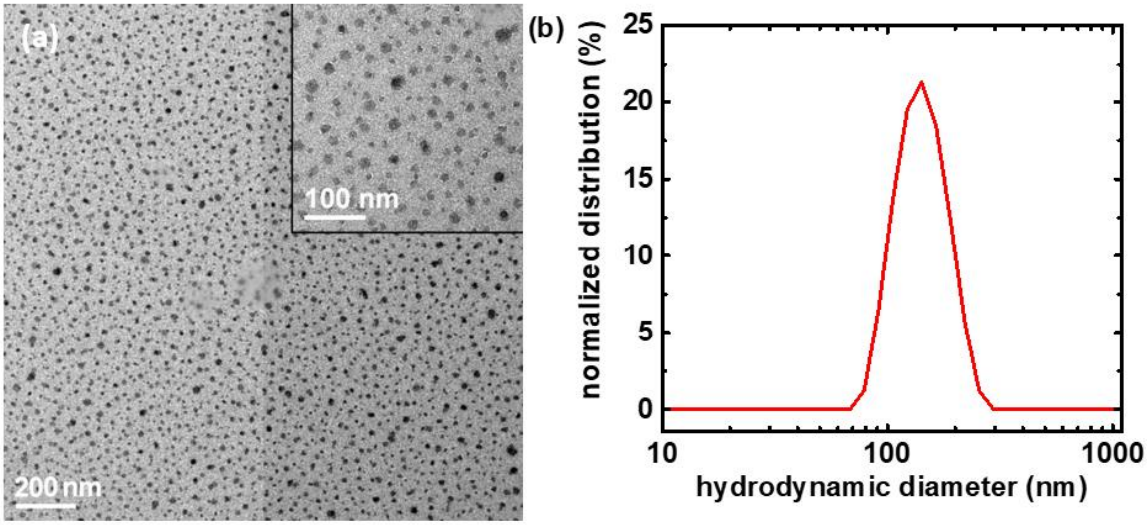

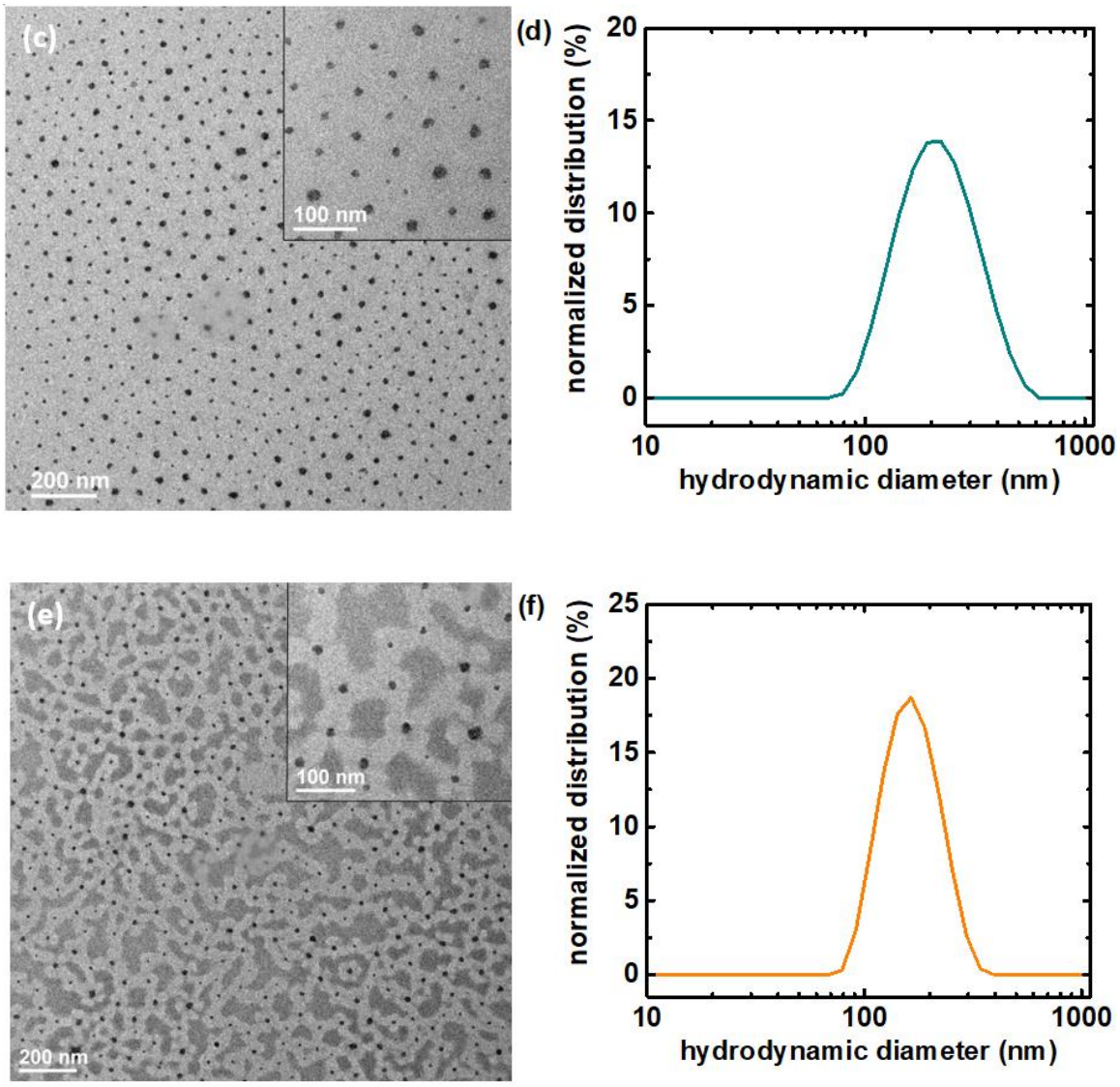

Figure A2-5. TEM images and DLS hydrodynamic size distributions by intensity (in THF) of (approximately) monolayer films of particle brushes grafted on silica NPs *via se*ATRP: P*t*BA (a,b; **Table A2-1**, entry 3), P*t*BA-*b*-PBA (c,d; **Table A2-1**, entry 7), and P*t*BA-*b*-PS (e,f; **Table A2-1**, entry 6).

Grafting of PBA resulted in an increase of the brush height (**Figure A2-5**c) which was in good agreement with the observed increase in hydrodynamic diameter to D_H = 195±1 nm (**Figure A2-5**d). Note that electron micrographs of SiO_2-P*t*BA-*b*-PBA particle brush monolayer such as shown in **Figure A2-5**c did not reveal insight into the state of

microphase separation of the block copolymer ligand. This is attributed to the very similar electron density and reactivity of P*t*BA and PBA segments that prevents contrast formation (or selective staining) of domains. To elucidate the microstructure, the glass transition temperatures were analyzed using DSC. DSC analysis of the P*t*BA brush modified silica NPs (**Table A2-1**, entry 3) exhibited a single T_g at ca. 44°C, which is approximately equal to the T_g of the P*t*BA homopolymer.[88] P*t*BA-*b*-PS diblock copolymers attached to silica NPs (**Table A2-1**, entry 6) showed two distinct T_g values at 46°C and 100°C, corresponding to the T_g values of P*t*BA[88] and PS[30, 80, 89] blocks, respectively. Also, two T_g values (-16°C and 42°C) were observed in P*t*BA-*b*-PBA diblock copolymers attached to silica NPs (**Table A2-1**, entry 7). In this case, however, T_g value of -16°C was in between the T_g of the PBA and P*t*BA homopolymers (-55°C[89] and 44°C[88], respectively), which suggested partial miscibility of the of the PBA block with the outer part of P*t*BA block. ~~Apparently,~~ ŧThe presence of the second T_g at 42°C, corresponding to the P*t*BA homopolymer suggests immiscibility of the most inner part of the P*t*BA chains, which are very densely packed, close to silica surface.

Analysis of the electron micrograph of the SiO_2-P*t*BA-*b*-PS system (**Figure A2-5**e) provides intriguing insight into the morphology of particle brush monolayer structures. We rationalize the microstructure observed in **Figure A2-5**e as a consequence of the symmetry-breaking effect of the polymer/air (and to a lesser extent the polymer/substrate) interface. To illustrate the idea, we note that the regular assembly of spherical SiO_2-P*t*BA-*b*-PS brush particles would be expected to result in an 'undulated' surface topology that is indicated in the upper image of **Figure A2-6**.

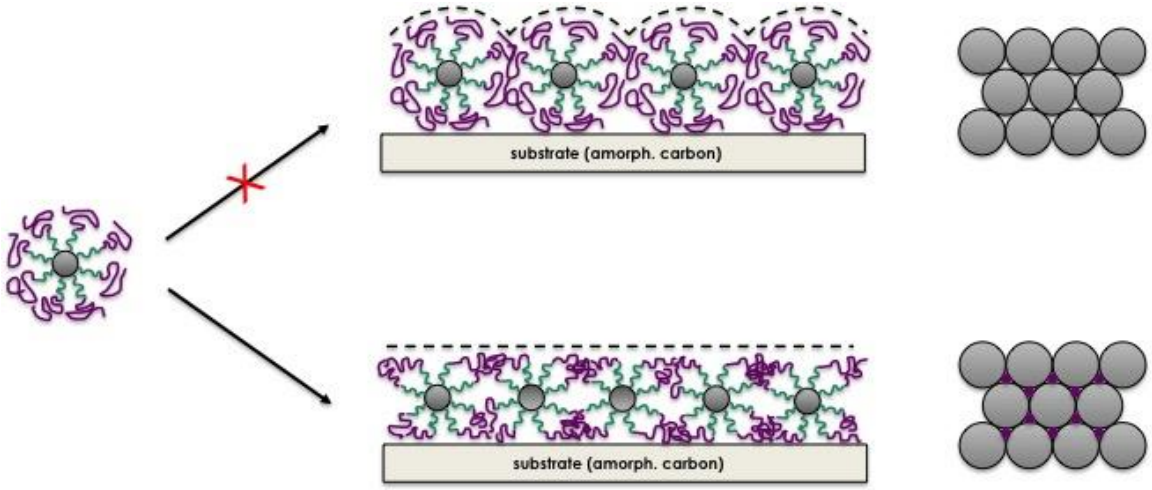

Figure A2-6. Illustration of the proposed structure formation process resulting in the morphology seen in **Figure A2-5**e. Relaxed PS segments (indicated as 'purple' block) stretch to fill in the void space in between adjacent brush particles and to minimize the total area of the polymer/air interface (indicated as black dotted line).

This situation is energetically unfavorable since it will create an excess surface area (and hence energy). To reduce the total interface area the relaxed brush segments are expected to stretch and fill the interstitial space as indicated in the lower panel of **Figure A2-6** (the energy penalty associated with the stretching of chains is considered negligible when compared to the interfacial energy of PS $_{PS}$ = 40 mJ/m^2).[90] Since only the 'outer' PS block is expected to be in the stretched regime this causes a 'redistribution' of PS chains that causes a characteristic six-fold contrast pattern in electron micrographs that is approximately observed in **Figure A2-5**e. We note that this process bears similarity to the segregation of filler additives to the void spaces in assembly structures formed by brush particles blended with homopolymer or nanoparticle fillers.[88, 89] To the best of our knowledge, this is the first example of such phase separation behavior of block copolymers grafted from nanoparticles.

A2.3. Conclusion

Well-defined densely grafted (co)polymer brushes were synthesized for the first time *via* a recently developed surface-initiated simplified electrochemically mediated atom transfer radical polymerization (SI-*se*ATRP) from 15.8 nm silica nanoparticles under constant potential preparative electrolysis conditions. The attractiveness of the presented method stems from the ability to prepare well-defined block copolymer brushes with the desired composition. The controlled/living characteristics of the system allowed for chain extension of the grafted P*t*BA brushes with a second PS or PBA block. Grafting densities up to ≈ 0.93 nm^{-2} were obtained. The rate of the polymerizations was enhanced by applying more negative potential values, which also resulted in an increase of grafting densities. Temporal control over polymerization was achieved by appropriately varying applied potential. All prepared (co)polymer brushes had narrow MWDs ($Đ$ = 1.20–1.32). Excellent particle polymer-grafted nanoparticle size uniformity was obtained and dispersions were stable without indication of any trace of nanoparticles aggregation. (P*t*BA-*b*-PS) block copolymers densely grafted from silica NPs show interesting morphological features in TEM. Relaxed outer PS segments stretch to fill in the void space in between adjacent brush particles and to minimize the total area of the polymer/air interface.

A2.4. Experimental Section

Materials. Silica nanoparticles (NPs), 30 wt% solution in methyl isobutyl ketone (MIBK-ST) were kindly donated by Nissan Chemical and used as received. Tetherable initiator, 3-(chlorodimethylsilyl)propyl 2-bromo-2-methylpropionate (BiBSiCl), was synthesized as described in a previous report.[76] Methanol (MeOH, Aldrich, > 99.8%),

tetrahydrofuran (THF, Aldrich, 99.5%), toluene (Aldrich, 99%), *N*,*N*-dimethylformamide (DMF, 99.9%, Acros), chlorodimethylsilane (Aldrich, 98%), 48 wt % aqueous hydrofluoric acid (HF, Aldrich, 99.99%), allyl alcohol (Aldrich, 99%), 2-bromoisobutyryl bromide (BriBBr, Aldrich, 98%), triethylamine (TEA, Aldrich, 99.5%), platinum cyclovinylmethylsiloxane complex (Gelest, 2% in cyclovinylmethylsiloxane), ammonium hydroxide aqueous solution (NH_4OH, 28.0-30.0%, Fisher), anhydrous magnesium sulfate ($MgSO_4$, Fisher), tetrabutylammonium perchlorate (TBAP, Aldrich, > 98%), and copper(II) bromide ($Cu^{II}Br_2$, Aldrich, 99.9%) were used as received unless otherwise stated. Tris(2-pyridylmethyl)amine (TPMA) was synthesized according to a published procedure.[91] Stock solutions of $Cu^{II}Br_2$ and TPMA were prepared according to a published procedure.[92] *tert*-Butyl acrylate (*t*BA, Aldrich, > 99%), *n*-butyl acrylate (BA, Aldrich, > 99%) and styrene (S, 99%, Aldrich) were passed through a column filled with basic alumina prior to use to remove any inhibitor. Platinum (Pt) wire, Pt mesh and Pt disk (3 mm diameter, Gamry) were purchased from Alfa Aesar, USA. Cyclic voltammetry and preparative electrolysis were conducted in an electrochemical cell kit (Gamry, USA).

Analysis. ^{1}H NMR spectra in $CDCl_3$, used for calculation of monomer conversion, were measured using Bruker Avance 300 MHz spectrometer. The apparent number-average molecular weights ($M_{n,app}$) and dispersities (*Đ,* M_w/M_n) were measured by size exclusion chromatography (SEC). The SEC was conducted with a Waters 515 pump and Waters 2414 differential refractometer using PSS columns (SDV 10^5, 10^3, 500 Å) with THF as eluent at 35 °C and at a flow rate of 1 mL/min. Linear PS standards were used for calibration. All samples were etched with HF before SEC measurement.[30] Thermogravimetric analysis (TGA) was performed on a TA Instrument TGA 2950 and the

data was processed with TA Universal Analysis software. The heating procedure involved four steps: (1) ramp up at 20 °C/min to 120 °C; (2) hold at 120 °C for 20 min; (3) high-resolution ramp up at 20 °C/min to 800 °C; (4) hold at 800 °C for 10 min. The organic contents of the samples were normalized to the weight loss between 120 °C and 800 °C. The grafting densities were calculated using a previously reported equation.[64]

$$\sigma_{\mathrm{TGA}} = \frac{\left(1 - f_{\mathrm{SiO_2}}\right) N_A \, \rho_{\mathrm{SiO_2}} d}{6 \, f_{\mathrm{SiO_2}} \, M_{\mathrm{n}}} \qquad \text{(S1)}$$

The value of $f_{\mathrm{SiO_2}}$ in the equation is the silica fraction measured by TGA after exclusion of any residual solvent; N_{A} is the Avogadro number; $\rho_{\mathrm{SiO_2}}$ is the density of silica NPs (1.9 g/cm^3); d is the average diameter of silica NPs; and M_{n} is the number-average molecular weight of polymer brushes. The glass transition temperature (T_{g}) of polymer grafted SiO_2 NPs with different compositions were measured by differential scanning calorimetry (DSC) using TA Instruments Q 2000. The same procedure was run three times, each involving the following steps: 1) hold at -80 ºC for 2 min; 2) heat to 130 ºC at a rate of 10 ºC/min; 3) hold for 2 min; 4) cool down to -80 ºC. The DSC data were analyzed with TA Universal Analysis and the T_{g} was directly acquired. Transmission electron microscopy (TEM) was performed using a JEOL 2000 EX electron microscope operated at 200 kV. All samples were dissolved in THF with concentration of 1 mg/mL, and solvent casting on Cu grids. To confirm results obtained from TEM, dynamic light scattering (DLS) using a Malvern Zetasizer Nano ZS at 25 °C with THF as dispersant was employed to determine Z-average hydrodynamic diameter and intensity-weighted distribution. The particles were suspended in filtered THF (220 nm PTFE filter) at low concentrations. Cyclic voltammetry and preparative electrolysis were recorded on a Gamry Ref 600 potentiostat. Each

electrolysis was carried out under N_2 atmosphere using a Pt disk for CV, (A = 0.071 cm^2) and Pt mesh for electrolysis, ($A \approx 6$ cm^2) working electrodes (WE). The counter electrode (CE, sacrificial anode) was Al wire (l = 15 cm, d = 1 mm). Values of potentials applied for preparative electrolysis were established from CV measurements at a 100 mV/s scan rate using $Ag/AgI/I^-$ reference electrode (RE) according to the previously published report.[93]

Surface modification of silica nanoparticles. Silica nanoparticles were modified as described in a previous report.[30, 64] The molar concentration of tetherable initiator was determined to be 1.5 initiator molecules per nm^2 of silica nanoparticles (assuming a sphere with a diameter of 15.8 nm).[26]

Synthesis of P*t*BA brushes from silica nanoparticles by SARA ATRP. Silica nanoparticles (0.098 g, 91 μmol, assuming ~1 accessible Br/nm^2), DMF (5 mL), *t*BA (5 mL, 34 mmol) and 0.07 mL of $Cu^{II}Br_2$/2TPMA stock solution (0.05 M in DMF) were mixed in a Schlenk flask and stirred for 24 h. The flask was heated to 55 °C and subsequently a Cu^0 wire (l = 1 cm, d = 1 mm) was added to the solution. Polymerization conditions were as follows: [*t*BA]/[SiO_2-Br]/[$Cu^{II}Br_2$]/[TPMA] = 1050/1/0.105/0.21, $[tBA]_0$ = 3.4 M in DMF, T = 55 °C, Cu^0 wire (l = 1 cm, d = 1 mm), V_{tot} = 10 mL. Samples were withdrawn periodically to follow the monomer conversion using ^{1}H NMR. The M_n and M_w/M_n were determined by THF SEC measurements (with PS standards). The final product was recovered by precipitation in methanol/water mixtures.

Reaction cell configuration for cyclic voltammetry. Electrochemical experiments were carried out under N_2 atmosphere using a Pt disk WE, a $Ag/AgI/I^-$ RE,

and an Al wire CE. TBAP (1.93 g, 5.6 mmol) was placed in an electrolysis cell maintained at 55 °C under N_2 purge. Then, 14 mL of N_2 purged *t*BA (96 mmol), 14 mL of N_2 purged DMF, and 0.19 mL of N_2 purged $Cu^{II}Br_2$/2TPMA stock solution (0.05 M in DMF) were added to the reaction cell. The CV of the catalyst complex was recorded (Figure 1a) and used for determining the appropriate applied potential ($E_{app} = E_{pc} - 120$ mV, $E_{app} = E_{pc} - 80$ mV, $E_{app} = E_{pc} - 40$ mV, and $E_{app} = E_{pc}$ vs. Ag/AgI/I^-).

Synthesis of P*t*BA brushes from silica nanoparticles by *se*ATRP. Silica nanoparticles (0.27 g, 91 μmol, assuming ~1 accessible Br/nm^2), TBAP (1.93 g, 5.6 mmol), DMF (14 mL), *t*BA (14 mL, 96 mmol), 0.19 mL of $Cu^{II}Br_2$/2TPMA stock solution (0.05 M in DMF) were placed in an electrolysis cell and stirred for 24 h. The mixture was purged with N_2 for 45 min, after which a CV was recorded (Figure 1a) using a Pt disk WE, a Ag/AgI/I^- RE, and an Al wire CE. Then a Pt mesh WE, Al wire CE, and Ag/AgI/I^- RE were immersed in the reaction solution and the selected potential ($E_{app} = E_{pc} - 120$ mV, $E_{app} = E_{pc} - 80$ mV, $E_{app} = E_{pc} - 40$ mV, and $E_{app} = E_{pc}$ vs. Ag/AgI/I^-) was applied using the controlled potential preparative electrolysis method. Polymerization conditions were as follows: [*t*BA]/[SiO_2-Br]/[$Cu^{II}Br_2$]/[TPMA] = 1050/1/0.105/0.21, $[tBA]_0$ = 3.4 M in DMF, T = 55 °C, [TBAP] = 0.2 M, V_{tot} = 28.2 mL. Samples were withdrawn periodically to follow the monomer conversion using ^{1}H NMR. The M_n and M_w/M_n were determined by THF SEC measurements (with PS standards). The final product was recovered by precipitation in methanol/water mixtures and dried under vacuum for 1 day.

Temporal Control in Synthesis of P*t*BA brushes from silica nanoparticles by *se*ATRP. Silica nanoparticles (0.27 g, 91 μmol, assuming ~1 accessible Br/nm^2), TBAP (1.93 g, 5.6 mmol), DMF (14 mL), *t*BA (14 mL, 96 mmol), 0.38 mL of $Cu^{II}Br_2$/2TPMA stock solution (0.05 M in DMF) were placed in an electrolysis cell and stirred for 24 h. The mixture was purged with N_2 for 45 min, after which a CV was recorded using a Pt disk WE, a Ag/AgI/I$^-$ RE, and an Al wire CE. Then a Pt mesh WE, Al wire CE, and Ag/AgI/I$^-$ RE were immersed in the reaction solution and a potential program ($E_{app} = E_{pc} - 80$ mV for the "on" stage and $E_{app} = E_{pc} + 720$ mV for the "off" stage vs. Ag/AgI/I$^-$) was applied using the controlled potential preparative electrolysis method. Polymerization conditions were as follows: [*t*BA]/[SiO_2-Br]/[$Cu^{II}Br_2$]/[TPMA] = 1050/1/0.021/0.042, $[tBA]_0$ = 3.4 M in DMF, T = 55 °C, [TBAP] = 0.2 M, V_{tot} = 28.2 mL. Samples were withdrawn periodically to follow the monomer conversion using ^{1}H NMR. The M_n and M_w/M_n were determined by THF SEC measurements (with PS standards). The final product was recovered by precipitation in methanol/water mixtures and dried under vacuum for 1 day.

Synthesis of P*t*BA-*b*-PS brushes from silica nanoparticles by *se*ATRP. The *se*ATRP method was used for the chain extension of SiO_2-*g*-P*t*BA-Br macroinitiator with S (Table 1, entry 3). Polymerization conditions were as follows: [S]/[SiO_2-*g*-P*t*BA-Br]/[$Cu^{II}Br_2$]/[TPMA] = 4000/1/0.4/0.8, $[S]_0$ = 4.3 M in DMF, $E_{app} = E_{pc} - 80$ mV vs. Ag/AgI/I$^-$ (Figure S3a), T = 55 °C, [TBAP] = 0.2 M, V_{tot} = 28.2 mL. Samples were withdrawn periodically to follow the monomer conversion using ^{1}H NMR. The M_n and M_w/M_n were determined by THF SEC measurements (with PS standards). The final product was recovered by precipitation in methanol/water mixtures and dried under vacuum for 1 day.

Synthesis of P*t*BA-*b*-PBA brushes from silica nanoparticles by *se*ATRP. The *se*ATRP method was used for the chain extension of SiO_2-*g*-P*t*BA-Br macroinitiator with BA (Table 1, entry 3). Polymerization conditions were as follows: [BA]/[SiO_2-*g*-P*t*BA-Br]/[$Cu^{II}Br_2$]/[TPMA] = 4000/1/0.4/0.8, $[BA]_0$ = 3.5 M in DMF, $E_{app} = E_{pc} - 80$ mV vs. Ag/AgI/I^- (Figure S5a), T = 55 °C, [TBAP] = 0.2 M, V_{tot} = 28.2 mL. Samples were withdrawn periodically to follow the monomer conversion using ^{1}H NMR. The M_n and M_w/M_n were determined by THF SEC measurements (with PS standards). The final product was recovered by precipitation in methanol/water mixtures and dried under vacuum for 1 day.

A2.5. References

(1) Rao, K. S.; El-Hami, K.; Kodaki, T.; Matsushige, K.; Makino, K., A Novel Method for Synthesis of Silica Nanoparticles. *J Colloid Interf Sci* **2005,** *289* (1), 125-131.
(2) Burns, A.; Ow, H.; Wiesner, U., Fluorescent Core-Shell Silica Nanoparticles: Towards "Lab on a Particle" Architectures for Nanobiotechnology. *Chem Soc Rev* **2006,** *35* (11), 1028-1042.
(3) Slowing, I. I.; Trewyn, B. G.; Giri, S.; Lin, V. S. Y., Mesoporous Silica Nanoparticles for Drug Delivery and Biosensing Applications. *Advanced Functional Materials* **2007,** *17* (8), 1225-1236.
(4) Slowing, I. I.; Trewyn, B. G.; Lin, V. S. Y., Mesoporous Silica Nanoparticles for Intracellular Delivery of Membrane-Impermeable Proteins. *J Am Chem Soc* **2007,** *129* (28), 8845-8849.
(5) Lu, J.; Liong, M.; Zink, J. I.; Tamanoi, F., Mesoporous Silica Nanoparticles as a Delivery System for Hydrophobic Anticancer Drugs. *Small* **2007,** *3* (8), 1341-1346.
(6) Torney, F.; Trewyn, B. G.; Lin, V. S. Y.; Wang, K., Mesoporous Silica Nanoparticles Deiver DNA and Cemicals into Pants. *Nat Nano* **2007,** *2* (5), 295-300.
(7) Li, Z.; Barnes, J. C.; Bosoy, A.; Stoddart, J. F.; Zink, J. I., Mesoporous Silica Nanoparticles in Biomedical Applications. *Chem Soc Rev* **2012,** *41* (7), 2590-2605.
(8) Tang, F.; Li, L.; Chen, D., Mesoporous Silica Nanoparticles: Synthesis, Biocompatibility and Drug Delivery. *Advanced Materials* **2012,** *24* (12), 1504-1534.

(9) Pyun, J.; Kowalewski, T.; Matyjaszewski, K., Synthesis of Polymer Brushes Using Atom Transfer Radical Polymerization. *Macromol Rapid Comm* **2003,** *24* (18), 1043-1059.
(10) Tsujii, Y.; Ohno, K.; Yamamoto, S.; Goto, A.; Fukuda, T., Structure and Properties of High-Density Polymer Brushes Prepared by Surface-Initiated Living Radical Polymerization. *Adv Polym Sci* **2006,** *197*, 1-45.
(11) Hui, C. M.; Pietrasik, J.; Schmitt, M.; Mahoney, C.; Choi, J.; Bockstaller, M. R.; Matyjaszewski, K., Surface-Initiated Polymerization as an Enabling Tool for Multifunctional (Nano-)Engineered Hybrid Materials. *Chem Mater* **2014,** *26* (1), 745-762.
(12) Fernandes, N. J.; Koerner, H.; Giannelis, E. P.; Vaia, R. A., Hairy Nanoparticle Assemblies as One-Component Functional Polymer Nanocomposites: Opportunities and Challenges. *MRS Communications* **2013,** *3* (1), 13-29.
(13) Kumar, S. K.; Jouault, N.; Benicewicz, B.; Neely, T., Nanocomposites with Polymer Grafted Nanoparticles. *Macromolecules* **2013,** *46* (9), 3199-3214.
(14) Hilburg, S. L.; Elder, A. N.; Chung, H.; Ferebee, R. L.; Bockstaller, M. R.; Washburn, N. R., A Universal Route Towards Thermoplastic Lignin Composites with Improved Mechanical Properties. *Polymer* **2014,** *55* (4), 995-1003.
(15) Khabibullin, A.; Mastan, E.; Matyjaszewski, K.; Zhu, S., Surface-Initiated Atom Transfer Radical Polymerization. *Adv Polym Sci* **2016,** *270*, 29-76.
(16) Radhakrishnan, B.; Ranjan, R.; Brittain, W. J., Surface Initiated Polymerizations from Silica Nanoparticles. *Soft Matter* **2006,** *2* (5), 386-396.
(17) Barbey, R.; Lavanant, L.; Paripovic, D.; Schüwer, N.; Sugnaux, C.; Tugulu, S.; Klok, H.-A., Polymer Brushes via Surface-Initiated Controlled Radical Polymerization: Synthesis, Characterization, Properties, and Applications. *Chem Rev* **2009,** *109* (11), 5437-5527.
(18) Zhou, Q.; Wang, S.; Fan, X.; Advincula, R.; Mays, J., Living Anionic Surface-Initiated Polymerization (LASIP) of a Polymer on Silica Nanoparticles. *Langmuir* **2002,** *18* (8), 3324-3331.
(19) Watson, K. J.; Zhu, J.; Nguyen, S. T.; Mirkin, C. A., Hybrid Nanoparticles with Block Copolymer Shell Structures. *J Am Chem Soc* **1999,** *121* (2), 462-463.
(20) Prucker, O.; Rühe, J., Synthesis of Poly(styrene) Monolayers Attached to High Surface Area Silica Gels through Self-Assembled Monolayers of Azo Initiators. *Macromolecules* **1998,** *31* (3), 592-601.
(21) Prucker, O.; Rühe, J., Mechanism of Radical Chain Polymerizations Initiated by Azo Compounds Covalently Bound to the Surface of Spherical Particles. *Macromolecules* **1998,** *31* (3), 602-613.
(22) Ohno, K.; Koh, K.; Tsujii, Y.; Fukuda, T., Fabrication of Ordered Arrays of Gold Nanoparticles Coated with High-Density Polymer Brushes. *Angewandte Chemie International Edition* **2003,** *42* (24), 2751-2754.
(23) Ohno, K.; Morinaga, T.; Koh, K.; Tsujii, Y.; Fukuda, T., Synthesis of Monodisperse Silica Particles Coated with Well-Defined, High-Density Polymer Brushes by Surface-Initiated Atom Transfer Radical Polymerization. *Macromolecules* **2005,** *38* (6), 2137-2142.
(24) Li, C.; Han, J.; Ryu, C. Y.; Benicewicz, B. C., A Versatile Method To Prepare RAFT Agent Anchored Substrates and the Preparation of PMMA Grafted Nanoparticles. *Macromolecules* **2006,** *39* (9), 3175-3183.
(25) Bartholome, C.; Beyou, E.; Bourgeat-Lami, E.; Chaumont, P.; Zydowicz, N., Nitroxide-Mediated Polymerizations from Silica Nanoparticle Surfaces: "Graft from"

Polymerization of Styrene Using a Triethoxysilyl-Terminated Alkoxyamine Initiator. *Macromolecules* **2003,** *36* (21), 7946-7952.
(26) Choi, J.; Hui, C. M.; Pietrasik, J.; Dong, H.; Matyjaszewski, K.; Bockstaller, M. R., Toughening Fragile Matter: Mechanical Properties of Particle Solids Assembled from Polymer-Trafted Hybrid Particles Synthesized by ATRP. *Soft Matter* **2012,** *8* (15), 4072-4082.
(27) Pyun, J.; Matyjaszewski, K., Synthesis of Nanocomposite Organic/Inorganic Hybrid Materials Using Controlled "Living" Radical Polymerization. *Chem Mater* **2001,** *13* (10), 3436-3448.
(28) Yoshikawa, C.; Goto, A.; Tsujii, Y.; Fukuda, T.; Yamamoto, K.; Kishida, A., Fabrication of High-Density Polymer Brush on Polymer Substrate by Surface-Initiated Living Radical Polymerization. *Macromolecules* **2005,** *38* (11), 4604-4610.
(29) Ohno, K.; Morinaga, T.; Takeno, S.; Tsujii, Y.; Fukuda, T., Suspensions of Silica Particles Grafted with Concentrated Polymer Brush: Effects of Graft Chain Length on Brush Layer Thickness and Colloidal Crystallization. *Macromolecules* **2007,** *40* (25), 9143-9150.
(30) Yan, J.; Kristufek, T.; Schmitt, M.; Wang, Z.; Xie, G.; Dang, A.; Hui, C. M.; Pietrasik, J.; Bockstaller, M. R.; Matyjaszewski, K., Matrix-free Particle Brush System with Bimodal Molecular Weight Distribution Prepared by SI-ATRP. *Macromolecules* **2015,** *48* (22), 8208-8218.
(31) Huang, Y.; Huang, X.; Schadler, L. S.; He, J.; Jiang, P., Core@Double-Shell Structured Nanocomposites: A Route to High Dielectric Constant and Low Loss Material. *ACS Applied Materials & Interfaces* **2016,** *8* (38), 25496-25507.
(32) Dang, A.; Ojha, S.; Hui, C. M.; Mahoney, C.; Matyjaszewski, K.; Bockstaller, M. R., High-Transparency Polymer Nanocomposites Enabled by Polymer-Graft Modification of Particle Fillers. *Langmuir* **2014,** *30* (48), 14434-14442.
(33) Ojha, S.; Dang, A.; Hui, C. M.; Mahoney, C.; Matyjaszewski, K.; Bockstaller, M. R., Strategies for the Synthesis of Thermoplastic Polymer Nanocomposite Materials with High Inorganic Filling Fraction. *Langmuir* **2013,** *29* (28), 8989-8996.
(34) Halim, A.; Fu, Q.; Yong, Q.; Gurr, P. A.; Kentish, S. E.; Qiao, G. G., Soft Polymeric Nanoparticle Additives for Next Generation Gas Separation Membranes. *Journal of Materials Chemistry A* **2014,** *2* (14), 4999-5009.
(35) Wright, R. A. E.; Wang, K.; Qu, J.; Zhao, B., Oil-Soluble Polymer Brush Grafted Nanoparticles as Effective Lubricant Additives for Friction and Wear Reduction. *Angewandte Chemie International Edition* **2016,** *55* (30), 8656-8660.
(36) Kim, D. J.; Kang, S. M.; Kong, B.; Kim, W.-J.; Paik, H.-j.; Choi, H.; Choi, I. S., Formation of Thermoresponsive Gold Nanoparticle/PNIPAAm Hybrids by Surface-Initiated, Atom Transfer Radical Polymerization in Aqueous Media. *Macromol Chem Phys* **2005,** *206* (19), 1941-1946.
(37) Wei, Q.; Ji, J.; Shen, J., Synthesis of Near‐Infrared Responsive Gold Nanorod/PNIPAAm Core/Shell Nanohybrids via Surface Initiated ATRP for Smart Drug Delivery. *Macromol Rapid Comm* **2008,** *29* (8), 645-650.
(38) Ma, H.; Hyun, J.; Stiller, P.; Chilkoti, A., "Non‐Fouling" Oligo (ethylene glycol)‐Functionalized Polymer Brushes Synthesized by Surface‐Initiated Atom Transfer Radical Polymerization. *Advanced Materials* **2004,** *16* (4), 338-341.

(39) Hua, Z.; Yang, J.; Wang, T.; Liu, G.; Zhang, G., Transparent Surface with Reversibly Switchable Wettability between Superhydrophobicity and Superhydrophilicity. *Langmuir* **2013,** *29* (33), 10307-10312.
(40) Yang, Q.; Tian, J.; Hu, M.-X.; Xu, Z.-K., Construction of a Comb-like Glycosylated Membrane Surface by a Combination of UV-Induced Graft Polymerization and Surface-Initiated ATRP. *Langmuir* **2007,** *23* (12), 6684-6690.
(41) Frost, S.; Ulbricht, M., Thermoresponsive Ultrafiltration Membranes for the Switchable Permeation and Fractionation of Nanoparticles. *Journal of Membrane Science* **2013,** *448*, 1-11.
(42) Zhi, S.-H.; Xu, J.; Deng, R.; Wan, L.-S.; Xu, Z.-K., Poly(vinylidene Fluoride) Ultrafiltration Membranes Containing Hybrid Silica Nanoparticles: Preparation, Characterization and Performance. *Polymer* **2014,** *55* (6), 1333-1340.
(43) He, K.; Duan, H.; Chen, G. Y.; Liu, X.; Yang, W.; Wang, D., Cleaning of Oil Fouling with Water Enabled by Zwitterionic Polyelectrolyte Coatings: Overcoming the Imperative Challenge of Oil–water Separation Membranes. *ACS Nano* **2015,** *9* (9), 9188-9198.
(44) Matyjaszewski, K., Atom transfer radical polymerization (ATRP): current status and future perspectives. *Macromolecules* **2012,** *45* (10), 4015-4039.
(45) Matyjaszewski, K.; Tsarevsky, N. V., Macromolecular Engineering by Atom Transfer Radical Polymerization. *Journal of the American Chemical Society* **2014,** *136* (18), 6513-6533.
(46) Jakubowski, W.; Matyjaszewski, K., Activators Regenerated by Electron Transfer for Atom ‐ Transfer Radical Polymerization of (Meth)acrylates and Related Block Copolymers. *Angewandte Chemie* **2006,** *118* (27), 4594-4598.
(47) Jakubowski, W.; Min, K.; Matyjaszewski, K., Activators Regenerated by Electron Transfer for Atom Transfer Radical Polymerization of Styrene. *Macromolecules* **2006,** *39* (1), 39-45.
(48) Simakova, A.; Averick, S. E.; Konkolewicz, D.; Matyjaszewski, K., Aqueous ARGET ATRP. *Macromolecules* **2012,** *45* (16), 6371-6379.
(49) Matyjaszewski, K.; Coca, S.; Gaynor, S. G.; Wei, M.; Woodworth, B. E., Zerovalent Metals in Controlled/“Living” Radical Polymerization. *Macromolecules* **1997,** *30* (23), 7348-7350.
(50) Konkolewicz, D.; Wang, Y.; Zhong, M.; Krys, P.; Isse, A. A.; Gennaro, A.; Matyjaszewski, K., Reversible-Deactivation Radical Polymerization in the Presence of Metallic Copper. A Critical Assessment of the SARA ATRP and SET-LRP Mechanisms. *Macromolecules* **2013,** *46* (22), 8749-8772.
(51) Konkolewicz, D.; Wang, Y.; Krys, P.; Zhong, M.; Isse, A. A.; Gennaro, A.; Matyjaszewski, K., SARA ATRP or SET-LRP. End of controversy? *Polym Chem-Uk* **2014,** *5* (15), 4396-4417.
(52) Matyjaszewski, K.; Jakubowski, W.; Min, K.; Tang, W.; Huang, J.; Braunecker, W. A.; Tsarevsky, N. V., Diminishing Catalyst Concentration in Atom Transfer Radical polymerization with Reducing Agents. *Proceedings of the National Academy of Sciences* **2006,** *103* (42), 15309-15314.
(53) Konkolewicz, D.; Magenau, A. J. D.; Averick, S. E.; Simakova, A.; He, H.; Matyjaszewski, K., ICAR ATRP with ppm Cu Catalyst in Water. *Macromolecules* **2012,** *45* (11), 4461-4468.

(54) Ribelli, T. G.; Konkolewicz, D.; Bernhard, S.; Matyjaszewski, K., How are Radicals (Re) Generated in Photochemical ATRP? *J Am Chem Soc* **2014,** *136* (38), 13303-13312.
(55) Pan, X.; Tasdelen, M. A.; Laun, J.; Junkers, T.; Yagci, Y.; Matyjaszewski, K., Photomediated Controlled Radical Polymerization. *Prog Polym Sci* **2016,** *62*, 73-125.
(56) Magenau, A. J. D.; Strandwitz, N. C.; Gennaro, A.; Matyjaszewski, K., Electrochemically Mediated Atom Transfer Radical Polymerization. *Science* **2011,** *332* (6025), 81-84.
(57) Park, S.; Chmielarz, P.; Gennaro, A.; Matyjaszewski, K., Simplified electrochemically mediated atom transfer radical polymerization using a sacrificial anode. *Angewandte Chemie International Edition* **2015,** *54* (8), 2388-2392.
(58) Chmielarz, P.; Fantin, M.; Park, S.; Isse, A. A.; Gennaro, A.; Magenau, A. J. D.; Sobkowiak, A.; Matyjaszewski, K., Electrochemically Mediated Atom Transfer Radical Polymerization (*e*ATRP). *Progress in Polymer Science* **2017,** *in press*.
(59) Treat, N. J.; Sprafke, H.; Kramer, J. W.; Clark, P. G.; Barton, B. E.; Read de Alaniz, J.; Fors, B. P.; Hawker, C. J., Metal-Free Atom Transfer Radical Polymerization. *J Am Chem Soc* **2014,** *136* (45), 16096-16101.
(60) Pan, X.; Lamson, M.; Yan, J.; Matyjaszewski, K., Photoinduced Metal-Free Atom Transfer Radical Polymerization of Acrylonitrile. *Acs Macro Lett* **2015,** *4* (2), 192-196.
(61) Zou, Y.; Kizhakkedathu, J. N.; Brooks, D. E., Surface Modification of Polyvinyl Chloride Sheets via Growth of Hydrophilic Polymer Brushes. *Macromolecules* **2009,** *42* (9), 3258-3268.
(62) Li, B.; Yu, B.; Huck, W. T. S.; Zhou, F.; Liu, W., Electrochemically Induced Surface-Initiated Atom-Transfer Radical Polymerization. *Angewandte Chemie International Edition* **2012,** *51* (21), 5092-5095.
(63) Yan, J.; Li, B.; Zhou, F.; Liu, W., Ultraviolet Light-Induced Surface-Initiated Atom-Transfer Radical Polymerization. *Acs Macro Lett* **2013,** *2* (7), 592-596.
(64) Yan, J.; Pan, X.; Schmitt, M.; Wang, Z.; Bockstaller, M. R.; Matyjaszewski, K., Enhancing Initiation Efficiency in Metal-Free Surface-Initiated Atom Transfer Radical Polymerization (SI-ATRP). *Acs Macro Lett* **2016,** *5*, 661-665.
(65) Song, Y.; Ye, G.; Lu, Y.; Chen, J.; Wang, J.; Matyjaszewski, K., Surface-Initiated ARGET ATRP of poly (glycidyl Methacrylate) from Carbon Nanotubes via Bioinspired Catechol Chemistry for Efficient Adsorption of Rranium Ions. *Acs Macro Lett* **2016,** *5* (3), 382-386.
(66) Discekici, E. H.; Pester, C. W.; Treat, N. J.; Lawrence, J.; Mattson, K. M.; Narupai, B.; Toumayan, E. P.; Luo, Y.; McGrath, A. J.; Clark, P. G.; Read de Alaniz, J.; Hawker, C. J., Simple Benchtop Approach to Polymer Brush Nanostructures Using Visible-Light-Mediated Metal-Free Atom Transfer Radical Polymerization. *Acs Macro Lett* **2016,** *5* (2), 258-262.
(67) Chmielarz, P.; Krys, P.; Wang, Z.; Wang, Y.; Matyjaszewski, K., Synthesis of Well-Defined Polymer Brushes from Silicon Wafers *via* Surface-Initiated *se*ATRP. *Macromol Chem Phys* **2017,** *in press*.
(68) Fantin, M.; Isse, A. A.; Venzo, A.; Gennaro, A.; Matyjaszewski, K., Atom transfer radical polymerization of methacrylic acid: A won challenge. *Journal of the American Chemical Society* **2016,** *138* (23), 7216-7219.
(69) Chmielarz, P.; Sobkowiak, A.; Matyjaszewski, K., A simplified Electrochemically Mediated ATRP Synthesis of PEO-b-PMMA Copolymers. *Polymer* **2015,** *77*, 266-271.

(70) Chmielarz, P.; Park, S.; Sobkowiak, A.; Matyjaszewski, K., Synthesis of β-Cyclodextrin-based Star Polymers *via* a Simplified Electrochemically Mediated ATRP. *Polymer* **2016,** *88*, 36-42.
(71) Chmielarz, P., Synthesis of Cationic Star pPolymers by Simplified Electrochemically Mediated ATRP. *Express Polymer Letters* **2016,** *10* (10), 810-821.
(72) Chmielarz, P., Synthesis of α-d-Glucose-based Star Polymers through Simplified Electrochemically Mediated ATRP. *Polymer* **2016,** *102*, 192-198.
(73) Lorandi, F.; Fantin, M.; Isse, A. A.; Gennaro, A., Electrochemically mediated atom transfer radical polymerization of n-butyl acrylate on non-platinum cathodes. *Polymer Chemistry* **2016,** *7* (34), 5357-5365.
(74) Chmielarz, P., Cellulose-based Graft Copolymers Prepared by Simplified Electrochemically Mediated ATRP. *Express Polymer Letters* **2017,** *11* (2), 140-151.
(75) Chmielarz, P., Synthesis of Mmultiarm Star Block Copolymers via Simplified Electrochemically Mediated ATRP. *Chemical Papers* **2017,** *71* (1), 161-170.
(76) Yan, J.; Pan, X.; Wang, Z.; Zhang, J.; Matyjaszewski, K., Influence of Spacers in Tetherable Initiators on Surface-Initiated Atom Transfer Radical Polymerization (SI-ATRP). *Macromolecules* **2016,** *49* (23), 9283–9286.
(77) Choi, J.; Dong, H.; Matyjaszewski, K.; Bockstaller, M. R., Flexible Particle Array Structures by Controlling Polymer Graft Architecture. *J Am Chem Soc* **2010,** *132* (36), 12537-12539.
(78) Munirasu, S.; Karunakaran, R. G.; Rühe, J. r.; Dhamodharan, R., Synthesis and Morphological Study of Thick Benzyl Methacrylate–Styrene Diblock Copolymer Brushes. *Langmuir* **2011,** *27* (21), 13284-13292.
(79) Ohno, K.; Tabata, H.; Tsujii, Y., Surface-Initiated Living Radical Polymerization from Silica Particles Functionalized with Poly(ethylene Glycol)-Carrying initiator. *Colloid Polym Sci* **2013,** *291* (1), 127-135.
(80) Hui, C. M.; Dang, A.; Chen, B.; Yan, J.; Konkolewicz, D.; He, H.; Ferebee, R.; Bockstaller, M. R.; Matyjaszewski, K., Effect of Thermal Self-Initiation on the Synthesis, Composition, and Properties of Particle Brush Materials. *Macromolecules* **2014,** *47* (16), 5501-5508.
(81) Konkolewicz, D.; Krys, P.; Góis, J. R.; Mendonça, P. V.; Zhong, M.; Wang, Y.; Gennaro, A.; Isse, A. A.; Fantin, M.; Matyjaszewski, K., Aqueous RDRP in the Presence of Cu0: The Exceptional Activity of CuI Confirms the SARA ATRP Mechanism. *Macromolecules* **2014,** *47* (2), 560-570.
(82) Magenau, A. J. D.; Bortolamei, N.; Frick, E.; Park, S.; Gennaro, A.; Matyjaszewski, K., Investigation of Electrochemically Mediated Atom Transfer Radical Polymerization. *Macromolecules* **2013,** *46* (11), 4346-4353.
(83) Krys, P.; Ribelli, T. G.; Matyjaszewski, K.; Gennaro, A., Relation between Overall Rate of ATRP and Rates of Activation of Dormant Species. *Macromolecules* **2016,** *49* (7), 2467-2476.
(84) Krys, P.; Matyjaszewski, K., Kinetics of Atom Transfer Radical Polymerization. *European Polymer Journal* **2017,** *89*, 482-523.
(85) Konkolewicz, D.; Schröder, K.; Buback, J.; Bernhard, S.; Matyjaszewski, K., Visible Light and Sunlight Photoinduced ATRP with ppm of Cu Catalyst. *Acs Macro Lett* **2012,** *1* (10), 1219-1223.

(86) Goel, V.; Pietrasik, J.; Dong, H.; Sharma, J.; Matyjaszewski, K.; Krishnamoorti, R., Structure of Polymer Tethered Highly Grafted Nanoparticles. *Macromolecules* **2011,** *44* (20), 8129-8135.
(87) Daoud, M.; Cotton, J. P., Star Shaped Polymers : a Model for the Conformation and its Concentration Dependence. *J. Phys. France* **1982,** *43* (3), 531-538.
(88) Sakar, D.; Erdogan, T.; Cankurtaran, O.; Hizal, G.; Karaman, F.; Tunca, U., Physicochemical Characterization of Poly(*tert*-butyl Acrylate-*b*-methyl Methacrylate) Prepared with Atom Transfer Radical Polymerization by Inverse Gas Chromatography. *Polymer* **2006,** *47* (1), 132-139.
(89) Danial, M.; My-Nhi Tran, C.; Young, P. G.; Perrier, S.; Jolliffe, K. A., Janus Cyclic Peptide–Polymer Nanotubes. *Nature Communications* **2013,** *4*, 2780.
(90) Lewin, M.; Mey-Marom, A.; Frank, R., Surface Free Energies of Polymeric Materials, Additives and Minerals. *Polymers for Advanced Technologies* **2005,** *16* (6), 429-441.
(91) Xia, J.; Zhang, X.; Matyjaszewski, K., Synthesis of Star-Shaped Polystyrene by Atom Transfer Radical Polymerization Using an "Arm First" Approach. *Macromolecules* **1999,** *32* (13), 4482-4484.
(92) Chmielarz, P.; Krys, P.; Park, S.; Matyjaszewski, K., PEO-b-PNIPAM Copolymers via SARA ATRP and eATRP in Aqueous Media. *Polymer* **2015,** *71*, 143-147.
(93) Park, S.; Chmielarz, P.; Gennaro, A.; Matyjaszewski, K., Simplified Electrochemically Mediated Atom Transfer Radical Polymerization using a Sacrificial Anode. *Angewandte Chemie International Edition* **2015,** *54* (8), 2388 –2392.